

**Influence of particle-scale properties and gravitational field on flow
properties of granular materials**

Babatunde Clement Arowosola

Submitted in accordance with the requirements for the degree of
Doctor of Philosophy

The University of Leeds
Institute of Particle Science and Engineering
School of Chemical and Process Engineering

January 2016

The candidate confirms that the work submitted is his own, except where work which has formed part of jointly authored publications has been included. The contribution of the candidate and other authors to this work has been explicitly indicated below. The candidate confirms appropriate credit has been given within the thesis where reference has been made to the work of others.

Chapter 5, 6 and 7 of the thesis contain some materials from the jointly-authored publications given below

Albaraki, S., Antony, S. J. & Arowosola, C. B. Visualising shear stress distribution inside flow geometries containing pharmaceutical powder excipients using photo stress analysis tomography and DEM simulations. *Powders and Grains*, 2013 Sydney, Australia. AIP Conference Proceedings, 706-709.

Antony, S. J., Arowosola, C. B., Amanbayev, T., Richter, L., Influences of particle-scale properties on the flow properties of powder media in low gravity environments: computational analysis. European Space Agency's International Conference on Dust and Grains in Low Gravity and Space Environment, ESA/ESTEC, 2012, The Netherlands

The work presented in the above publications was carried out by the candidate (Babatunde Arowosola). The whole work was carried out under the supervision of Dr S. J. Antony.

This copy has been supplied on the understanding that it is copyright material and that no quotation from the thesis may be published without proper acknowledgement.

The right of Babatunde Arowosola to be identified as Author of this work has been asserted by him in accordance with the Copyright, Designs and Patents Act 1988.

© 2016 The University of Leeds and Babatunde Arowosola

Acknowledgement

This research project would not have been successful without the efforts of my project Supervisor in the Institute of Particle Science and Engineering, University of Leeds, who endlessly provides the discipline, patience and encouragement to excel in my chosen career.

I would like to acknowledge the privilege given to learn and the support granted to me by the entire staff of the School of Chemical and Process Engineering, University of Leeds. I would like to express my special appreciation and gratitude to my project supervisor; Dr S. J. Antony. He has been a tremendous mentor who has greatly helped me in the acquisition of educational, social and moral knowledge. I am grateful to Dr L. Richter for his continuous support through the supervisor to this work. I also thank Dr B Manoj, PSG College of Technology, Mrs Judes Sujatha, Government College of Engineering at Nagercoil and my colleague Dr Saeed Albaraki for their timely help especially in some of the experimental characterisation work. I would also like to acknowledge Professor T. Amanbayev for his assistance whenever required.

I would like to express my special thanks and profound gratitude to my wife, Olajumoke Arowosola, for her constant moral and financial support and all the sacrifice made on my behalf over the years. I would also like to appreciate my daughter, Taraoluwa Arowosola and son, Taminiire Arowosola who both are constant motivation for me to be focused on my goal.

My appreciation also goes to Herbert Osei Baidoo (RIP) for his support and believe in me, my friends and colleagues, Grace Adeola Olugbenga, Kelechi Anyikude, Olayode Sodipo, Sesan Solaru, Fisayo Banks Alonge, Faith Bamiduro and especially Dr George Okeke who was always there to give that gently shove when required.

My special regard goes to my beloved parents, Mr. and Mrs. Simeon Arowosola, my lovely sisters, Damilola Oluwagbolahan, Ayomipo Latilo and Oluwatosin Arowosola for their spiritual, moral and financial support.

Ultimately, I am grateful to God Almighty for his grace, favour and love showered upon me.

Abstract

The complexities in the processing behaviour of granular materials under different gravitational environments pose challenges to the researchers in a number of multidisciplinary fields. The micromechanical behaviour of granular materials is inherently heterogeneous due to its discrete nature. Generally, the macroscopic behaviour of granular materials can be determined by accounting for the inter-particle interactions that exist within. Although significant progress has been achieved in the past especially on the transport, handling and storage of granular materials in confined geometries under earth gravity using experimental and computational methods, the micromechanical behaviour of granular materials under low-gravitational environments is still poorly understood. Out of the several approaches proposed in the literature in understanding the complexities in granular materials, discrete element modelling (DEM) has evolved as an important tool in evaluating the role of particle scale properties on the flow and compaction characteristics of granular materials. The primary focus of this research is to understand the micromechanical properties of granular materials, primarily their flow and compaction characteristics under different gravitational environments. Hence, three dimensional DEM is applied in this study under earth, mars and lunar (EML) gravity conditions.

In this study, in order to attain a fundamental level understanding of the flow behaviour of granular materials through confined geometries under varying gravity conditions, a comprehensive level of simulations were performed. Initially, sandstone materials as simulants used to represent space grains in space exploration activities are experimentally characterised to obtain two key input material parameters viz., particle size distribution and adhesion force between the grains. These key input parameters, in addition to their other physical properties reported in the literature are fed as input parameters in the three-dimensional DEM simulations for studying their flow and compaction characteristics under EML gravities. Further, investigations on the prediction of maximum shear stress distribution in a hopper containing granular materials under static filling were analysed under earth gravity using three dimensional DEM. The predicted results are compared with an advanced experimental approach using Photo-stress analysis tomography (PSAT). Studies show that the predicted DEM and experimental results for the maximum stress distribution are in good agreement under earth gravity. The hopper internal angle is seen to influence the stress profile quite significantly. Additionally, these DEM results agree qualitatively

well with the common Walker's theoretical predictions for the stress distribution along the hopper walls with dependence on hopper internal angle under earth gravity. The PSAT analysis, though performed only under earth gravity under static condition validates the usefulness of inputting measured particle-scale properties in the DEM simulations.

Thereafter, different continuum approaches and DEM simulations are used to investigate the effect of particle scale properties and gravity on the flow characteristics of granular materials through hoppers. Continuum theories based on discrete layer approach and Kirya's structural model for gravity effects on flow properties of grains in hoppers is performed and compared with that of DEM simulations. Most results obtained on the effect of various particle scale properties agree with existing studies in literature where available. Granular flow is seen to depend on gravity using both the continuum and DEM simulations and these results further agree qualitatively with predictions from a limited practical parabolic flight test operation. Based on this analysis and to further understand the influence of particle scale properties on granular flow, parametric analysis is carried out using DEM simulations. The analysis provides understanding of the complex behaviour of the grains and its response under EML gravity levels. Granular packing, granular bed density, cohesion, hopper geometry (orifice and internal angle), friction effect, angle of repose and combined adhesion strength and size distribution (for real samples) of the granular materials were all observed to have significant effect on granular flow under EML gravity levels distinctly. From all the analysis, the influence of gravity on granular flow is observed to be most sensitive under the lunar gravity. This could imply that the lunar in-situ resource utilization (ISRU) processes may require wider exit openings or non-gravity driving forces to have an effective output from the various processes as compared to process utilization on earth. To improve the granular flow, applying a granular flow aid is investigated for a horizontal piezo vibrator across the hopper containing granular bed under EML gravity levels using DEM. Analysis indicates that the piezo-vibrator technique could improve the flow of grains through a hopper under low gravity levels. To aid the design of the vibrator, its effective impact to improve flow is however shown to depend on the horizontal amplitude and frequency of the vibrator. Furthermore DEM simulations are performed to assess the quality of granular filling in a collection chamber from continuous flow and staggered flow outputs. Continuous flow mechanism is seen to be more effective in processing of grains as against staggering the flow especially under a low gravity level. Finally, the

compaction properties of granular media with ice contents under different gravity levels is analysed using DEM simulations.

Overall, this thesis presents vital information on the role of particle scale properties on flow and compaction characteristics of granular materials under varying gravity environments. In the future, the understandings reported in this thesis could help to design suitable flow and compaction processes in different engineering and science disciplines, especially in space/low gravity explorations to meet with the ever growing needs for technology advancements.

Table of Content

Acknowledgement	iii
Abstract	iv
Table of Content	vii
List of Figures	xv
List of Tables	xxv
Nomenclature	xxvii
Chapter 1	1
1 Research Introduction	2
1.1 Introduction	2
1.2 Motivation, Research Challenges and Aims of the Thesis	6
1.3 Structure of the Thesis	10
Chapter 2	13
2 Background and Literature Review	14
2.1 Introduction	14
2.2 Granular Materials	14
2.3 Processing Granular Materials	16
2.4 Properties of Granular Materials	17
2.4.1 Particle size	17
2.4.2 Packing fraction	19
2.4.3 Porosity	19
2.4.4 Density	20
2.4.5 Friction	21
2.4.5.1 Wall friction	21
2.4.5.2 Internal friction	22
	vii

2.4.6	Cohesion and adhesion	22
2.4.6.1	Van der Waals force	23
2.4.6.2	Liquid bridge force	25
2.4.6.3	Electrostatic force	26
2.5	Stresses within Granular Material	26
2.6	Contact Force Distribution	30
2.7	Granular Flow	30
2.8	Stress and Force Distribution in Granular Flow Devices – Silos and Hoppers	34
2.8.1	Janssen theory and assumptions	37
2.8.2	Jenike theory	38
2.8.3	Walter and Walker’s method	38
2.8.4	Stress analysis using finite element method and discrete element method simulations	39
2.9	Hopper Design	40
2.9.1	Flow modes	42
2.9.1.1	Mass flow	42
2.9.1.2	Funnel flow	44
2.9.1.3	Expanded flow	45
2.9.2	Hopper geometry	46
2.9.3	Hopper design problems: Current challenges	48
2.10	Particle Flow in Hopper	50
2.10.1	Approaches adopted for analysing particle flow	51
2.10.2	Continuum theory	53
2.10.3	Discrete element model (DEM)	55
2.11	Relevance of Flow Properties of Granular Materials under Low Gravity	59

2.12	Characterization of Particle Scale and Flow Properties	62
2.12.1	Flow function	63
2.12.2	Complete discharge time	63
2.12.3	Hausner ratio	64
2.12.4	Carr index	64
2.12.5	Angle of repose	65
2.12.6	Shear test	67
2.13	Improving Granular Flow Rate and Discharge Aids of Hoppers	70
2.13.1	Granular flow rate	70
2.13.2	Discharge aids	72
2.13.3	Vibrational methods	73
2.14	Conclusions	75
	Chapter 3	77
3	Experimental Characterisation of Granular Samples for Key Particle-Scale Properties	78
3.1	Particle Size Distribution Measurement	78
3.2	Adhesion Force Measurement	85
3.2.1	Adhesion force measurement using atomic force microscopy	85
3.2.2	Adhesion force measurement using colloidal force microscopy	89
	Chapter 4	92
4	Stress Analysis and Shear Deformation of Granular Materials in Granular Flow under EML Gravity	93
4.1	Introduction	93
4.2	Basics and Background of Photo-Stress Analysis Tomography (PSAT)	95
4.3	Prediction of Maximum Stress within Granular Materials in Hoppers Using DEM 3D Simulations	97

4.3.1	Prediction of maximum shear stress distribution across the hopper section (horizontal section) using DEM simulations under earth gravity level	102
4.3.2	Prediction of maximum shear stress distribution across the hopper section (horizontal section) using DEM simulations under mars and lunar gravity level	105
4.4	Prediction of Shear Stress within Granular Materials in Hoppers along the Vertical Wall Using DEM 3D Simulations under Static Filling Condition	107
4.4.1	Prediction of stress distribution along the vertical hopper walls using DEM simulations under earth gravity level	110
4.4.2	Prediction of stress distribution on vertical hopper walls using DEM simulations under mars and lunar gravity level	114
4.5	Conclusion	116
Chapter 5		118
5	Effect of Gravity on Granular Flow: Some Theoretical Approaches and DEM Simulations	119
5.1	Analysis of Granular Flow using Discrete Layer Approach (DLA)	119
5.1.1	Discrete layer approach model and parameters used in granular flow investigation	119
5.1.2	Effect of height of the granular filling (Lagrange coordinates , ξ) in the hopper	122
5.1.3	Effect of flow rate Q on discharge completion time	123
5.1.4	Internal angle on granular discharge completion time	125
5.1.5	Effect of hopper orifice opening width on granular flow	128
5.1.6	Particle velocity on completion time	131
5.1.7	Particle height on granular discharge completion time	132
5.2	Influence of Gravitational Field on Granular Flow Using Kirya's Structural Model (Continuum Analysis)	134
5.2.1	Gravity effect of granular flow using Kirya structural model	135
5.2.2	Impact of particle size on granular flow under gravity level using Kirya's structural model	141

5.2.3	Impact of friction coefficient on granular flow under gravity level using Kirya's structural model	143
5.3	Gravity Effect of Granular Flow using DEM Model	147
5.3.1	Qualitative validation of gravity effect on granular flow with parabolic flight campaign	157
5.4	Conclusion	163
	Chapter 6	164
6	Influences of Particle-Scale Properties and Hopper Geometry on the Flow Behaviour of Granular Materials under Earth, Mars and Lunar Gravities: Parametric Analysis Using Three-Dimensional DEM Simulations	165
6.1	Introduction	165
6.2	DEM Model to Predict the Influence of Granular Packing on Granular Flow under EML Gravitational Field	167
6.3	Effect of Cohesion (Granular Bond Strength) on Granular Flow under EML Gravitational Field	170
6.3.1	Constant slit opening size of hopper	170
6.3.2	Varying slit opening sizes of hopper	173
6.4	Effect of Contact Stiffness on Granular Flow under EML Gravitational Field	177
6.5	Effect of Density of Particles on Granular Flow under EML Gravitational Field	179
6.6	Effects of Hopper Internal Angle on the Granular Flow under EML Gravity Level	181
6.7	Influences of Friction Coefficient on Granular Flow under EML Gravitational Field	185
6.8	Effects of Angle of Repose Formed by Grains of Granular Flow under EML Gravity Levels	188
6.9	Influence of Combined Effects of Particle Size Distribution (PSD) and Adhesion Strength of Grains on Granular Flow	191
6.10	Conclusions	198

Chapter 7	200
7 Granular Flow Aids and Flow Improvement	201
7.1 Introduction	201
7.2 Horizontal Vibration Induced Hopper Flow under EML Gravity Levels	202
7.3 Staggered Vs Continuous Granular Flow in a Hopper under EML Gravity Levels	223
7.4 Conclusion	230
Chapter 8	232
8. Compaction Properties of Granular Media with Ice Content	233
8.1 Brief Background on Lunar Explorations	233
8.2 Lunar Soil and Simulants	235
8.3 Compaction on Ice-Bonded Lunar Soil using Three Dimensional DEM	237
8.4 Compaction of Ice-Bonded Granular materials for Earth and Mars Gravity Levels	251
8.5 Conclusions	254
Chapter 9	256
9 Conclusions and Future Recommendations	257
9.1 Conclusions	257
9.1.1 Investigations on the stress analysis and shear deformation of granular materials under EML gravity	258
9.1.2 Gravity effects on granular flow using theoretical approaches and DEM simulations	259
9.1.3 Influences of particle-scale properties and hopper geometry on granular flow behaviour under earth, mars and lunar gravity levels using DEM simulation	260
9.1.4 Enhancing granular flow under EML gravity	261
9.1.5 Compaction properties of ice-bonded granular media	262
9.2 Future Recommendations	263
References	264

List of Publications	303
Appendix A	304
A.1 Theory and concept of DEM modelling	305
A.2 DEM Calculation Cycle	305
A.2.1 Force displacement relations	306
A.2.2 Law of motion	309
A.2.3 Contact law	310
A.3 Contact Force Models	311
A.3.1 Contact stiffness models	311
A.3.1.1 Linear contact model	311
A.3.1.2 Hertz-Mindlin contact model	313
A.3.2 Slip model	314
A.3.3 Bonding model	315
A.3.3.1 Contact-bond model	315
A.3.3.2 Parallel-bond model	316
A.3.4 Alternative contact models	318
A.4 Critical Time-Step Determination	318
A.5 Contact Detection Algorithm	321
A.6 Energy Tracing in DEM Simulations	322
A.6.1 Body work	322
A.6.2 Bond energy	323
A.6.3 Boundary work	323
A.6.4 Frictional work	324
A.6.5 Kinetic energy	324
A.6.6 Strain energy	324

A.7	Measurement Logic	325
A.7.1	Coordination number	325
A.7.2	Porosity	325
A.7.3	Sliding fraction	327
A.7.4	Stress measurements	327

List of Figures

Fig. 1. 1	Example of ExoMars surface layers of typical low gravity terrestrial planets (e.g. mars and moon)	5
Fig. 1. 2	A typical SPDS station (credit ESA)	8
Fig. 1. 3	Scope of thesis	12
Fig. 2. 1	Typical types of granular materials – Sand particles, Beads, sand pile and grains (Short, 2011)	15
Fig. 2. 2	Spherical particle	18
Fig. 2. 3	Packing arrangements for (a) monodispersed spheres (b) polydispersed spheres (Baranau and Tallarek, 2014).	19
Fig. 2. 4	Inter-particle strength governed by intermolecular, electrostatic and capillary forces (Juliano and Barbosa-Cánovas, 2010)	24
Fig. 2. 5	Liquid bridge between two spheres of equal radius	25
Fig. 2. 6	Contact force networks of granular matter (Majmudar and Behringer, 2005)	30
Fig. 2. 7	Application of granular flows: (a) An avalanche on the Liberty Wall Range, USA; (b) The buckling of a grain silo; (c) Eroded cliff faces in the Valles marinerie canyon on Mars (Cawthorn, 2008)	32
Fig. 2. 8	Different configurations to study granular flows; (a) Plane shear (b) annular shear (c) vertical silo (d) Inclined plane (e) heap flow (f) rotating drum (Forterre and Pouliquen, 2006)	33
Fig. 2. 9	The stress σ , in the hopper as a function of position (\mathbf{r}, θ)	35
Fig. 2. 10	Radial stress field (Schulze, 2006b)	36
Fig. 2. 11	Schematic of different types of hopper (Woodcock and Mason, 1987)	41

Fig. 2. 12	Pattern of flow within a hopper	43
Fig. 2. 13	A basic expanded flow hopper (Roberts, 1992)	46
Fig. 2. 14	Effective storage volume of a hopper	47
Fig. 2. 15	Common hopper design problems	50
Fig. 2. 16	Illustration of the circular polariscope set-up	52
Fig. 2. 17	Angle of repose, θ	66
Fig. 2. 18	Shear testers (Schweddes, 2003)	67
Fig. 2. 19	Schulze ring shear tester (Schulze, 2007)	69
Fig. 2. 20	Classification of vibratory discharge aids (Bates et al., 2007)	74
Fig. 3. 1	Morphologi G3 by Malvern	79
Fig. 3. 2	SEM images and size distributions of granular simulant JS1 – JS4 and JB1 – JB4	84
Fig. 3. 3	AFM set-up (Mironov, 2004)	86
Fig. 3. 4	Illustrative diagram of the Leonard-Jones potential	87
Fig. 3. 5	Illustrative diagram of a cantilever-particle interaction (Mironov, 2004)	88
Fig. 3. 6	Typical output from an AFM adhesion force experiment (Mironov, 2004)	89
Fig. 3. 7	Schematic representation of AFM and CFM	90
Fig. 4. 1	Schematic diagram of PSAT (circular polariscope) set up	96
Fig. 4. 2	Initial compact state of the hopper generated using PFC ^{3D}	98
Fig. 4. 3	Hopper geometry for angles 30, 45, 60, and 90 degrees	100
Fig. 4. 4	Contact forces within the granular bed for angles 30, 45, 60, and 90 degrees	101

Fig. 4. 5	Schematic cross section showing the measurement sphere used for stress measurement across the granular bed horizontally in the hopper	102
Fig. 4. 6	Superimposed plot for maximum shear stress distribution across granular bed for 30°, 45°, 60° and 90° under earth gravity using DEM simulations and PSAT experiments	104
Fig. 4. 7	Superimposed plot for maximum shear stress distribution across granular bed for 30°, 45°, 60° and 90° under earth, mars and lunar gravity using DEM simulations	106
Fig. 4. 8	Variations in the static normal and shear stresses with the bed height (a) hopper half angle 10°, (b) hopper half angle 20° (Chou and Chen, 2003)	108
Fig. 4. 9	Schematic cross section showing the measurement sphere used for stress measurement vertically along the hopper wall	110
Fig. 4. 10	Predictions of wall stress distribution for hoppers with internal angles of 30°, 60° and 90° using DEM simulations under earth gravity	111
Fig. 4. 11	Comparison between numerical and theoretical predictions of wall pressure distributions for end of filling and beginning of discharge (Wang and Ooi, 2015)	112
Fig. 4. 12	Comparison between DEM and Walker's predictions of wall stress along the hopper for 30°, 60° and 90° under earth gravity	113
Fig. 4. 13	Superimposed plot for shear stress distribution vertically along the hopper walls for 30°, 60° and 90° under earth, mars and lunar gravity using 3-dimensional DEM simulations	115
Fig. 5. 1	Schematic cross section of DS bounded by walls	120
Fig. 5. 2	Variation of Lagrange coordinates, ξ within the media	123
Fig. 5. 3	Effect of flow rate on completion time using DLA model	124
Fig. 5. 4	Time to empty the hopper with flow rate variation using DLA model	125
Fig. 5. 5	Variation of the internal angle α for $\xi=0.2$ and 0.3 respectively using DLA model	126

Fig. 5. 6	Comparison of the theoretical and experimental discharge rates at different internal hopper angle (Albaraki and Antony, 2014)	126
Fig. 5. 7	Time to empty the hopper (completion time) with the hopper angle (α) variation	127
Fig. 5. 8	Effect of flow rate on varying hopper orifice opening a for both 0.05m and 0.2m	129
Fig. 5. 9	Time to empty the hopper against flow rate Q for different hopper outlet size at $\xi = 0.3$	130
Fig. 5. 10	Time to empty hopper against hopper outlet size for $\xi = 0.2$ and 0.3	131
Fig. 5. 11	Velocity gradient with x at $\xi = 0.3$	132
Fig. 5. 12	Effect of particle height, h on the completion time for the granular flow of one dimension through the hopper media	133
Fig. 5. 13	(a) Zone of flow out of the granular particles. (b) Expanded view of Zone D	135
Fig. 5. 14	Variations of mass flow rate versus gravity g when hourglass is evacuated (◆) or filled by air (♠) (Le Pennec et al., 1995)	139
Fig. 5. 15	Variations of gravity effect on flow rate using continuum theory	140
Fig. 5. 16	Impact of particle diameter (a) $10\mu m - 100\mu m$ (b) $100\mu m - 104\mu m$ on the gravity effect on flow rate using Kriya's structural model	142
Fig. 5. 17	Impact of friction coefficient on the gravity effect on flow rate using Kriya's structural model	144
Fig. 5. 18	Variation of particle diameter and friction coefficient (a-e) on flow rate at different gravity level	146
Fig. 5. 19	Geometry arrangement of a wedge shaped hopper	148
Fig. 5. 20	Geometry constraint in a wedge shaped hopper	148

Fig. 5. 21	Particles confined in a wedged shaped hopper	149
Fig. 5. 22	Geometry arrangement of conical hopper and confined particles within the hopper	150
Fig. 5. 23	Flow of particles under gravity for both hopper model types	151
Fig. 5. 24	Time evolution of the effect of gravity	153
Fig. 5. 25	Gravity effect on volumetric flow rate using DEM	154
Fig. 5. 26	Volume of basalt spheres in the hourglass experiment as a function of gravity level (Hofmeister et al., 2009)	154
Fig. 5. 27	Validation of gravity effect between Kirya's continuum theory and DEM	155
Fig. 5. 28	General information from DEM simulation profile during hopper flow	156
Fig. 5. 29	Still from December 2012 TUM/LRT parabolic flight experiment with 2D hoppers (set of 3 hoppers of different throat diameters (credit: P. Reiss TUM/LRT)	157
Fig. 5. 30	Flow of sandstone materials under lunar gravity conditions ceased	159
Fig. 5. 31	Mass flow of sandstone materials under lunar gravity and 2g0 gravity levels	160
Fig. 5. 32	Influence of EML gravity levels on mass flow	161
Fig. 5. 33	Influence of EML gravity on mass and volume flow rate	162
Fig. 6. 1	Conical hopper with confined grains for granular flow under EML gravity levels	166
Fig. 6. 2	Influence of packing fraction on granular flow under EML gravity	168
Fig. 6. 3	Snapshots of the system during discharge process at mid flow for loose and dense packed grains under EML gravity levels	169
Fig. 6. 4	Effect of cohesion on granular flow using three dimensional DEM under EML gravity	171

Fig. 6. 5	DEM snapshots of clumps created due to cohesive bonds (3N) and particles with no cohesive bonds during granular flow	172
Fig. 6. 6	Cohesion effect on particle flow at low bond strength under EML gravity using DEM	173
Fig. 6. 7	Superimposed gravity effect of hopper slit opening on granular flow of low and high cohesive particles using DEM	175
Fig. 6. 8	DEM profile showing ceased flow of grains under lunar gravity	176
Fig. 6. 9	Effect of particle stiffness on granular flow in hopper under EML gravity level using DEM	178
Fig. 6. 10	Density effects on granular flow rate through hopper under EML gravity levels using DEM	180
Fig. 6. 11	Influence of hopper angle on granular flow under earth, mars and lunar gravity	182
Fig. 6. 12	Formation of arc during granular flow at high internal angle in DEM simulation	183
Fig. 6. 13	Typical DEM simulation profiles showing the displacement of particles at 30° and 90° hopper internal angle	184
Fig. 6. 14	Experimental results showing major stress principal directions inside stress responsive granules at 30° and 90° internal angle hopper geometry (Albaraki and Antony, 2014)	184
Fig. 6. 15	Effect of (a) wall friction and (b) particle friction on granular flow in hopper under EML gravity levels	187
Fig. 6. 16	EML gravity effect on angle of repose of cohesionless granular material	189
Fig. 6. 17	Angle of repose predictions from DEM simulations using cohesionless granular materials	190

Fig. 6. 18	Typical flow profile for PSD of soil samples JS1 and JB1 at $\frac{3}{4}$ flow under gravity flow	194
Fig. 6. 19	Particle size distribution dependence on granular flow for JS1 to JS4 soil simulants under EML gravity levels	195
Fig. 6. 20	Particle size distribution dependence on granular flow for JB1 to JB4 soil simulants under EML gravity levels	196
Fig. 7. 1	Initial position of grains just after samples attained equilibrium	204
Fig. 7. 2	Profiles of particle contacts at different stages of flow: for the cases of no vibrator and vibrator with sinusoidal frequency 1Hz, 3Hz, 5Hz, 7Hz, and 10Hz under gravity flow (Mars gravity)	206
Fig. 7. 3	Profiles of contact force distribution at different stages of flow: for the cases of no vibrator and vibrator with sinusoidal frequency 1Hz, 3Hz, 5Hz, 7Hz, and 10Hz under gravity flow (Mars gravity)	209
Fig. 7. 4	Velocity distribution profiles at different stages of flow: for the cases of no vibrator and vibrator with sinusoidal frequency 1Hz, 3Hz, 5Hz, 7Hz, and 10Hz under gravity flow (Mars gravity)	211
Fig. 7. 5	Displacement profiles at different stages of flow: for the cases of no vibrator and vibrator with sinusoidal frequency 1Hz, 3Hz, 5Hz, 7Hz, and 10Hz under gravity flow (mars gravity)	213
Fig. 7. 6	Average bulk flow rate at different stages of flow: for cases of no vibrator and vibrator with sinusoidal frequency 1Hz – 10Hz under Mars gravity	214
Fig. 7. 7	Profiles of particle contacts at different stages of flow: for the cases of no vibrator and vibrator with sinusoidal frequency 20Hz, 50Hz and 250Hz under gravity flow (Mars gravity)	216

Fig. 7. 8	Profiles of contact force distribution at different stages of flow: for the cases of no vibrator and vibrator with sinusoidal frequency 20Hz, 50Hz, and 250Hz under gravity flow (Mars gravity)	218
Fig. 7. 9	Velocity distribution profiles at different stages of flow: for the cases of no vibrator and vibrator with sinusoidal frequency 20Hz, 50Hz, and 250Hz under gravity flow (Mars gravity)	219
Fig. 7. 10	Displacement profiles at different stages of flow: for the cases of no vibrator and vibrator with sinusoidal frequency 20Hz, 50Hz, and 250Hz under gravity flow (mars gravity)	221
Fig. 7. 11	Average bulk flow rate for cases of vibrator with sinusoidal frequency 1Hz – 250Hz under EML gravity	222
Fig. 7. 12	Pictorial view of a hopper and collection chamber designed using DEM simulations	224
Fig. 7. 13	Flow profiles obtained from staggered and continuous flow of grains from hopper using DEM simulation	228
Fig. 7. 14	Effect of staggered flow against continuous flow system (a) normalized with earth gravity (b) normalized with continuous flow under each gravity level	229
Fig. 8. 1	Lunar landing Site Chart – Nearside of the Moon with locations of Apollo, Surveyor and Lunar (Sibille et al., 2005)	234
Fig. 8. 2	Footprint in lunar soil with few rocks on the regolith (NASA photo AS11-40-5877)	235
Fig. 8. 3	Relative effects of three (3) common modes of ice contents on lunar soil strength	237
Fig. 8. 4	DEM profile for ice-bonded simulated lunar regoliths at isotropic state before applying axial compaction under lunar gravity	241
Fig. 8. 5	DEM profile for ice-bonded simulated lunar regoliths at steady state (post-peak)	243

Fig. 8. 6	DEM simulation results of axial stress measured against the axial strain for ice bonded grains of modes 1, 2 and 3 under lunar gravity	245
Fig. 8. 7	DEM simulation results of mean stress measured against the axial strain for ice bonded grains of modes 1, 2 and 3 under lunar gravity	246
Fig. 8. 8	DEM simulation results of friction energy measured against the axial strain for ice bonded grains of modes 1, 2 and 3 under lunar gravity	247
Fig. 8. 9	DEM simulation results of kinetic energy measured against the axial strain for ice bonded grains of modes 1, 2 and 3 under lunar gravity	248
Fig. 8. 10	DEM simulation results of axial stress, mean stress, frictional and kinetic energy measured against the axial strain for ice-bonded grains of modes 1, 2 and 3 under lunar gravity	250
Fig. 8. 11	DEM simulation results of axial stress, mean stress, frictional and kinetic energy measured against the axial strain for ice-bonded grains of modes 1, 2 and 3 under earth gravity	252
Fig. 8. 12	DEM simulation results of axial stress, mean stress, frictional and kinetic energy measured against the axial strain for ice-bonded grains of modes 1, 2 and 3 under mars gravity	253
Fig. A. 1	Description of the particle-particle contact (ITASCA, 2004)	307
Fig. A. 2	Description of the particle-wall contact (ITASCA, 2004)	308
Fig. A. 3	Schematic description of the overlap, δ during collision	310
Fig. A. 4	Linear Spring-Dashpot Model for DEM simulations in (a) normal and (b) tangential directions	312
Fig. A. 5	An approximate of the Hertz-Mindlin Model (EDEM, 2012)	313
Fig. A. 6	Constitutive behaviours for point contact (ITASCA, 2004)	316

Fig. A. 7	Parallel bond idealization depicted as a cylinder of cementitious material	317
Fig. A. 8	Single mass-spring system	319
Fig. A. 9	Multiple mass-spring system	319
Fig. A. 10	Calculation cycle in PFC3D for the force-displacement law at particle-wall contacts	322
Fig. A. 11	Relevant quantities for porosity computation in a system with 4 clumps and 2 particles (ITASCA, 2004)	326

List of Tables

Table 2. 1	Advantages and Disadvantage of mass flow in hoppers (Rhodes, 2008b)	44
Table 2. 2	Advantages and Disadvantage of funnel flow in hoppers	45
Table 2. 3	Classification of flow behaviour based on flow function (Jenike, 1964b)	63
Table 2. 4	Scale of flowability for Carr index and Hausner ratio (Abdullah and Geldart, 1999)	65
Table 2. 5	Typical angle of repose and flow behaviour (Woodcock and Mason, 1987)	66
Table 2. 6	Classification of Discharge Aids (Woodcock and Mason, 1987)	72
Table 2. 7	Selection of vibrations based on application (Bates et al., 2007)	75
Table 3. 1	Adhesion force input values of granular soil simulants	90
Table 4. 1	Parameters used in DEM model to analyse stress distribution	99
Table 5. 1	System description outlining type of investigation and parameters used in DLA model for granular flow investigation	121
Table 5. 2	Description of parameters used in investigating the impact of gravity on flow using Kirya's structural model	138
Table 5. 3	Description of parameters used in investigating the impact of particle size on flow under varying gravity level using the Kriya's structural model	141
Table 5. 4	Description of parameters used in investigating the impact of friction coefficient on flow under varying gravity level using Kirya's structural model	143
Table 5. 5	Constant values used in investigating gravity effect in 3D DEM simulation	152
Table 5. 6	Sandstone properties used in DEM simulation for granular flow under EML gravity	158
Table 6. 1	Standard values for the conical hopper geometry used in simulating granular flow under EML gravity levels	166

Table 6. 2	Parameters used to study the effect of packing fraction on granular flow under EML gravity	168
Table 6. 3	Material properties used in DEM simulations for cohesion effect with constant hopper slit opening size	171
Table 6. 4	Material properties used in DEM simulations for cohesion effect with varying hopper slit opening size	174
Table 6. 5	Material properties used in DEM simulations for particle stiffness effect	177
Table 6. 6	Material properties used in DEM simulations for density effect	180
Table 6. 7	Material properties used in DEM simulations for density effect	182
Table 6. 8	Material properties used in DEM simulations for friction effect	186
Table 6. 9	Parameters used in DEM simulation of gravity effect of angle of repose	188
Table 6. 10	Standard values for the conical hopper geometry used in simulating granular flow under EML gravity levels for different particle size distribution	192
Table 6. 11	Parameters used in DEM simulation on the effect of combined particle size distribution and adhesion force on granular flow under EML gravity levels	192
Table 7. 1	Hopper parameters and Microscopic material properties used in simulating vibrational induced gravity flow under EML gravity levels	202
Table 7. 2	Hopper parameters and Microscopic material properties used to simulate the stop-flow system under EML gravity levels	224
Table 8. 1	Micro-properties and compression conditions used in the DEM simulation for compression of ice-bonded lunar regolith	238

Nomenclature

Acronyms

DEM	Discrete Element Model
PFC	Particle Flow Code
DLA	Discrete Layer Approach
CFM	Colloidal Force Microscopy
AFM	Atomic Force Microscopy
PSD	Particle Size Distribution
PSAT	Photo-stress Analysis Tomography
FEM	Finite Element Model
SPDS	Sample Preparation and Distribution System
DS	Dosing Station

Chapter 1

Research Introduction

1 Research Introduction

1.1 Introduction

The physics of granular materials has a long standing history. Prominent scientists over the past years have contributed significantly to the early study of granular materials (Bagnold, 1966, Rayleigh, 1906, Bagnold, 1941, Reynolds, 1885, Faraday, 1857, Coulomb, 1773). Developing on these early days, the physical approach gave rise to engineering fields studying granular flows, pattern formation and packing. These noble efforts helped to progress the field of granular mechanics significantly. However, the study of granular materials under different process environments is still poorly understood. The understanding of granular materials is unique and complex in nature. Granular matter ranges from grains to ice floes drifting across the polar seas, to natural rocks, sands, seeds, beads, sugar, pharmaceutical pills, to extra-terrestrial icy and non-icy particles. Thus, granular matter is a system of interest in many fields such as: engineering, physics, geology, material science, biology and astronomy. Duran (1999) emphasized the fact that aggregates tend to obey universal laws, however, the fundamentals and applications of granular matter needs further understanding. Consequently, many interesting collective phenomena have been attributed to granular materials (Franklin and Shattuck, 2015, Acton, 2012, Jaeger et al., 1996b) and thus attract interest increasingly from the engineering science community. Research into these granular materials and their properties could be further broken down into different particle scales – molecular, macro, micro and nanoscale. Studies of the properties of granular materials in their micro and nanoscale have been gaining more attention in various applications in most natural and engineering processes. Particulate materials in their micro and nanoscales have been shown to behave differently compared with macro or molecular scale (Li et al., 2009, Antony, 2007). An understanding of these materials in the micro and nanoscale can aid in predicting their behaviour in the larger scale as well. Since the granular material is said to consist of grains in contact and surrounding voids (Satake et al., 1999), the micromechanical behaviour of granular materials can therefore be discontinuous and heterogeneous consisting of many discrete particles which exhibit complex interactions. The overall bulk constitutive relationships are then determined by the contact interactions between two adjoining particles and also by the individual characteristics of all the single particles (Oda and Iwashita, 1999). Relevant theories have been established in order to characterize and analyse the behaviour of granular materials and several

approaches have been studied: A macroscopic approach based on continuum mechanics (Sawyer and Tichy, 2001, Savage, 1998, Jenkins, 1987a, Jenkins and Richman, 1985) and a microscopic approach considering a complete discrete structure based on the discrete element modelling (DEM) theory (Cundall & Strack, 1979)(Clearly, 2004, Williams et al., 2004, Rycroft et al., 2009b). However, a complete theory for the mechanical behaviour of granular materials has not yet been established (Rycroft et al. 2009b). A distinguishing feature between flows of granular materials and other solid-fluid mixtures is that in granular flow, the direct particle interactions play a vital role in the flow mechanics. Thus, most of the energy dissipation and momentum transfer in granular flow occurs when particles are in contact with each other or with a boundary (Markowich, 2007).

In processing granular materials, the flow state of granular materials is seen as extremely complex because they are regarded to be the least predictable of all materials in relation to flowability (Behringer et al., 1999). The complex interactions between individual particles and interactions with the surrounding gas or liquid and walls introduce new challenges not faced in particle free liquid or gas systems. This complexity revolves around the large number of factors that can change the rheological properties of the granular materials. These factors including physical, mechanical and external properties are such as: particle size, angularity, shape, particle interaction, stiffness, cohesion, flow rate, container surface effects, and storage time (Cagnoli and Romano, 2010, Mollon and Zhao, 2013, Peng et al., 2014, Zhu et al., 2013a, Clearly and Sawley, 2002). Existing analysis in dealing with this complexity involves mostly the use of the continuum approach (Tejchman, 2013, Rycroft et al., 2009a). However, most of the current industrial granular materials as well as research materials can flow like a fluid depending on the boundary conditions (Behringer et al., 1999). An attempt has been made over the years to understand and exploit the flowability of granular materials so as to ease handling and storage problems, yet the design of granular systems is still not fully accomplished. This is in part due to the lack of clear understanding of the most basic flow mechanism of granular materials. Application of the science of granular materials has not fully matured to identify all material properties that can control and optimise flow behaviour. In view of this, the flow properties are evaluated by first creating an understanding of the continuum theory and then applying the three dimensional discrete element model (DEM) at later stages here.

Antony (2007) has been able to apply particle characterization techniques in micro and nanotechnologies such as atomic force microscopy (AFM) to study the inter-particle interactions and design the particulate assemblies. These inter-particle interactions are microscopic quantities that help define stress and strain tensors and the response of materials to localized stress applied to its boundary is a fundamental property of any granular material (Socolar, 2003). In the past, continuum theories based on the principles of plasticity and elasticity have been applied to analyse the behaviour of soil in the engineering length scale and as such, extended to a generalized one to include granular structures (Satake et al., 1999). In the application of continuum mechanics, constitutive models need to be determined and are usually the most difficult aspect. The constitutive model used in continuum approaches usually involves a lot of material constants, which sometimes have no clear physical meaning (Duran, 1999). Granular materials are seen as packed assemblies of particles in which interactions between particles occur and the material constants have explicit meanings (Satake et al., 1999). However, the material constants as used in continuum approaches may be implicitly expressed in the geometry of a packed assembly of particles. As a result, the discrete element model approach (DEM) (Cundall and Strack, 1979) becomes a more realistic way in analysing granular materials in which the particle arrangement is modelled explicitly.

The discrete element approaches have their own difficulties in simulating real granular materials and as such when in application, it is certain that idealized assemblies of particles are modelled. Even with the idealized models, the discrete element approaches help to study and analyse the micromechanics of granular materials in a way that cannot be achieved using continuum approaches (Satake et al., 1999). It is however worth noting that the two types of approaches are complementary and have their roles in the modelling and analysis of granular material behaviour. DEM was first developed for rock mass problems by Cundall (1971) and later applied to granular materials by Cundall and Strack (1979). DEM has an algorithm that is based on the finite difference formulation of the equation of motion and usually avoids the process of inversion for stiffness matrices. This type of algorithm helps to handle large number of particles in simulations (Satake et al., 1999).

The application of these modelling techniques helps to provide access to understand the internal behaviour of the particulate assemblies. This can be analysed characteristically in many ways with

major and increasing attention on flowability and shear deformations behaviour (Moreno-Atanasio et al., 2004). When shear is applied in granular media, generally, there is distribution of forces through a network of contacts known as force chains (Antony, 2007) which is dependent on the interparticle contacts as a response to the shear. Force chains in granular materials have been studied by scientists extensively (Liu et al., 1995, Mueth et al., 1998). A load transmitted by a relatively rigid stressed chain of particles is exhibited by the particulate system and thus forms a sparse network of contacts known as ‘strong contacts’. The strong force chains are then separated by the remaining particles which are slightly loaded and known as ‘weak contacts’ (Antony, 2007). Granular materials also exhibit instability inherently in relation to flow performance. An example of this instability can be such as, when a sudden cessation occurs during the free flow of granular materials which can be initiated by the formation of a bridge (arch formation), by adhesion to the surface of the medium or by any other means due to the various discrete particle properties or environmental factors. Thus, to be able to predict the flow performance of granular materials, there is need to have knowledge of the handling and processing conditions (as applied under different gravity conditions), as well as the characteristics of flow of the materials under earth and low gravity conditions.



Fig. 1. 1 Example of ExoMars surface layers of typical low gravity terrestrial planets (e.g. mars and moon)

This can be achieved by understanding how granular materials are affected by various discrete particle properties as well as the processing characteristics of the flow handling device. In industries, to allow processing of materials, storage is required. Containers are often cylindrical, and can range in size from capacities measured in grams to thousands of tonnes (Nedderman,

1992). One practical problem involved in designing the storage and handling device of particulate materials is the attainment of an adequate flow of material and the control of the flow at a desired rate. Hoppers are common devices used in the processing and handling of granular materials. The optimal design and control of hoppers requires essentially accurate prediction of the discharge rate. This accuracy is crucial for various industrial applications. Inherent particle characteristics such as particle size, particle shape, particle size distribution, angularity, particle bed packing all influence the material flow. Being able to predict flow performance of granular materials would enhance many operational advantages such as reducing arch formation and improving product quality.

DEM models have been used to study the flow of granular materials (Wang and Ooi, 2015, Zhou et al., 2013, Clearly, 2004, Xu et al., 2002). DEM is an effective method to study the fundamentals of granular flow at particle or microscopic scale (Zhu et al., 2005). DEM simulations for both cohesive (Nguyen et al., 2014) and non-cohesive (Datta et al., 2008) materials have given many significant insights into the microscopic details at particle-level and also provide information that aids in understanding the complexities surrounding granular materials. As these complexities exist in the handling of granular materials under earth gravity, there are very limited systematic studies under three dimensional conditions and very little and limited information on granular behaviour under low gravities exist which makes granular material more complex under low gravity.

It has been shown statistically by Duran (1999) that the processing of granular materials and its aggregates consumes roughly 10% of all energy produced under earth gravity. Thus, any advanced understanding in the physics and role of granular media within the universe is bound to have a profound impact on the economy.

1.2 Motivation, Research Challenges and Aims of the Thesis

Granular materials have been the subject of several research in engineering over many decades due to their importance in industrial processes. A wide range of process and industries, for example pharmaceutical, nuclear processing, civil, space and mechanical engineering industries engage in dealing with their products in granular particulate forms such as powders and grains. The characteristics and processing behaviour when viewed in smaller scales (such as micro,

nanoscales, etc.) is different and complex. Even when carefully designed using continuum principles, large silos used for storage can completely block as a result of the formation of arches and also in some cases collapse due to unforeseen fluctuations in stress (Claudin and Bouchaud, 1997, Vanel et al., 2000). In terms of flow and shear behaviour, it is important that the effect of single-particle scale properties on their macroscopic behaviour is probed further. As known, many industries rely on transporting and storing granular materials as well as processing them. Yet, the technology for handling and controlling granular materials is poorly developed. An estimate according to Jaeger et al. (1996a) show that 60% of the capacity of most industrial plants is wasted due to problems associated with the transport of these materials which eventually leads to inefficient performance in equipment. This gives the motivation to study and understand the long term challenging issues associated with the flow process of granular materials under earth gravity and as such, any improvement in our understanding of the behaviour of granular materials should have a profound impact on industry.

Furthermore, gravity could play a significant role in governing the processing behaviour of granular materials. This information for three-dimensional granular system is lacking in the literature, but much sought in space engineering applications. This investigation helps to provide an insight and a better understanding of the properties and mechanics of extra-terrestrial exploration with the aid of numerical investigation of how extra-terrestrial geo-materials will respond to loading actions and flow under reduced gravitational fields in the lunar and Martian (Liu et al., 2010) environments. The analysis of the force structures in granular particles at different gravities can be used in the future for addressing problems that are being faced in the lunar or deep space stellar (Liu and Li, 2010).

One of the key challenges in the exploration of the Moon and Mars of the ExoMars laboratory (Fig. 1.2) is the design of its Sample Preparation and Distribution System (SPDS) for the Martian gravity conditions. Of the many sub-stations within the SPDS, the dosing and crushing stations are of vital importance to the design process which has great challenges.

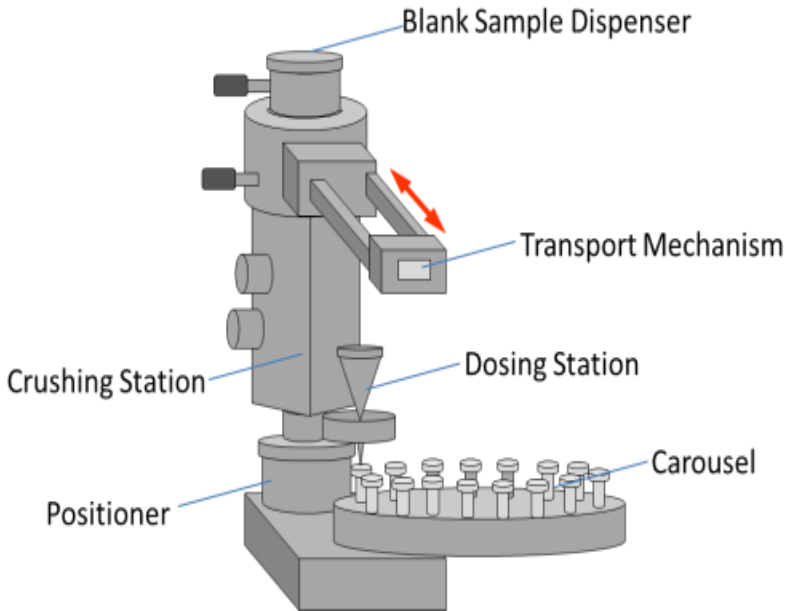


Fig. 1. 2 A typical SPDS station (credit ESA)

Flow properties of granular materials through the components of SPDS is not well understood convincingly but approached and addressed here by understanding the flow and shear behaviour of the geo-materials under lower gravity environments, also in comparison with earth gravity environment.

Also, the anticipated results under earth gravity environment of this investigation would be very useful in the design process within the chemical and particulate process industries as well as in various engineering applications. As a benchmark to the investigation within low gravity environment, a series of parabolic flight tests have been performed studying and analysing the effect of gravity using simulant powders by the space agencies. The continuum and DEM approaches are of advantage due to the complex nature of experiments as well as the low time frame availability of low gravitational conditions in parabolic flight tests. The application of theoretical and DEM approaches can help to understand the flow properties of the geo-materials under low gravity environment. Due to the variation in gravity and different properties within the lunar and Martian regoliths (Fig.1.1), it was suggested that many of the design rules as applied under earth gravity environments may not apply.

The aim of the thesis is to fully investigate the role of particle scale properties on granular flow under different gravity conditions. The thesis is based on the general study of the shear and flow behaviour of granular materials as applied in both earth and space (lower gravity) environments.

With the increase in the process and handling of bulk particulate solid in industries, achieving smooth and reliable flow from the storage devices as a function of gravity is becoming critical and more important than before. The significance of this study is attributed to the challenges faced in spacing industries dealing with particulate materials, for example, the exploration of the Moon and Mars (Chung and Ooi, 2008, Moreno-Atanasio et al., 2004) grounds which requires in-situ resource utilization found in regoliths as well as the ExoMars laboratory.

The research aims of this thesis can then be achieved as summarised:

- Parametric analysis of granular flow using continuum theory with the aid of the Lagrange concept
- Parametric analysis of gravity effect through DEM computational simulation using three-dimensional DEM (PFC^{3D})
- Extensive analysis of flow and shear behaviour of granular materials in a hopper under Earth, Lunar and Martian (EML) regolith conditions.
- Examining ways to improve granular flow characteristics in hoppers under earth, mars and lunar (EML) gravity environments

Here, continuum theory and the discrete element model (DEM) have been developed to help evaluate the flow properties of granular media through a hopper which is one of the most common granular handling devices. The evaluation and analysis is performed under various gravitational fields. Whilst DEM is increasingly being used to model granular materials, careful validation and comparison with other numerical methods and simulations are rare. It is also to be noted that, the added advantage in this project is understanding the microscopic properties in terms of the internal dynamics and particle scale properties. The project also aids in the ability to relate macroscopic flow properties in terms of particle scale behaviour in addition to the case of earth gravity using three-dimensional modelling. As much as possible, key particle scale properties are measured for real soil samples, which are subsequently used in the DEM modelling studies.

1.3 Structure of the Thesis

This thesis is composed of nine chapters in total. The general introduction to the project including the scope and significance is presented in **Chapter 1**. **Chapter 2** gives an introduction to granular materials and their flow properties including information about applications and recent developments. Possible techniques required to analyse granular flow which has been proposed and applied by researchers as well as the techniques adopted are also discussed in this chapter. Furthermore, the concepts of the theoretical and numerical modelling approach used in predicting the influence of particle scale properties on granular flow as well as the concept behind the hopper design are discussed here. Also, gravity effect on granular flow, stress analysis and flow discharge aids are discussed in this chapter. The characterization of experimental key scale properties of selected particle simulants is explained briefly in **Chapter 3** using Atomic Force Microscopy and particle size analyses. The chapter gives an overview of the particle size distribution for different granular samples used in the SPDS station for space research. **Chapter 4** provides the stress and shear deformation predictions of granular materials in funnels using photo-stress analysis and compared with three dimensional DEM simulations. The chapter discusses the stress distribution and contact force network within granular materials. **Chapter 5** is divided into sections to investigate low gravitational granular flow using both theoretical and numerical approaches. A simple theoretical method using the continuum theory is explained initially. It gives an overview of the continuum theory using the discrete layer approach (DLA) and provides information about the developed Lagrangean flow model by adopting DLA. The predictions of the macroscopic flow properties and behaviour of granular materials during flow and sensitivity analysis are shown, which helps to provide an insight into the flow behaviour of granular materials. Further, the theoretical analysis of granular flow (cohesionless) under different gravity environments (g -values) using Kirya's structural model (Kirya, 2009) are presented which directly accounts for g value. Finally, the theoretical results are compared with corresponding DEM simulations. Predictions are carried out for the effects of particle scale properties such as friction and particle sizes on macroscopic flow behaviour. Supporting results from literature and practical flight simulation test are also reported where applicable and available. **Chapter 6** further applies DEM to systematically predict and analyse micro-properties of granular materials (for both cohesion and cohesionless) under earth, mars and Lunar gravity. Investigations are done on the angle of repose,

the cohesive nature of the material, particle-particle friction, particle-wall friction, hopper angle, density, hopper orifice and packing fraction. The results are obtained and analysed using the PFC^{3D} simulations and supported where applicable and available. **Chapter 7** provides result on the vibration effect in hoppers as one of the aids to improve granular discharge. The impact of horizontal vibration on granular flow under the EML gravity levels are presented in detail. Further investigations are carried out on staggering flow against continuous flow of granular materials from the hopper to see its effect on the discharge rate under EML gravity levels. **Chapter 8** briefly discuss the introduction of ice bonding to replicate the lunar regolith and predict its response under compaction under the EML gravity levels. Finally, the wholistic understandings on the micromechanical characterisation of granular materials (including flow properties) are summarised in the conclusion in **Chapter 9**. Furthermore, recommendations, projected applications and future work are suggested. **Appendix A** provides information on the computational method (DEM) used in this research in comparison with other computational methods. Here, there is a detailed discussion on the principles, applications and theory behind the discrete element modelling (DEM) software package, PFC^{3D} (ITASCA, 2004) used. This chapter gives a general background on DEM, concepts of PFC^{3D} simulation codes used and types of contact model used. Also here, examples of work done using PFC^{3D} and its validation are highlighted.

The key methodologies used in this thesis are presented in Fig. 1.3.

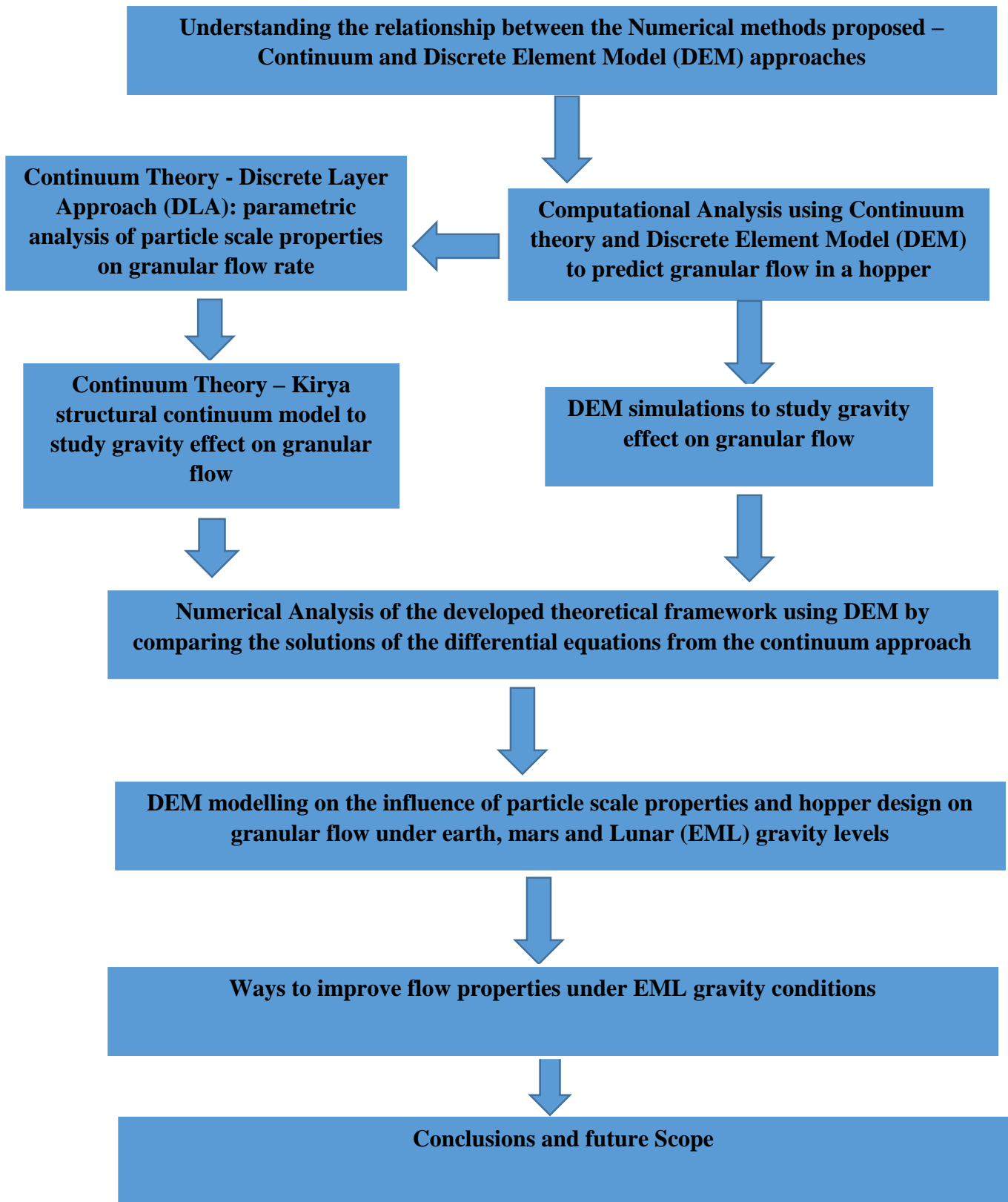


Fig. 1. 3 Scope of thesis

Chapter 2
Granular Materials:
Background and Literature Review

2 Background and Literature Review

2.1 Introduction

This chapter provides brief insight into the background information on granular materials, its applications, recent development into its flow behaviour and properties as reported in literature. Different techniques adopted by other researchers as compared to techniques and approaches used within the scope of this research are discussed under different gravity levels. Literature on numerical modelling to predict the behaviour of granular materials under earth, lunar and mars gravity environments as well as discussions on the impact of various particle-scale properties on granular flow are also presented.

2.2 Granular Materials

Granular materials are known to consist of many individual particles or grains in different densities such as rocks, sand, pebbles, snow and powders. These individual particles or grains are in contact with surrounding particles and voids (Satake et al., 1999) and some regarded as large conglomerations of particles having macroscopic properties, which are quite common in the industry. Despite such seeming simplicity in granular materials, their behaviour is distinctively different from any of the other standard and familiar forms of matter such as solids liquids or gases. Granular matter are considered now as an additional state of matter in its own right (Jaeger et al., 1996b). For example, when granular materials collide or slide past each other, energy is lost due to inelasticity and friction. This energy loss known as dissipation within granular materials is different from ordinary liquids or gases where energy is conserved as a result of collisions between atoms and molecules. The study of granular materials and their related problems have been widely studied and discussed in variety of engineering field e.g. (Chang et al., 1992, Kachanov, 1980, Chang et al., 1997, Matsuoka and Sun, 1995, LI and YU, 2010). These continuous efforts in trying to understand the science of granular materials has a long history and thus resulted in recent development in theoretical, computational and experimental researches. Classical theories such as thermodynamics and statistical mechanics have difficulties in describing granular materials due to dissipation and the irrelevance of temperature (Richard et al., 2005). Many basic products, including a variety of building materials, chemicals, pharmaceuticals, food, etc. are granular and

due to the properties of granular materials, inefficiency occurs in the operations of most processing plants. These inefficiencies sometimes lead to catastrophic failures which in turn result to a collapsing grain vessel. In fact, a study by Merrow (1988) showed that two of the most common problems encountered in processing granular materials occur during the transportation and handling. However, beyond the practical importance of granular materials, scientists and engineers took interest in the science behind granular materials because of their unusual form of matter and interesting properties which are not fully understood yet. Based on the present understanding, the granular materials form a collective system as a result of the collision of the particles and its rubbing together which in turn plays an important role in determining the response of the granular materials.

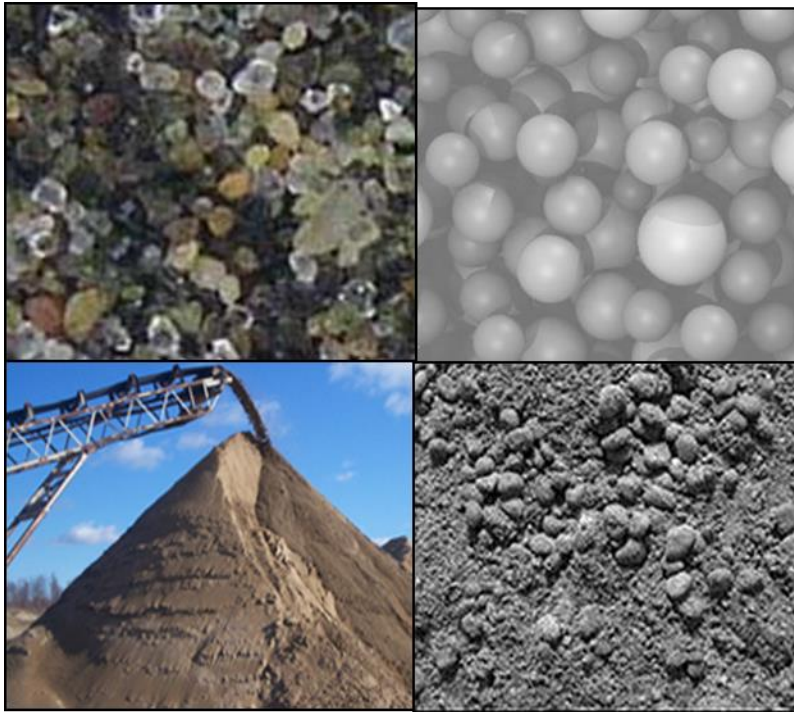


Fig. 2. 1 Typical types of granular materials – Sand particles, Beads, sand pile and grains (Short, 2011)

For example, when considering sand pile as shown in Fig. 2.1, each particle interacts with the surrounding particles, but these short range interactions help to determine the response of the whole pile. Thus, the science of granular materials could be said to be based on a few basic ideas:

- Gravity exerts a downward force on each particle.
- Friction between the particles depends on the size and nature of the particles and also on the medium (if any) between the particles.

- The existence of friction between the particles and the granular storage device.
- Mechanical energy has been lost during the movement of particles and when they bump together.

2.3 Processing Granular Materials

Granular materials are found everywhere in nature and can be said to be the second most-manipulated material in industry (Richard et al., 2005). Over the years, there has been increase in the use of granular materials in various industries such as the pharmaceutical industry, agriculture, energy production, chemical and process industries, mechanical, automotive, powder metallurgy, mining and space industries. Most of these industrial applications require the storage, handling, processing and charging of the granular materials which are often stored in devices such as hoppers, bins or silos. Overtime, granular materials are being studied in different applications such as textile treatment (Srinivasan et al., 2008), mineral processing, food processing, pharmaceutical manufacture (Shah et al., 2008), and space exploration (Brucks et al., 2008). Agricultural industries are known to store, process and transport grains, powders and pills. The basic technologies involved in the processing of granular materials such as wheat, cocoa, corn, powdered milk have lacked major improvements in the agriculture industry due to the outstanding problems concerning the processing, transport and storage of granular materials (Duran et al., 2012). A typical plant in the agriculture industry treats hundreds of thousands of tons of various grains per year and it is not uncommon that the storage/processing device, usually hoppers and silos get damaged due to problems that arise during granular processing. Most of the problems encountered with granular materials of agricultural origin are exclusively of two types – flow blockage caused by arch effect, and granular separation. Aggregates used in civil constructions are generally found in granular form and it is well known that their characteristics depend on the physical properties of the single grains and on the way these grains interact with each other (Thom and Brown, 1988). Mining and construction industries rely on the extraction, transportation and handling of rocks, gravels and sand. The variety of granular materials handled especially in bulk is almost endless which varies from dust to rocks, in temperature from deep-frozen to near-molten and in value from refuse to gold.

2.4 Properties of Granular Materials

Granular materials constitute a number of distinct macroscopic physical and mechanical properties in nature and these properties are important in designing or selecting equipment for its handling or storage (Antony et al., 2004). Several examples exist in the industry of problems and process failure which is attributed to the insufficient attention paid to the properties of granular materials used (Woodcock and Mason, 2013, Jaeger and Nagel, 1992). For understanding the behaviour of granular materials, their characterization can be analysed by means of the descriptive features of the behaviour of the material in its bulk form such as the way it compacts, its flow properties and also by means of the constituent particle feature e.g. size, density, porosity etc. The properties considered and analysed are the physical and mechanical properties at single-grain scale and they are summarised below.

2.4.1 Particle size

The size of a particle is a very important physical property to be considered when handling granular materials in most industrial applications. The influence of particle size on other particulate material property is high which evaluates and control the quality and performance of the granular materials (Fu et al., 2008, Horiba, 2014). In addition to controlling the product quality within the industry, a better understanding of the effect of particle size on granular behaviour and process will help to improve product performance (Hu et al., 2009), improve yield or output (Menardo et al., 2012), and optimize efficiency of the process (Plumpton, 2013). During granular flow or mixing, particulate materials with similar and narrow distributions are less prone to segregation (Sommier et al., 2001) and this makes the effect of particle size and its distribution common and vital within processing industries. The size of a particle has direct influence on dissolution rate (Sun et al., 2012), delivery efficacy (Eniola-Adefeso and Charoenphol, 2008), appearance (Bernardin, 2009), stability in suspension (Jian et al., 2012), packing density and porosity (Samoilov et al., 1996), flowability and handling (Mullarney and Leyva, 2009, Hart, 2015).

However, Hare et al. (2011) have also shown that particle size can be affected by particle breakage while Gosens et al. (2010) reported that the particle sizes can increase by agglomeration as the materials are processed at different stages.

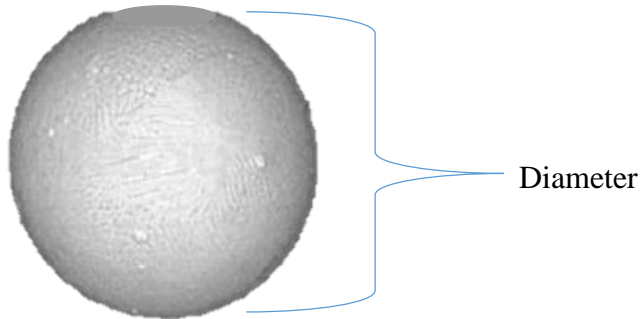


Fig. 2. 2 Spherical particle

Particles are in three dimension and for simplicity, it is convenient to describe the particle and its properties by a single dimension such as radius or diameter (Fig 2.2) using the concept of equivalent spheres (Woodcock and Mason, 1987). Further, a monodispersed spherical particle can be described by a single dimension such as particle diameter (Fig.2.2) while that of a polydispersed particle can be described by an average particle diameter as well as supporting size distribution information to quantify the average value. As such, most studies indicate that spherical particles show good flowability as compared with irregular shaped particles (Barbosa-Cánovas and Juliano, 2005). Controlling the particle size of granular materials influences the appearance properties including gloss and tinctorial strength in the paint and pigment industry (Merkus, 2014); colour and flavour of chocolates within the cocoa production (Minifie, 2012); hydration rate and strength within the cement industry (Bentz et al., 1999); particle behaviour during die filling (Hart, 2015), compaction and sintering; the critical characteristics such as absorption rates (Haleblian, 1975), dissolution, discharge rates, flow behaviour within the pharmaceutical industry, nanotechnology and so many other industries (Horiba, 2014). In general, theory shows that reduction in particle size will lead to decrease in powder flowability (Juliano and Barbosa-Cánovas, 2010) and in contrast, similar particle size may exhibit contrasting flow behaviour due to influence of other granular properties (Kaye et al., 1995). The sizes of particles are measured using methods such as microscopy (DiMemmo et al., 2011), sieving (Dishman, 2006), sedimentation techniques (Gupta, 1959), optical and electrical sensing zone method (Nollet, 2004), laser light scattering techniques (Syvitski, 2007), and surface area measurement techniques (Horiba, 2014).

2.4.2 Packing fraction

In granular flow, packing fraction is the fraction of space filled by the granular materials within the medium representative volume which can satisfactorily characterize a packing with its related parameters such as porosity. Packing density can often alone satisfactorily characterize a packing (Yang et al., 2003). This is generally defined as the ratio between solid volume and total volume and the percentage of the total volume not occupied by the particles is referred to as voidage (ϵ).

$$\epsilon = \frac{\text{volume of voids}}{\text{total volume of particles and voids}} = \frac{V_{voids}}{V_{solids} + V_{voids}} \quad (2.1)$$

Thus, in a bed of material having unit volume, the packing fraction is known as:

$$1 - \epsilon \quad (2.2)$$

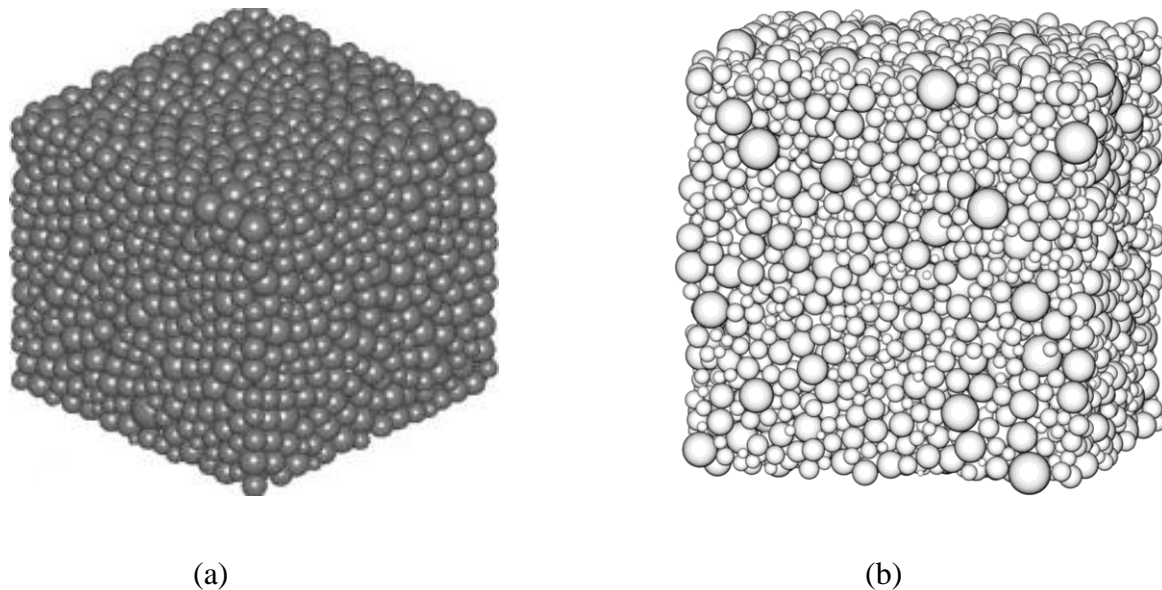


Fig. 2.3 Packing arrangements for (a) monodispersed spheres (b) polydispersed spheres (Baranau and Tallarek, 2014).

2.4.3 Porosity

The term porosity as applied to bulk granular materials could be referred to as voidage, ϵ or void fraction which is a measure of the voids in a granular bed. Porosity can also be defined in terms of

the structure of individual constituent particles as the ratio of the pore volume within a particle to the total volume inclusive of pores (Woodcock and Mason, 1987). The intricate pore structure of porous materials play an essential role in determining their bulk behaviour (Hihinashvili and Blumenfeld, 2011). There are many methods for measuring porosity, a few of which are by direct measurement (Kuila et al., 2014), imbibition method (Joekar Niasar et al., 2009), mercury injection (Johnson, 1998), gas expansion (Washburn and Bunting, 1922), density methods (Mwaikambo and Ansell, 2001) and petrographic methods (Layman, 2004). Most of these methods however require knowledge of the bulk volume of the material.

2.4.4 Density

With relevance to granular material handling, density, ρ can be categorized into bulk density ρ_b and particle density ρ_p . The bulk density relates to the overall material and defined as the mass of the material within a medium divided by its total volume including voids as seen in equation 2.3 (Woodcock and Mason, 1987).

$$\rho_b = \frac{m_{grains} + m_{voids}}{V_{grains} + V_{voids}} \quad (2.3)$$

Understanding the importance of bulk density of granular materials is essential to help in designing storage vessels, conveying systems or any other medium used in handling granular materials. Relatively, the values of bulk densities are qualified with an indication of the materials concerned since the voidage depends on the packing of the granular materials (Woodcock and Mason, 1987). Bulk density measurements are summarised by Abdullah and Geldart (1999). Generally, the bulk density of a material depends on the particle size (Johanson, 1995, Hollenbach et al., 1983), moisture content (Ganesan et al., 2008) and chemical composition (Rosentrater, 2006). Thus, it could be said that for grains of variable particle sizes, the bulk density will depend on the packing and the extent to which smaller grains are accommodated with the larger ones.

The particle density is thus described for a single particle and defined as the mass of the particle divided by the volume. This implies the average particle density for a bulk material will be defined by the true volume occupied by the particles without the voids (Woodcock and Mason, 2013). Thus, the relationship between the bulk density and the particle density is (Woodcock and Mason, 1987):

$$\rho_p = \frac{\rho_b}{(1-\varepsilon)} \quad (2.4)$$

The arrangement and interlocking of grains are impacted on the mechanical behaviour of the granular assembly as well as its structure. In many recent applications, engineers do not have the tools available to consider the changes in density of granular materials in design methods used (Salot et al., 2009).

2.4.5 Friction

When surfaces come in contact with each other, the interatomic and intermolecular forces existing between the contacting surfaces gives rise to friction. Friction is regarded as the force resistance of the relative motion between contacting surfaces of any solid. Thus,

$$F = \mu N \quad (2.5)$$

where F is the frictional force, μ is the coefficient of friction and N is the normal force.

The coefficient of friction μ is a dimensionless value which describes the force of friction between two contacting bodies and the external force. The types of friction that occur in dry granular materials are known as static friction and dynamic friction. The static friction resists relative motion between non-moving surfaces and can be measured using the centrifugal friction apparatus (Dunkin and Kim, 1996), using the tribometer (Burnfield and Powers, 2006), estimated via the angle of repose (Franklin and Shattuck, 2015), etc. The dynamic friction resists relative motion between moving surfaces that remain in contact and can be measured using the program data acquisition (Redfern et al., 1990), using tribological studies (Sivamani et al., 2003), and estimated via the angle of repose (Franklin and Shattuck, 2015). In a granular media, particles in contact with each other gives rise to particle-particle friction (internal friction) while particles in contact with the boundary or walls give rise to particle-wall friction (wall friction).

2.4.5.1 Wall friction

The friction between particles and the wall of the granular media in a granular assembly is the wall friction. The particle to wall friction exists such that a normal force is required to press the particle against a constraining wall and a shear force is required to cause the material to slide along the surface of the wall. Wall friction is often a dominating factor in the rheology of granular materials

which leads to rat-holing and erratic flow especially with cohesive materials (Onwulata, 2005). Schulze (2008) and Iqbal and Fitzpatrick (2006) have analysed the fundamentals of wall friction. Wall friction is affected by particle size and shape and its effect on process parameters depends on so many factors such as surface roughness, surface material, surface wear and corrosion (Kulkarni et al., 2010). In contrast, Iqbal and Fitzpatrick (2006) reported that particle size has no significant effect on wall friction which indicates that there may be a size range that can account for the effect on wall friction. The flowability of materials is also reported by Iqbal and Fitzpatrick (2006) to decrease with increasing wall friction angle by carrying out the studies at relatively high particle size ranges $> 100\mu\text{m}$.

2.4.5.2 Internal friction

This is the friction caused when solid particles flow against each other. The internal friction is very important in the design, handling and storage of materials. In a granular media, when the internal friction between the particles increases, the direction alignment of strong contacts becomes highly anisotropic (Antony, 2007). The internal angle of friction has been reported to influence the packing density with no direct link between the internal friction and the packing structure of the material (Kojima and Elliott, 2012). This can be measured using cubical triaxial tester and controlled shear test (Kandala and Puri, 2000, Schellart, 2000).

2.4.6 Cohesion and adhesion

In a granular media, attractive forces exist between constituent particles and these forces are known as cohesive forces. Cohesion influences the flowability (Zhu et al., 2013b) and at a low attraction force under a gravitational field, the rate of flow tends to be high while higher interparticle attractive forces will exhibit low flow rate and often no flow (Moreno-Atanasio et al., 2004). Thus, the cohesive forces that exists within granular materials help to predominantly determine their flowability. The cohesive nature of particles has been shown to be an attribute to flowability issues due to the liquid bridge formation as well as the interlocking forces such as friction (Schulze, 2008).

Within a granular media such as hoppers and chutes, adhesion describes the ability of particles to stick to the walls or surfaces of the containing media (Woodcock and Mason, 1987). The particle adhesion is mainly caused by surface forces such as van der Waals, electrostatic (Krupp, 1967),

liquid bridges or capillary forces (Butt and Kappl, 2009). Adhesion models exist which are applicable under different adhesion limits. The JKR model (Johnson et al., 1971) assumes that short range forces exist within the contact area. It has been shown by Figueroa et al. (2009), that this model is more appropriate for soft materials with notable deformation due to adhesion while a DMT model (Derjaguin et al., 1975) describes the weaker attraction between stiff materials. Interparticle adhesive forces can be measured with the aid of highly sophisticated techniques such as Atomic Force Microscopy (AFM) (Butt et al., 2005). An AFM helps to get a measure of the adhesive force (pull-off) required to separate particles. AFM operations are generally classified into image formation and others (force spectroscopy and potential mapping). Also, information on force displacement relationship relevant for contact modelling can be obtained using AFM. The accuracy of these microscopic measurements such as AFM has been criticised for its uncertainty due to the idealisation of the particle shape (Tykhoniuk et al., 2007). The mechanism giving rise to adhesion is described in the following section.

2.4.6.1 Van der Waals force

Van der Waals forces are as a result of the intermolecular forces of attraction between molecules and the impact of these forces is seen to be of more significance for smaller size particles as highlighted in Fig. 2.4. Different types of Van der Waals forces exist but the London dispersion force is the most important contributor to Van der Waals forces (Hamaker, 1937). The London dispersion force is an induced dipole interaction created by the electrostatic charge fluctuations. Van der Waals forces are short range which is dominant in dry systems and for stiff particles with smooth surfaces; they can be calculated using Hamaker's (1937) calculation as given in equation 2.6.

$$f_o = \frac{AR}{12s^2} \quad (2.6)$$

Where A is the Hamaker's constant, R is the sphere radius and s is the separation between the particles.

In many practical industrial situations, it is difficult to determine the Hamaker's constant. However, Hamaker proposed a macroscopic approach where A can be expressed as

$$A = \pi^2 C_f \rho_a^2 \quad (2.7)$$

Where C_f is a constant and p_a is the number of atoms per unit volume of contacting bodies which is also a material property.

The JKR model assumed that all short range forces exist within the contact area while the DMT model considers non-contact forces acting outside the contact area. Both of these models are applicable under different adhesion limits and both provide an expression for van der Waals force calculation based on the surface energy (γ) concept as provided in equations 2.8 and 2.9.

$$f_{o_{DMT}} = -2\pi\gamma R \quad (2.8)$$

$$f_{o_{JKR}} = -\frac{3}{2}\pi\gamma R \quad (2.9)$$

According to Figueroa et al. (2009), the JKR model is more applicable to soft and large spheres with soft materials having notable deformation due to adhesion, while the DMT model is more suitable for small and stiff spheres describing the weaker attractions between stiff materials.

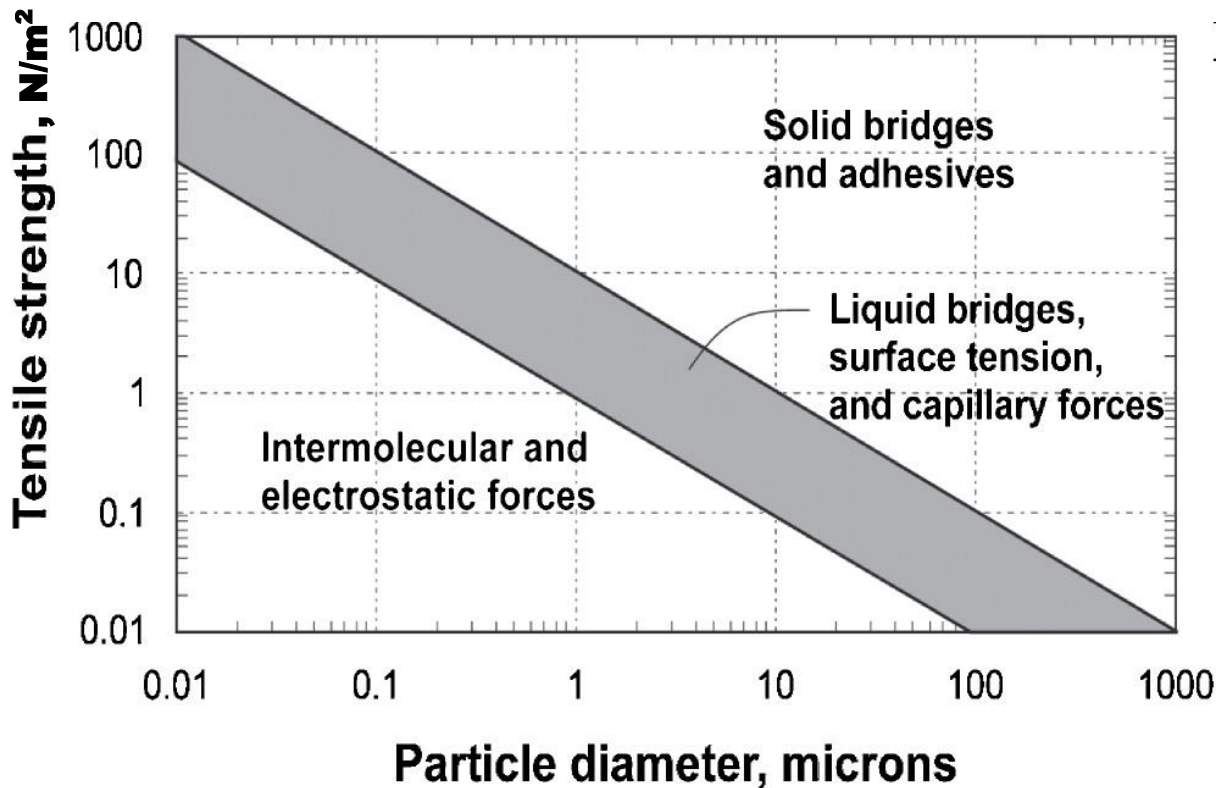


Fig. 2. 4 Inter-particle strength governed by intermolecular, electrostatic and capillary forces (Juliano and Barbosa-Cánovas, 2010)

2.4.6.2 Liquid bridge force

The liquid bridge force arises from capillary interactions found in many situations where particles are partially wetted by low viscosity liquid (Megias-Alguacil and Gauckler, 2009). A stable bridge is formed at points of contacts of the particles which then produce a resultant attractive force between the particles. The attraction forces are as a result of the capillary pressure present and the surface tension of the liquid existing between the particles. Seville et al. (2000) gave an expression for the liquid bridge force as the force which exists between spheres of equal radius arising from the surface tension of the liquid and the difference in capillary force as given in equation 2.10 while for liquid bridge that exist between non equal spheres (Chen et al., 2011) is given in equation 2.11:

$$F_{ls} = 2\pi r\gamma + \Delta p r^2 \pi \quad (2.10)$$

$$F_{ls} = 2\pi R\gamma \quad (2.11)$$

where Δp the pressure difference between atmosphere and liquid bridge, r is the size of the liquid bridge.

A typical example of the liquid bridge formation between two spheres of equal radius is given in Fig. 2.5.

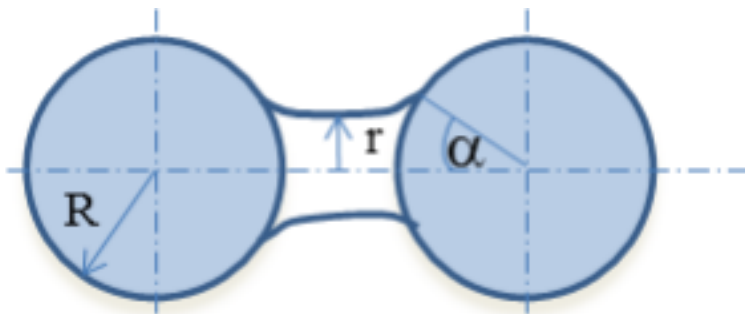


Fig. 2.5 Liquid bridge between two spheres of equal radius

In most cases, the advent of the capillary forces leading to the liquid bridge leads to undesirable events which can affect the tensile strength, agglomeration behaviour and flow properties (Rabinovich et al., 2005, Schubert, 1984).

2.4.6.3 Electrostatic force

The formation of potential difference between particles or triboelectric charging gives rise to electrostatic forces. The triboelectric charging force (F_{tel}) exists between a point charge (Q) and its image charge (Q') and can be expressed via the classic Coulomb's law as given in equation 2.12.

$$F_{tel} = \frac{-QQ'}{4\pi\epsilon_0 l^2} \quad (2.12)$$

where ϵ_0 is the permittivity of free space and l is the distance between the charges. In cases where the electrostatic adhesion is as a result of the potential difference ΔU between particles of different work function, the force of attraction is expressed as given in equation 2.13.

$$F_{vel} = \pi\epsilon_0 \frac{R(\Delta U)^2}{l} \quad (2.13)$$

Electrostatic forces have been reported to be able to profoundly impact flow of granular materials which can be both beneficial and detrimental to industrial operations (LaMarche et al., 2010).

Adhesion may also arise from other forces such as magnetic forces, solid bridge forces and mechanical interlocking. However in granular mechanics, to fully understand the flow properties and behaviour of granular materials, certain conditions relating to the shear behaviour and its response must be met. This means that there is a need to analyse and understand the stress distribution characteristics within the granular materials under the external loading environments.

2.5 Stresses within Granular Material

Stress as indicated is a continuum mechanical concept but for discrete grains, the evident of non-uniformity of stress should be appreciated when measured at the individual grain scale or grain clusters (Kuhn and Antony, 2004). The behaviour of granular materials such as powders, soil or ceramic materials are historically being described by the constitutive laws which are derived from continuum mechanics (Zeuch et al., 2001). In recent times, this behaviour of the materials can be characterized when the materials are considered as a collection of discrete particles and there are increasing number of studies making use of discrete element simulation (Cundall and Strack, 1979). This characteristic behaviour can be shown with the aid of micromechanics approach

(Emeriault and Chang, 1997). Due to the discrete nature of particles, the stress-strain relationship of a granular assembly should be derived with the inter-particle properties put into consideration (Liao et al., 1997). Deresiewicz (1958) and Duffy and Mindlin (1957) have developed the stress-strain relationship for regular packing of equal sized spheres and for random packing of spheres (Bathurst and Rothenburg, 1988, Walton, 1987, Jenkins, 1987b). Within the assembly, particles are bound to rotate and this effect on the stress-strain relationship has also been studied (Chang and Liao, 1989). To a large extent, the kinematic hypothesis used to relate displacement and strain assumes that the strain is uniform in the packing and that every particle that is within the assembly displaces in accordance with the applied strain of the assembly (Liao et al., 1997). The external forces applied are tolerated disproportionately by specific grains which are arranged in irregular and inconsistent networks of force chains (Kruyt and Antony, 2007, Liao et al., 1997). This leads to force being transmitted within the granular materials both at low and high strains and the manner in which the inter-granular forces are distributed. The average stress tensor which can also be known as the Cauchy stress σ_{ij} in a granular assembly can be directly computed as a sum of the dyadic products associated with its M contacts as (Liao et al., 1997):

$$\sigma_{ij} = \frac{1}{V} \sum_{xy \in M} l_i^{xy} f_j^{xy} \quad (2.14)$$

where V is the assembly volume and each product is for a contact xy between particles x and y . The pair x and y is an element in the set M of all contacts. The branch vector l^{xy} connects the centre of mass of a particle x to the centre of mass of particle y ; and f^{xy} is the contact force exerted by particle x on y .

By decomposing the contact force vectors into normal and tangential components,

$$f^{xy} = f^{xy,n} n^{xy} + f^{xy,t} t^{xy} \quad (2.15)$$

$$l^{xy} = l^{xy} n^{xy} \quad (2.16)$$

Equations 2.15 and 2.16 are for spherical particles where the length of branch vector is l^{xy} and thus equation 2.15 can be rewritten as:

$$\sigma_{ij} = \frac{1}{V} \sum_{xy \in M} l^{xy} [f^{xy,n} (n_i^{xy} n_j^{xy}) + f^{xy,t} (n_i^{xy} t_j^{xy})] \quad (2.17)$$

Equation 2.17 is the notation of generic stresses in which n^{xy} is the outward unit normal of particle x at contact xy while, t^{xy} is the unit tangential vector aligned with the tangential component of contact force, $f^{xy,t}$.

Equations 2.14 to 2.17 have been widely used as a basis for development of constitutive law of granular mechanics as reported in the works of Christoffersen et al. (1981) and Walton (1987). The stress and strain tensors as discussed are necessary to formulate some problems in a consistent manner, since the degree of freedom of contact forces and movements at grain level becomes tremendously large for discrete systems.

The manner in which force is been transmitted internally within granular materials have a unique feature. Particles within a granular assembly are under stress, supporting the weight of the material above them in addition to any applied load/boundary. Particulate materials subjected to external boundary loading exhibit stress propagation through inter-particle contacts usually in a non-homogeneous manner through a chain-like network of contacts (Ketterhagen et al., 2009a, Mueth et al., 2000, Kruyt and Antony, 2007, Antony, 2007). The bulk shear strength of particulate materials is a combination of small proportion of force transmitting through the formation of structural entities referred to as strong force chains (Antony, 2007). The transmission of forces is implied to be mostly heterogeneous such that the characteristic length scale of the force chains is generally greater than the mean particle size (Radjai et al., 1998). These kind of observations have been made from photo-elastic studies of birefringent grains (Howell et al., 1999, Antony and Chapman, 2010, Antony et al., 2015b), computer simulations using DEM (Cundall and Strack, 1979) and combined FEM-DEM (Munjiza, 2004). In application to granular materials, photo-elastic studies were mostly reported under two dimensional conditions (Antony et al., 2015a, Kruyt and Antony, 2007) while the DEM simulations accounted for both two dimensional and three dimensional conditions (Cundall and Strack, 1979, Zhu et al., 2008, Matuttis et al., 2000). The link between the structural alignment of the force network and bulk mechanical properties of granular systems is quite significant (Quintanilla et al., 2001). The transmission of forces further leads to anisotropic deformation characterized by shear banding and strain localization (Murthy et al., 2012). During the movement of the particles, there is some degree of internal momentum transport due to the motion of individual particle relative to the bulk material. Thus, Force chains and stress distributions are regarded as characteristics of granular materials.

Knowledge of stress distributions within the granular materials contained is essential to allow structural design of the silo and hopper shell and attachments, and to allow estimation of likelihood and location of cohesive arch formation during flow (Ooi et al., 1996, Zhao and Teng, 2004). In most real applications, any slight amount of disorder within the materials due to particle size variation or packing conditions is amplified by the nature of the interparticle friction forces and interaction. This then allow stresses to be transmitted along the force chains within the granular bed through a fraction of particle contact network (Baxter, 1997, Antony, 2007). Force derived from the movement and interaction of particles within the bed is not uniformly distributed due to the discrete nature of the particles with some forces relatively high compared to the remainder within the bed. Kruyt and Antony (2007) have been able to show that the number of contacts having force greater than the average normal force on the strong contacts generally accounts for less than 20% of the total contacts. The strong contacts predominantly orientate themselves towards the direction of greatest resistance to flow known as the major principal stress (Radjai et al., 1998). The weak contacts which constitute forces lower than the average contact force are largely orientated along the major principal stress and provide the substantial majority of the total number of sliding contacts within the particle media (Radjai et al., 1998, Antony, 2007). As many of the weak contacts slide, while the strong contacts rarely slide, changes in friction are reported to hardly alter the macroscopic properties of the granular bed. This indicates that the stresses on the weak contacts are almost unchanged by inter-particle friction (Antony and Kruyt, 2009). The manner in which forces are distributed within the granular bed depends on the location of the contacts within the bed. The particle bed structure determines if the force chains are isotropic or anisotropic (Antony et al., 2004, Antony et al., 2005). However, spherical particles tend to have lesser stress ratio than the non-spherical particles as the latter have high resistance to rolling (Kuhn and Antony, 2004).

Understanding the force network further helps to properly analyse the stress and strain measurement within the granular bed. Although the forces within the particulate assembly in the granular bed are highly dependent on the specific orientation and properties of each particle, the macroscopic properties such as the normal and shear stress-strain relationships can be reproduced regardless of the orientation of the bed.

2.6 Contact Force Distribution

The manner in which force is transmitted within granular materials is unique (Antony, 2007). When particles get to collide, they tend to create contacts which determine the distribution of forces within the particulate system (Antony, 2007). The transmission of these forces is through heterogeneous network of chain-like contacts known as ‘force chains’ as shown in Fig 2.6.

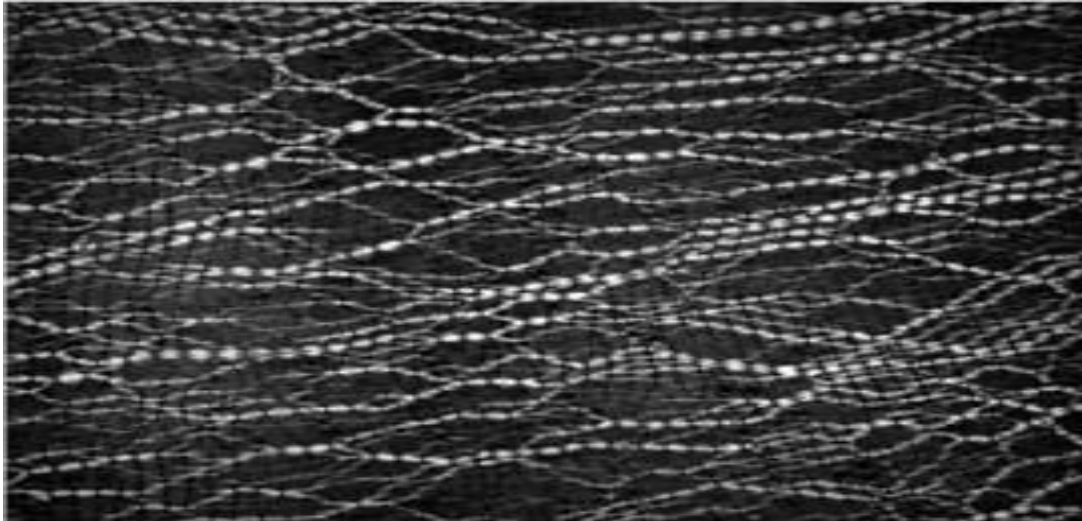


Fig. 2. 6 Contact force networks of granular matter (Majmudar and Behringer, 2005)

In the distribution of both contact forces and contact network, anisotropy is observed in sheared systems. Also within spatial correlations, anisotropy occurs which provides a quantitative replacement for the force chains (Majmudar and Behringer, 2005). Thus, the stress which the material exerts within the granular media is very important. Stress is also exerted on the walls of the storage bin of the granular media along different height as described by Janssen (Schulze, 2006b). The pressure on the walls of the storage media is through shear stress transmission which is an effect of the high contact forces between the granular materials as well as the static friction existing between the particles and the wall boundaries (Schulze, 2007, Jaeger et al., 1996b).

2.7 Granular Flow

Granular matter is involved everywhere in everyday life and impacts many natural and industrial processes with the processes involving granular materials all-prevailing in the industry. Understanding the nature of granular flow primarily helps in the design of virtually any medium

involved in its handling and storage (Woodcock and Mason, 2013). In the understanding of granular flow, there is limited advancement as the behaviour of flow has not been fully ascertained. A vast range of the behaviour exhibited by granular flow has been reported (de-Gennes, 1999, Kadanoff, 1999, Jaeger et al., 1996a). Thus, good analysis of particulate material flow plays a vital role in many industrial processes which includes generic particle flow in and from hoppers, silos, bins and conveyors belts. A granular medium can be termed as a collection of macroscopic particles with size typically greater than $100\mu\text{m}$ and this media means non-Brownian particles which interact solely by friction and collision. However, smaller sizes of particles below $100\mu\text{m}$ tend to behave as powders and when the sizes further fall below $1\mu\text{m}$, they are characterized as colloids (Forterre and Pouliquen, 2006). In the case of granular media, particles are too large to experience what is known as Brownian motion and thus, the statistical average over different configuration may not be possible. The interactions between the particles within the granular media play a very important role in determining the flow properties and as such granular flow is established when these interactions dominate the mechanics in which the flow pattern can be quite different from those of conventional fluids. A thorough understanding of the flow properties of the granular materials is yet to be established as against the apparently similar fields of fluid and soil mechanics and as a result the lack of understanding leads to failure (Fig. 2.7) or inefficiency of the storage or flow medium. Two categories among the variety of granular materials should be considered separately i.e. cohesive and non-cohesive granular materials and it has been shown that the cohesive forces affect the static, quasistatic and flow properties of powders (Lumay et al., 2009).

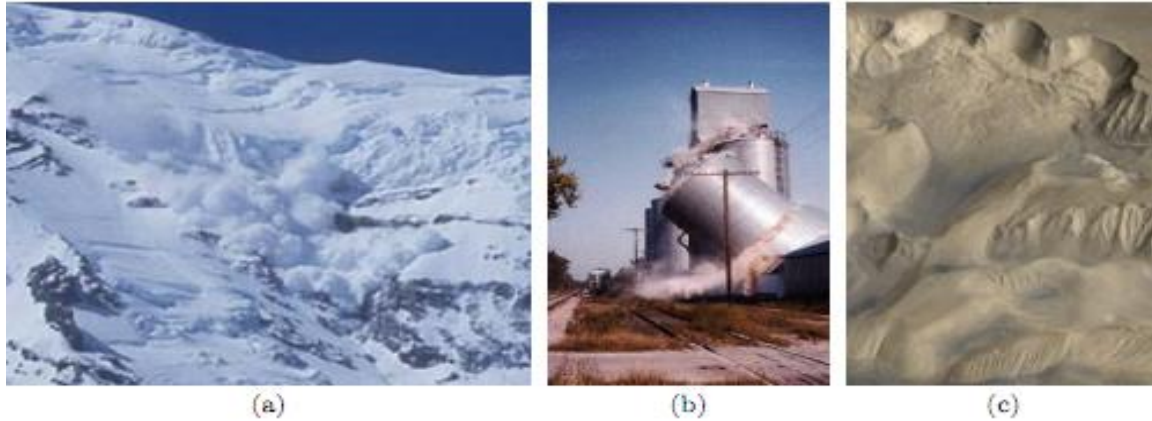


Fig. 2. 7 Application of granular flows: (a) An avalanche on the Liberty Wall Range, USA; (b) The buckling of a grain silo; (c) Eroded cliff faces in the Valles marinerie canyon on Mars (Cawthorn, 2008)

In order to describe the different flow regime of a granular media, different frameworks have been developed by researchers such as Forterre and Pouliquen (2006) who investigated the use of plasticity theories to describe the dense quasi-static regime where the deformations are very slow and particle interaction by frictional contacts exist. Within the domain of granular flow, though, the summation of a number of different effects may determine the flowability of grains, large transient structures known as force chains occurring from the distribution of attractive forces between constituent particles through heterogeneous network of chain-like contacts dominate the rheology and these force chains are known to be quasi-linear sequence of particles with large normal forces at their contacts (Antony, 2007). Thus, at low force of attraction, the granular materials can easily flow under the influence of gravity. Granular flow is studied in different configurations where a simple shear can be achieved as well as the measurement rheological properties as shown in Fig. 2.8. These geometries are divided into two families: confined and free surface flows.

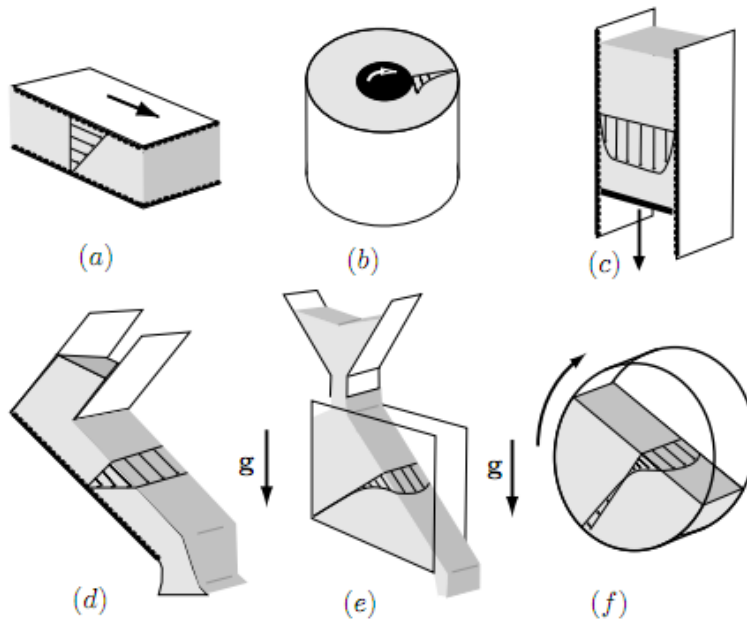


Fig. 2.8 Different configurations to study granular flows; (a) Plane shear (b) annular shear (c) vertical silo (d) Inclined plane (e) heap flow (f) rotating drum (Forterre and Pouliquen, 2006)

Fig. 2.8 are examples of confined flows where Fig. 2.8a represents the plane shear geometry in which shear is applied as a result of the motion of the wall; Fig. 2.8b is such that the material is confined within two cylinders and sheared by the rotation of the inner cylinder and the vertical chute flow configuration; Fig. 2.8c shows the flow of material due to gravity in between the two vertical rough walls. On the other hand, Fig. 2.8d to 2.8f are examples of free surfaces flow with Fig. 2.8d showing the flow of granular material on a rough inclined plane; Fig. 2.8e represents flow at the surface of the pile while Fig. 2.8f shows the flow in a rotating drum. The last three cases (Fig. 2.8d to 2.8f) have its driving force as gravity (Midi, 2004).

Challenges have been associated with problems dealing with granular materials in different regimes of motion during flow. These regimes are distinct and are: static, slowly deforming, and rapidly flowing (Babic et al., 1990). The flow regime encountered in granular flow is such that the volume fraction of the material has a high value which approached the maximum value. The behaviour of granular materials depends strongly on the combination of some non-dimensional parameters and the granular material is said to be in static regime when the non-dimensional strain rate is zero. The well-established Mohr-Coulomb criterion governs the initiation of motion and the past failure motion is initially obtained by particle sliding or rotation over neighbouring particles against friction. Thus, the granular material gradually shifts from the friction-dominant quasi-static

regime to a more agitated, collision dominant rapid flow regime as the non-dimensional strain rate increase (Shen and Babic, 1999). In the quasi-static regime, there is a constant support of the boundary force by the force chains which are within the granular material. Same cannot be said with the transitional regime as the internal force chains are continuously destroyed and regenerated by particles' relative motion due to the decrease in solid concentration (Shen and Babic, 1999). In understanding this concept of granular flow and the theory behind it, different techniques have been adopted over time.

2.8 Stress and Force Distribution in Granular Flow Devices – Silos and Hoppers

The study of hopper flow has been reported to be closely related to understanding the stress distribution in a hopper (Fan and Zhu, 1998). Problems encountered decades ago in relation to the stress distribution calculations in hoppers still remain challenging (Moreea and Nedderman, 1996, McGlinchey, 2005, Drescher, 1992). Understanding stress distribution within granular materials not only helps in predicting reliable flow of materials from hoppers but the knowledge is also required for the mechanical design of the hopper vessel walls (Ooi et al., 1996, Chen et al., 1998, Song, 2004, Zhao and Teng, 2004). Stress distributions within granular materials stored in hoppers have been the subject of research for the past century (Janssen, 1895) and have developed continually over time (Jenike, 1964b, Enstad, 1975, Matchett, 2004, Schulze, 2008). The stress profile that exists in granular packing in a hopper can be compared to the classical theory of Janssen (Landry, 2004) and the stress deviation also related to the Coulomb failure criterion (Kamrin and Bazant, 2007). Jenike (1964b) postulated that the magnitude of stress in the hopper is proportional to the distance from the apex of the hopper and also depends on the angle as represented in Fig. 2.9. The stress is written as:

$$\sigma = \sigma(r, \theta) \quad (2.18)$$

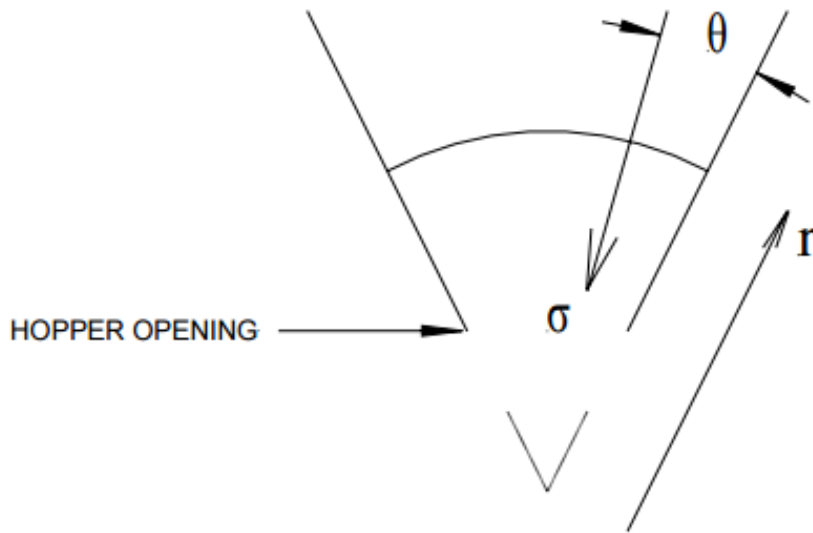


Fig. 2. 9 The stress σ , in the hopper as a function of position (r, θ)

A lack of consideration of the internal stress and force distribution can result in a catastrophic failure in grain hoppers (Carson, 2000). Thus, having a good knowledge of stress distributions within the granular materials contained is critical to the desirable structural design of the hopper as well as to allow for easy estimation of possible location of the cohesive arch formation. In granular media, force is transmitted from one boundary to another through interparticle contacts (Antony, 2007). The contacts distributed will determine the force distribution within the particles and allow changes in the internal structure of the granular media. This force distribution in the hopper is non-uniform and it is reported by Qiu et al. (2014) that the strong force chains are more dominant in the lower part of the hopper and the vicinity of the inclined wall. As reported by Radjai et al. (1997) and Kuhn (2003), the non-uniformity of the contact force can even be said to occur for an isotropic and homogenous assembly of particles which is subjected to homogenous applied boundary loading. The transmission of forces is through the network of force chains correlated over length scales larger than average particle size (Antony, 2007). Geng et al. (2001) and Majmudar et al. (2007) have been able to discuss the important qualitative observation of stress distribution experimentally by studying the optical stress of two-dimensional light-transmitting photoelastic discs (Antony et al., 2015a, Antony et al., 2015b). The experimental studies reveal that load is transmitted by relatively rigid heavily stressed chains of particles forming a relatively sparse network of contacts known as strong contacts while the remaining particles separating the strong force chains have light loads known as weak contacts (Antony, 2007). Recent investigations

by Albaraki et al. (2013) used the photo-stress analysis tomography (PSAT) to probe the distribution of stress and the stress field within assemblies in the hopper. Their study showed that the non-homogenous distribution of shear resistance zone increased with the hopper angle which is further supported with DEM simulations. FEM and DEM simulations are also widely available increasingly on the study of granular materials (Cundall and Strack, 1979, Schmidt and Wu, 1989, Kamath and Puri, 1999, Li et al., 2004, Landry et al., 2004, Mio et al., 2009). Despite its capability, DEM had fallen short of industrial requirements based on the number of particles that can be represented by the computer program (Clearly and Sawley, 2002, Li et al., 2004, Kruggel-Emden et al., 2010). This limitation is however been reviewed with recent improvements (Clearly, 2004, Nasato et al., 2015).

Stress and force distribution in hoppers vary at different stages of granular material processing and according to Jenike (1961) and Jenike (1964b), there exists a passive stress state during hopper discharge and the vertical stress present within the granular solid are an approximate proportion of the diameter of the hopper at any single point. Jenike (1961) assumed this type of relationship to be linear and termed it Radial Stress Field as shown in Fig. 2.10.

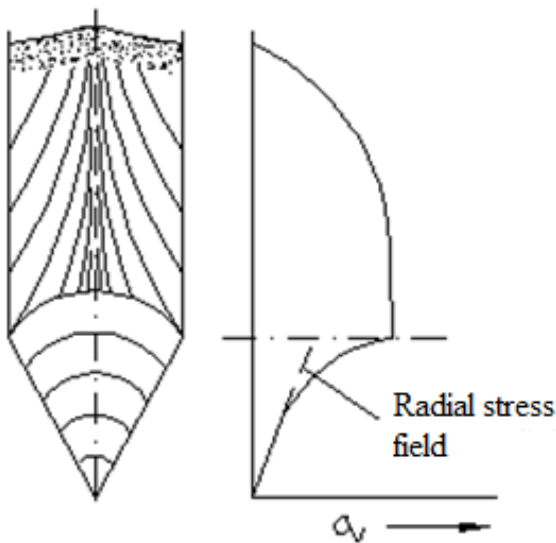


Fig. 2. 10 Radial stress field (Schulze, 2006b)

The radial stress field shows major principal stress distribution after discharge of some material and that the radial stress field is only valid close to the hopper outlet (Pitman, 1986). However, the validity of the radial stress field method has been questioned by Moreea and Nedderman (1996). During hopper filling of granular materials, the stress can be said to be higher as compared to

during discharge (Schulze, 2006b). Understanding the stress profiles and distribution in a hopper can then be considered to determine the critical hopper outlet diameter for arching and this helps to solve one of the major practical problems in hopper design. Most of the experimental methods and models studied are limited to either static packing of the granular materials or results obtained or reported selectively at different loading stages. Antony (2001) reported that force distribution in granular media will depend on the packing condition, shear history and single-particle properties. Most of the studies on stress distribution till date still apply or base their theories with respect to the fundamentals of pioneered assumptions for radial stress, silo wall pressure and velocity fields of granular materials described and corrected by Janssen (1895), Johanson and Jenike (1962) and Walker (1966) as briefly outlined in the next section.

2.8.1 Janssen theory and assumptions

Janssen's theory is so critical to understanding many aspects of granular silos. Janssen (1895) performed experiments on a tall silo and developed theory relating to the silo pressures which is almost universally referenced. A simple interpretation to measure the vertical wall pressure exerted by the granular materials can be expressed as given in equation 2.19.

$$P_v = \frac{\rho^0 g D}{4\mu K g_c} \left(1 - \exp\left(-\frac{4\mu K z}{D}\right) \right) \quad (2.19)$$

Where ρ^0 is the density, g is gravity, D is the height of the silo, μ is the friction coefficient, K is the Janssen's constant, g_c is the gravity constant conversion factor and z is the silo diameter.

The Janssen's constant K is referred to as the ratio of the vertical stress to the horizontal stress on the wall. In a silo e.g. the maximum stresses due to the Janssen equation are proportional to the diameter D of the silo and inversely proportional to the wall friction coefficient μ . It was shown that stresses acting on silo walls can be calculated following the Janssen equation. The prediction of the Janssen's constant however presents a problem as it cannot be derived satisfactorily with the help of known properties such as angle of internal friction (Martínez et al., 2002), angle of wall friction (Jenike et al., 1973) and granular bulk density (Haque, 2013). Modifications were made to Janssen's theory by introducing a distribution factor, D (Walker, 1966, Walters, 1973b, Nedderman, 1992). The value of D was shown to vary and the variation could be neglected in an active case while it is to be considered in the passive state (Nedderman, 1992). The importance of

the distribution factor lies in analysing stress in a conical hopper where passive failure is likely to occur. In general, it was concluded that Janssen's equation is based on multiple assumptions which are not defined satisfactorily yet (Landry et al., 2004, Bratberg et al.).

The Janssen theory helps to describe pressures in a parallel-sided vessel by assuming a constant vertical pressure in a horizontal plane as briefly discussed earlier. This assumption has been shown to be inconsistent (Landry et al., 2004). It was later suggested that the distribution of pressure and stress on single particle will greatly be influenced by the location of the particles along the horizontal axis and the boundary (Jaeger et al., 1996a, Geng et al., 2001, Antony and Chapman, 2010). The corresponding theory for a converging channel came much later, and is normally attributed to Walker (1966), though it was first derived by Dabrowski (1957) and was probably also found by Jenike and others in the late 1950s (Rotter 2009).

2.8.2 Jenike theory

Jenike (1964b) reviewed Janssen's work and extended it to include silos and hoppers. New methods were introduced to address the static and dynamic stress states and further classified the stress states and wall pressure in the hopper section of the silo as active stress state and passive stress state (Jenike and Johanson, 1969, Jenike et al., 1973). The method of characteristics was also first applied to flow of granular materials in a hopper by Jenike (1961) which helps validate the radial stress theory. Jenike assumed that the major principal stress is in direct proportion to the distance from the apex of the hopper. The measurement of the shear stress on the hopper wall considered the balanced weight of the granular materials in the hopper according to the vertical pressure and the angle of friction between the bulk solid and the wall. Jenike and Johanson (1969) then suggested a value for the Janssen's constant K as 0.8 to be applicable to most granular solids in hopper flow. It was also suggested that the radial stress field is only valid within the hopper close to the hopper apex and the stress value tends towards zero as it approaches the hopper apex (Jenike and Johanson, 1969, Jenike et al., 1973, Pitman, 1986, Davidson and Nedderman, 1973).

2.8.3 Walter and Walker's method

Walker (1966) extended Janssen's theory by proposing a differential slice method with vertical sides and calculated the average stresses in a conical hopper. A further extension to the approximate theory of Walker was done by Walters (1973b) by distinguishing between the stresses

developed during the initial filling of the silo and those developed during flow. Also, Walters (1973b) further proposed a more accurate extended differential slice with sides aligned with the hopper wall and calculated the averaged stresses in the conical hopper. Walker gave various assumptions about the distribution of stress components using the Walker's differential slice model (Walker, 1966) and primarily assumed that at any level within the material bed, there is an equal hydrostatic pressure and vertical pressure since there is no shear stress present in the vertical direction. The major difference between the theories of Walter and Walker is the inclusion of the wedge effect in the stress distribution estimation (Schulze, 2006b).

2.8.4 Stress analysis using finite element method and discrete element method simulations

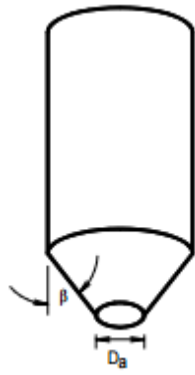
Computer simulations is been employed in estimating stress distributions within granular materials. According to Kamath and Puri (1999), finite element methods (FEM) have been used to model stress distributions over a considerable length of time and was applied to granular materials initially by Haussler and Eibl (1984). Initially, prediction of stress distribution using FEM has been restricted to cohesionless materials but overtime, FEM has been developed by various authors (Kamath and Puri, 1999, Zhao and Teng, 2004, Goodey et al., 2006). FEM models require complex continuum properties to accurately replicate real stress applications and experimental data is not readily available in sufficient quantity to verify FEM methods (Malone and Xu, 2008). It was realised that simple models using hoppers in two-dimension (Kamath and Puri, 1999, Wójcik and Tejchman, 2009, Yang et al., 2011) and more complex three-dimensional shell models to replicate stresses in the hopper walls (Sadowski and Rotter, 2011, Gallego et al., 2011) were used in FEM simulations for stress distributions within granular materials.

The Discrete element method (DEM) on the other hand is widely employed in granular mechanics. It uses individual particles as separate entities in the model (Langston et al., 2004) and has great potentials to help compute stress distributions within granular materials. DEM helps to calculate the trajectories, spins and orientations of all the particles and their interactions with other particles and their environments are modelled (Clearly and Sawley, 2002). A detailed description of the principles of DEM is provided in chapter three.

Generally, recent studies explain the role of single-particle properties (micro and nanoscales) on the stress distribution within the particulate assemblies and the ability to establish anisotropy in the force contact (Antony et al., 2004, Antony and Sarangi, 2006). Thus, in order to have better understanding of the influence of particle-scale properties on the texture of force networks and stress distribution within the hopper, a thorough knowledge of existing principles of hopper design is required.

2.9 Hopper Design

Generally, hoppers are used for storing and discharging granular materials as applied in many industries e.g., granulates in pharmaceutical industry, catalysts and powders in chemical industry, pellets in iron and steel making industry and cement in construction industry. Prior to the 1960's, the design of storage bins were mostly by trial and error but this idea was all changed through the works of Andrew W. Jenike in the 1960s (Jenike, 1961). Jenike developed the theory and applied it in the material flow in storage vessels putting into consideration the equations and measurement of necessary material properties (Jenike, 1961). Generally, hoppers come in variety of shapes and designs such as conical, square opening, chisel, wedge, pyramid, pyramid square opening, cylindrical flat bottomed slot opening and cylindrical flat-bottomed circular opening as shown in Fig. 2.11.



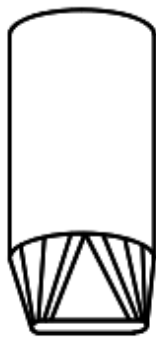
(A) Conical hopper



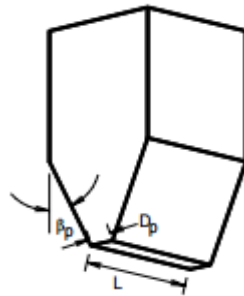
(B) Square opening



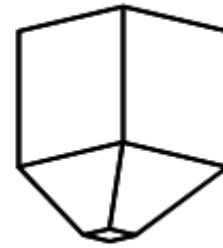
(C) Chisel



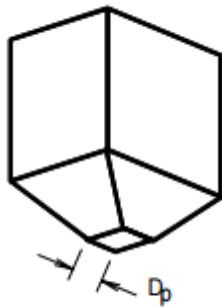
(D) Transition



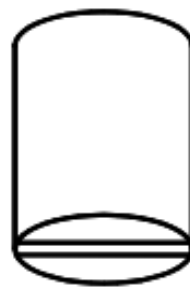
(E) Wedge



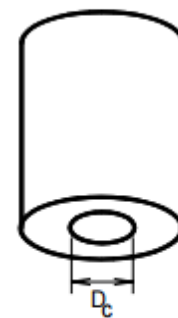
(F) Pyramid



(G) Pyramid, square opening



(H) Cylindrical, flat-bottomed slot opening



(I) Cylindrical, flat-bottomed circular opening

Fig. 2. 6 Schematic of different types of hopper (Woodcock and Mason, 1987)

Analysing the granular flow from an energy approach, Brown (1961) assumed the total kinetic and potential energies will be at a minimum for materials to flow. The design of gravity-flow storage hoppers is also seen to be material dependent and hoppers should be designed or selected to handle

materials based on product specification. Recent research show that simulation is fast becoming commonly used in hopper designs (Li et al., 2004, Kruggel-Emden et al., 2010) with the aid of FEM and DEM. The design of hoppers must be done such that they can be easily loaded and on the other hand easily to unload. The design of the hopper plays a vital role in the processing of particulate materials which includes flow rate of particles out of the hopper, (if it flows at all); how much of the stored materials are discharged; the holding capacity of the hopper and so on. With many free flowing granular materials, the flow and discharge pattern within the hopper is very important among other issues such as flow modes, stress, hopper geometries and hopper design problems.

2.9.1 Flow modes

Flow of particulate materials within the hopper can be categorised into two primary distinct types namely: mass flow and funnel flow (alternatively ‘core flow’ or ‘plug flow’) (Clearly and Sawley, 2002, Ketterhagen et al., 2009b). Flow could exist as a combination of these two flow types which is known as expanded flow. This pattern of flow occurring during the discharge of materials from a hopper has been investigated by so many researchers using different experimental technique, for example using Digital Particle Image Velocimetry, DPIV (Albaraki and Antony, 2014).

2.9.1.1 Mass flow

An important distinguishing characteristic in mass flow is that all materials though not necessarily with the same velocity begin to move in the bin when the outlet is open which includes materials near the walls (Fig. 2.12a). Mass flow is also characterised to usually have low particle to wall friction coefficient and its design aids easy flow of materials through smaller outlets. Generally, the mass flow characteristic in a hopper can be recognised by the steep wall slopes of the converging section, small included angle, and absence of sharp transitions among others (Woodcock and Mason, 1987, Nguyen et al., 1980). Examples of the mass flow hopper geometry design are shown in Fig. 2.11(a-f). Also, the effect of the indefinite storage on the nature of the product helps in determining the mass flow pattern in the hopper (Rhodes, 1998). During the discharge from a hopper exhibiting mass flow, the stress distribution is such that a stable arch does not occur and there will not be any stoppage of flow.

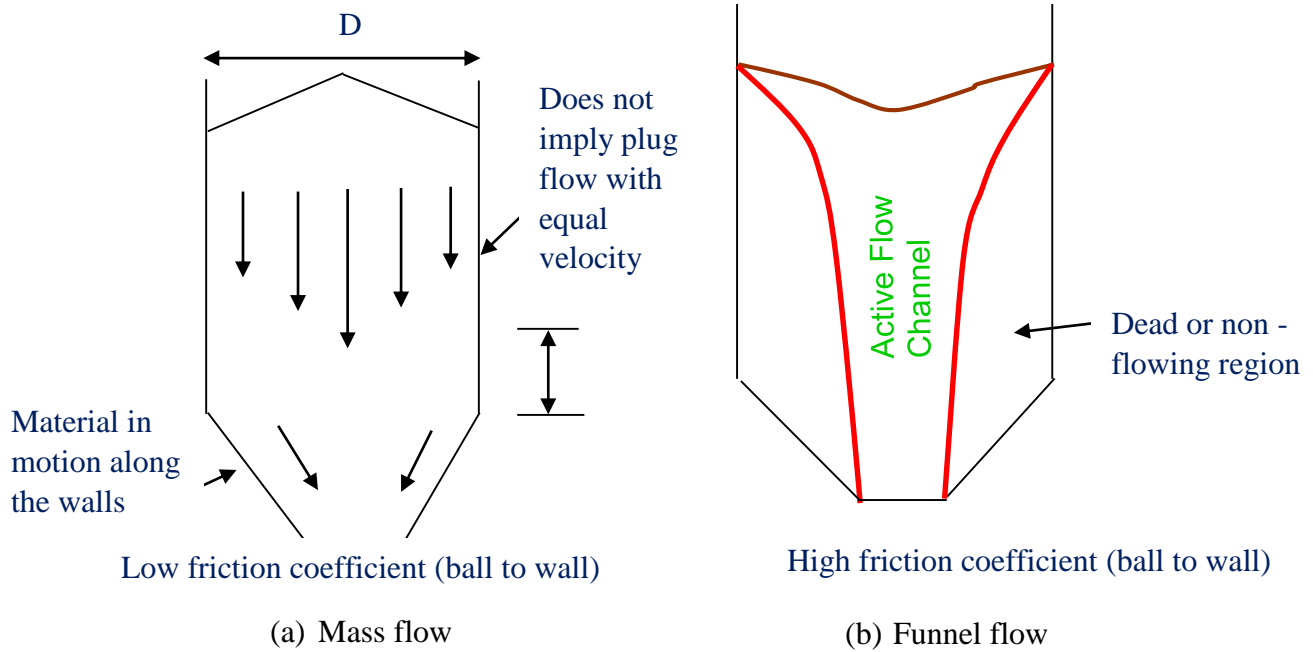


Fig. 2.7 Pattern of flow within a hopper

Generally, mass flow is regarded as the preferred flow pattern and its required slope angle from the vertical axis depends on the particle-particle friction and particle-wall friction (Rhodes, 1998). The advantages and disadvantages of mass flow are given in Table 2.1.

Table 2. 1 Advantages and Disadvantage of mass flow in hoppers (Rhodes, 2008b)

Advantage	Disadvantage
<p>i. Flow is uniform and steady flow can be closely approached irrespective of the head of material in the hopper bin.</p> <p>ii. Flow is more consistent</p> <p>iii. Channeling, hang-ups, flooding and surging are absent</p> <p>iv. Reduced radial segregation</p> <p>v. Pressure is relatively uniform across any horizontal section of the hopper bin</p> <p>vi. Stresses on the wall are more predictable</p> <p>vii. Effective use of full hopper capacity with no dead regions.</p> <p>viii. A first-in = first-out flow pattern can be achieved.</p>	<p>i. Enhanced wear of wall surfaces</p> <p>ii. Higher stress on the walls</p> <p>iii. Requires a lot of head room</p>

2.9.1.2 Funnel flow

Funnel flow is that in which the materials move in a central core with stagnant material near the walls. The materials flow through a channel formed by the materials in the central core of the hopper (Rhodes, 2008a). However, the materials around the near wall region is known as the dead or non-flow region (Fig. 2.12b) in which the discharge is essentially irregular (Woodcock and Mason, 1987). Materials at the bottom lower region in the hopper are stagnant until the hopper is almost empty. Though it is generally known that funnel flow depends on the hopper angle (Klinzing et al., 2013, Maynard, 2013), it was shown by Nguyen et al. (1980) that the existence of funnel flow in a hopper also depends strongly on the hopper geometry. Examples of funnel flow

hopper geometry design are shown in Figs. 2.11(g – i) and Fig 2.12 as funnel flow could also exist in conical hoppers.

Table 2. 2 Advantages and Disadvantage of funnel flow in hoppers

Advantage	Disadvantage
i. Low head room required	i. Ratholing ii. Segregation iii. First in = Last out iv. Time consolidation effects can be severe v. Poor distribution of stresses on walls may cause hopper collapse vi, Flooding vii. Reduction of effective storage capacity

2.9.1.3 Expanded flow

A transition occurs between both flow patterns and usually seen in a composite hopper (Woodcock and Mason, 1987). An expanded flow exist which is a combination of both mass flow in the hopper exit and funnel flow in the bin above the hopper as shown in Fig. 2.13. An added advantage of expanded flow may be in the case of hoppers or bunkers with multiple outlets (Roberts, 1992). The expanded flow is normally used in retrofit situations and it's a useful method to optimise storage capacity while mass flow is still maintained and thus allow for uniform flow at outlet (Woodcock and Mason, 1987).

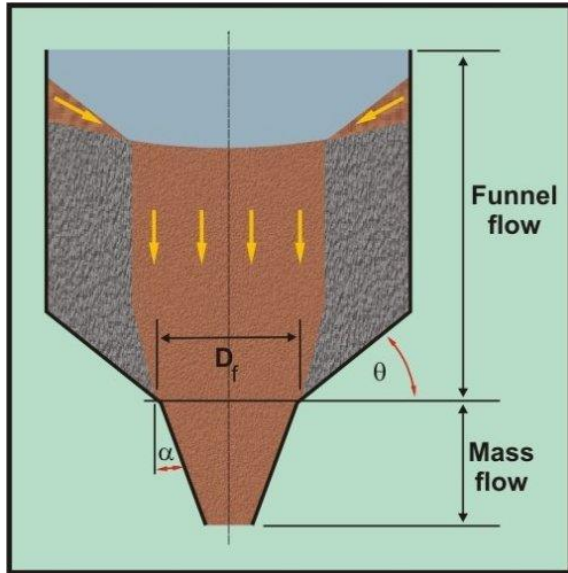


Fig. 2. 8 A basic expanded flow hopper (Roberts, 1992)

Generally, the conditions on the hopper geometry have been studied to classify different flow patterns by Jenike (1964a) in which the stress was balanced at the exit against the strength of materials. The operation of a hopper in any of the flow modes depends on the flow properties of the granular material and its interactions with the hopper walls. Other major aspects to consider in designing a hopper can be categorised into two (Maynard, 2013); measured parameters and calculated parameters. The measured parameters include cohesion, stress, inter-particle friction, wall friction, and compressibility/permeability etc. while the calculated parameters include outlet size, hopper angles, discharge rates, etc.

2.9.2 Hopper geometry

Various factors influence the overall geometry of the hopper such as shape, diameter, width, total height to the upper free surface, hopper angle and hopper outlet size. In addition to these factors, an important factor is also the volume or mass of product required to be stored (Woodcock and Mason, 1987). The volume of the hopper can be estimated conveniently by dividing the hopper into sections as shown in Fig.2.14.

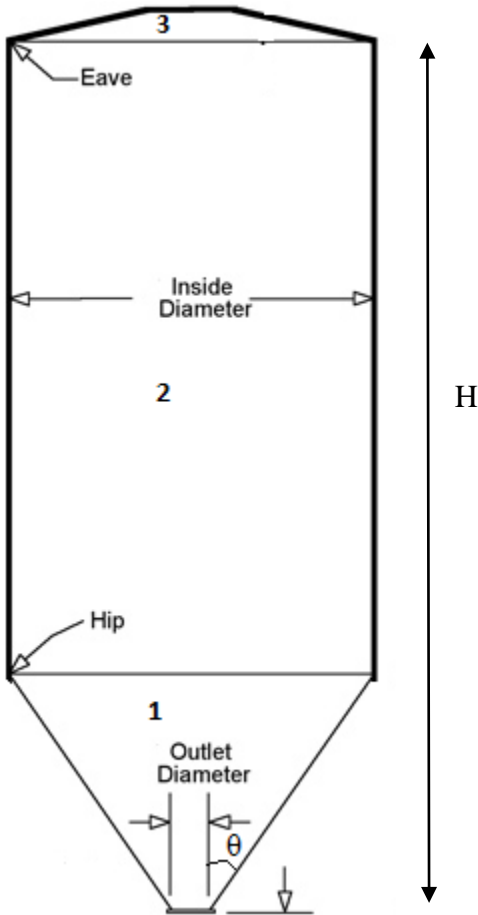


Fig. 2. 9 Effective storage volume of a hopper

As indicated in Fig. 2.14, each section of the hopper will have its own volume and thus, the total volume of the hopper will be the addition of each section volume as

$$V_{\text{total}} = \text{Vol.1} + \text{Vol.2} + \text{Vol.3} \quad (2.20)$$

Generally, hoppers are designed to have a height H between one and four times the diameter D i.e.

$$D < H < 4D \quad (2.21)$$

An understanding of Jenike's philosophy to determine the geometry inter-related parameters is necessary and very important to determine the outlet size and cone angle (Jenike, 1964a). The magnitude of the hopper outlet also helps to determine the flow pattern as well as the discharge rate of the grains where Nedderman (1992) showed that the flow rate is independent of the diameter of the hopper, D as long as:

$$D > 2.5D_o \quad (2.22)$$

and,

$$D > D_o + 30d_p \quad (2.23)$$

where D is the hopper diameter, D_o is the outlet size and d_p is the average particle diameter.

The hopper angle, θ is the angle of the converging section in the hopper as shown in Fig. 2.14. The hopper angle has been studied and shown to have impact on: flow pattern (Nguyen et al., 1980); complete drainage from the hopper which was deduced to be the critical drainage angle (Kalsoum and Resnick, 1985); granular flow by probing the spatial and temporal distribution of the velocity fields (Albaraki and Antony, 2014).

2.9.3 Hopper design problems: Current challenges

Hoppers are designed to help in the storage and handling of grains to give reliable gravity discharge. However, many problems still occur during flow which is attributed to the design of the hopper as well as the granular material properties. Problems associated to hopper design can be classified into two types: inadequate discharge of material from the hopper outlet or segregation of material during flow. Examples of the types of problems commonly encountered are:

- Incomplete emptying (Schulze, 2006a): This is as a result of the existence of dead spaces within the bin which prevents the bin from discharging completely.
- Very slow flow (Woodcock and Mason, 2013): Slow flow is usually not desired as it does not allow granular materials to exit the hopper in adequate time required to feed the follow on process.
- No flow (Woodcock and Mason, 1987): Granular materials tend not to flow due to arching or doming that occurs in the hopper. This usually occurs due to the high cohesive nature of the materials which enables the particles to form arch bridges or domes. The bridges and dome holds overburden materials in place and stops granular flow completely. Another type of arch known as mechanical arch (Schulze, 2006a) can also occur as a result of particles interlocking each other at the converging section above the hopper outlet. (Fig. 2.15b).

- Ratholing/Piping: Ratholing or piping is a characteristic of cohesive materials and mostly only occur in hopper exhibiting funnel flow pattern (Woodcock and Mason, 1987). It usually occurs when the materials in the centre of the hopper discharges, forming a hole through the centre of the materials while the materials close to the walls remain stagnant without flowing. (Fig. 2.15a). Schulze and Schwedes (1990) indicated that the risk of ratholing increase with time consolidation.
- Flushing (Woodcock and Mason, 1987): Fairly cohesive materials that do not form a stable dome but strong enough to slow down the discharge rate tend to allow air to penetrate into the packed material and this results to flushing. Due to the air penetration, sluggish particle flows exist and the penetration frees each layer of the material continuously (Fig. 2.15c).
- Segregation: Granular medium with different size and density particles tend to allow for segregation due to vibrations and percolation (Schulze and Schwedes, 1990). This is observed when small particles move through the void space between larger particles.
- Time Consolidation: consolidation in materials within the hopper can lead to considerable increase in strength of the bulk material (Woodcock and Mason, 1987). The increase in the storage time of the materials within the hopper increases the time consolidation effects due to loss of entrained air, settling and re-arrangement of the constituent particles and thus become more tightly packed together (Schulze, 1996).
- Caking: This is a very important effect which causes problems in the handling and storage of granular materials that undergo variations in humidity and temperature. Caking is defined as the process where loose particles interact to form a coherent mass which then leads to flow resistance (Juliano and Barbosa-Cánovas, 2010). The interacting particles undergo a physiochemical bonding due to the changes in humidity. As known that higher stress leads to stronger attractions, it has been shown that compaction stress significantly affect the cake strength of particles and these caking effects has been reported by Griffith (1991).

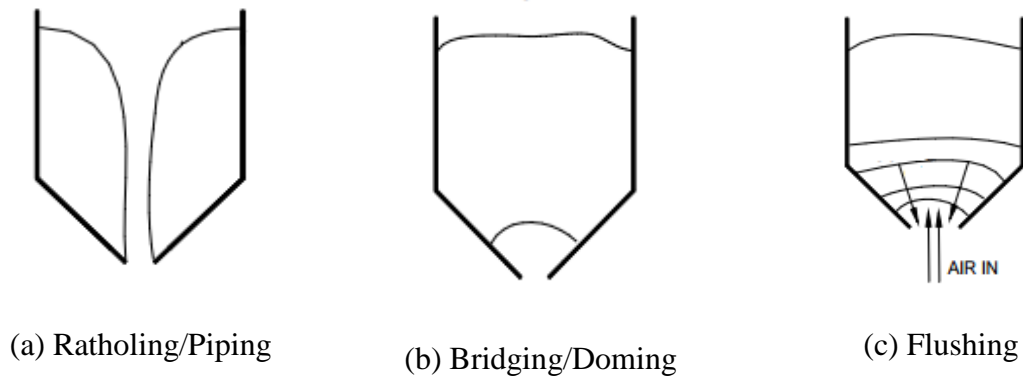


Fig. 2. 10 Common hopper design problems

Currently there is lack of knowledge of stresses and strains in the hopper flow device both in static and dynamic state. Also, the information to analyse all of these design problems under low gravity is lacking. These problems in the hopper design are however literally expected even under low gravity conditions and the effect of material properties are continuously been investigated under variable conditions to give reliable gravity discharge. In addition to the optimal design of the hopper, the particle scale properties and flow properties are required to be understood to have reliable flow.

2.10 Particle Flow in Hopper

Granular flow in a hopper is allowed to discharge freely under the influence of gravity as a common practice. However, failure to understand the fundamental principles of granular solids often results to unsatisfactory performance. Considerable attention over time has been shifted to the problem of granular flow in hopper experimentally, theoretically and numerically. In the early 1960s, the basic principles of plasticity to study bulk solids was applied by Johanson and Jenike (1962) in which the materials were treated as perfect plastic solid according to the Mohr-Coulomb condition. The equilibrium equations involved in the hopper has been solved by Jenike (1964a) (steady gravity) with a radial stress field in which the mean stress in the material was assumed to vary linearly with the radial distance from the top of the hopper. Understanding the behaviour of granular materials flowing in hopper is motivated by the need to determine the bin/hopper geometries and design that allows the free flow of granular materials. It also helps to devise

reasonable methods to help predict the stress that develop on the hopper walls and to characterize scale-up factors for the transport of materials.

2.10.1 Approaches adopted for analysing particle flow

Over the past few decades, granular flow has been investigated using different approaches individually or in combination and these approaches are further categorized under numerical modelling, theoretical model and experimental approach.

Several experimental and theoretical works have based their theory on the basic assumptions introduced (Jenike, 1961, Jenike, 1964b, Johanson and Jenike, 1962) on the velocity fields and radial stress in the flow of granular materials as explained earlier. Examples of experimental approaches include: the application of the particle image velocimetry (PIV) technique for granular flow (Lueptow et al., 2000); Optical flow digital particle image velocimetry (OF-PIV) technique (Quenot et al., 1998), application of DPIV technique to granular flow in two-dimensional hoppers (Albaraki and Antony, 2014, Steingart and Evans, 2005); the shear cell technique (Craig et al., 1986, Yu et al., 1994, Hopkins et al., 1991); Application of the particle tracking velocimetry (PTV) in the study of granular flow (Jian et al., 2002). The photo stress analysis tomography (PSAT) technology has been applied to probe the distribution of stress inside hopper geometries in static filling and their characteristics help to infer some dynamic flow characteristics (Albaraki et al., 2013). Photo-stress analysis tomography (PSAT) is a method mostly applied in shear deformation as well as stress analysis which upon application can be used in component testing, analysis of stress in grains or powder assembly (Antony and Chapman, 2010). The theory behind photonic stress analysis is based on the birefringence of particulate materials. The term birefringence has to do with the ability to divide light passing through into two components. Birefringence only occurs on the application of stress and also at each point; the refractive indices magnitude is directly related to the state of stress at that point (Antony and Chapman, 2010). The maximum shear stress exhibited by the particles under mechanical load or gravity is measured with the aid of a circular polariscope as seen in Fig. 2.16.

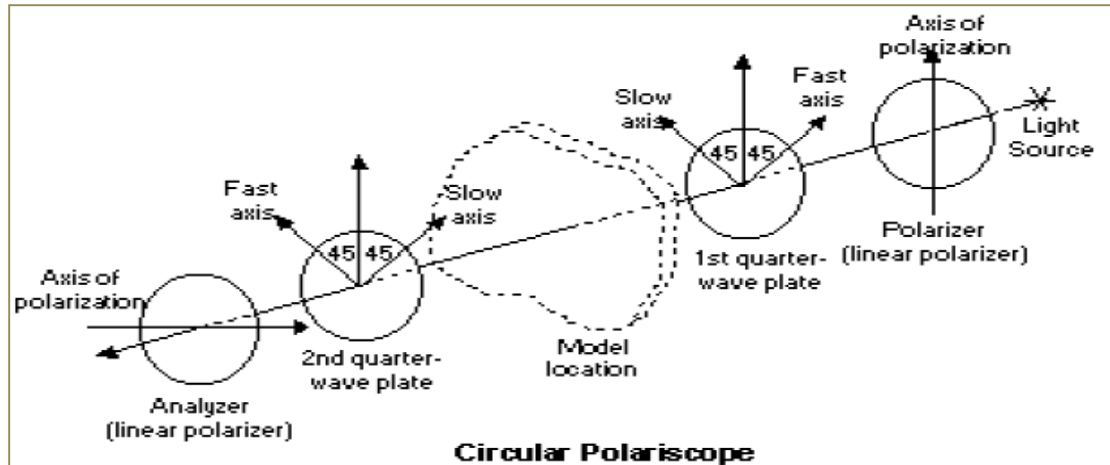


Fig. 2. 11 Illustration of the circular polariscope set-up

This process illustrated allows polarised light to be produced and viewed from the analyser. The birefringent materials allow light to be transmitted through it at a speed which is proportional to the major and minor principal stress components (σ_{11} and σ_{22} respectively). The differences between these stress components are then associated to the fringe orders shown by the material and thus, to the maximum shear stress τ_{max} as well (Antony and Chapman, 2010, Antony et al., 2015b, Antony et al., 2015a). Most of the experimental approaches have their limitations where only flow close to the transparent wall is observed.

Continuum postulates were also developed to help to understand and analyse granular flow and its flow properties and continuum models have been analysed and summarised by Jenkins (1987a). In continuum models, a granular material is assumed as a continuum and granular flow is modelled based on the fundamental principles of continuum mechanics (Hill and Wu, 1991, Wu and Schmidt, 1992).

Several numerical approaches have also been used such as FEM (Wu et al., 2007), molecular dynamics (Zheng and Hill, 1998) and DEM (Clearly and Sawley, 2002, Zhu and Yu, 2004, Langston et al., 1995).

Generally, these approaches can be categorized into two length scales: microscopic and macroscopic. In the microscopic scale which is also known as particle scale, granular materials is a discrete system that have discontinuous physical properties with respect to position and time. However, on the macroscopic scale which is also known as bulk scale, granular material is a continuum system whose physical properties are continuous (Zhu et al., 2005). Thus, based on

these two scales, the continuum theory on a macroscopic scale and DEM on a particle scale are the approaches adopted which is supported with the PSAT technology and experimental flight simulation test in this research which will be discussed further.

2.10.2 Continuum theory

Continuum theory can be said to be a part of mechanics which deals with kinematic analysis as well as the mechanical behaviour of materials which are modelled as a mass continuous rather than as discrete particles. Rycroft et al. (2009b) gave an insight on continuum mechanics and how the properties are averaged over discrete particles in which the application of continuum mechanics depends on fundamental notion of a mesoscopic volume “element”. Modelling materials using continuum theory assumes that the material fills the medium in which it occupies completely and does not take into cognisance the atomic nature which is not so continuous. Several approach of the continuum theory has been applied to construct relevant theories of granular material in its behaviour and performance analysis. However, it has been noted that there is still no general continuum model which can help describe the many phenomena of dense granular flow as seen in parabolic flow (Medina et al., 1998, Nedderman and Tüzün, 1979, Choi et al., 2004); transitioning to plug flow (Rycroft et al., 2006) in a draining silo, wide shear zones (Fenistein et al., 2004) and localised shear bands (Mueth, 2003) in Couette cells, and Bagnold scaling for inclined plane flows (Silbert et al., 2001, Pouliquen, 1999). Although in the hydrodynamics of dilute granular materials and molecular fluids, accurate continuum models have been shown to be systematically derived by averaging over particle collisions in an idealized element (Jenkins and Savage, 1983). The application of continuum theories such as elasticity and plasticity to analyse the behaviour of soil in engineering length scale has been reported by Oka et al. (1999). The Cosserat theories are known to be more advanced theories within the continuum mechanics approach. Other more advanced theories are such as micro-mechanics (Yang and Misra, 2012), micropolar (Zhang-ji, 1987), non-Newtonian models (Sochi, 2010), hypoplastic or hypoelastic models (Tejchman, 2008), viscoelastic (Daniel and Kim, 2002), turbulence models (Hutter and Jöhnk, 2013), etc. In order to represent the stresses that occur within the granular materials, Goodman and Cowin (1971) and Goodman and Cowin (1972) developed a continuum theory which accounts for situations where the stress levels are less than 10psi. Their concept assumes that materials contained in the void is

a gas and have no interaction with the granules and as well the mass distribution is related to the volume distribution of granules. Thus the distributed volume is given as,

$$V_t = \int v dV \quad (2.24)$$

and the distributed mass can be defined as,

$$M = \int \rho_s v dV \quad (2.25)$$

Where the function v is an independent kinematical variable called the volume distribution function which can be defined as

$$0 \leq v(x, t) < 1 \quad (2.26)$$

This volume distribution function v is represented as a continuous function which depend on position and time and within a granular system, v can be said to be either zero (if void) or one (if granule) at any position and time. The distribution density ρ_s can be related to the classical mass density or bulk density, ρ and volume distribution function v as seen in equation 2.27 (Massoudi, 2004).

$$\rho = \rho_s v \quad (2.27)$$

As many material parameters could influence on the behaviour of granular flow, it is difficult to agree on a single constitutive relation that can cover the operation of all the flow regimes of the granular flow. Other material properties can also influence flow behaviour such as size (Antony and Ghadiri, 2006), shape, viscosity on surface roughness (Craig et al., 1987), geometry of the particles, inter-particle friction, etc. (Schulze, 2007).

Continuum model using the discrete layer approach (DLA) which is based on the concept of hybrid Lagrange continuum approach (Antony and Amanbayer, 2011) and the Kirya structural continuum model which accounts for the gravity term (Kirya, 2009) are also reported in the past, which will be applied later in this research study. The continuum based theories help to understand the macroscopic behaviour of the granular material.

2.10.3 Discrete element model (DEM)

The numerous application and complex nature of particulate solids has resulted in the increasing use of numerical methods to simulate bulk material behaviour. The discrete element modelling (DEM) theory can be used to model the movement and interaction of stressed assemblies of rigid spherical particles. The DEM approach allows for the use of complex particle contact physics (Johnson and Hopkins, 2005) and it is particularly adequate for the modelling of granular materials in its non-cohesive or cohesive nature. DEM was first introduced by Cundall (1971) for the analysis of rock-mechanics problems and then later to model how soil particles behave when subjected to dynamic loading conditions (Cundall and Strack, 1979). An in depth understanding and description of the method is as given in a two-part paper by Cundall (1988) and Hart et al. (1988). The dynamics of assemblies of particles and the micromechanical interactions that exist between grains can be explicitly described with the aid of DEM methods. This in-turn helps to provide a means of improving our ability to improve the representation of microstructure as well as complex micromechanical processes (Johnson and Hopkins, 2005). This can be compared in the work of Baker (1998) where FEM including surface contacts was used to simulate uniaxial strain compression of spherical particles aggregate. The macroscale deformation of the aggregate was qualitatively replicated while tracking the evolution in the microstructure responsible for the behaviour of the material. Though the FEM approach could represent the microstructure and grain rearrangement, the important grain scale micromechanical process could not be modelled and this lead to some limitations. This brought to an understanding that DEM is more suitable to represent individual grains and assemblies of grains and also, the micromechanics at grain contact level can be quantified. DEM is particularly useful in processing materials that undergoes large-scale deformation which are discontinuous and depends on the microscale contact process, internal breakage of contact bonds and compaction of broken fragments (Johnson and Hopkins, 2005). During the application process of the DEM approach, the model helps to store the particle shapes, velocities and locations; it helps find the contacts; helps calculate the forces and moments that exist at each contact; helps calculate the conditions at which the contact bonds are formed, the growth and rupture; and as well help calculate the movement of each particle that exist within the aggregates (Cundall and Strack, 1979, Johnson and Hopkins, 2005).

In DEM, when particles interact, they are treated as a dynamic process with equilibrium states developing whenever there is a balance in the internal forces (Cundall and Strack, 1979). In order to find the contact forces and displacements of a stressed assembly of particles, the movement of the individual particles are traced. This movement result from the propagation through the particle system of disturbances caused by specific wall and particle motion as well as other body forces. The propagation speed depends on the physical properties of the discrete system due to the process being dynamic. The numerical behaviour is thus represented numerically by a time-step algorithm in which there is an assumption that the velocities and accelerations are constant within each time-step. The explicit finite method for continuum analysis as used by Bathe and Wilson (1976) is seen to have identical solution scheme to the DEM concept. The FEM helps to break down objects or flows into bunch of small spheres or circles relating to the system as a whole. The DEM concept is based on the idea that a chosen time-step may be small and during a single time-step, the propagation of disturbances is from any particle to its nearest neighbour and the forces acting on a particle are determined exclusively by its interaction with the particles it interacts with. DEM deals with individual particles within the system and provides data according to each individual sphere or circle (Williams et al., 1985). Thus, within a model, DEM regards each particle as its own or as many tiny finite elements while the finite element method can only be regarded to be more of a continuum model (Parker and O'Brien, 2009). In order to be able to simulate the non-linear interaction of larger number of particles without excessive memory requirements in DEM, the use of an explicit rather than an implicit numerical scheme is required (Cundall, 1988). In DEM applications, the calculations performed alternate between the applications of Newton's second law to particles and a force displacement law at the contacts (Cundall and Strack, 1979). The Newton's second law is used to determine the motion of each particle which arises from the contact and body forces while the force-displacement law helps to update the contact forces which arises from the relative motion at each of the contacts. The Newton's equations of motion are used to describe the finite number of discrete interacting particles and related to translational and rotational motions (Zhu et al., 2005).

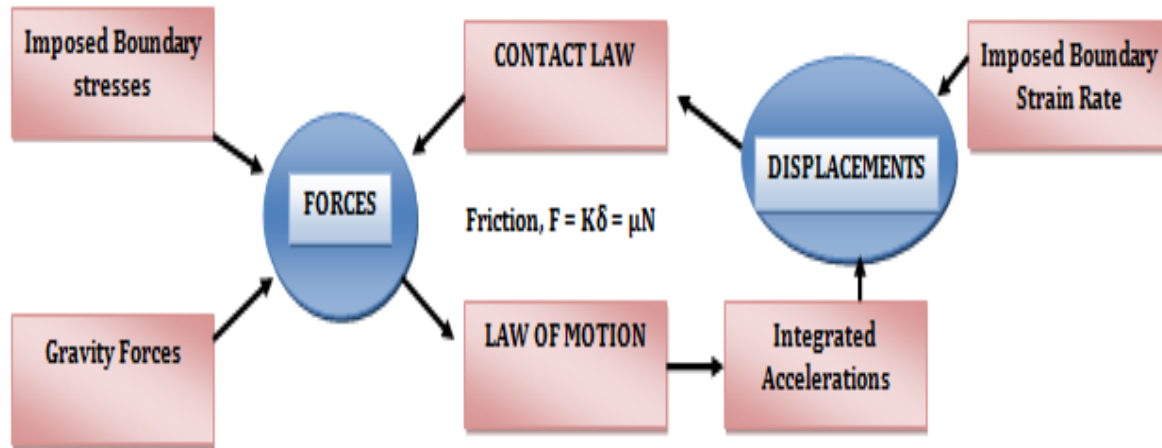


Fig. 2. 12 DEM basic concept – typical calculation cycle

The DEM has been shown to be an effective method to study the fundamentals of granular flow at a particle or microscopic scale (Zhu et al., 2005). Though, macroscopic properties such as stress and velocity can also be obtained using FEM, the approach depends on the constitutive relationship of the materials which ignores the microscopic structural effect of granular flow. This drawback in FEM thus leads to the increased investigations of granular flow using DEM. In order to model a cohesive material using DEM, a local cohesion is introduced for each contact by adding an attractive force. The type of attractive forces could be any of the adhesion forces explained earlier which helps determine the extent of the cohesive nature of the material.

The developments made in the past decade have significantly extended the applicability of DEM methodology to even broader challenges. The application of DEM in the simulation of granular flows shows useful potential in understanding the behaviour of dry granular flows as initially proposed by Cleary and Campbell (1993). Many engineering fields now adopt DEM as an analysis tool in dealing with granular matter, for example, processes in the pharmaceutical industries, agricultural industries, geo-mechanics, aerospace, and more recently in space exploration. DEM is often regarded as soft particle Molecular Dynamics which is very similar to Molecular Dynamics (MD). The principle and approach of both DEM and MD are similar in finding the trajectories of particles obeying the classical mechanics principles of Newton's equation of motion in which the particles are updated gradually in many discrete steps (Plimpton, 1995). MD however is more useful and applicable to study thermodynamic properties of atoms and molecules while DEM is generally applicable to the simulation of greater than micron-scale particle motions under the

prescribed boundary conditions. The size of the simulation often results in a computationally intensive simulation technique but with well-developed algorithms, the computational complexity can be reduced considerably (Arévalo et al., 2007). The discrete particles are treated as a continuum by averaging the physical properties across the particles and the use of DEM to study small-scale engineering problems often aids in validating more large scale models qualitatively. Following the successive applications of DEM, it has often been considered as a standard for comparing the predictions with continuum level theories and other computational models for granular material flows. DEM simulations can therefore be used to determine essentially flow properties of all particles within a granular system. DEM exhibits the following properties:

- Can handle large number of particles
- Short-range forces existing between the particles, though, long range effects can be modelled with more computing power (Antony and Sarangi, 2006).
- Simulation is dominated by the computational time of the forces

The DEM analysis begins with a collection/creation of particles in a designated region or collector and each particle is represented by a sphere or/and geometrically well-defined volume. Though more involved non-spherical particles are also considered in DEM by previous studies (Antony et al., 2005, Hyodo et al., 2006, Zhou et al., 2013). The interaction of the particles is considered as a dynamic process with developing state of equilibrium after the balance of the internal forces. The movement of the individual particles is traced to help determine the contact forces and displacement of the particles under stress. The macroscopic behaviour of the particulate system is captured by calculating the trajectories of each individual particle within the mass and time evolution of the trajectories (Cundall and Strack, 1979). In addition to the current position and velocity of a particle, the physical properties of the particles also help to calculate the current forces acting on the particle. These forces range from friction, gravity, pressure from inter-particle contacts and storage wall contacts to other effects that may be caused by cohesion. This is a dynamic process and the speed at which the forces are propagated depends on the physical properties of the discrete system. The dynamic behaviour is achieved numerically by a time-stepping algorithm which assumes that the velocities and accelerations are constant within each time step. During a time-step, disturbances will only propagate from one particle to its immediate

neighbour and the forces acting on any particle are determined exclusively by its interaction with the particles in which it is in contact with.

DEM methodology is based on the model of Cundall and Strack (1979) and can be summarized below;

- Generation of an initial particulate assembly which results in orienting all particles under imposed boundary conditions
- Assigning boundary strain to the assemblies and subsequent displacement of the individual particles
- Computation of the forces acting on each particle is done from the initial data, the physical laws and contact models
- Simulation which consists of the initialization, the explicit time stepping and post processing of the simulation outcome data

DEM simulations for both cohesive and non-cohesive materials have given many significant insights into the microscopic details at particle-level and also provide information that aid in understanding the complexities surrounding granular materials. As these complexities exist in the handling of granular materials under earth gravity, very little and limited information on granular behaviour under low gravities exist which makes granular material more complex under low gravity.

2.11 Relevance of Flow Properties of Granular Materials under Low Gravity

Investigations of granular flow under low gravitational field help to gain a better understanding of the space exploration activities on planets and other small bodies in the solar system. An interesting feature is to understand how the particles (soil grains) will behave under reduced gravity conditions, for example, the flow or discharge rate, force structures and stress pattern. Various techniques and studies have been intensively developed so far to understand the impact of various material properties on the hopper design and granular flow under earth gravity ($g = 9.8\text{m/s}^2$). However, it is unsure that these predictions will apply under lower gravity conditions as the soil properties, environmental conditions and gravity are completely different. In these type of conditions, numerical methods are useful tools in studying granular flow and its mechanisms under

low gravity environment; thereby providing the basic knowledge to improve the applicability of theoretical models. Studies have been conducted to analyse how particles at micro and nanoscales behave at reduced gravity conditions in different phases such as gas-liquid and gas-solid (Wang et al., 1990). Reduced gravity conditions have also been predicted to play a role in particle dispersions and not just limited to liquids (Liu and Li, 2010). Several experiment works have investigated the effect of gravity on granular materials using different techniques. The effect of gravitational field and atmosphere on the behaviours of granular material has been studied by Johnson et al. (1970). Euler – Euler model (using two phase turbulent models and kinetic theory of granular flow) was used to simulate gas particle dispersions in a downer (Liu and Li, 2010). The behaviour of the particles was predicted under earth (9.81 m/s^2), lunar (1.667 m/s^2) and micro (0.0098 m/s^2) gravities and it was reported that as the gravity reduces, the particle collision decreases and hence the velocity (Liu et al., 2010).

An experiment of granular flow in a rotating drum was conducted by Klein and White (1990) to investigate the effect of gravity on the angle of repose. Hofmeister et al. (2009) also performed a set of reduced gravity measurements to analyse the flow behaviour of granular matter using a quasi-2D hourglass. This was carried out under coarse-vacuum conditions and with a tilting avalanche box. They were able to determine the volume flow through the orifice, the repose and friction angles and the flow behaviour of particles close to the surface. The current studies later focus on the behaviour of granular material using spherical particles in three dimension under varying gravity environment with much interest on the earth, mars and lunar gravity. The experimental result can be used to support and compare some of the modelling studies carried out here in order to correlate the experimentally obtained result with the numerical approach.

The analysis of the effect of cohesion and gravity on the bulk behaviour of powders using Distinct Element Method has been investigated by Moreno-Atanasio et al. (2004). DEM simulation was carried out in analysing polydispersed assembly of glass beads which were initially compressed isotropically in the absence of gravity. It was shown that gravity did not appreciably affect the isotropy of the system.

Chung and Ooi (2008) also studied the influence of gravity on bulk behaviour of granular particulate solid under different loading scenarios such as confined compression, rod penetration into a granular medium and discharging through an orifice. It was then shown that with respect to

the force transmission in the confined compression, gravity had no noticeable effect; for the rod penetration case, the loading gradient was linearly proportional to the gravity; and finally for the flow in the orifice discharge, the mass flow rate was proportional to the square root of the gravity and there was as well an increase in the angle of repose with reduced gravity. This study was done using the three dimensional DEM method. In the present study, the effect of gravity on the flow regime using both the continuum and discrete approach will be used to define the flow properties of the granular media.

In cases of powder movement in common industrial powder processing and transfer operations, gravity has been found to be the primary driving force. This was shown by Walton et al. (2007) using micron-scale pharmaceutical powders in an experimental study with the aid of a centrifuging, rotating drum- avalanche. The gravity levels were varied from $12.5g_0$ to $1200g_0$ with a factor of 100 variations in the gravity level and a clear transition was seen from clumps to avalanche flow and then free flowing as gravity increased. They also studied the effect of particle size on the flow properties and it was concluded that terrestrially, the larger the particle sizes (100 to $200\mu\text{m}$), the less cohesive and free flowing they are and vice versa. A decrease in the particle size leads to an increase in the surface area per unit mass and the effect of surface energy will be significant (Walton, 2004, Maugis and Pollock, 1984). A typical reason responsible for the cohesiveness of powders in the regolith is such that at low particle sizes, higher cohesion exists which is relative to other forces acting on the particle (Walton et al., 2007).

The study of gravity on bulk behaviour of particulate solid was also carried out by Nakashima et al. (2011). A comparative investigation of data collected through experimental and numerical means was carried out which was related to particles through a hopper under low gravity conditions. Two dimensional DEM was used to simulate the angle of repose and it was reported that gravity effects on the angle of repose is negligible. This observation will however be further looked into later in this thesis to be able to compare using the three dimensional DEM simulation for the variation in the angle of repose with gravity.

Parabolic flight test have also been used to investigate the effect of gravity levels on granular flow (Hofmann et al., 2013, Franzen et al., 2008). The stress-strain relationship of granular material at low effective confining stress was investigated by Sture et al. (1998) during a space shuttle using triaxial compression tests in the microgravity environment. These experiments were able to give

some insight in the gravity dependence of surface and volume flows of granular assemblages under reduced gravity levels. It was suggested that over-consolidation and grain interlocking may be effective under microgravity and materials will dilate at high strain levels.

Though several experimental studies have been performed investigating the effect of gravity level on granular flow, limited numerical study exists. Various numerical techniques have been used as reported earlier to investigate granular flow; the discrete element model is increasingly becoming useful in the study of granular flow under microgravity fields. The effects of particle scale properties and geometry on macroscopic flow properties can be obtained under low gravity using three dimensional DEM.

2.12 Characterization of Particle Scale and Flow Properties

The macroscopic behaviour of granular materials are strongly influenced by particle-scale properties (Antony, 2007). So many investigation techniques have been applied to characterize particles and its flow properties at the macroscopic scale. However, the behaviour of the particulate media when viewed at the microscale level and below is extremely complex as compared to the macroscopic level (Jaeger et al., 1996b). Overtime, theories have also emerged (Drescher et al., 1995) which links the macroscale behaviour to the microscale phenomena acting on the particle level. Many methods and devices has been proposed and developed to help determine and characterize flow properties and behaviour of powder and granular materials (Schweddes, 2003). To be able to characterize the flow properties of bulk solids, the flowability of the bulk solid needs to be known. Flowability is the ability of the materials to flow based on its cohesive nature. Flowability testing is required to compare the flowability of each product's requirement of quality control, model processes and validation. Practical ways to measure flow properties include the use of shear testers (Schulze, 2007, Crowe, 2005). Additionally, a number of empirical methods for the flow behaviour indicators have been defined in literature to characterize flowability such as flow function, complete discharge time, compressibility index (Hausner ratio and Carr index) and angle of repose. These are described briefly as follows.

2.12.1 Flow function

Flow function first proposed by Jenike (1964b) is a method employed to characterise powder flowability by considering the ratio of the unconfined yield strength, σ_c , and major principal stress at steady state flow, σ_1 , as expressed in equation 2.28.

$$ff_c = \frac{\sigma_1}{\sigma_c} \quad (2.28)$$

Thus, from equation 2.28, it can be deduced that as the inverse ratio of the unconfined yield strength to the major principal stress reduces, the ff_c increases which implies improved flowability (Table 2.3). Based on Jenike's classification, Table 2.3 gives the flow behaviour classification as a function of the flow function.

Table 2.3 Classification of flow behaviour based on flow function (Jenike, 1964b)

Flow function, $ff_c = \sigma_1/\sigma_c$	Flow Behaviour
$ff_c < 1$	Hardened
$1 < ff_c < 2$	Very Cohesive
$2 < ff_c < 4$	Cohesive
$4 < ff_c < 10$	Easy flowing
$10 < ff_c$	Free flowing

It is however required to note that the flow function is dependent on the major principal stress, σ_1 , and is not considered a material property.

2.12.2 Complete discharge time

The complete discharge time flow test (Kishino, 2001, Clearly and Sawley, 2002) is employed to determine the time required for the granular material to discharge through the hopper. A larger discharge time is related to greater cohesive strength of the material. A number of factors however may affect the flow time of the materials such as particle size, size distribution, shape, density, particle to particle friction, particle to wall friction and permeability of the material (Bell, 2001).

The discharge time test have a few limitations in that the interaction among these parameters are unknown and the test method itself does not consider the solid stress due to self-weight of the material. Though some researchers do not fully agree with the discharge time test as a result of these limitations, the discharge time test is still a good indicator of flow behaviour.

2.12.3 Hausner ratio

The Hausner ratio (HR) is a measure of compressibility index which is the ratio of tapped density to the loose bulk density. It relates to the gain in cohesive strength after the compaction of granular materials and thus can be used to determine the cohesion of a material. The magnitude of the Hausner ratio increases with cohesion as shown in table 2.5. The bulk density of a material changes with the process conditions such as consolidation stress and materials with little gain in bulk density. $HR < 1.25$ is considered to be non-cohesive. The Hausner ratio is limited in its application such that it does not consider the bulk density of the material and a slight change in bulk density can cause a change in the strength of the material. As a result, materials can have same Hausner ratio and still have different flow behaviour due to the difference in their bulk densities. Also, the magnitude of the force required to achieve the tapped density is unknown and on application of external stress, Hausner ratio cannot accurately determine the cohesive strength. Thus, it can be concluded that Hausner ratio is not a fully accurate measure to predict bulk flow behaviour (Sarraguça et al., 2010).

2.12.4 Carr index

The Carr index (CI) is determined from compressibility which can be used as a flow indicator (Carr, 1965). It is a relative measure of inter-particle interactions and can be said to be the ratio of increase in bulk density due to tapping. A scale of material flow using Carr index is presented in Table 2.4. Carr index measurement to characterise flow depends on other factors such as particle size, particle size distribution, shape, adhesion, etc. (Yang et al., 2005) and as a result cannot be regarded as an independent measurement for characterising flow. The Carr index can be expressed as given in equation 2.29.

$$CI(\%) = 100 \frac{(V_0 - V_f)}{V_0} \quad (2.29)$$

Where V_0 represents the untapped volume and V_f represents the tapped volume.

Table 2.4 Scale of flowability for Carr index and Hausner ratio (Abdullah and Geldart, 1999)

Flow Character	Carr Index	Hausner Ratio
Excellent	≤ 10	1.00 – 1.11
Good	11 – 15	1.12 – 1.18
Fair	16 – 20	1.19 – 1.25
Passable	21 – 25	1.26 – 1.34
Poor	26 – 31	1.35 – 1.45
Very Poor	32 – 37	1.46 – 1.59
Extremely Poor	> 38	> 1.60

Though in certain circumstances, Carr index and Hausner ratio can both give quick and rough measure of the cohesion of materials; the measurement techniques have limitations and not widely accepted for not having strong theoretical basis.

2.12.5 Angle of repose

When materials flow out through a medium and fall on a flat horizontal surface, they tend to form a conical pile at an inclined angle to a maximum value without slumping. This value is known as the critical angle of repose (Fig. 2.17) and depends principally on the nature of the materials involved (Woodcock and Mason, 1987). Wouters and Geldart (1996) and Ganesan et al. (2008) indicated that the angle formed between the horizontal plane and the sloped line is known as the angle of repose. There are two types of angle of repose test: static and dynamic angle of repose. For granular materials, the static angle of repose is the internal angle between the surface of the pile and the horizontal surface and this can range between 0° to 90° .

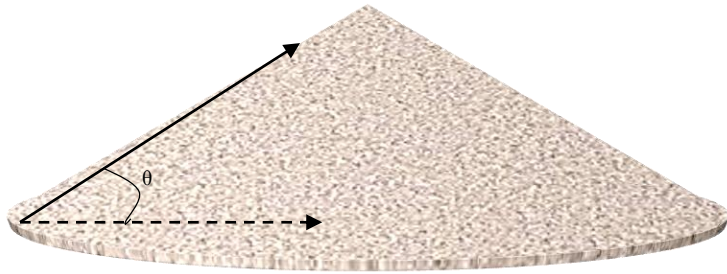


Fig. 2. 17 Angle of repose, θ

The static angle of repose test can be highly influenced by the test conditions such as height of fall during pouring. The dynamic angle of repose is the angle at which the bulk material surface can remain stable in a drum rotating at certain speed (Kleinhans et al., 2011). Theory indicates that the angle of repose of a bulk solid material could be used as crude evidence of its likely behaviour as presented in Table 2.5.

Table 2. 5 Typical angle of repose and flow behaviour (Woodcock and Mason, 1987)

Angle of Repose	Flow Behaviour
25 – 30°	Very free flowing
30 – 38°	Free flowing
38 – 45°	Fair flowing
45 – 55°	Cohesive
> 55°	Very cohesive

Table 2.5 should however only serve as a qualitative guide to the flow properties of granular material. Based on the guide in Table 2.5, many researchers have studied the effect of angle of repose on material flowability (Cain, 2002, Bodhmag, 2006) and also supported that lower angle of repose is as a result of free flowing materials while higher angle of repose is due to the cohesive nature or poor flow of the material. In contrast to the general assumptions (Salisbury and Glaser, 2013, Nakashima et al., 2011) that angle of repose does not depend on gravity, Kleinhans et al. (2011) showed that both static and dynamic angle of repose depend on gravity. Studies have also

described experimentally the angle of repose as a function of hopper angle as well as relating the angle of repose with the critical drainage angle above which the hopper drains completely (Kalsou and Resnick, 1985). The angle of repose is therefore suggested not to be a very robust means of quantifying granular flow as reported in literature (Lindberg et al., 2004, Schulze, 2008, Kulkarni et al., 2010).

2.12.6 Shear test

The aim of a shear test is to measure the yield limit (also known as yield locus) of a consolidated bulk solid (Schulze, 1994). The use of shear testers are supported by well-established physical theory and developed by many researchers to analyse complex bulk system. Shear testers can be classified into direct and indirect shear testers as shown in Fig. 2.18.

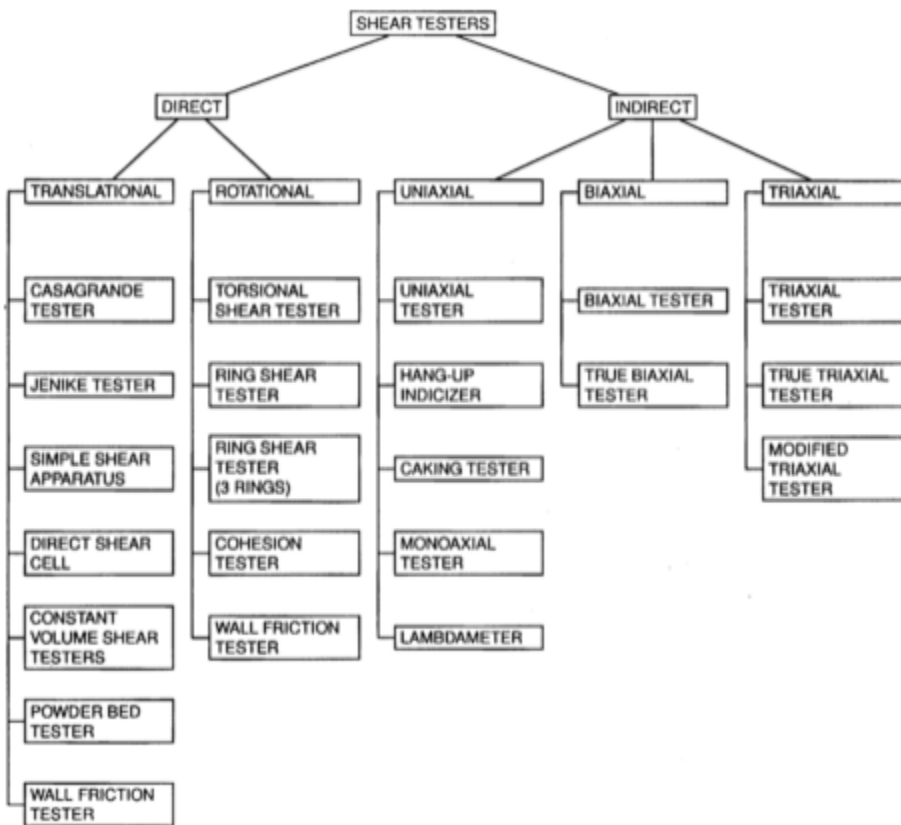


Fig. 2.18 Shear testers (Schwedde, 2003)

In direct shear testers, there is a predefined failure zone which materials are forced to fail through and the direction of principal stress rotates during the test. However, with indirect shear testers, the materials fail along the weakest plane and the direction of the principal stress remains same during the test. Direct shear testers can measure flow properties such wall friction angle, internal and effective friction angle, yield loci and flow function. The most commonly used shear testers are the Jenike shear tester and ring shear tester which will briefly described.

The Jenike shear tester is a translational tester which was the first tester designed for powder technology purposes such as measurement at small stresses (Schulze, 2006a). The Jenike shear tester is based on the principle of plastic failure with Mohr-Coulomb failure criterion and shear is applied by translation motion. Comprehensive details on the operation of the Jenike shear tester can be found as reported by Jenike (1964b), Schwedes (2003) and Schulze (2006a, 2007). Although the Jenike shear tester is more widely accepted, it has some limitations and disadvantages such as: The translation motion limits the amount of shear displacement that can be applied for shearing; Also, during the initial state of shear, it is difficult to maintain a constant powder density and at low consolidation stress, it is difficult to measure flowability; Additionally, the Jenike shear tester is not cost effective for many industries as a large amount of material sample is required.

The limitation caused by the translation motion in the Jenike shear tester was overcome by a torsional shear tester by Peschl (Bell, 2001). The Peschl shear tester rotates the bottom half of the cylindrical specimen against the stationary top half. A disadvantage with this tester is that there is an uneven amount of shear across the radius of the shear cell as particles towards the outside edge of the cell have increased the amount of shear travel as compared to particles at the centre of the cell. This in turn will introduce stress inhomogeneity along the radius of the cell.

The problem of the non-uniformity in the shear displacement in rotational tester can be minimized by introducing an annular ring shape at the shear cell instead of the circular one. This ring shear tester was first developed for bulk handling by Carr and Walker (1968) but too difficult to operate. Similarly, a technically improved ring shear tester was then developed by Schulze (1994). The Schulze ring shear tester (Fig. 2.19) is a better engineering improvement of the Jenike and Peschl shear tester to measure flow properties including wall friction, bulk density and angle of internal friction.

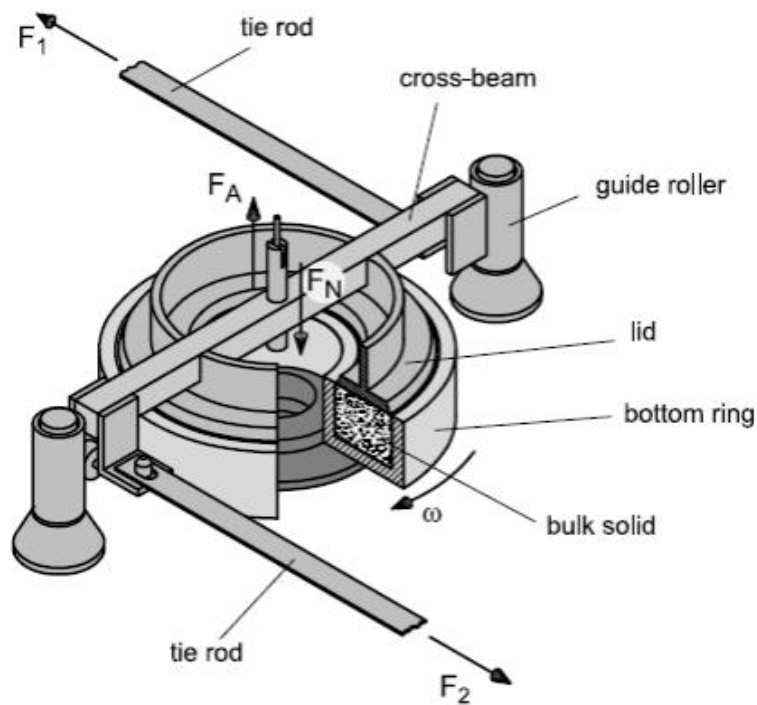


Fig. 2. 19 Schulze ring shear tester (Schulze, 2007)

The Schulze ring shear tester is able to measure the yield locus with smaller normal loads and very useful in designing silos and hoppers. A detailed description on the principle and operation of the Schulze ring shear tester is given by Schulze (2008). The Schulze shear tester is not solely for the design of silos and hoppers but required for quality control, product development and screening purposes. The Schulze ring shear tester has an advantage over the other types of shear testers in terms of its easy usage and time required to perform tests.

The indirect shear testers can also be applied to carefully measure the mechanical behaviour of cohesive materials. The uniaxial, biaxial and triaxial testers are briefly explained.

The uniaxial shear test is used to show the relationship between the major principal stress at steady state, σ_1 , and the unconfined yield strength, σ_c . The uniaxial shear test is a simple technique to evaluate the flowability of bulk materials (Freeman and Fu, 2011, Bell et al., 2007). Three main steps are involved in performing a uniaxial test as given below:

- Confined compression: This is the application of vertical consolidation load over a certain length of time.

- Unloading: The removal of load and confinement is done here in order to observe the failure point of the granular bed.
- Unconfined compression: This is the final step where vertical load is applied until the sample fails. The stress point of failure is known as the unconfined yield strength, σ_c .

This concept related to the stress state and yielding is detailed by Nedderman (1992) and Schwedes (2003). One of the advantages of the uniaxial test is that shorter time requirement for characterising the flowability in terms of unconfined yield strength. The limitation of the uniaxial test however, is that it does not provide critical information regarding bulk flow measures such as wall and internal friction.

In the biaxial tester, both methods of consolidation, either steady state flow or uniaxial compression can be realised. The biaxial shear tester is able to estimate the measurement of both stresses and strains (Schwedes, 2003). The triaxial test is also an indirect shear tester in which all the principal stresses in three dimensions are measured or applied. This tester is the standard shear tester in soil and granular mechanics. The true biaxial and triaxial tester (Thakur et al., 2013, Schwedes, 2003) can be used for a careful measurement of the mechanical behaviour of cohesive materials but not widely used in the industry due to its cost and time consumption.

These shear testers discussed are necessary for material characterization to be able to give information about the materials which may influence granular flow during processing. Details on improving the flow of particles are briefly described in the next section.

2.13 Improving Granular Flow Rate and Discharge Aids of Hoppers

2.13.1 Granular flow rate

The flow rate of granular materials, for example through a conical hopper has been reported to depend on properties of the granules and cone angles under negligible or constant environmental conditions such as temperature and relative humidity (Mazumder et al., 2008). Due to the growing interest in hopper usage in industrial applications, so many studies have been done on the granular flow through an orifice (Nedderman, 1992, Tüzün et al., 1982). When granular materials are discharged by gravity from the hopper, it has been reported that the height of the granular layer does not depend on the flow rate (Mankoc et al., 2007). However, there is contrasting report by

Wilson et al. (2014) that under submerged conditions, the discharge rate depends on the hopper filling height. Thus investigations under a different gravity environment are required to predict how the granular discharge rate will be affected. Nedderman et al. (1982) reported using a first order approximation that the flow rate is independent on the hopper diameter D provided:

$$\begin{cases} D > 2.5D_o \\ D > D_o + 30d_p \end{cases} \quad (2.30)$$

where D is the hopper diameter, D_o is the outlet diameter and d_p is the particle diameter.

The flow rate of particles flowing through the orifice is widely predicted using the law proposed by Beverloo et al. (1961) in the form

$$W = C_{\rho_b} \sqrt{g} (D_o - kd_p)^{5/2} \quad (2.31)$$

where W is the average mass discharge rate through the orifice, ρ_b is the apparent density, C is the empirical discharge coefficient, g is the acceleration due to gravity and k is the empirical shape coefficient. In the study of Beverloo, different materials having different particle properties were used and allowed to flow in different types of orifices. Equation 2.31 can also be expressed as a volume flow rate V as:

$$V = C \sqrt{g} (D_o - kd_p)^{5/2} \quad (2.32)$$

Overtime the concerning issues of equation 2.32 varies between the dependence of the flow rate on 5/2 power of the orifice diameter and the two empirical coefficients (C and k) which is required to be determined for different types of grains and hopper material. Despite the abundance studies of a reasonable good agreement of the granular flow rate achieved with the Beverloo equation in the literature experimentally and numerically, it is still difficult to find works where the flow rate is measured covering several outlet sizes and other discrete properties. Some of the studies cover very big orifices where the k value has little or negligible influence while others cover small orifices without reaching the high D_o values.

Several factors have been reported to impact the granular discharge rate from a hopper under gravity such as the bulk granular properties, hopper design variables and type of flow (Crewdson et al., 1977, Kurz and Rumpf, 1975, Walker, 1966, Suiker and Fleck, 2004). A comprehensive investigation was also made to study the parameters affecting the discharge rate using the DEM

approach (Anand et al., 2008). Using the DEM, several parameters such as hopper fill height, hopper width, particle-particle and particle-wall friction, hopper internal angle, hopper outlet width, particle diameter and several granular material properties can be investigated in three dimension to predict its impact on granular flow rate even under variable gravity conditions (Wang and Ooi, 2015, Franklin and Shattuck, 2015, Xu et al., 2002). During granular flow, there may be need to control or aid the discharge rate from a gravity-flow hopper as a solution to the problem of poor flow. This is usually achieved by incorporating into the design of the hopper some form of discharge aids to help to improve the granular flow.

2.13.2 Discharge aids

Discharge aids are devices that can help to stimulate or improve granular flow out of a hopper. Discharge aids which are also known as flow promoting devices helps to initiate flow when arching and/or ratholing occurs. It also helps to improve flow i.e. by changing the flow pattern between funnel and mass flow or increase the discharge rate (Schulze, 2007). It is very important to select the right discharge aid as this may either provide a satisfactory solution to the poor flow problem or may have negative effects and create more problems. It is noted that discharge aids should not be a substitute to hopper design but only applicable if necessary under which a gravity flow hopper will not naturally be suitable for the nature of product required or other constraints as well as the environmental conditions as well. Discharge aids can be classified into two – Active devices and Passive devices (Woodcock and Mason, 1987). This can further be grouped as seen in Table 2.6.

Table 2.6 Classification of Discharge Aids (Woodcock and Mason, 1987)

Active Devices	Passive Devices
Vibratory	Hopper shape and construction e.g. plane flow hoppers, friction liner, etc.
Pneumatic	Insert systems e.g. cone-in-cone, inverted cone, etc.
Mechanical	

There are quite a few circumstances leading to the use of discharge aids where reliable gravity flow is not feasible such as:

- The poor flow nature of the material requiring larger outlet size than required for the downstream process
- Uncontrolled variability in the flow properties of materials
- Discharge rate from the hopper required for reliable flow is either extremely high or low

Each of these discharge aids have their advantages and drawbacks and emphasis is on the vibrational methods within the scope of this study.

2.13.3 Vibrational methods

The vibration method is used to address flow problems such as arching, bridging, ratholing or incomplete withdrawal of materials which stick on the hopper walls (Jaeger et al., 1996a). The governing principles of the successful application of vibration are poorly understood generally (Bradley, 1998, Mather, 1998). They show result of its mixed conclusions on its impact on flow (Carroll and Colijn, 1975). Despite the limited and mixed effect of vibrations on flowability as reported, vibrations as a means of discharge aid is widely used in industry with many different form of vibrating devices. Granular materials under excitation via vibrated flow can exhibit a wide range of pattern and thus said to be a complex system. The effect of vibration was first studied by Takahashi et al. (1968) and Suzuki et al. (1968) experimentally via the vertical oscillation of the wedge hoppers and flat bottom bins. Prior to the use of vibrational discharge aids, the crude application of impact using the hammer technique was a ‘standby’ processes which caused hammer rash due to indentations on the hopper walls which may in-turn obstruct flow (Matchett, 2004). The vibratory aid could either cause the hopper walls to vibrate (external discharge) or operate directly internally on the stored materials (internal discharge) as shown in Fig. 2.20.

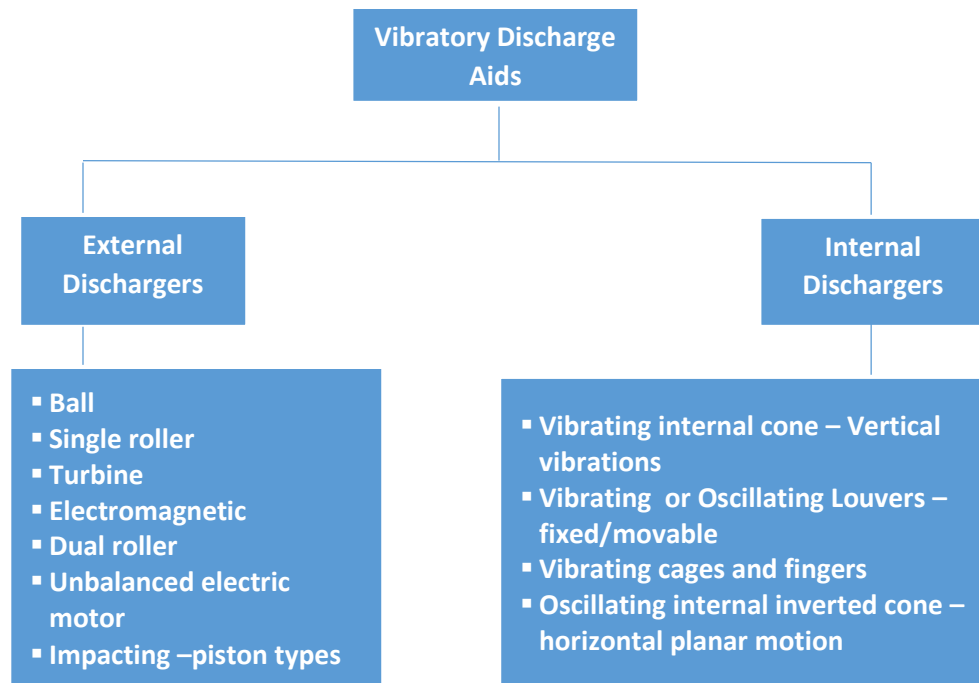


Fig. 2. 13 Classification of vibratory discharge aids (Bates et al., 2007)

Based on application, the external vibratory discharges are employed within the scope of this research to avoid any contact of external devices with the internal granular materials. The external vibratory aids can either be applied as linear or rotary vibrators. The former vibrates the hopper wall perpendicularly while the latter produce components of force both perpendicular and parallel to the hopper wall. The vibratory devices produces resulting forces as functions of their mass, amplitude and frequency (Bates et al., 2007) and depending on their design, the vibrational frequency can generally range from 14 Hz to about 1300 Hz and amplitude from about 0 to more than 60mm (Woodcock and Mason, 1987). However, in specific terms, frequency ranges of 10 Hz to 500 Hz and amplitude 0.25 mm to 12.5mm are used depending on the energy source (Bates et al., 2007). The vibration source is very important and should be placed appropriately to avoid no improvement in flow (Matchett, 2004). The rotary vibrators impart a radial impulse and exert stresses parallel to the hopper wall (Woodcock and Mason, 1987) and by vibrating the wall in vertical and/or horizontal directions help maintain a continuous movement of the material. The rotary vibrators are generally operated at higher frequencies and lower amplitudes than most other types of vibrators and have achieved success in promoting flow of difficult products (Woodcock

and Mason, 2013). Based on the application of the vibrators, it is selected in terms of its frequency and amplitude as shown in Table 2.7.

Table 2.7 Selection of vibrations based on application (Bates et al., 2007)

Vibration Type		Application
Frequency	Amplitude	
Low Frequency (< 30 Hz)	High Amplitude	Coarse or large particles, material sticking to the wall, wet materials and electrostatic problem
Medium to High Frequency (30 Hz to 60 Hz)	Low Amplitude	Compacting materials, fine dry powder discharge, wall friction reduction
Very High Frequency (> 60 Hz)	Low Amplitude	Hopper cleaning, chute flow, de-aeration, fine dry powder discharge

It is apparent that both the vibrational frequency and amplitude are very vital to the impact of the vibrator on the hopper and the enclosed materials. As against the conventional methods, flow can be enhanced through very small hopper outlets and vibration over the whole hopper is more effective than when it is applied to a section of the cone (Matchett, 2004). Generally, flow can be promoted using vibration for systems where reliable flow is impossible by gravity alone provided the selection is right.

2.14 Conclusions

Granular materials are undoubtedly prevalent in the world at macro and micro scales from the macro-scale of construction materials to micro-scale of grains and powders used in industries. In spite of the vast use of granular materials within so many industries, the knowledge of its flow properties is still not well established. Many experimental mathematical model techniques and in recent times FEM and DEM have been employed for analysing granular flow mostly under earth gravity. The flow behaviour has been regarded to be exceedingly complex and not yet well established, however very much needed in the design of operating capabilities in the industry and in recent development such as of space explorers as EXOMARS where gravity effects could

strongly influence granular flow. Experiments as applied under low gravity such as using parabolic flights are expensive, yet low gravity levels are only available for a short duration (~ few seconds). Alternatives such as using: virtual experiments are not yet well studied for low gravitational granular flows; continuum theories which mostly do not account for the inherent discrete nature of the grains but probably less expensive; Discrete element modelling (DEM) which accounts for the discrete nature of the grains, however could be computationally extensive and expensive. Particle scale properties and hopper design have been widely speculated to play a major part in earth gravitational granular flows and this speculation is extended to granular flow under low gravity levels. Individual properties have a particular effect on granular flow and the combined effect makes the study of granular flow complex. It is therefore suggested that understanding these individual factors affecting granular flow will largely aid to understand the rheology of granular flow and help to understand its complexity. Though such information on the behaviour of granular flow is available under earth gravity, it is much limited under low gravity levels. As a motivation to this research, the understanding is further applied under low gravity conditions as a stepping stone to understand the flow behaviour on the surfaces of Mars, Moon or other asteroid size bodies. Investigations on the effect of hopper design, the force field indicating the stress and strain within the granular assembly and the particle scale properties affecting the rheology under earth gravity (1g) could be extended and validated for low gravity studies. The computational methods discussed using continuum theory and DEM using the simulation software PFC^{3D} by ITASCA are applied in later chapters to study gravitational effects on granular flow. The continuum theory developed is based on the Lagrangean model and Kirya structural model for non-cohesive flow. The DEM concept is based on contact model which takes into account particle interactions within the granular media. DEM models using PFC^{3D} could provide useful estimates of the effects of particle scale properties on stress and force distributions, velocity distributions and general flow behaviour within the granular media. It is therefore proposed that the DEM model could be used to establish an understanding of the flow behaviour of granular materials as well as bridge the knowledge gap on the flow behaviour between the low gravity regolith and earth gravitational granular flow. The model will further help design hoppers to be used in the SPDS within the ExoMars laboratory during the exploration of the Mars and Moon. The concepts and methodology of DEM is given in Appendix A while the key particle-scale properties for real grains can be characterised experimentally as described in the next chapter.

Chapter 3

EXPERIMENTAL CHARACTERISATION OF GRANULAR SAMPLES FOR KEY PARTICLE-SCALE PROPERTIES

3 Experimental Characterisation of Granular Samples for Key Particle-Scale Properties

In the current study, sandstones materials are used as representative samples of lunar grains. Though the current thesis work is dominantly based on DEM simulations, it is important to ensure that the input parameters of particle-scale properties are realistic and truly represented in the DEM simulations. Previous studies have characterized the physical properties in detail (Tucker et al., 2012, Lumay et al., 2012). However, in the current investigations, two most important parameters viz; particle size distributions (PSD) of the actual samples and adhesion force between the grains of the different samples are characterized experimentally. The focus of this chapter is the experimental characterization of the grains to get information using particle size analyzer and colloidal force microscopy (CFM) for eight different granular samples coded as JS1, JS2, JS3, JS4, JB1, JB2, JB3, and JB4 (Table 3.1). The samples are designed to represent the simulants used in space engineering applications of Martian and Lunar soils.

3.1 Particle Size Distribution Measurement

Malvern particle analyser is used to obtain the size distribution of different granular material samples used in this study. The size distribution of the samples are also used as input in DEM simulations to study the influence of particle-scale properties and gravity on granular flow from a hopper. Size distribution of the particles could influence the processing behaviour of particulate system. In process industries, mostly, bulk solids which comprises of a large number of particles of non-uniform size is encountered and to have a complete understanding of the materials, it is necessary to know the particle size distribution. In general, particle size distribution within sheared granular materials are part of the factors that can influence the bulk system frictions and anisotropy (Antony and Ghadiri, 2006, Antony et al., 2005) as well as the final product properties (Breitung-Faes and Kwade, 2011). Particle size distribution can be expressed as frequency distribution or cumulative curves which is normally depicted by a histogram. The size distribution aids in having the particle sizes in different ranges and can be based on number, surface, mass or volume. A wide distribution of the particle size is reported to have significant impact on granular flow (Calvert et al., 2009). For example, Mullarney and Leyva (2009) showed that spherical particles containing a mixture of elongated and small size spherical particles are likely to have better flow as compared

to non-spherical particle mixture. Reduced flow is however reported for size distribution with finer particles as it encourages cohesive arching (Lumay et al., 2012). Similarly, a distribution having more of the larger particle sizes may lead to segregation problems during flow as the smaller particles tend to migrate through the unoccupied voids to the bottom which further creates non-uniformity in the sample (Abdullah and Geldart, 1999).

For each of the samples investigated, an average particle size distribution of ten measurements was taken to ensure full dispersion and stability of the sample. The Morphologi G3 (Fig. 3.1) developed by Malvern Instruments, UK, was used for the size distribution analysis



Fig. 3. 1 Morphologi G3 by Malvern

The Morphologi G3 consists of automated dispersion and an optical microscope equipped with magnification lenses ranging from 2.5X to 50X which has the capacity to measure particle sizes ranging between 0.5 and 3000 μm . The samples to be analysed were dispersed using calibrated spoons into the dispersion capsule and enclosed with 6 μm aluminium foils. The aluminium foil serves as a protection to the sample collector. The sample dispersion on to the slide is carried out under controlled conditions of dispersion pressure, injection time and settling time with an instantaneous pulse of compressed air. High quality information about the morphology of the particle and 2D images of the scanned particles are provided by the Morphologi G3 equipment. Ten measurements were taken for each sample and average particle sizes are plotted against

volume percent using the Weibull distribution analysis (Famoye, 1995) and the scanning electron microscopy (SEM) image of the granular simulants given as shown in Fig. 3.2. All the measured size distributions are represented in terms of Weibull fit and the equations related to the Weibull constants are given as:

$$F(X_i) = 1 - e^{-(X_i/\beta)^\alpha} \quad (3.1)$$

where $F(X_i)$ is percentage of cumulative particle size distribution (%), X_i is the size of particles (μm), β is the Weibull scale parameter and α is the Weibull shape parameter. Expanding equation (3.1),

$$y = 1 - e^{-(X_i/\beta)^\alpha} \quad (3.2)$$

$$y = a - (a - b)e^{-(kx)^d} \quad (3.3)$$

$$y = 1 - e^{-(kx_i)^d} \quad (3.4)$$

where $a = 1$, $b = 0$, $x = x_i$, $1/\beta = k$ and $\alpha = d$

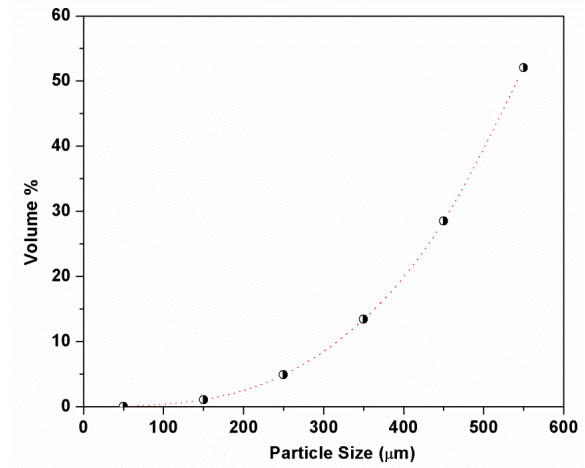
The Weibull parameters for each soil sample are given in Table 3.1. From the particle distribution, most of the particles are less than 550 μm in the case of JS1, less than 188 μm for JS2, less than 375 μm for JS3, and less than 425 μm for the JS3 samples. For the JB samples, the distribution is observed to consist more of larger particles and as a result, for JB1, all the particles are less than 460 μm , for JB2, less than 850 μm , for JB3, less than 1850 μm and for JB4, the particles are less than 575 μm . The whole distribution of size of the particles in the different samples are provided in Fig. 3.2.

Granular
Simulant

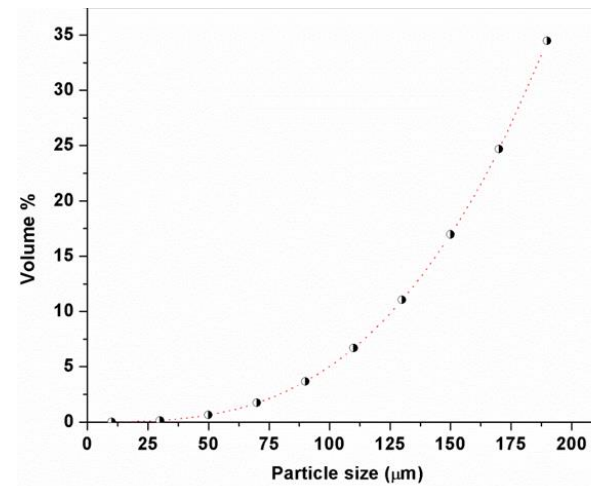
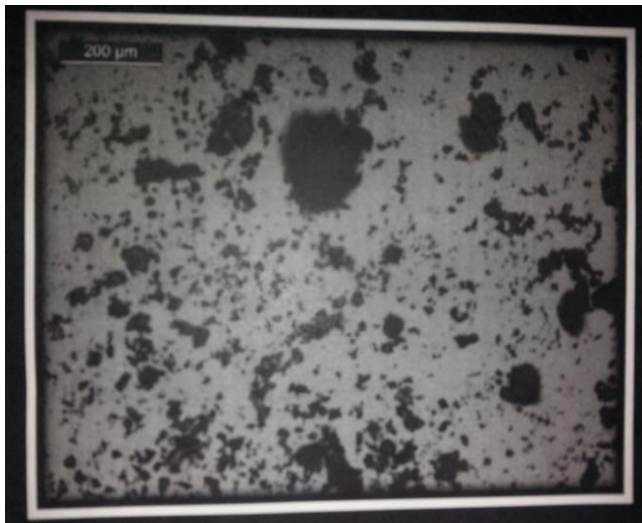
SEM Image

Size Distribution

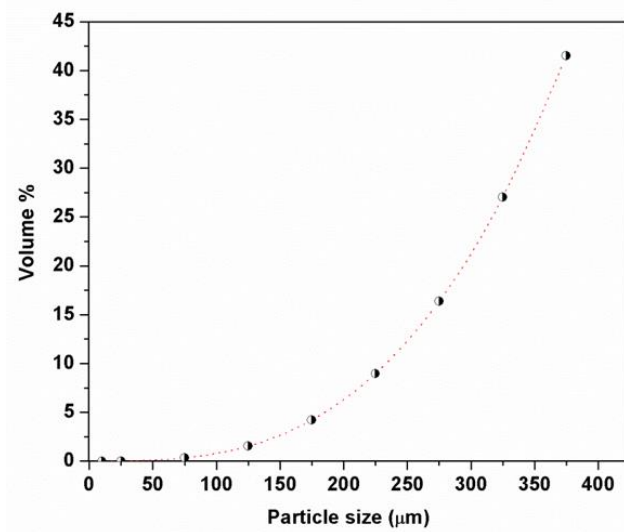
JS1



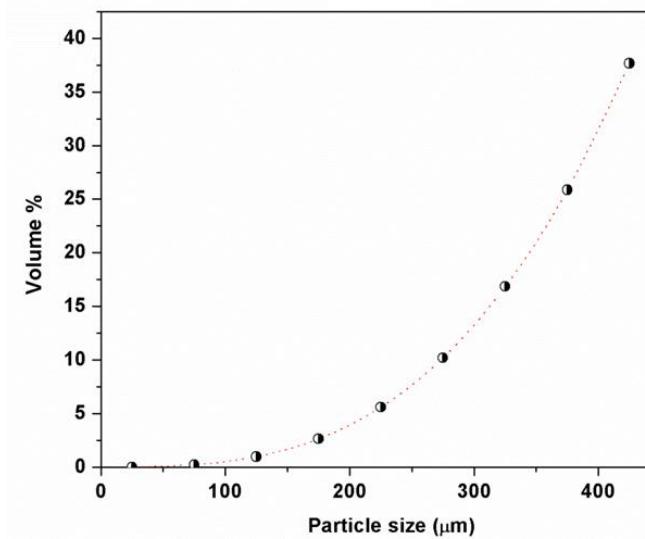
JS2



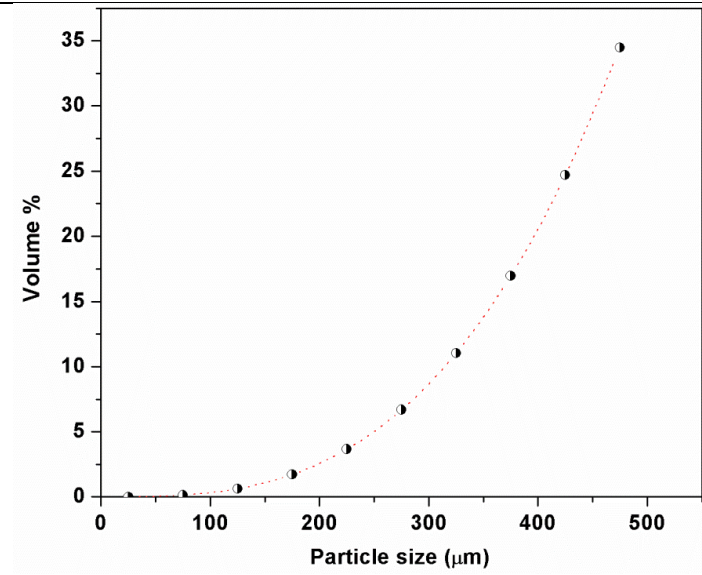
JS3



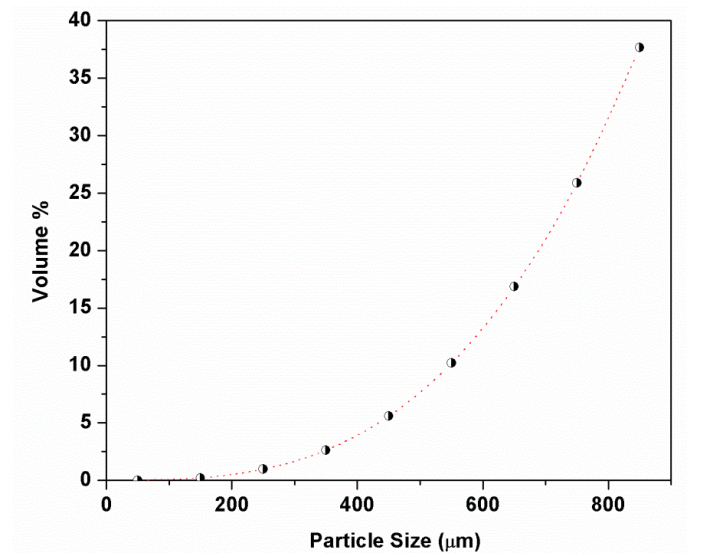
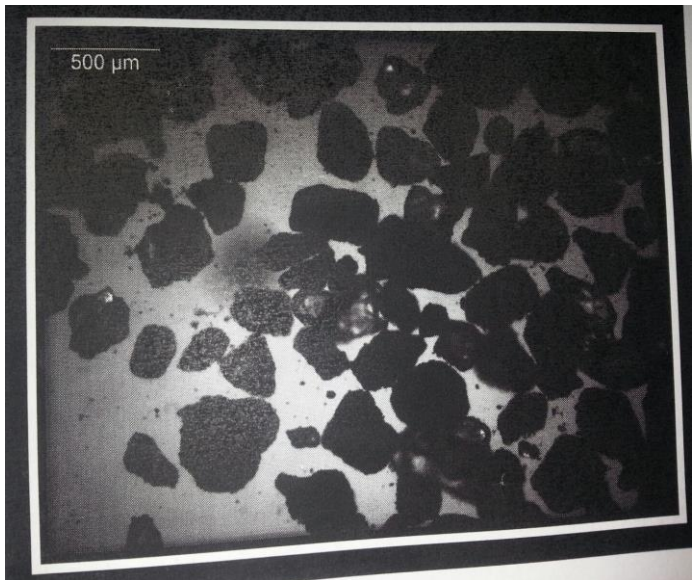
JS4



JB1



JB2



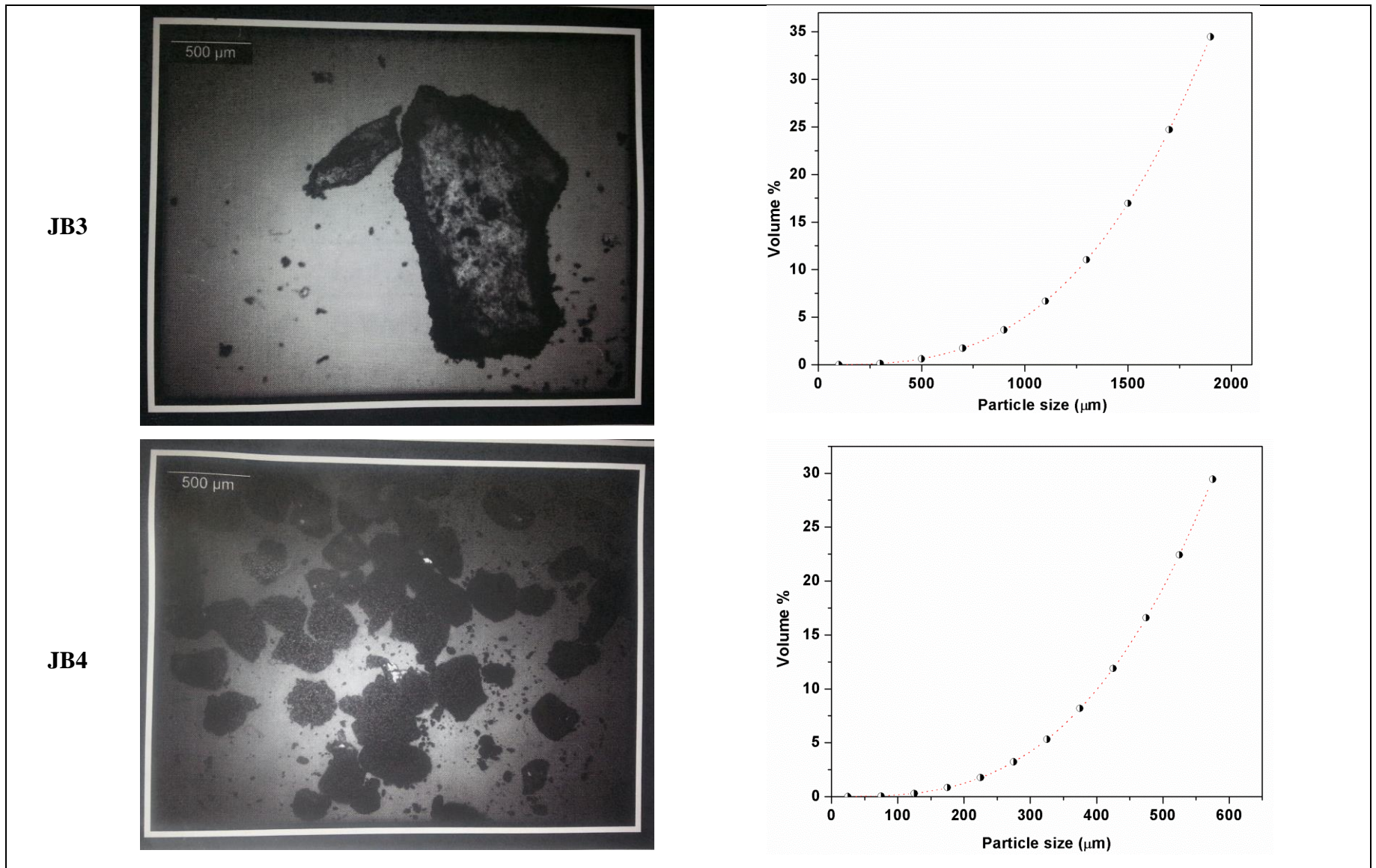


Fig. 3. 2 SEM images and size distributions of granular simulant JS1 – JS4 and JB1 – JB4

3.2 Adhesion Force Measurement

Inter-particle forces can be examined by applying atomic force microscopy principles using two methodologies namely:

- Atomic Force Microscopy (AFM) – which is in form of cantilever-particle interactions
- Colloidal Force Microscopy (CFM) – which is a modified version of Atomic Force Microscopy in form of particle-particle interactions. This is the main technique applied in this investigation to measure the force of adhesion between the grains.

The working principles will be briefly highlighted in this section.

3.2.1 Adhesion force measurement using atomic force microscopy

Atomic force microscopy (AFM) is a type of scanning probe microscope (SPM) that is used for force measurements. AFM aids the measurement of the interaction force between the tip of a sharp cantilever probe supported on a flexible cantilever and the sample surface at a distance (Butt et al., 2005). The amount of force between the probe and the soil sample depends on the stiffness of the cantilever and the distance between the probe and the sample surface. Image resolution of the particle surface is acquired with the aid of AFM by measuring the small vertical and lateral deflections of the elastic cantilever as shown in Fig. 3.3.

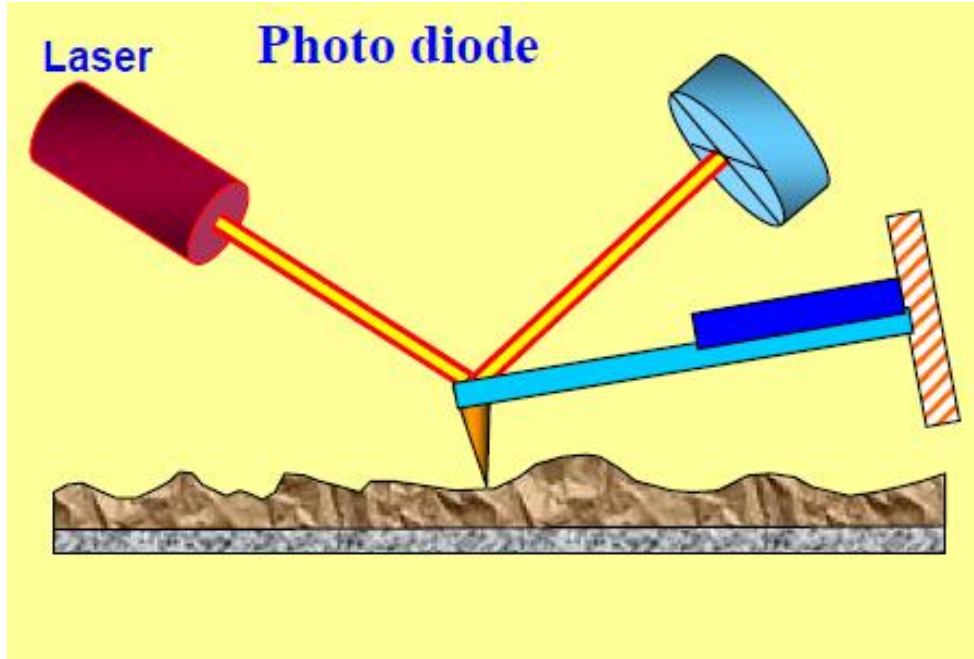


Fig. 3. 3 AFM set-up (Mironov, 2004)

As described in chapter 2, the interactive forces obtained from AFM can be explained qualitatively by taking into account the van der Waals forces which is dominant. The van der Waals potential energy of two atoms located at a distance r from each other is approximated by the exponential function known as Leonard-Jones potential (Fig. 3.4).

$$U_{LD}(r) = U_0 \left\{ -2 \left(\frac{r_0}{r} \right)^6 + \left(\frac{r_0}{r} \right)^{12} \right\} \quad (3.5)$$

The long-distance attraction caused by a dipole-dipole interaction is represented by the first term of the sum in equation 3.5 while the second term considers the short range repulsion due to the Pauli Exclusion Principle. The parameter U_0 is the equilibrium distance between atoms for which the energy value is minimum.

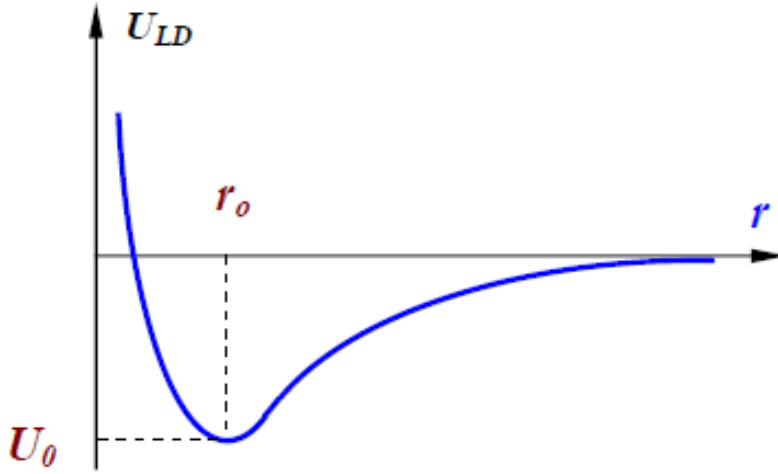


Fig. 3. 4 Illustrative diagram of the Leonard-Jones potential

The measurement represented in Fig.3.4 allows for the estimation of the interaction force of a tip with a sample. Thus, the energy of the interaction can be illustrated in equation 3.6.

$$W_{PS} = \iint_{V_P V_S} U_{LD}(r - r') n_P(r') n_S(r) dV dV' \quad (3.6)$$

where, $n_S(r)$ and $n_P(r')$ are the densities of atoms in the sample and in the tip.

Subsequently, the force which affects the tip from a surface can be calculated from equation 3.7.

$$\check{F}_{PS} = -grad(W_{PS}) \quad (3.7)$$

From equation 4.3, the force generally consist of both the component normal to the sample surface and a lateral component which lies in the plane of the sample surface (Mironov, 2004). During contact with the sample surface, the probe predominantly experience repulsive van der Waals forces (contact mode) while as the tip moves further away from the surface, the attractive van der Waals forces (non-contact mode) become dominant. The amount of force experienced by the cantilever as the probe tip moves towards the sample surface and further away is measured by force curves (Johnson et al., 2009).

Force curve analysis can be used to determine properties such as elasticity and adhesion forces (Hilal et al., 2009) and for most industrial particles, the shape of the measured force-separation curve ($\Delta Z = f(z)$) is complex in nature as shown in Fig. 3.5.

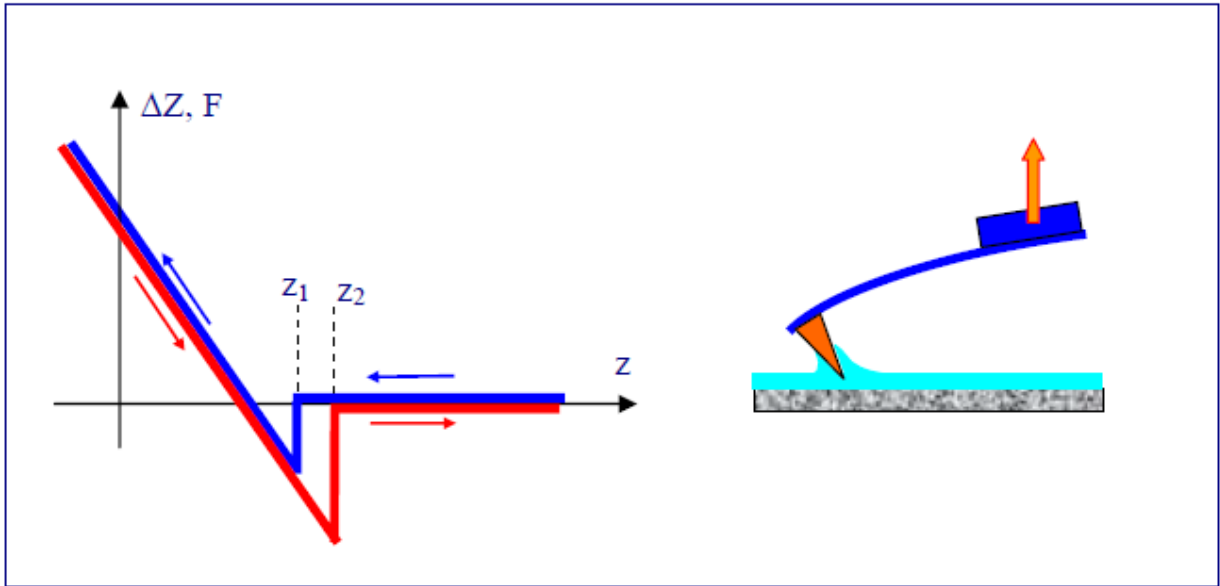


Fig. 3. 5 Illustrative diagram of a cantilever-particle interaction (Mironov, 2004)

Fig. 3.5 is a schematic representation of an approach-retraction curve for a particle-cantilever interaction in which the capillary effect within the snap-off distance ($z_2 > z_1$) is illustrated.

Spectroscopy measurements can be obtained when the probe approaches the surface via the contact mode operation. In this contact mode, adhesion forces have a significant effect on the cantilever movement during the probe withdrawal from the sample (Butt et al., 2005). The forces result in the deflection of the cantilever before it breaks contact with the surface. The adhesion force can then be calculated assuming the force is a linear function of the probe displacement relative to the sample surface. The force can be described using Hooke's law as given in equation 3.8.

$$F = k \times \Delta H \quad (3.8)$$

where, F is the force, k is the cantilever stiffness and H is the cantilever deflection as illustrated in Fig. 3.6.

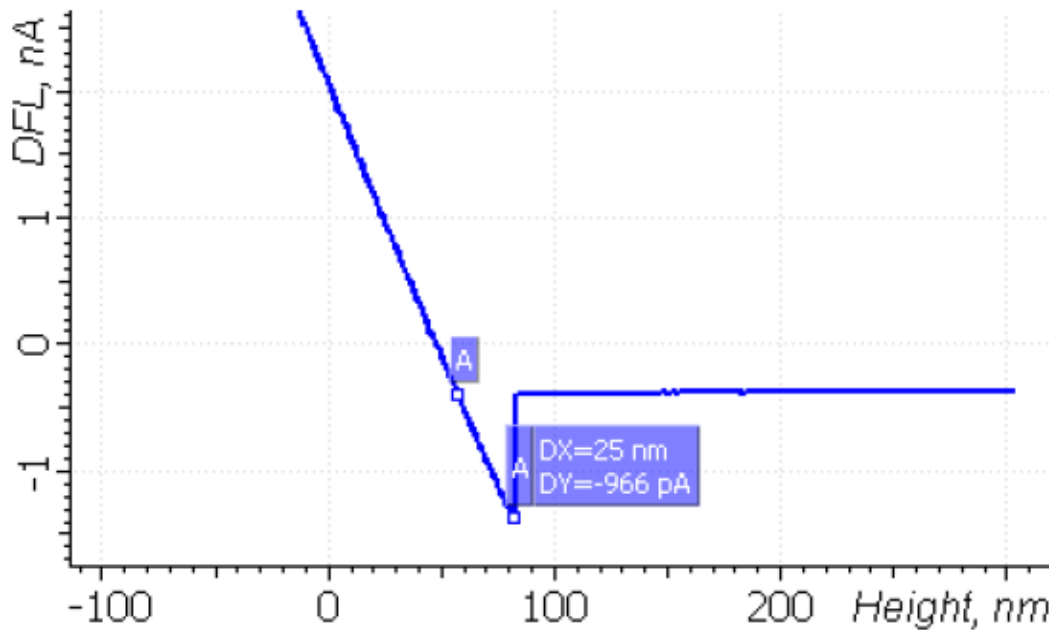


Fig. 3.6 Typical output from an AFM adhesion force experiment (Mironov, 2004)

From Fig. 3.6, the values of DX and DY are the ΔH and ΔDFL respectively. These measures are subsequently calibrated to the interaction force-separation measures using the calibration constants which is recommended by equipment suppliers.

3.2.2 Adhesion force measurement using colloidal force microscopy

The colloidal force microscopy is a modified AFM technique which basically uses a standard AFM for the force measurements. In this technique however, the AFM cantilever makes use of a colloidal probe (Borkovec et al., 2012). The colloidal probe is normally obtained by attaching a colloidal particle to the tip of the cantilever (Fig. 3.7). In this study, the attached colloidal particle is represented by the grinded soil particle of about $10\mu\text{m}$ from individual samples. The inter-particle interaction force is extracted as a function of the separation distance between the particles by recording the reflection of the cantilever as a function of the vertical displacement of the AFM scanner from the surface of another particle fixed on the substrate. Other calculations are similar to the AFM calculation theory as described in section 3.2.1.

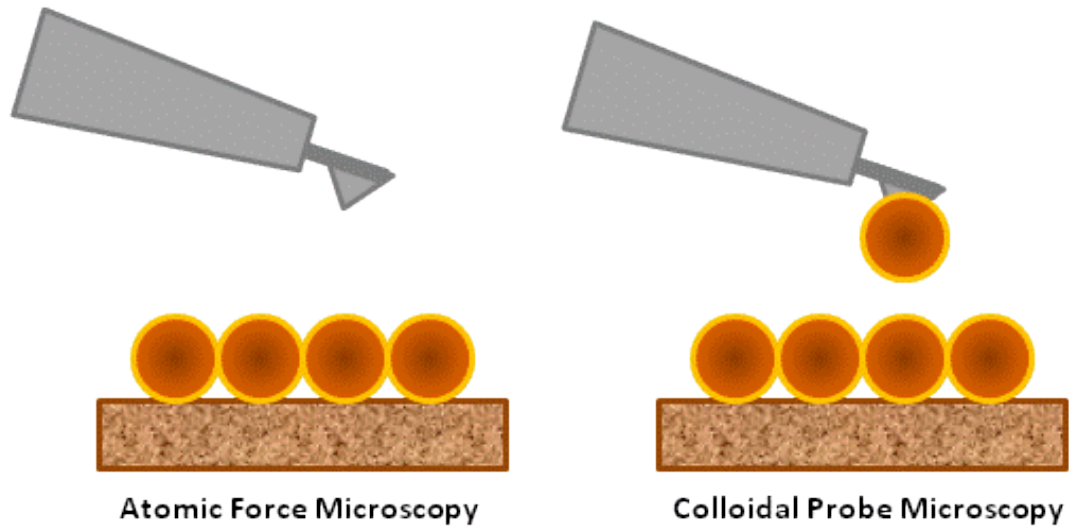


Fig. 3. 7 Schematic representation of AFM and CFM

After the interparticle adhesion force, F_{Adhesion} is measured for the given type of soil samples with the data normalized to the actual size of the particles (F_{Adhesion}/R , where R is the average radius of similar interparticle size used) for easy comparison between the samples as given in Table 3.1.

All the measurements for the adhesion force presented below are based on the average value of three measurements for each type of samples. The deviation of F_{Adhesion}/R is within 6% error limit which is reasonably good tolerance level in particle characterisation measures.

Table 3. 1 Adhesion force input values of granular soil simulants

Soil sample	Weibull scale parameter, β	Weibull shape parameter, $\alpha = d$	$k = 1/\beta$	R^2	F_{Adhesion}/R (N/M)
JS1	444.45	6.06	0.00225	0.9787	0.0008
JS2	166.11	6.26	0.00602	0.9985	0.0058
JS3	289.02	4.77	0.00346	0.9965	0.0079
JS4	323.62	3.39	0.00309	0.9788	0.0043
JB1	2127.65	3.61	0.00047	0.9904	0.0067
JB2	724.63	2.97	0.00138	0.9996	0.0064
JB3	1724.13	2.71	0.00058	0.9986	0.0074
JB4	2439.02	4.78	0.00041	1	0.0057

The above presented experimentally characterized values, in addition with other grain scale properties available from literature(Zhu, 2010) will be fed as input parameters in DEM simulations in the following chapters.

Chapter 4

STRESS ANALYSIS AND SHEAR DEFORMATION OF GRANULAR MATERIALS IN GRANULAR FLOW UNDER EML GRAVITY

4 Stress Analysis and Shear Deformation of Granular Materials in Granular Flow under EML Gravity

The primary methodology used in the current research programme is based on DEM simulations. Hence it would be desirable to validate the stresses predicted by DEM for a hopper containing granular materials and to compare it with experimental results. Ideally, it would be nice to have such a comparison under dynamic flow conditions. However, an experimental methodology to examine such a result within granular materials is not yet well established.

Hence, the purpose of this chapter is to perform the above comparison for a static filling of pharmaceutical granules (pharmaceutical excipient powders) represented by starch. The reference material used in this chapter is different from that of the following chapters due to the birefringence nature required for the materials to be used in the experiment. Photostress analysis tomography (PSAT) experimental methodology is used here to obtain the stress distribution within granular filling inside hoppers of different opening angles (static condition) and compared with corresponding DEM simulation results.

4.1 Introduction

Historically, continuum methods have constituted the majority of studies/investigations analysing stress distributions within a media with an increasing proportion in recent times making use of DEM. The laboratory experiments on real materials rely on estimates of the macroscopic stress and strain states from boundary measurements which themselves depend on assumptions made about the material behaviour. Most experimental techniques undertaken to measure flow patterns and stresses are reported to be very expensive and usually not repeatable (Wang and Ooi, 2015). Also, the development of stress in granular materials requires measurements of single particle interactions experimentally. These measurements have however been limited due to the practical difficulties of distinguishing individual grains (Ding et al., 2013). A lot of success in stress predictions in hoppers has been gained using FEM (Goodey et al., 2006), however, the FEM method sees the granular material as a continuum and is unable to evaluate the dynamic behaviour of individual particles within the granular media. This has led to an increase in the use of DEM

simulations which shows great ability to help describe precisely material properties and all resultant observations are quantifiable. The environmental condition applied in the use of DEM also offers control over experiments and non-intrusive measurements and provides computer graphics which permits visualisation of the internal micro/nano mechanical processes. Over time, DEM simulations have been used in parallel with experiments to probe the propagation of force chains and to understand the flow behaviour of granular media. Murthy et al. (2012) reported the characterization of force chains using DEM simulations based on micro-level descriptions of interparticle contact friction, particle density and degree of polydispersity. A variety of DEM and continuous FEM simulations have been developed to describe the stresses in granular media due to the difficulty of experimental verification. Most DEM simulations overtime has been confined to 2D systems (Landry, 2004) with recent applications in 3D systems. The main advantage of DEM is that highly complex systems can be modelled without oversimplifying the assumptions (Langston et al., 2004).

DEM has been proven to be successful in describing the flow of particles in a number of process geometries under earth gravity. Examples of such extensive review can be found (Wang and Ooi, 2015, Zhu et al., 2008). Most of the investigations in the literature is focussed more on process geometries under earth gravity. Efforts have been made in this work to overcome this gap as related to other gravity environments such as the Mars and Lunar gravities even in 3-dimensional systems which are largely unexplored. Overtime, as experimental techniques have not been readily available to accurately measure the stress distribution within a granular media, results from DEM have not been easily verified. In the absence of adequate experimental techniques, DEM is utilised in this research for 3D systems supported by PSAT experiments to assess the stress distribution within the granular media at least under earth gravity in order to further justify results under mars and Lunar gravity levels.

Recent studies show the usefulness of PSAT to understand the influence of wall boundaries on the nature of shear stress experienced by an inclusion for the positions close to the wall boundaries (Antony and Chapman, 2010) and also to obtain the stress distribution within inclusions in particulate system (Antony et al., 2015b). The working principle and brief background of the PSAT technology are given in the next section.

4.2 Basics and Background of Photo-Stress Analysis Tomography (PSAT)

The basic and working principles of the photo-elasticity methodology are well established (Dally et al., 1978). PSAT is based on the birefringence of materials which is an opto-mechanical phenomenon. Induced stresses in birefringent materials usually cause changes in their refractive index and the application of PSAT analysis utilizes the induced birefringence to examine the distribution of stress within the assembly (Antony et al., 2015b). Basically, the birefringent particles optically respond to stress when viewed under a circular polariscope setup (Dally et al., 1978, Drescher and De Jong, 1972, Antony et al., 2015b). The direction and magnitude of the components of the maximum shear stress at various points can be obtained by utilizing the fringe patterns that characterizes the light retardation passing through the circular polariscope. The observed fringes can be categorised into two: isochromatic and isoclinic fringes. The isochromatic fringes help to determine the maximum shear stress via the fringe order using stress-optics law as given in equation 4.1 (Dally et al., 1978, Majmudar and Behringer, 2005).

$$\sigma_1 - \sigma_3 = \frac{nf}{t} \quad (4.1)$$

where, σ_1 is the major principal stress, σ_3 is the minor principal stress, n is the measured fringe order, f is the material fringe coefficient and t is the thickness of coating.

Isochromatic fringes are lines of constant principal stress difference which at any point in the birefringent material can be related to the magnitude of the maximum shear stress τ_{max} (equation. 4.2).

$$\tau_{max} = \frac{\sigma_1 - \sigma_3}{2} \quad (4.2)$$

On the other hand, Isoclinic fringes provides information on the direction of the principal stresses in the assembly. These isoclinic fringes occur when the principal stress direction coincides with the axis of polarization of the polarizer (Dally et al., 1978). However, for convenience when only the maximum shear stress is required, the use of a circular polariscope (Fig. 4.1) will help eliminate the isoclinic fringes. Alternatively, in situations where both the maximum shear stress and the directions of the principal stresses are required at any point of interest in the birefringent material, image capturing and digital imaging techniques (Patterson, 1988, Ramesh, 2000, Ramesh et al., 2011) are used which allow for the separation of the isochromatic and isoclinic fringe patterns.



Fig. 4. 1 Schematic diagram of PSAT (circular polariscope) set up

The PSAT experimental rig shown in Fig. 4.1 consists of a linear polariser, two quarter wave plates, an analyser, light source and the birefringent sensor material hopper (angle of hopper = θ)

In this investigation, the application of PSAT technology which is limited to two dimensional conditions is found to be adequate and relevant to support the three dimensional DEM simulations for near axisymmetric fillings (Timoshenko and Goodier, 1970) in the hopper funnel geometry. In axisymmetric cases, a planar section is taken and treated as a two dimensional case in which the radial coordinates are translated into planar coordinates to be used in PSAT analysis. The PSAT results are then compared with DEM simulation results as discussed in the following sections.

4.3 Prediction of Maximum Stress within Granular Materials in Hoppers Using DEM 3D Simulations

DEM in three dimensional systems is applied as a method of analysing the stress distribution through granular materials in hoppers via inter-particle contacts. The way stress is distributed within granular materials in hoppers is fundamental to understanding the phenomena observed in hoppers and as such, stress distribution predictions are essential. The assessment of the distribution of stresses should analyse the variation in radial, vertical, and angular position. The aim here is to predict and understand the stress distribution profiles across the horizontal width of the bed and along the hopper wall in the granular packings along different heights within the hopper under earth, mars and Lunar gravity levels. These predictions are done for various hopper internal angles. Also, experimental support is provided using the PSAT technology to the very best possible under earth gravity conditions.

When hoppers are filled with granular materials, stresses develop within the material which is fundamental to understanding the flow properties of granular material as well as the problems encountered during flow. The distribution of stress in hoppers helps to understand phenomena such as arching, velocity discontinuity, stress fluctuations, etc. Thus the correct design of hoppers will require adequate prediction of the stresses that occur via the inter-particle contacts and pressure exerted on the hopper walls by the materials (Wang and Ooi, 2015).

In this work, a conical hopper is modelled using the DEM model with the aid of PFC^{3D} simulation software (explained in appendix A). The DEM model represents a conical hopper which is defined by two flat walls and a cone-shaped general wall. An assembly of spherical particles having specified particle diameters which are randomly distributed with specified target porosity is generated at an initial compact state as shown in Fig. 4.2.

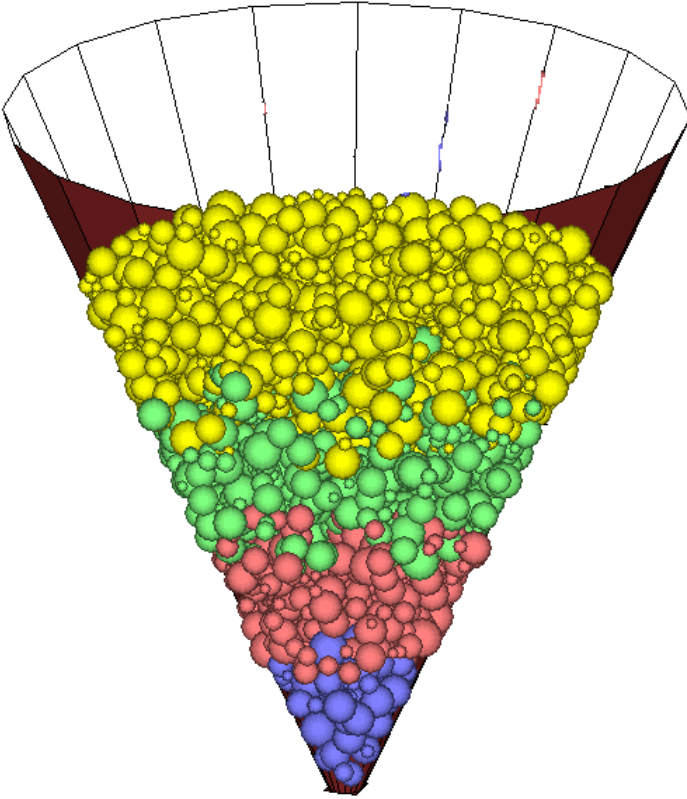


Fig. 4. 2 Initial compact state of the hopper generated using PFC^{3D}

The cone-shaped general wall is fixed which confines the flow of particles within the hopper in an irregular assembly. The hopper is initially filled with non-cohesive spherical particles at given desired porosity with the assembly allowed to reach equilibrium after compaction under gravity. The particles are uniformly distributed using a radius multiplier to achieve the desired porosity. The DEM simulation is performed using PFC^{3D} software and the parameters used are summarized in Table 4.1. A linear contact model is employed to describe the force-displacement relation in normal and tangential directions between the two contacting entities, particle-particle/particle-wall interactions as discussed in chapter three. All the contacts are assumed to have equal normal contact stiffness K_n and tangential contact stiffness K_s .

Table 4.1 Parameters used in DEM model to analyse stress distribution

Hopper dimensions	Granular properties	Other properties
Wall normal stiffness (Pa) 1e7,	Density kg/m ³ 708	$g (m/s^2) = 9.8$ (earth), 3.77 (mars), 1.67 (Lunar)
Wall shear stiffness (Pa) 1e7,	Particle minimum radius (m) 300e ⁻⁶	Initial Porosity 0.16
Hopper height (m) 0.09	Particle average radius 6.5e ⁻⁴	Measurement sphere 3.2 x average diameter (Fig 5.5 and 5.9)
Hopper orifice opening (m) 0.005	Particle radius ratio 3.3	
	Particle normal stiffness K_n (Pa) 1e7	
	Particle shear stiffness K_s (Pa) 1e7	
	Radius multiplier 1.4	

The DEM microscopic parameters such as the contact stiffness are determined by a calibration process to correlate with the macroscopic parameters such as Young's modulus used in the experimental investigations. Other microscopic material parameters used in DEM simulations are obtained from PSAT experiments as input parameters.

The measurement of stress adopted here is via the measurement sphere technique as discussed in section A.7 in the appendix. This technique makes use of the averaging procedure by obtaining average values from three measurement circles which helps make the step from the micro-scale to continuum. This averaging procedure is used because stress is a continuum quantity and does not exist at individual points in a particle assembly in the discrete medium. The hopper dimensions and particle properties are given in Table 4.1. This measurement technique provides the truest measurement of the material properties which may differ from the physical laboratory measurement not able to replicate the measurement logic and take into account the discrete nature of the particles. The material properties used for this study are input from the PSAT experiment. In DEM computations to measure the stress quantities, only particles with centroids contained within the measurement sphere are considered (Figs. 4.5 and 4.9). The maximum stress is

calculated from the stress components obtained from the measurement sphere for varying internal angles of the hopper (Fig. 4.3) under earth, mars and Lunar gravity levels.

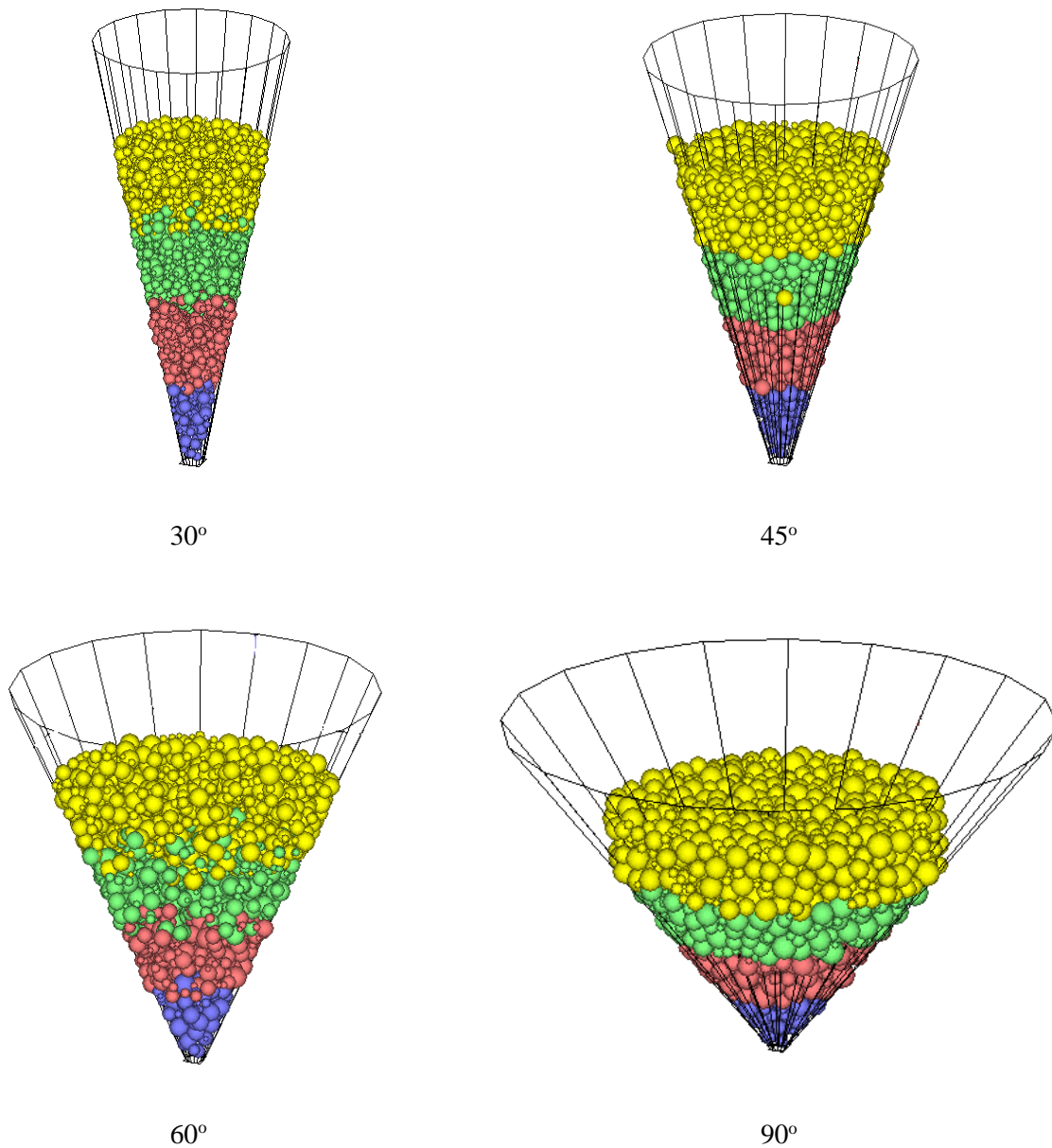


Fig. 4.3 Hopper geometry for angles 30, 45, 60, and 90 degrees

Stress is measured using the stress and velocity-gradient tensor measurement procedures of Potyondy and Cundall (2004). The stress measurement is computed within the region based on the contact forces (Fig. 4.4), contact orientations and the porosity of the region. In DEM analysis, the position and velocity of every particle is obtainable at every time-step.

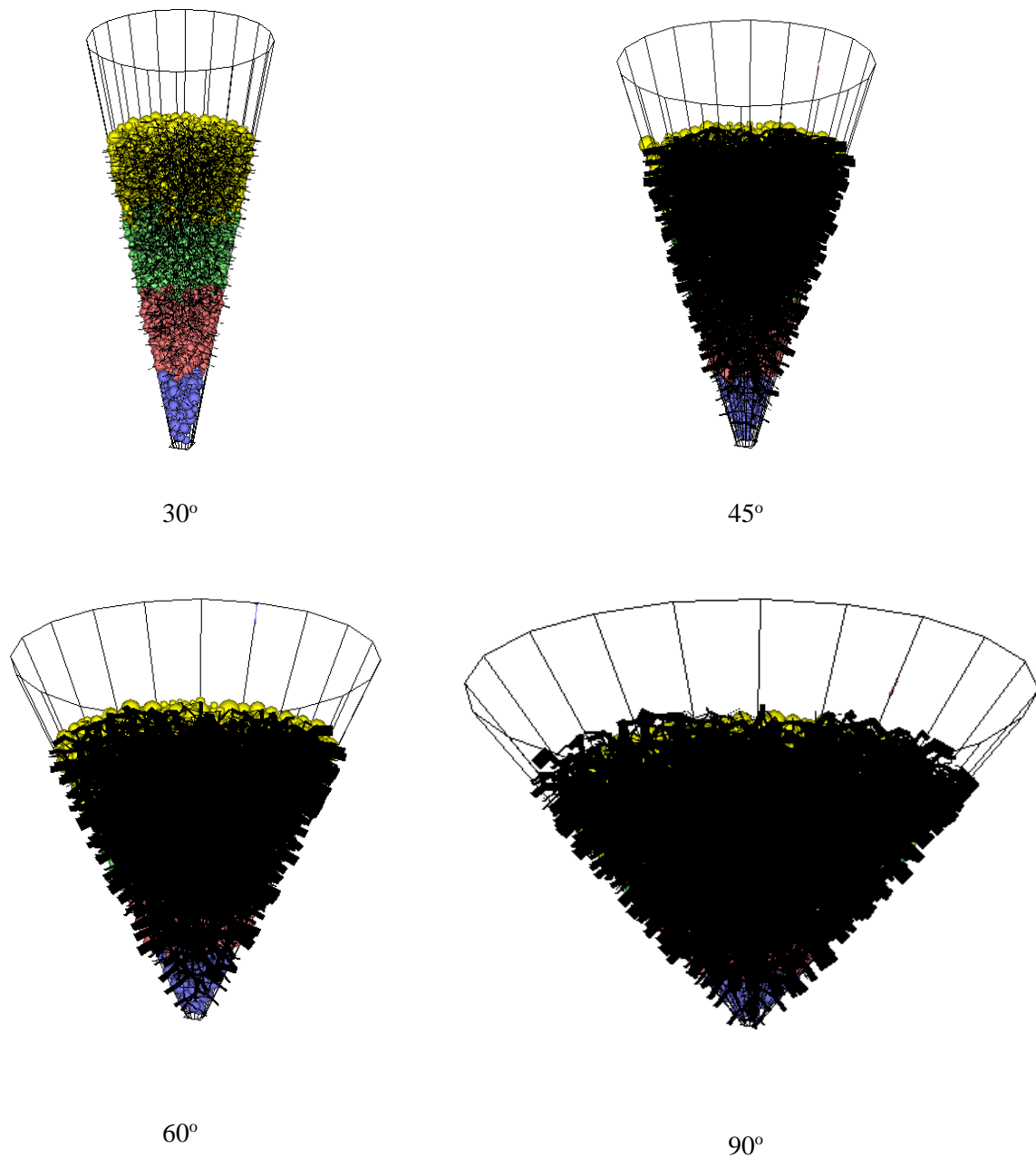


Fig. 4. 4 Contact forces within the granular bed for angles 30, 45, 60, and 90 degrees

The stress is computed based on the assumptions that (a) external applied forces are absent and (b) each of the particles is in full-force equilibrium. A body force (gravity) is necessary to support a stress field that varies linearly in space.

4.3.1 Prediction of maximum shear stress distribution across the hopper section (horizontal section) using DEM simulations under earth gravity level

The particles are compacted within the hopper and allowed to reach equilibrium after which the maximum shear stress is tracked along different scanning points at a given height. Analysis was done through the horizontal section of the hopper at a bed height ($H/2$) for angles 30, 45, 60 and 90 degrees (Fig 4.3) under earth gravity. The measurement spheres are used to compute the stress at various scanning points along the width of the hopper. The diameter of the measurement sphere was fixed to an average value based on variation test of the diameter beyond which there is no significant change in the stress components.

The stress that exists due to the inter-particle interaction across the horizontal width of the granular bed in the hopper (Fig. 4.5) is measured and analysed under earth gravity.

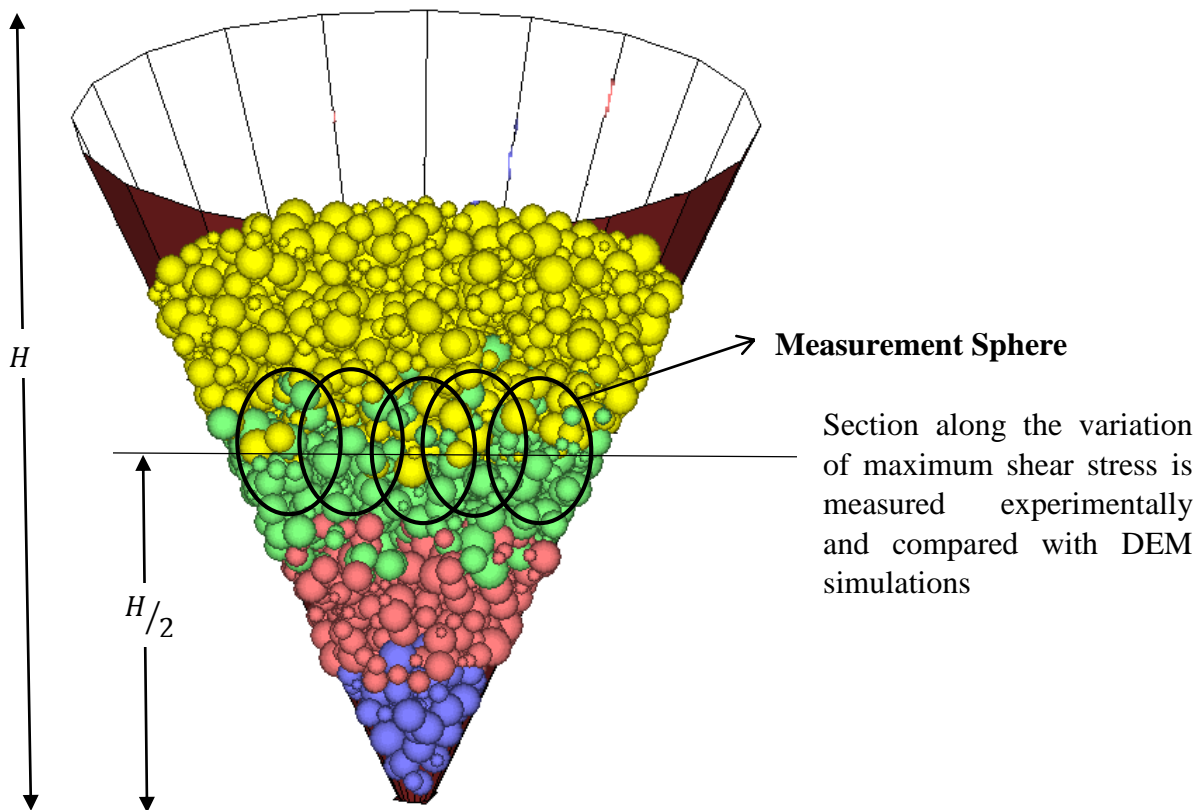


Fig. 4.5 Schematic cross section showing the measurement sphere used for stress measurement across the granular bed horizontally in the hopper

From the results presented in Fig. 4.6, it was found that stress is higher along the walls of the hopper and tends to decrease approaching the mid-section of the hopper. This result is an indication of the static initial stress state. The DEM results in Fig 4.6 was normalised with the highest maximum shear stress value for each hopper internal angle and it showed that the maximum shear stress is very low at the middle of the hopper for 90° hopper angle. Here, there are indications that there are more stresses acting along the wall and particles close to the hopper wall tend to be displaced more towards the wall. The stress magnitude is observed to reduce rapidly along the width of the bed. The particles towards the wall could be termed as the passive particles that fall within the passive region of the hopper which is expected to exist during flow especially for hoppers with high internal angles. The materials towards the wall could then be regarded to be highly dense. For the 60° simulations in Fig. 4.6, it was shown that the stress is also higher at the walls of the hopper as seen at 90° but with less magnitude. The stress also tends to reduce along the width of the hopper towards the middle of the hopper. For 30° and 45°, the stress distribution tends towards being uniform along the width of the hopper though with some traces of high stress along the hopper walls. Higher stress field is however experienced at these lower angles along the hopper width. It can then be deduced that the maximum shear stress distribution tends towards uniformity across the hopper width as the hopper internal angle reduces under earth gravity level.

These maximum shear stress distribution predictions are supported with results obtained from PSAT experiments. The PSAT technology was used to evaluate the magnitude of the maximum shear stress across the width of the hopper at height $H/2$. The granular bed height was kept constant for all hopper angle variation. A description of the detailed experimental set up can be found in Antony and Chapman (2010). The granular materials used are novel pharmaceutical birefringent stress responsive materials (JASA 100) with the particle parameters as used in DEM simulations. The particle sizes are also distributed uniformly having a normal size distribution.

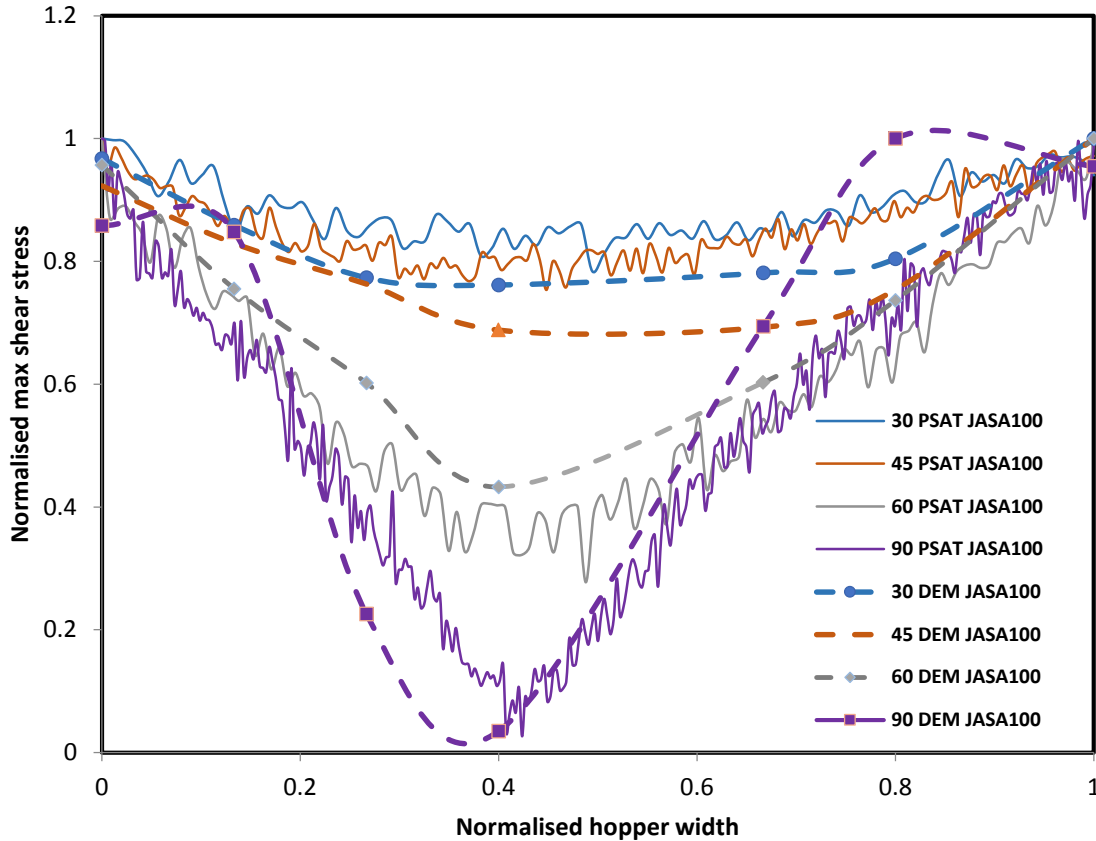


Fig. 4.6 Superimposed plot for maximum shear stress distribution across granular bed for 30°, 45°, 60° and 90° under earth gravity using DEM simulations and PSAT experiments

The results shown in Fig 4.6 further confirms that both PSAT and DEM show similar trends. The maximum shear stress obtained tend to be more uniform across the width of the hopper as the internal angle of the hopper decreases. It also indicates that for increasing hopper internal angle, the stress tend to decrease at the middle of the hopper away from the walls. Further from the PSAT results, the direction of the major principal stress tends to be in the vertical direction at low hopper angles (30°) and deviates to act normal to the wall with increasing hopper angle (Albaraki et al., 2013).

There is no large amount of detailed experimental data available in the literature pertaining to stress distributions along the horizontal width of the hopper under earth gravity level and literally does not exist for lower gravity investigations. The PSAT experiment however helped to understand and justify, to a large extent, the stress distribution predictions by DEM across the horizontal width of the granular bed under earth gravity levels. Further analysis is done using DEM simulations under mars and lunar gravity levels

4.3.2 Prediction of maximum shear stress distribution across the hopper section (horizontal section) using DEM simulations under mars and lunar gravity level

This is a relatively new area of research in understanding static stress distribution within granular materials under mars and lunar gravity levels. Since there are no enormous proportions of studies carried out under Mars and Lunar gravity, preliminary information about its internal composition and gravitational effect on its materials can be obtained using DEM simulations. The loading of the materials is due to gravity and the particles are uniformly distributed. The granular materials are allowed to reach equilibrium before obtaining the value of the stress components using the measurement sphere averaging procedure.

The max shear stress was predicted across the granular bed in a hopper at height $H/2$ with varying internal angle of 30° , 45° , 60° and 90° . Results presented in Fig 4.7 for lower gravity level simulations indicate that gravity does not affect the stress distribution of the material. Thus the way in which stress is being distributed across the width of the static granular bed does not depend on gravity.

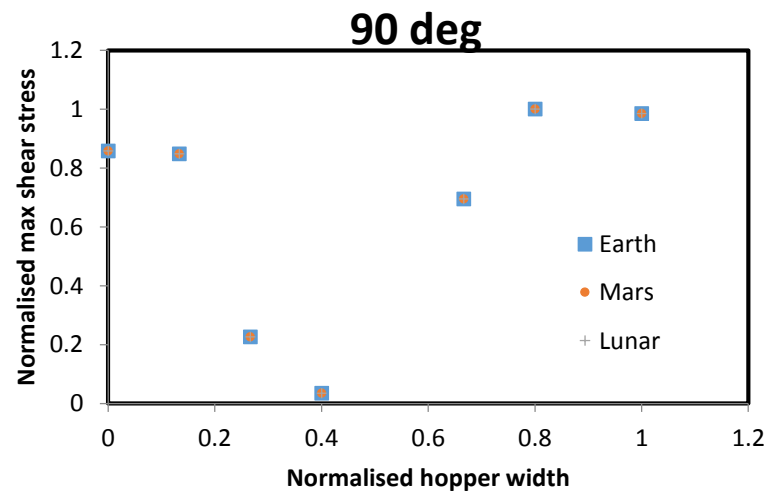
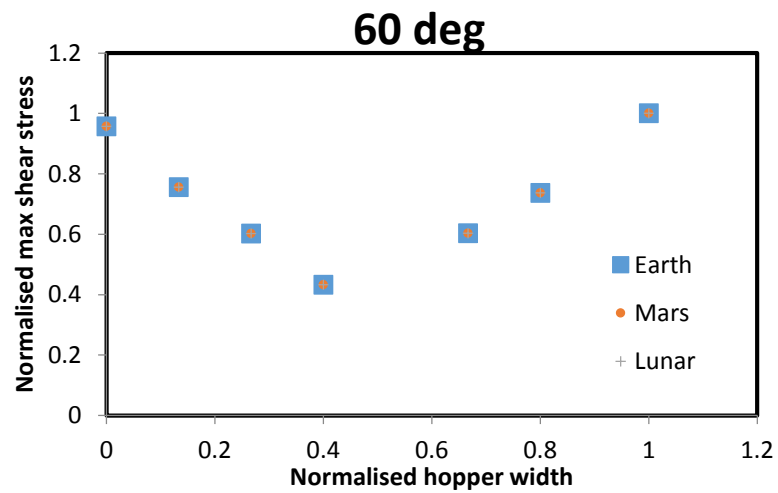
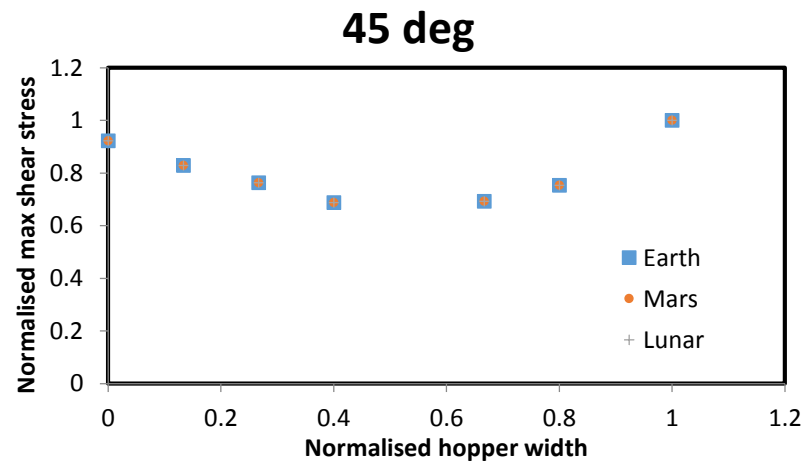
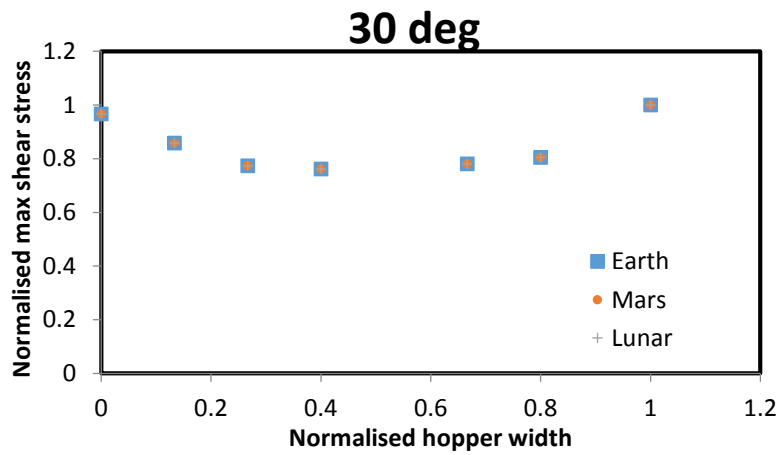


Fig. 4.7 Superimposed plot for maximum shear stress distribution across granular bed for 30°, 45°, 60° and 90° under earth, mars and lunar gravity using DEM simulations

The hopper internal angle effect on the stress distribution was also evident but similar to the effect under earth gravity. The stresses developed on the walls are observed to be higher compared to the stresses across the granular bed horizontally.

The transmission of stresses through the stationary bed has been investigated using DEM simulations under earth, mars and lunar gravity. This investigation focused on the forces exerted from the weight of the material under gravity loading in which the maximum shear stress has been evaluated. Further analysis is required to understand the forces exerted on the stationary walls which are the results of the transmitted stresses from the boundaries of the hopper. Next, the stresses acting on the side wall is evaluated.

4.4 Prediction of Shear Stress within Granular Materials in Hoppers along the Vertical Wall Using DEM 3D Simulations under Static Filling Condition

For many years, research on the prediction of pressure or stresses on the walls of silos and hoppers has been governed by experimental and analytical studies (Walker, 1966, Walters, 1973a). This recently has gained more interest with numerical methods such as DEM and researchers are employing these numerical methods to evaluate the wall pressures of silos and hoppers. It has already been explained that the bulk solids behave differently from liquid even in similar container, thus, the pressure distribution also behaves differently. Within a granular bed, stress occurs as a result of the frictional forces between the solid particles and the walls of the hopper which in effect means that the walls are supporting part of the weight of the bulk particles. Analytical analysis has been briefly detailed in chapter two about the theories of Janssen, Jenike, Walker and Walters. Walker extended the stress distribution estimation into hoppers and derived a set of formula for the prediction of flow pressure on hopper walls with or without surcharge. In Walker's formula, a factor called the distribution factor cannot be exactly evaluated and seen as a weakness or limitation to the theory. It was also noted that when Walter's theory was used to predict hopper pressures under static condition, it was only valid for very steep hoppers (Arnold et al., 1978). Jenike and his co-workers also described methods for predicting the static (initial) pressures on hopper walls (Jenike and Johanson, 1969, Jenike et al., 1973). The filling pressure is assumed to be at a maximum value at some intermediate height and the stress distribution can be estimated

based on the equilibrium of the bulk materials stored in the hopper. The flow pressure distribution on the hopper wall is predicted to consist of a pressure peak at the top of the hopper which decreases linearly to an intermediate value at an intermediate height and then decreases linearly again towards zero at the hopper apex (Jenike et al., 1973). These theories however are intrinsically based on assumptions for simplicity and often not able to describe other complex situations outside which they are formulated for.

Based on these theories, experimental and numerical methods have been used to estimate the static stresses in hoppers, for example, in a wedge shaped hopper (Chou and Chen, 2003). The stresses on the wall in a circulatory two-dimensional wedge hopper were predicted using differential slice and Runge-Kutta (order 4) methods as shown in Fig. 4.8. The stresses were carried for two different half angles 10° and 20° and plotted in relation to the bed height.

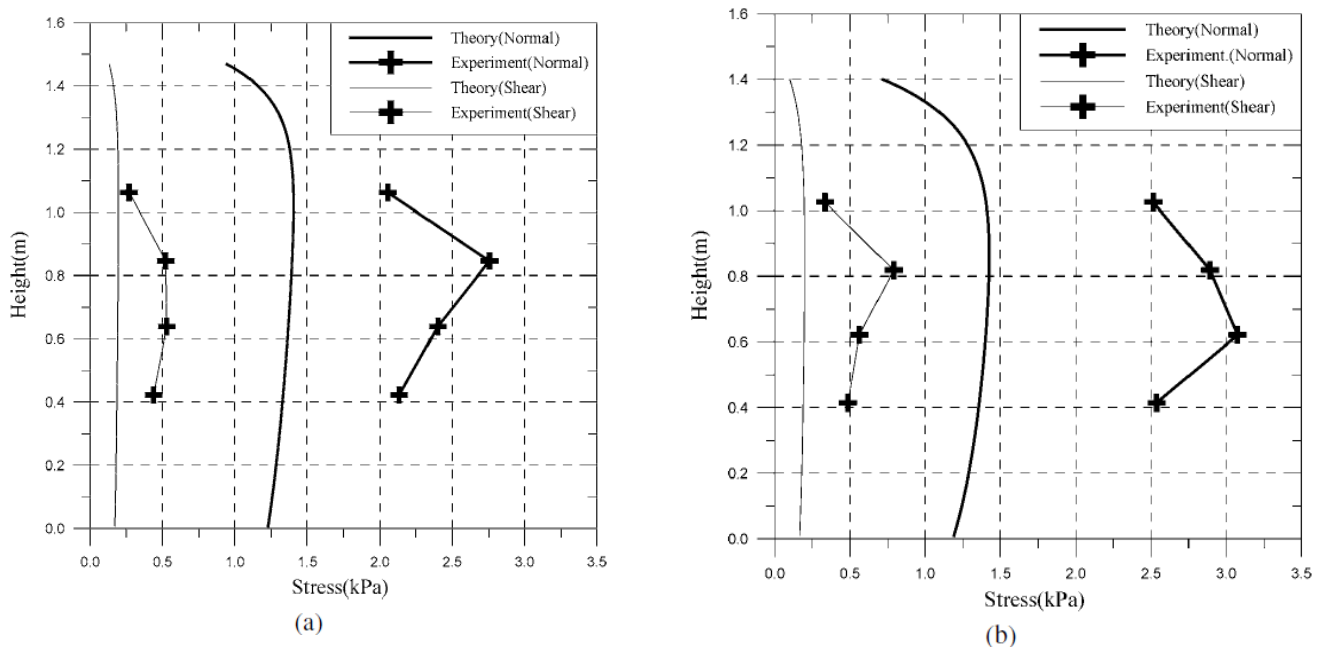


Fig. 4.8 Variations in the static normal and shear stresses with the bed height (a) hopper half angle 10° , (b) hopper half angle 20° (Chou and Chen, 2003)

Other experimental investigations have been done to measure the stress and corresponding flow pattern (Chen et al., 2005, Ding et al., 2013). These operations are however not repeatable and not cost effective. In recent times, the use of numerical techniques for the study of stresses and flow characteristics in hoppers is increasing with increasing improvements in the computational

technique and power. One of the techniques is the FEM method which has overtime gained some success in the prediction of stress and flow patterns in silos and hoppers (Goodey et al., 2006). This FEM method however regards the granular mass as a continuum which does not consider the individual particle behaviour of the granular media. The current most sought after numerical technique, DEM helps to address the particle scale behaviour of the granular media and shows a great ability to meet the requirements with quality predictions (González-Montellano et al., 2012). Recently, DEM models have been used to predict the stresses distributions and flow patterns in silos and hoppers (González-Montellano et al., 2011, Balevičius et al., 2011) and it shows a great advantage over the experimental measurements and continuum analysis.

In the present work, a conical hopper is modelled using DEM according to geometry dimensions in Table 4.1 with random filling. The particles are allowed to fall into the hopper under gravity until it reached an equilibrium state. The three-dimensional DEM is further used to investigate the stress distribution along the vertical wall at different heights within the hopper under earth, mars and lunar gravities. As discussed earlier, the measurement sphere technique is adopted and only particles with centroids contained within the measurement sphere are considered (Fig. 4.9). The maximum stress is calculated from the stress components obtained from the measurement sphere for varying internal angle of the hopper under the earth, mars and Lunar gravity levels.

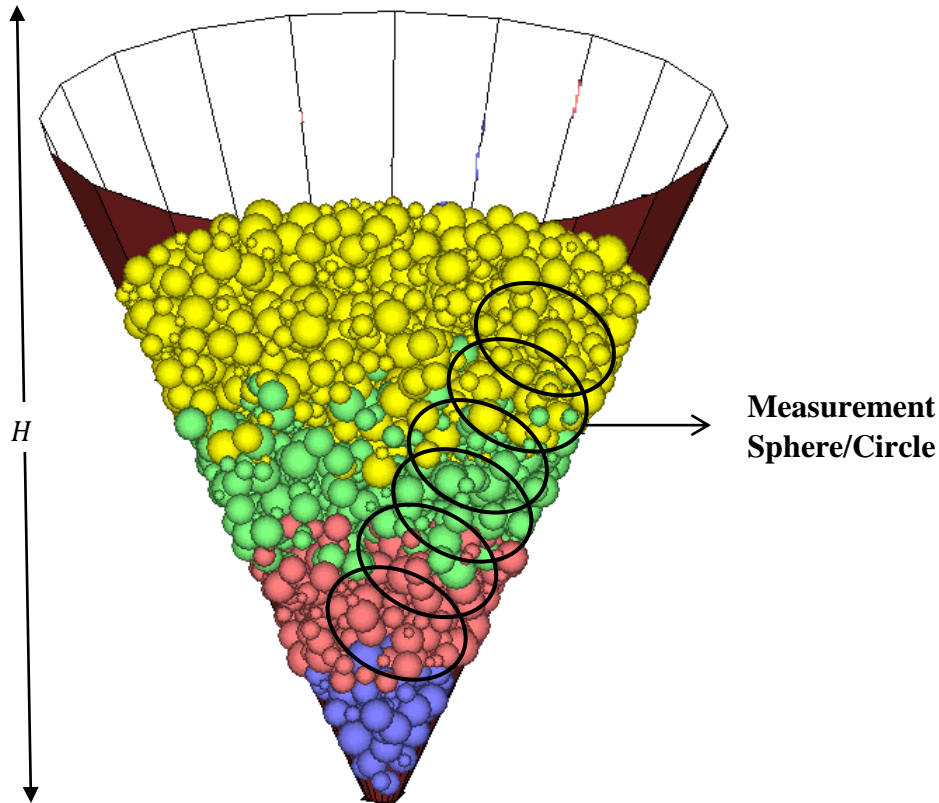


Fig. 4.9 Schematic cross section showing the measurement sphere used for stress measurement vertically along the hopper wall

4.4.1 Prediction of stress distribution along the vertical hopper walls using DEM simulations under earth gravity level

The investigations of the wall stress on the hopper walls shows the predicted wall shear stress distribution on the walls under earth gravity level (Fig. 4.10). The measurements are extracted at different heights along the hopper wall by adopting the averaging procedure as explained earlier. The first set of analysis was done along the walls of the hopper horizontally for angles 30° , 60° and 90° under earth gravity. The measurement spheres are used to compute the stress at various scanning points along the wall of the hopper. The diameter of the measurement sphere was fixed to an average value based on variation test of the diameter beyond which there is no significant change in the stress components.

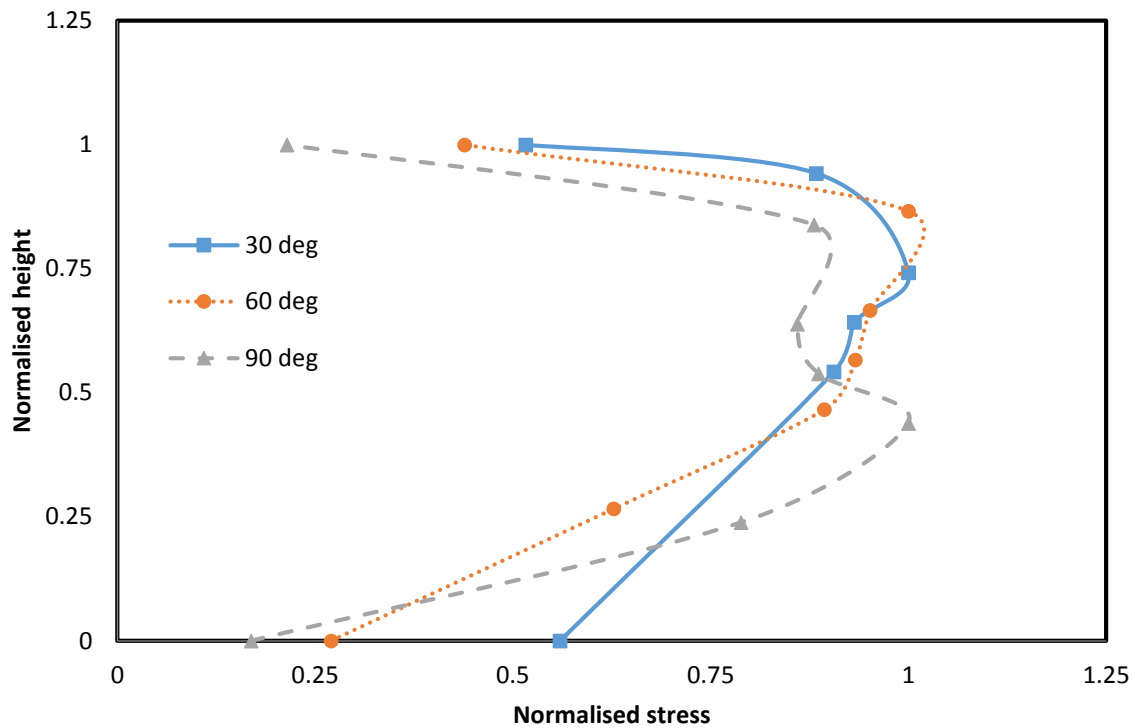


Fig. 4.10 Predictions of wall stress distribution for hoppers with internal angles of 30°, 60° and 90° using DEM simulations under earth gravity

Presented in Fig 4.10 is the shear stress distribution along the wall of the hopper. The shear stress is normalised with the maximum shear stress value for each hopper internal angle and the hopper height is also normalised with the maximum height. Through Fig. 4.10, it is found that under earth gravity, the stress has its peak at an intermediate height for all the angles investigated. The stress increases from the top of the hopper to an intermediate height and then decreases towards the zero at the hopper apex. The same trend is seen for all the angles 30°, 60° and 90°. The peak of the stress value for a 90° hopper is observed to occur at a low intermediate height compared to 30° and 60° hoppers. Also, at the hopper apex, the stress is much higher for 30° hoppers than for 60° and 90° hoppers. The presented predictions follow a trend where the filling pressure and the discharge pressure were investigated using DEM (Fig. 4.11).

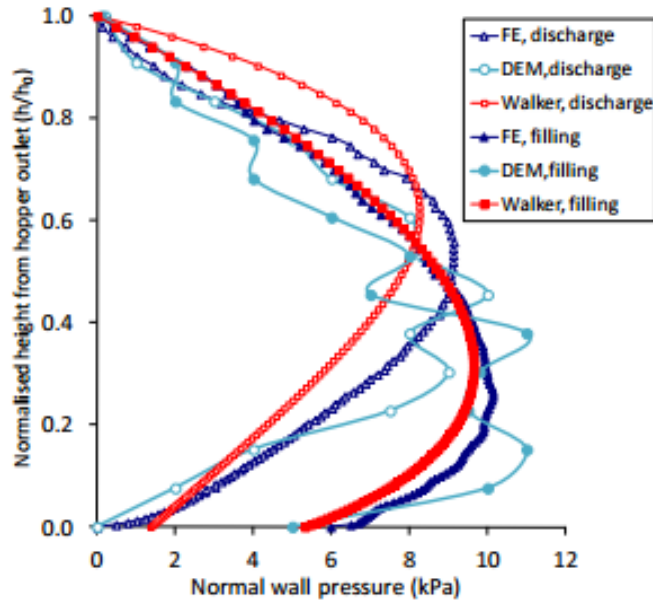


Fig. 4. 11 Comparison between numerical and theoretical predictions of wall pressure distributions for end of filling and beginning of discharge (Wang and Ooi, 2015)

It was reported that pressure peaks existed at an intermediate height at the lower part of the hopper for DEM simulations and decreases towards the upper part of the hopper (Wang and Ooi, 2015). Despite the few discrepancies with the walker’s theory, the result provided a verification of the FEM and DEM models employed to predict reliable wall pressure.

Walker’s theory (Walker, 1966) which has been extensively used as a classical theory to analyse wall stress in conical hoppers, is also employed as a comparison with the present predictions. This is done for each of the angles investigated as shown in Fig. 4.12.

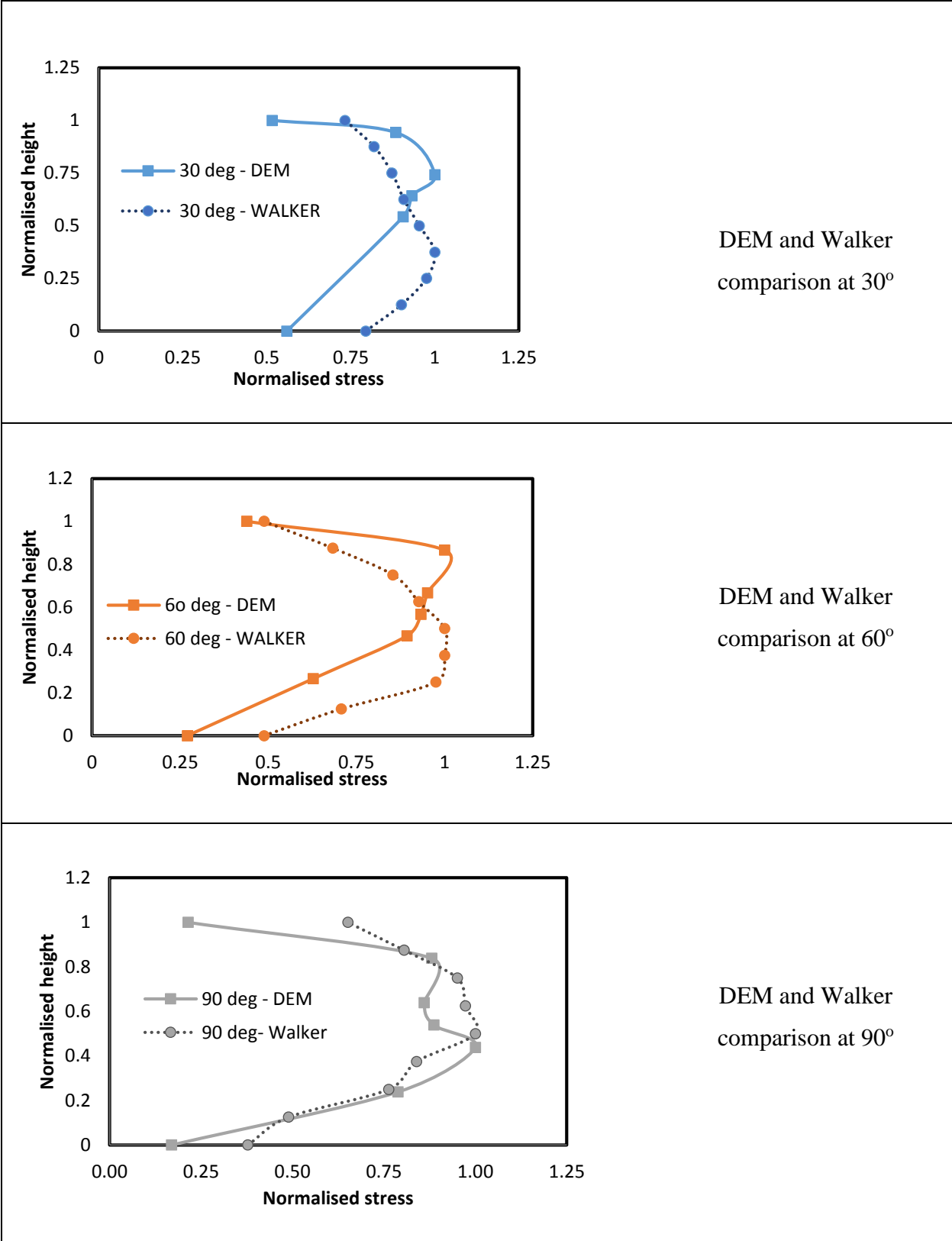


Fig. 4.12 Comparison between DEM and Walker's predictions of wall stress along the hopper for 30°, 60° and 90° under earth gravity

Through Fig. 4.12, predictions made using the DEM model follows similar and consistent trend for all angles with the classical Walker's theory. For 30° and 60° , the stress peak is seen to be at different intermediate height along the walls of the hopper, which could be related to the assumptions made in Walker's equations. However, for 90° , the stress peak is observed at similar intermediate height along the wall of the hopper. Both the numerical DEM model and the Walker's theory are applied here to predict the static shear stress. Additionally, the predicted results indicate that the assumptions made by Walker may not apply to all the different internal angles and the results show the potential of DEM simulations.

4.4.2 Prediction of stress distribution on vertical hopper walls using DEM simulations under mars and lunar gravity level

Further, the effect of gravity levels is investigated on the stress distributions along hopper walls for different hopper internal angles of 30° , 60° and 90° using DEM simulations. Gravity levels studied are the EML (earth, mars and lunar) gravity which are consistent with the previous investigation of the stress distribution across the granular bed width. These predictions are for the static stress distributions. The particles are under the influence of gravity and were filled via gravity filling randomly as initially explained. Results showing the stress distributions along the hopper walls using three dimensional DEM for lower gravity simulations are presented in Fig. 4.13.

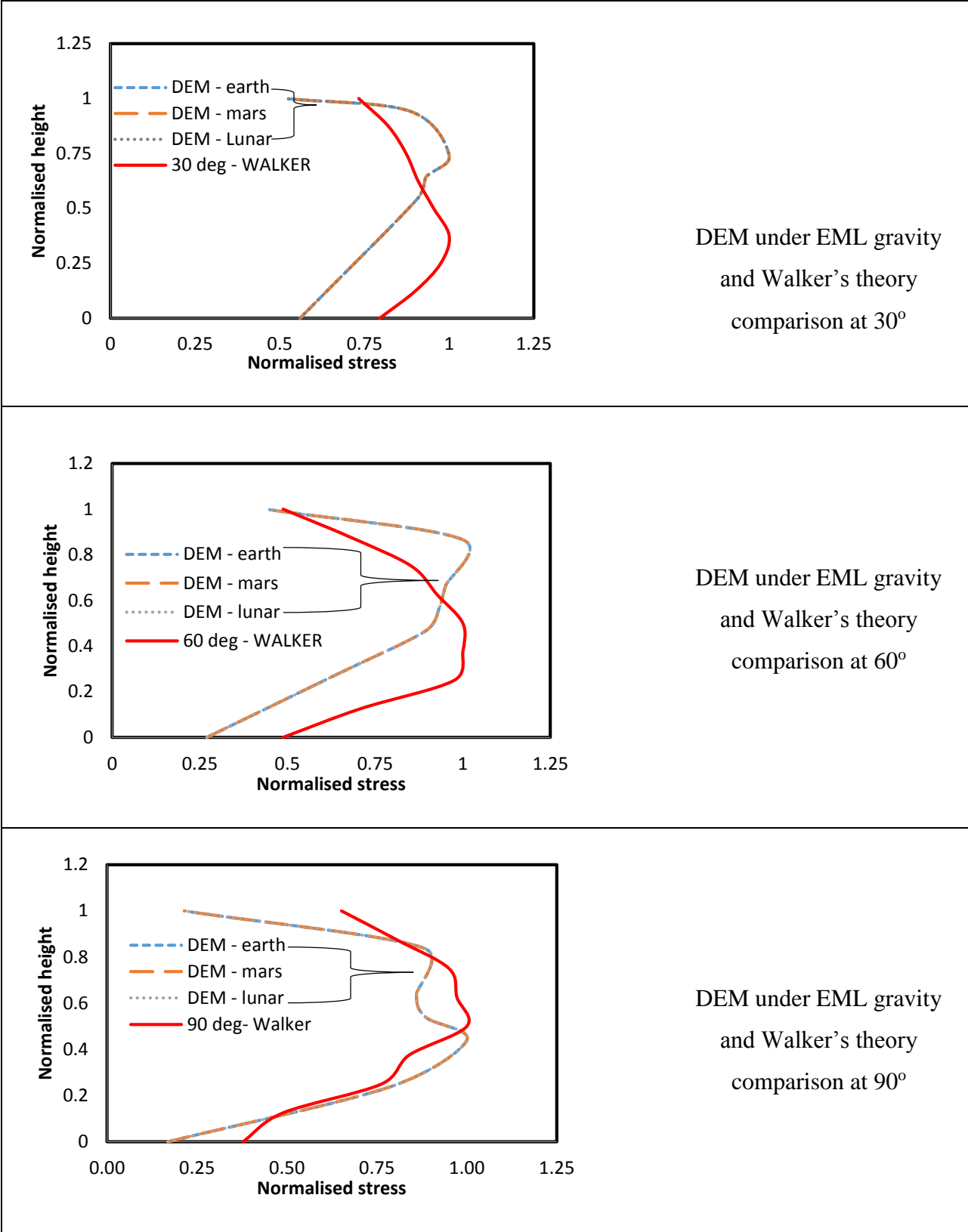


Fig. 4.13 Superimposed plot for shear stress distribution vertically along the hopper walls for 30°, 60° and 90° under earth, mars and lunar gravity using 3-dimensional DEM simulations

This indicate that gravity does not necessarily affect the stress distribution of the material even on the hopper walls. This has been discussed earlier given that gravity plays no role in the static stress distribution across the bed. The hopper angle effects however, still exist under low gravity and expected to behave similarly under earth, mars and lunar gravity. Again, it is to note that further investigations on the dynamic stress distributions may prove otherwise regarding the effect of gravity.

4.5 Conclusion

The discrete element method has been applied to describe the stresses that develop in hoppers across the granular bed and along the hopper walls under the earth, mars and lunar gravities. Experiments were also carried out to support the predictions of the stress distributions existing across a granular bed in the hopper under earth gravity. The results obtained from experiments were used to complement the DEM results under earth gravity alone while the DEM simulations were applied to the stress distribution predictions under mars and lunar gravities. The stress distributions along the hopper walls were compared with the classic Walker's theoretical predictions under earth gravity and further estimated under mars and lunar gravities.

The maximum stress distributions evaluated using three dimensional DEM simulations were observed to correlate with the PSAT experimental results. The predictions indicate that the granular materials close to the hopper walls tend to be highly stressed compared to the granular materials towards the mid hopper. The static stresses tend to reduce towards the mid hopper from both ends of the hopper walls. The stress distribution was also observed to depend on the hopper opening angle and at 30° the stresses were predicted to be almost uniform in the granular bed across the hopper horizontally. The mid hopper is seen to have the lowest stress at the 90° hopper opening and this can be related to the type of flow expected during the hopper design. The PSAT and DEM results were observed to be similar under earth gravity. The stress distribution predictions were then extended in a new dimension under the mars and lunar gravity in view of the ongoing and proposed space exploration. This novel concept was established using DEM simulations for different hopper opening internal angle which was compared with the DEM results under earth gravity. Conclusions from the results show that gravity plays little or no role in the stress distribution of the granular materials under static conditions. Same materials were used

under earth, mars and lunar gravity. The effect of the opening angle was however still observed under mars and lunar gravity as seen under earth gravity.

The stress along the hopper walls were then predicted using DEM simulations and supported by the theoretical Walker's theory (Walters, 1973b). After filling the granular materials, the maximum stress on the wall observed to be at an intermediate height along the walls and not at the beginning or outlet of the hopper for all hopper opening angles 30° , 60° and 90° investigated. It is also concluded that gravity does not affect the distribution of the static stress along the hopper walls and the distribution is similar to the response predicted under earth gravity.

For the first time, three dimensional DEM has been developed and applied to probe and predict the stress distribution under static filling in granular bed in a hopper under earth, mars and lunar gravities. More complex behaviour may be experienced in dynamic stress distribution under these gravities which is proposed for future work. The novel work done to predict stress distribution in this study is currently under proposed application practically in Mars and Moon exploration and will serve as a benchmark for further dynamic stress studies. In this sense, the simulated synthetic material provides a single framework within which a large spectrum of behaviours exhibited by solid materials can be captured under different gravity levels.

Concerning the complexities of predicting and evaluating stresses in granular materials which is a complex task, the current research has clearly shown the usefulness, reliability and excellence of characterizing the particle scale properties realistically and feeding them into DEM modelling which is validated in view of the above comparisons. This further gives confidence and allow researchers to postulate and test micro-mechanisms and, if successful, predict behaviours that cannot yet be encompassed by existing experimental or continuum theories as reported in the following chapter where dynamic evaluations are performed using DEM simulations.

Chapter 5

EFFECTS OF GRAVITY ON GRANULAR FLOW: SOME THEORETICAL APPROACHES AND DEM SIMULATIONS

5 Effect of Gravity on Granular Flow: Some Theoretical Approaches and DEM Simulations

In this chapter, initially, two types of theoretical approaches viz., (i) Discrete Layer Approach (DLA) and (ii) Kirya's structural model are considered to evaluate the gravitational flow characteristics of granular materials. It is worth stating that DLA approach does not explicitly account for the gravity term, but is used implicitly to qualitatively evaluate the characteristics of granular flow inside the hoppers under various discharge regimes. Then, DEM simulations are performed to evaluate the flow characteristics of grains under low gravity and the results are compared with Kirya's model predictions. The last part of this chapter deals with comparing qualitatively certain flow characteristics predicted by DEM with experimental parabolic flight test results.

5.1 Analysis of Granular Flow using Discrete Layer Approach (DLA)

This section provides results obtained from continuum modelling parametric studies in predicting granular flow using the discrete layer approach (DLA). Investigations have been carried out to estimate the gravitational flow behaviour of granular particles based on continuum theories. The continuum based theories are carried out to understand the macroscopic behaviour of the granular material using DLA which is basically a hybrid Lagrange continuum approach. The model accounts for factors such as the flow rate, discharge completion time, velocity, Lagrange coordinate, hopper geometry which captures the large particle height, internal angle and hopper width opening. Results regarding each of these individual factors and their influence on granular flow are presented and discussed in detail here.

5.1.1 Discrete layer approach model and parameters used in granular flow investigation

The behaviour of granular particulates is estimated based on hybrid Lagrange continuum theories in a hopper (Fig. 5.1). Fig. 5.1 depicts the geometry of the dosing station (DS) as used in the Sample Preparation and Distribution System (SPDS) as much as possible. The flow characteristics is predicted by developing a one-directional Lagrangean flow model in which it is assumed that the media flow out with the intensity Q (m^2/s) with a large particle existing in the media with

height h . This assumes that the dimensions of the hopper along the thickness direction are sufficiently long so that the flow properties are independent of the thickness direction. Hence, flow rate is simplified in m^2/s unit in this case only. Fig. 5.1 shows a schematic illustration of the geometry and parameters used to define the geometry. The initial position of the granular material contained within the geometry is presented in Table 5.1.

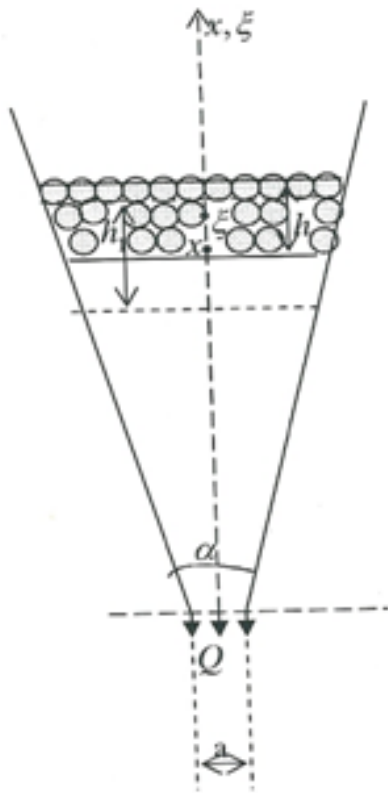


Fig. 5. 1 Schematic cross section of DS bounded by walls

where h and h_1 are depth of a typical granular layer under consideration at time 0 and t respectively; Q is the flow rate; a , is the width of the slit opening; x, ξ are the Euler and Lagrangean coordinates.

Table 5.1 System description outlining type of investigation and parameters used in DLA model for granular flow investigation

Type of Investigation	Parameter description
Effect of Lagrange coordinates , ξ	(1) $\xi = 1\text{m}$ and 2m (2) $Q = 0.2\text{m}^2/\text{s}$ (3) $a = 0.1\text{m}$ (4) $\alpha = \pi/3$ (5) $h = 0.001\text{m}$
Effect of flow rate Q on discharge completion time	(1) $\xi = 0.2\text{m}$ and 0.3m (2) $Q = 0.001 - 0.005\text{m}^2/\text{s}$ (3) $a = 0.1\text{m}$ (4) $\alpha = \pi/3$ (5) $h = 0.001\text{m}$
Internal angle on granular discharge completion time	(1) $\xi = 0.2\text{m}$ and 0.3m (2) $Q = 0.003\text{m}^2/\text{s}$ (3) $a = 0.1\text{m}$ (4) $\alpha = \pi/2, \pi/3, \pi/4, \pi/5, \pi/6$ (5) $h = 0.001\text{m}$
Hopper slit opening on granular flow	(1) $\xi = 0.2\text{m}$ and 0.3m (2) $Q = 0.001 - 0.005\text{m}^2/\text{s}$ (3) $a = 0.04 - 0.2\text{m}$ (4) $\alpha = \pi/3$ (5) $h = 0.001\text{m}$
Particle velocity on completion time	(1) $\xi = 0.3\text{m}$ (2) $Q = 0.003\text{m}^2/\text{s}$ (3) $a = 0.1\text{m}$ (4) $\alpha = \pi/3$ (5) $h = 0.001\text{m}$
Particle height on granular discharge completion time	(1) $\xi = 0.2\text{m}$ and 0.3m (2) $Q = 0.003\text{m}^2/\text{s}$ (3) $a = 0.1\text{m}$ (4) $\alpha = \pi/3$ (5) $h = 0.001\text{m}$

The Lagrange coordinate, ξ is employed as the initial coordinate of the centre of the large particle with the conditions as;

$$\begin{cases} t = t_o : x = \xi \\ t > t_o : x = f(\xi, t) \end{cases} \quad (5.1)$$

where x = the Euler coordinate of the centre of the large particle and t is the time in seconds. The area of the large particle is assumed to be constant since the media is incompressible and the

following formulas were derived to use as a model to analyse the behaviour of the granular particulates.

$$x = \frac{h}{h_1} \left(\xi + \frac{1}{2 \tan \alpha_1} \right) - \frac{1}{2 \tan \alpha_1} \quad (5.2)$$

$$h_1 = (h_{11} - h_{12}) / \tan \alpha_1, \quad \alpha_1 = \alpha / 2 \quad (5.3)$$

$$h_{11} = \sqrt{\left(\xi \tan \alpha_1 + \frac{a}{2} + \frac{h}{2} \tan \alpha_1 \right)^2 - (t - t_o) Q \tan \alpha_1}, \quad (5.4)$$

$$h_{12} = \sqrt{\left(\xi \tan \alpha_1 + \frac{a}{2} - \frac{h}{2} \tan \alpha_1 \right)^2 - (t - t_o) Q \tan \alpha_1}, \quad (5.5)$$

A one-directional Lagrangean flow model was developed to aid the prediction of flow characteristics. The schematic representation of the geometry and parameters used to define the geometry and initial position of granular material which is contained within the geometry is represented in Fig 5.1. Two different heights of the hopper were considered in this study i.e. when $\xi = 0.2$ and $\xi = 0.3$ as case 1 and 2 respectively. The results were analysed by tracking the position x of the topmost thin discrete layer as it moves from time = 0, t_o to a time t . The time to empty T_{empty} which will further be analyzed corresponds to the time when x approaches or equal zero.

5.1.2 Effect of height of the granular filling (Lagrange coordinates , ξ) in the hopper

Here, the analysis is based on the conditions associated to the Lagrange coordinate ξ as represented in equation 5.1. The flow of the particle is monitored by estimating the time required to empty the hopper media for different cases of ξ as a function of the position x of the layer with time, t .

The result was observed to comply with the conditions imposed where at time, $t = 0$, $x = \xi$ and at a higher Lagrange coordinate, ξ (initial coordinate of center of large particle), the time required to complete one dimensional granular flow through the media increases.

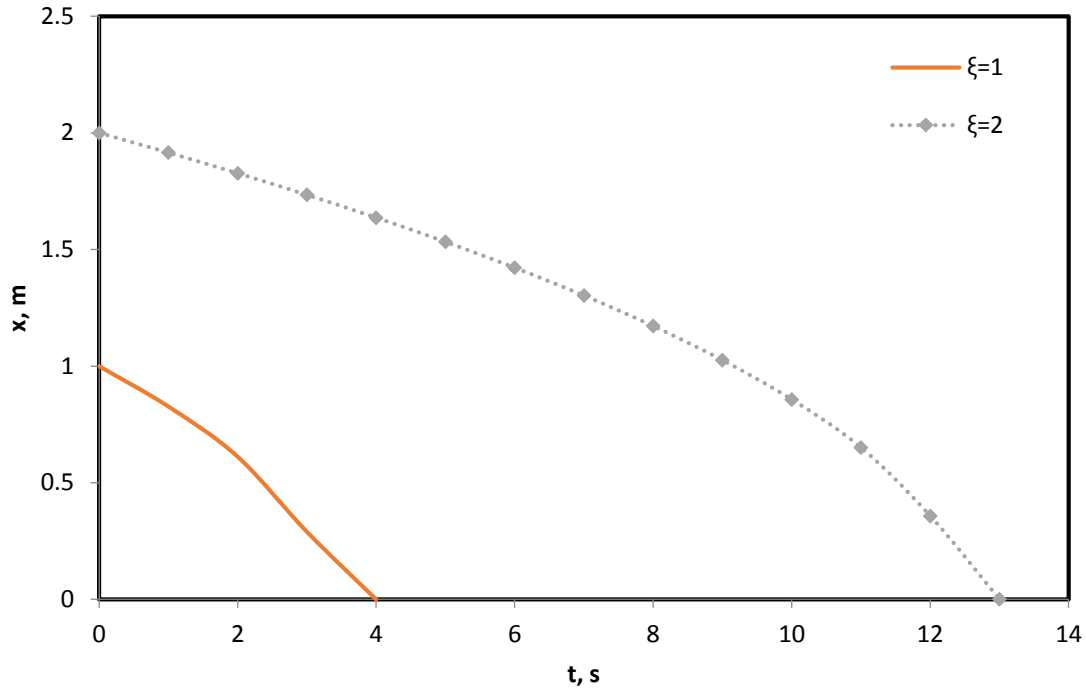


Fig. 5.2 Variation of Lagrange coordinates, ξ within the media

The result from Fig. 5.2 thus indicate that for both $\xi = 1$ and 2, as the completion time increases, the Euler coordinate of centre of large particle (which is a function of ξ and time t) decreases until it reaches approximately 0.

5.1.3 Effect of flow rate Q on discharge completion time

Previous analysis has shown that the conditions imposed on the application of the Lagrange coordinate ξ have been met. As a result, further analysis has been done on estimating the flow rate and its effect on the time required to empty the particle from the hopper media. The value for the Lagrange coordinate ξ used in this analysis is 0.2 and 0.3 and other values as given in Table 5.1.

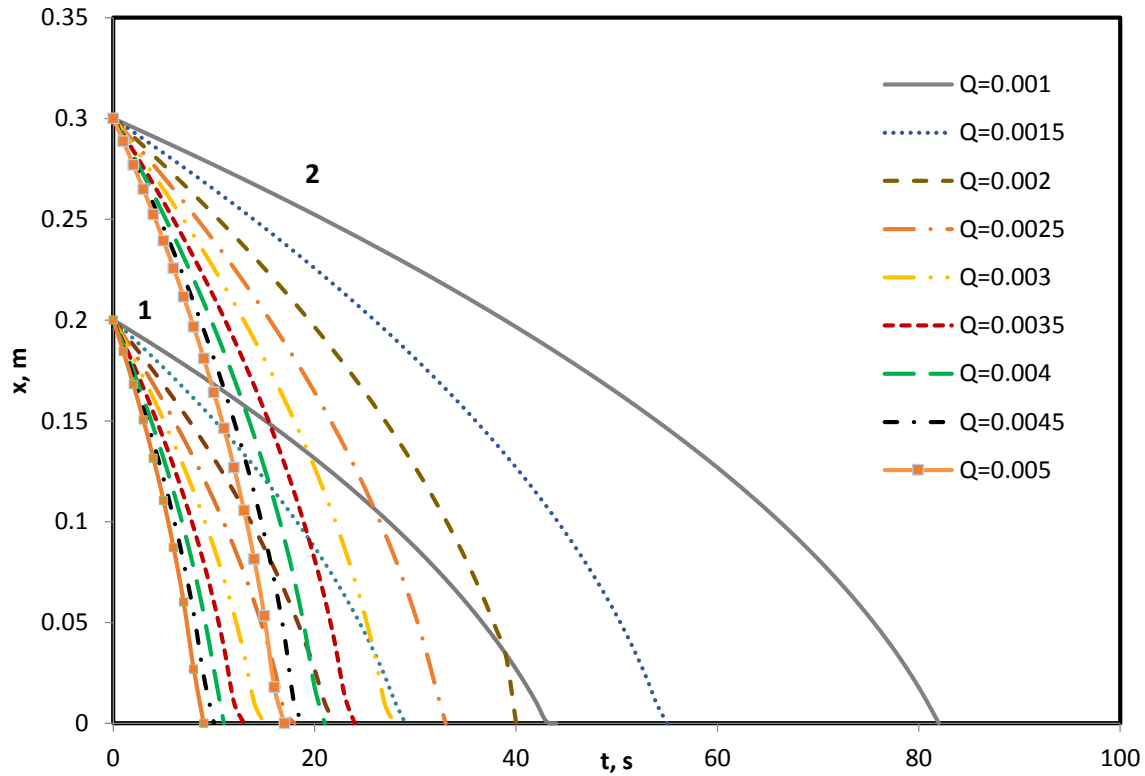


Fig. 5.3 Effect of flow rate on completion time using DLA model

The results presented in Fig. 5.3 indicates that as the flow rate reduced, the completion time increased and it was deduced that low flow rates leads to higher completion time for the granular flow of one dimension through the media. As can be seen from Fig. 5.3, for the Lagrange coordinate $\xi = 0.3$ at a low flow rate of about $0.001\text{m}^2/\text{s}$, the completion time was observed to be about 82 seconds while for flow rate of $0.005\text{m}^2/\text{s}$ the completion time was about 17 seconds which is very low.

A further study is done to check the relationship between the time to empty the media (completion time) and the flow rate for both $\xi = 0.2$ and 0.3 respectively.

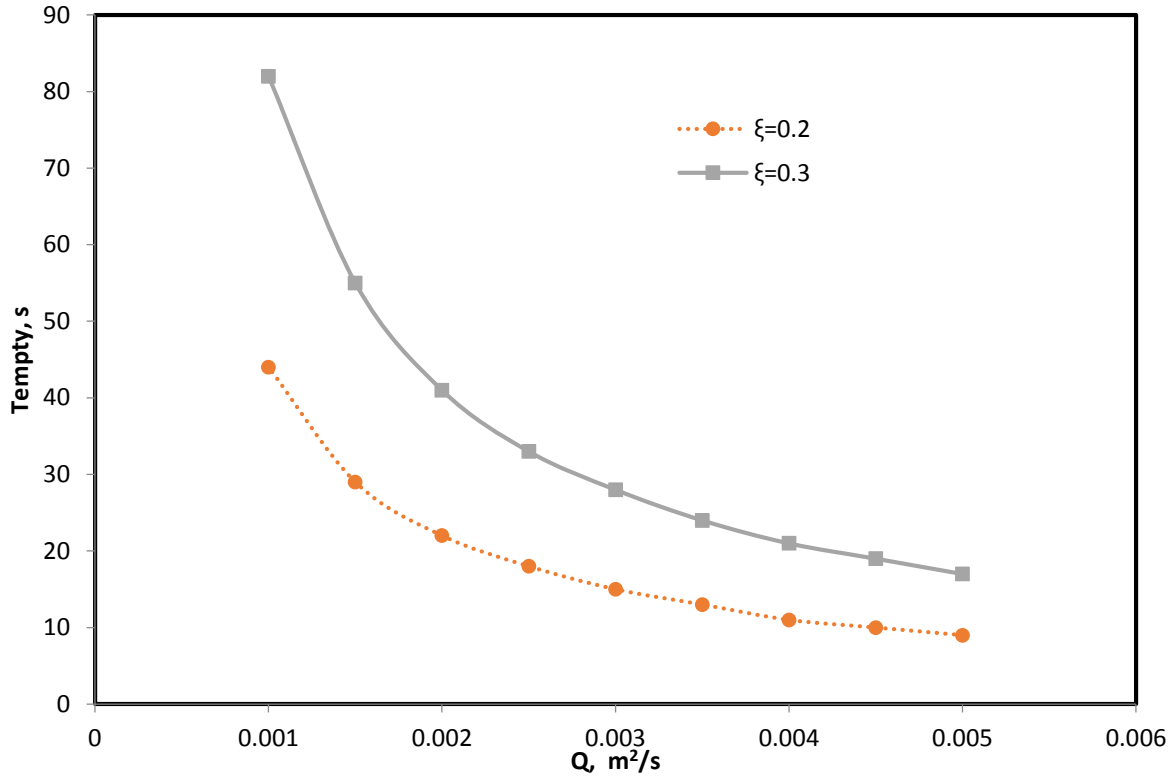


Fig. 5.4 Time to empty the hopper with flow rate variation using DLA model

As expressed in Fig. 5.4, results further indicate that the time to empty the hopper completely decreased as flow rate, Q increased. This implies that granular materials flowing out of a hopper at high flow rate will take shorter time to be completely emptied and at a lower granular flow, the time required to completely empty the hopper is high. This agrees with theoretical reasons (Schulze and Schwedes, 1990) as well as practical applications. The DLA model also tends to indicate that at some very high flow rate, the impact of the Lagrange coordinate ξ may not be effective.

5.1.4 Internal angle on granular discharge completion time

As discussed in chapter 2, hopper internal angle is a factor in theory that could impact granular flow (Mazumder et al., 2008). In view of this, the variation in the internal angle is represented in Fig. 5.5 with the initial coordinate ξ set at 0.2 and 0.3 respectively. The same trend still exists for the impact of the Lagrange coordinate ξ but as the hopper angle increased from 30° ($\pi/6$) to 90° ($\pi/2$), the completion time increased.

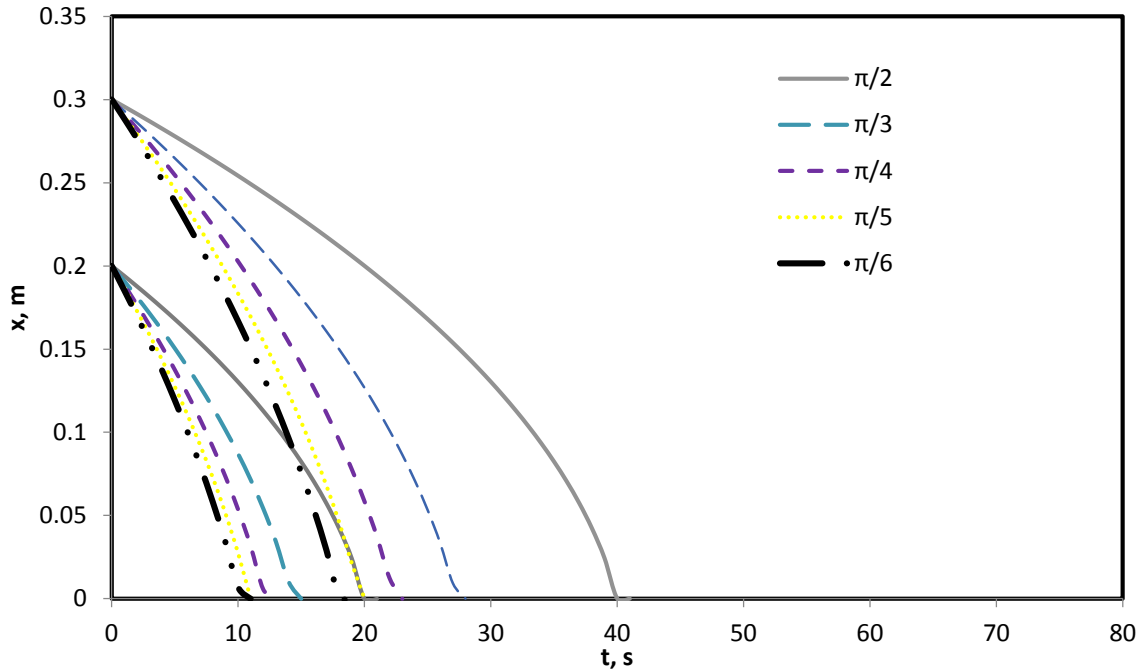


Fig. 5.5 Variation of the internal angle α for $\xi=0.2$ and 0.3 respectively using DLA model. The comparison of theoretical (Rose and Tanaka, 1959) and experimental results (Albaraki and Antony, 2014) obtained from literature for flow properties of grains under earth gravity indicate that the discharge rate is the highest for the lowest internal angle. The discharge rate is then related to the time in which it took for the hopper to be completely emptied as shown in Fig 5.6.

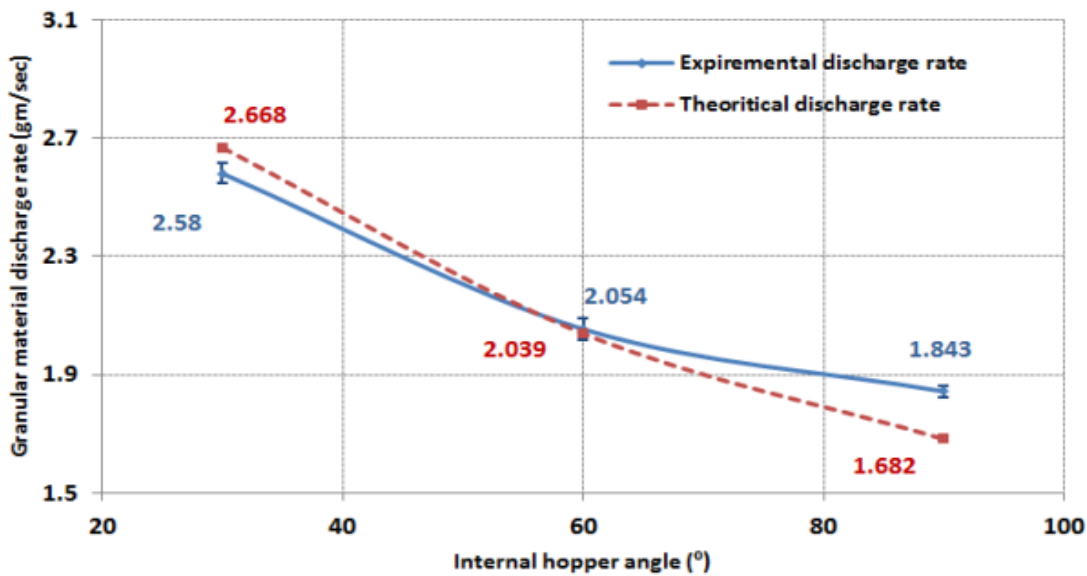


Fig. 5.6 Comparison of the theoretical and experimental discharge rates at different internal hopper angle (Albaraki and Antony, 2014)

Results obtained experimentally by Albaraki and Antony (2014) were qualitatively compared with results reported in this study represented in Fig. 5.7. The analysis was done to further represent the completion time as a function of the hopper angle for $\xi = 0.2$ and 0.3 .

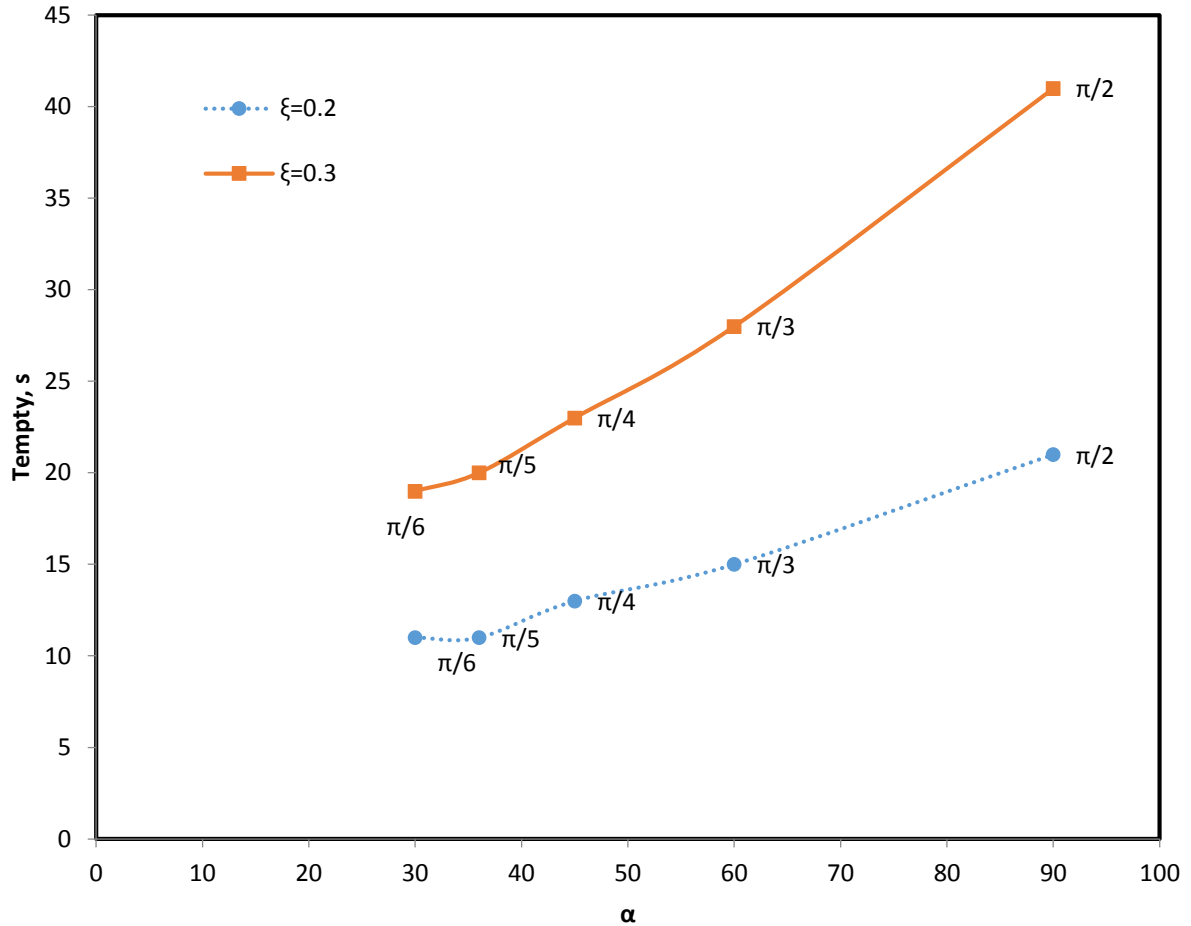


Fig. 5.7 Time to empty the hopper (completion time) with the hopper angle (α) variation

Following the analysis of the result presented in Fig. 5.7, it was clearly predicted that the hopper internal angle will affect the granular flow. The time required to empty the hopper is predicted to increase with internal angle (Antony and Albaraki 2014). Further analysis is done using the DEM simulations in later chapters to further establish the impact of the internal angle on granular flow.

5.1.5 Effect of hopper orifice opening width on granular flow

As reported in chapter two, research in early years proposed that granular flow is dependent on both the nature of particles and hoppers. It has been shown from Beverloo's equation presented in equation 2.21 that granular flow rate is dimensionally proportional to $\rho g^{1/2} D_0^{5/2}$ (Beverloo et al., 1961, Mankoc et al., 2007) where D_0 is the hopper orifice opening. The hopper orifice outlet can be said to be a very important factor that can impact the time required to empty the hopper which in turn impacts the granular discharge rate. It can then be confidently established that a power law relationship holds between the rate of flow of the material and the size of the hopper orifice which is given by a general relationship in equation 5.6.

$$W = A(D_0)^n \quad (5.6)$$

This indicates that the granular flow rate of material increases with the increase in the outlet size. Using the DLA model in the same trend as seen earlier, the relationship between the time to empty the hopper media (completion time) and the hopper outlet size a , is investigated for both $\xi = 0.2$ and 0.3 respectively. The initial analysis was carried out for different flow rates when the outlet size $a = 0.05\text{m}$ and 0.2m as presented in Fig. 6.8. All other parameters are as given in Table 5.1.

Results presented in Fig. 5.8 follow same trend for the different Lagrange coordinate ξ as reported earlier. However, interestingly, the time required to empty the hopper was seen to be high for larger outlet size of the hopper which is contrary to some reports from literature. The result indicated that the time to completely empty the hopper increases with the hopper outlet size.

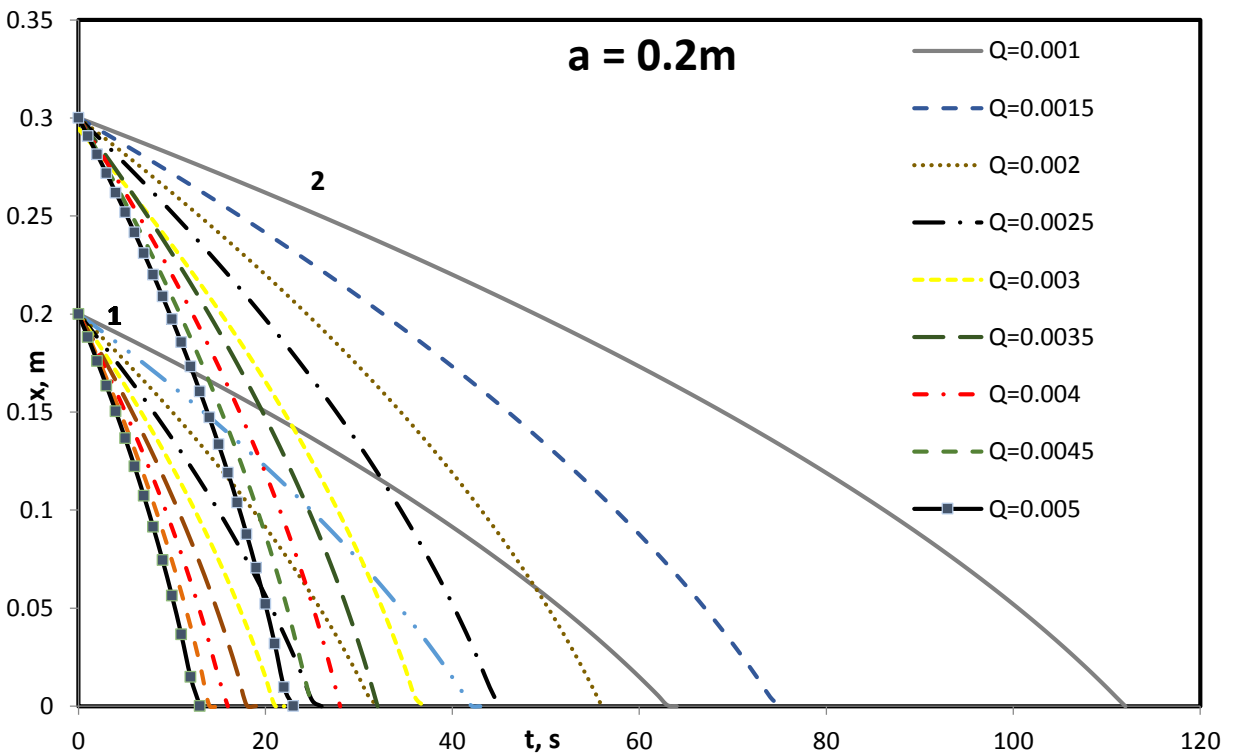
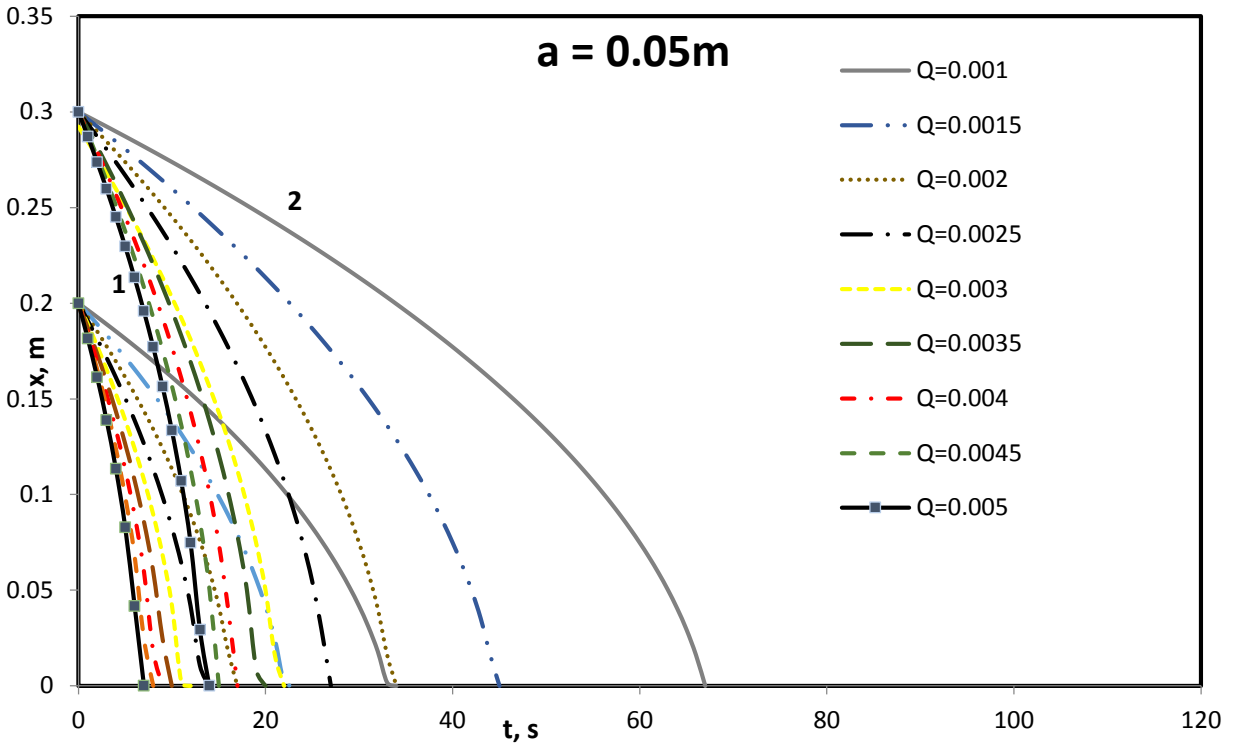


Fig. 5.8 Effect of flow rate on varying hopper orifice opening a for both 0.05m and 0.2m

Further results are presented in Fig. 6.9 to represent the time to completely empty the hopper with the granular flow rate for different hopper outlet sizes a of 0.05, 0.1 and 0.2m at $\xi = 0.3$.

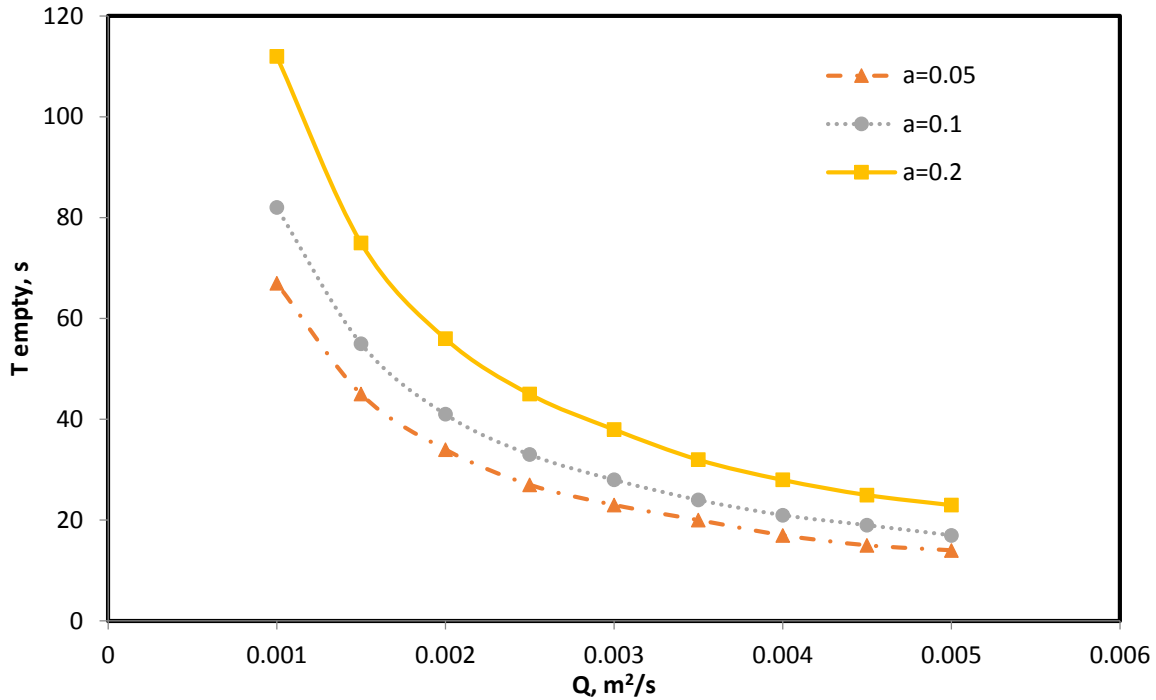


Fig. 5.9 Time to empty the hopper against flow rate Q for different hopper outlet size at $\xi = 0.3$

It can then be deduced from Fig. 5.9 that below flow rate $Q = 0.003m^2/s$, there is a significant change in the completion time but above the said value, there is no much difference in the completion time. This aids the conclusion that $0.003m^2/s$ is a reasonable flow rate to be used at $\xi = 0.3$. The hopper outlet size was observed to vary in contrast to literature in which even at same flow rate, more time was required to completely empty the hopper at larger outlet size than at lower outlet size. This is further analysed for various hopper outlet sizes as a function of the total empty time as represented in Fig. 5.10.

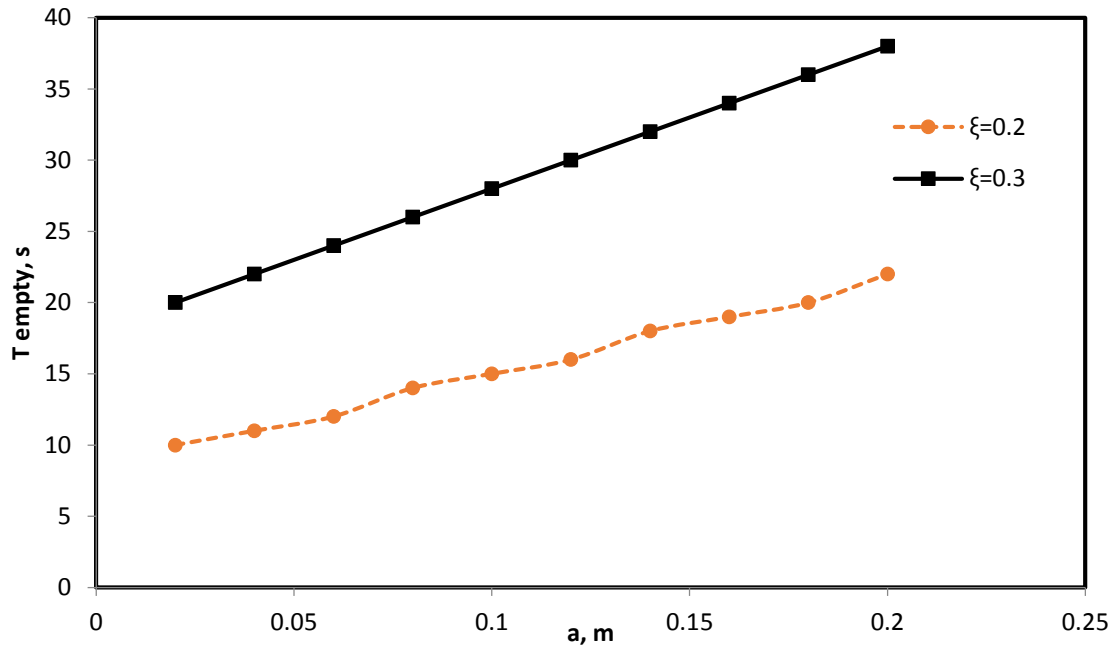


Fig. 5.10 Time to empty hopper against hopper outlet size for $\xi = 0.2$ and 0.3

Results shown in Fig. 5.10 further helps to establish that using the DLA model developed, the effect of the hopper outlet was not as expected. This is deduced from the outcome which indicated that an increase in the outlet size is directly proportional to increase in the time required to empty the hopper. This can be attributed to the assumption that an increase in the hopper orifice may imply a bigger or larger hopper and thus, for a bigger hopper, there will be more granular particles which will lead to an increase in the completion time. Also, as reported by Mankoc et al. (2007), the $5/2$ power law which is generally accepted to determine the effect of hopper orifices on flow rate are satisfactory only for small range openings. Improvements may be made on this DLA model to help account for the differences in the hopper outlet orifice impact on granular flow.

5.1.6 Particle velocity on completion time

The DLA model was also used to further monitor the velocity profile of the particle during granular flow in the hopper. The particle inside the hopper was tracked in both space and time to obtain the velocity properties. Continuum equations have been developed previously by Nedderman and Tüzün (1979) from a constitutive law relating the horizontal velocity and downward velocity gradients. This model has been used in various experiments (Nedderman and Tüzün, 1979, Tüzün et al., 1982) with some researchers disagreeing with the constants used within the model

(Samadani et al., 1999, Choi et al., 2005). The simple DLA model proposed in this study was observed to help capture the velocity along the hopper length during flow all through to the orifice.

The velocity of the particle was studied as the completion time for the granular flow of one dimension through the media changes with time using equation 5.7.

$$v = \frac{dx}{dt} = -\frac{1}{2} \frac{hQ}{h_1 h_{11} h_{12}} \{ \xi \tan \alpha_1 + a/2 \} \quad (5.7)$$

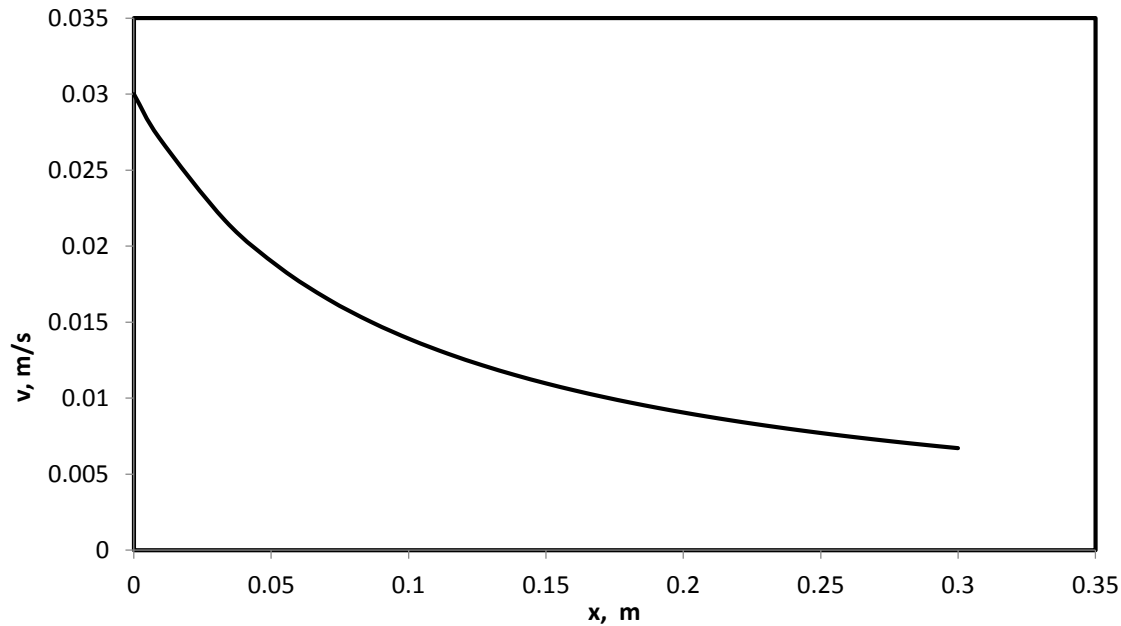


Fig. 5.11 Velocity gradient with x at $\xi = 0.3$

The outcome of the velocity gradient investigation is represented in Fig 5.11 and it indicates that at lower values of x i.e. as the granular flow of one dimension through the media approaches the exit, the velocity increases. This implies that the velocity is at a maximum at the exit of the hopper during granular flow (Cox and Hill, 2005).

5.1.7 Particle height on granular discharge completion time

The effect of the particle height represented by the granular layer on granular flow is investigated using the DLA model. Studies have shown the difference in fluid flow rheology and granular flow rheology. It is known that pressure at a point at a Newtonian fluid depends on the height of the fluid, density and acceleration due to gravity and hence it can be said that flow rate decreases with the height of the fluid. However, this does not hold for granular flow as the pressure at any point

in a granular material is largely independent of the height of the material. Therefore, contrary to fluids, for a gravity discharged hopper, the flow rate does not depend on the granular layer (Mankoc et al., 2007). Generally, in past studies, it has been found experimentally that the height of a granular material has no significant influence on flow rate. Good theoretical reasons for the observations are described by Nedderman (1992) and Nedderman et al. (1982) among many others. The height, h of the large particle is investigated during flow to determine if there will be any change in the time required to complete the granular flow with the centre of the particle using the DLA model. This is literally supposed to have little or no effect with its tolerance at 0.001. Thus, h is varied from 0.001 to 0.1m with $x = x/a$. All parameters used in this investigation are as reported in Table 5.1.

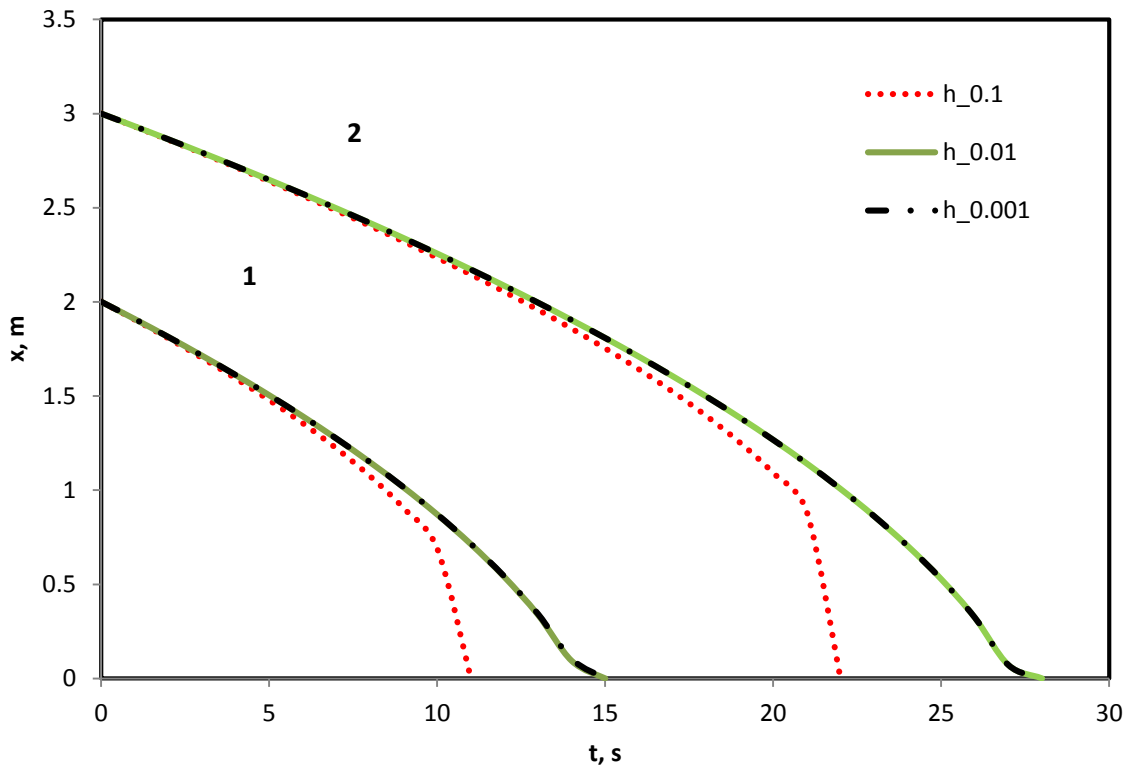


Fig. 5.12 Effect of particle height, h on the completion time for the granular flow of one dimension through the hopper media

Fig 5.12 indicates that between height $h = 0.01\text{m}$ and $h = 0.001\text{m}$ for both cases of $\xi = 0.2$ and 0.3 , there was no difference and the tolerance level was below 0.001. However, when h was increased to 0.1m , the completion time for both cases reduced. This effect can be related to the Janssen effect (Janssen, 1895) which ideally indicate that when the thickness of the layer is

greater than a value close to 1.2 times the diameter of the hopper, the pressure at the bottom of the hopper will saturate due to the Janssen effect which makes the flow rate constant (Mankoc et al., 2007). This indicates that a limit will exist for the magnitude of the height to have reasonable effect on granular flow.

The data obtained by varying various properties and hopper dimensions enables the testing of the DLA model of gravity flow inside the hopper geometry thoroughly. The achieved results in this section have provided a solid foundation in further applying the gravity influence developed using another continuum approach, Kirya's structural model in the next section and later compared with the discrete element model (DEM).

5.2 Influence of Gravitational Field on Granular Flow Using Kirya's Structural Model (Continuum Analysis)

The objective of this section is to investigate the impact of different gravity on the discharge rate of granular materials from hoppers. Following up on the DLA model to account for the gravity term, Kirya's structural model which is a continuum approach was used to carry out this investigation. The results obtained for predicting the gravity effect on granular flow are provided and discussed in detail in this section.

Gravity-driven flow of granular materials is very vital in the understanding of the planet to respond to varying gravitational fields. This is also important for human exploration and construction on the Moon and Mars in the near future. Gravity has been predicted to influence the particle collision as well as velocity under different gravity conditions of dense gas particle flows in gas-fluidization reactor (Liu et al., 2010). Due to the lower gravity levels on terrestrial surfaces, the flow behaviour of the regolith under variable environmental conditions is fairly unknown. Most granular shear flow from industrial applications (processing of grains, ore and pharmaceutical) to geological situations (including landslides and sand piles on a beach) to space explorations (EXOMARS) have their determinant factor as gravity, but the effect of variable low gravity acceleration is largely unexplored. Low gravity experiments such as using parabolic flights are expensive, yet low gravity levels are only available for a short duration. Although several previous investigations both experimentally and theoretically have been done on discharge rate of granular materials under 1g (earth gravity), a number of uncertainties and unanswered questions still remain. Further, more

intrusive virtual experiments using theoretical/modelling approaches are not yet well understood for low gravitational granular flows. At a microscopic or particle scale, granular materials are known to be discrete with discontinuous physical properties with respect to position and time while at a macroscopic or bulk scale; it is a continuum system with continuous physical property (Zhu et al., 2005). Based on these considerations, this section will focus on the prediction of flow rate of granular materials under varying low gravity in hoppers using the Kirya's structural model. The results presented here as well as other results obtained earlier using the DLA approach under 1g provide a platform for further investigations on how particle-scale properties influence the flow properties of granular materials under varying levels of gravity conditions.

5.2.1 Gravity effect of granular flow using Kirya structural model

The continuum based theory proposed, developed and applied to predict the influence of gravity on granular flow rate is based on the Kirya structural continuum model for non-cohesive flow (Kirya, 2009). This is used to study the exit velocity of granular material through the chunk of the medium. This approach is aimed at understanding to what extent gravity can affect the granular flow rate from the hopper as shown in Fig. 5.13.

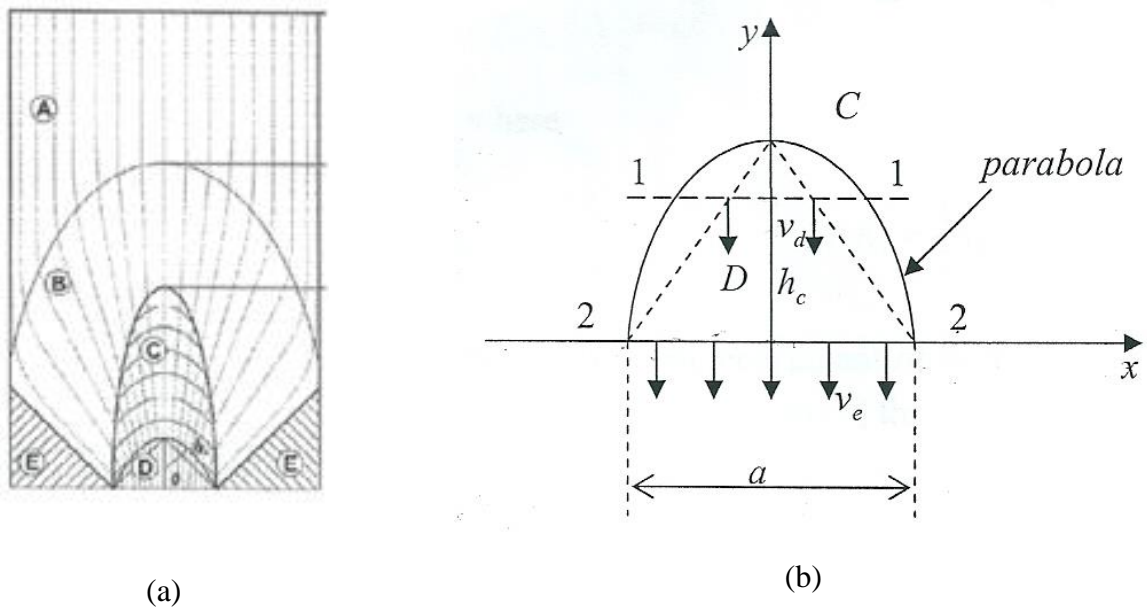


Fig. 5.13 (a) Zone of flow out of the granular particles. (b) Expanded view of Zone D

Considering the exit zone, D, of a hopper as represented in Fig. 5.13a, there is a collision of the granular particles with each other continuously and in a chaotic movement. The granular material

in this zone is said to be in free disperse state and the movement can be described by the Navier Stokes equations for granular materials. The boundary between dynamic arc C, and the exit flow, zone D can be illustrated using the Moor circle which can then be represented in the form of a parabola as shown in Fig. 5.13b. This can further be expressed mathematically from the parabola in Fig. 5.13b as:

$$y = h_c \left[1 - \left(\frac{2x}{a} \right)^2 \right] \quad (5.8)$$

Where h_c represents the height of the parabola which can also be defined as:

$$h_c = \frac{a}{4} \frac{1 + \sin\varphi}{\cos\varphi} = \frac{a}{4} (f + \sqrt{1 + f^2}) \quad (5.9)$$

where,

$$f = \tan\varphi \quad (5.10)$$

In the granular material, f is the coefficient of friction while φ is the angle of internal friction.

The exit velocity of the granular material can further be expressed as:

$$v_e = \frac{1}{\sqrt{1+\zeta}} \sqrt{2gy + v_d^2} \quad (5.11)$$

where v_d is the velocity of the particles at a point of intersection and can be expressed as

$$v_d = \sqrt{\frac{2g\sigma_2}{\gamma}} \quad (5.12)$$

where,

$$\sigma_2 = \gamma \left(\frac{1}{f} + f - \sqrt{1 + f^2} \right) x \quad (5.13)$$

Replacing equation 5.12 and 5.13 into equation 5.11 gives

$$v_e = \frac{1}{\sqrt{1+\zeta}} \sqrt{2g \left(y + \frac{\sigma_2}{\gamma} \right)} \quad (5.14)$$

Thus, the exit velocity can be obtained from equation 6.14.

The volume expenditure of granular material through the chunk is given as

$$Q = \frac{2}{3} a^{3/2} \sqrt{g} \frac{1}{\sqrt{1+\zeta}} \frac{K_1^{3/2}}{K_1 \chi'} \left[1 - \left(\frac{\chi'}{K_1} \right)^{3/2} \right] \quad (5.15)$$

where, Q is the flow rate, g is gravity, a is the outlet opening and:

$$K_1 = \frac{1}{2} (f + \sqrt{1 + f^2}) \quad (5.16)$$

$$\chi' = f + \frac{1}{f} - \sqrt{1 + f^2} \quad (5.17)$$

From equation 5.15, ζ is the coefficient of loss which can be calculated in the zone of flow out during the movement of the granular material. ζ is further defined as:

$$\zeta = K_2 \frac{k^2 d^2 l}{h^3} \quad (5.18)$$

where K_2 is any dimensionless coefficient dependent on the conditions of flow out from the tank and obtained from experiments; l is the length of the channel; k is the kinetic coefficient which characterizes the loss of the mechanical energy flow by collisions between the particles.

Based on the mathematical expression from equations 5.15 to 5.18, a computational scheme was developed to describe the behaviour of granular flow. This computational scheme is used in analysing the predictions of the gravitational field effect in relation to $1g$ (earth gravity) on the flow rate, Q of the particles flowing from the hopper.

A summary of the parameters used in carrying out investigations on gravity effect on granular flow using the Kirya structural model in this study are presented in Table 5.2.

Table 5.2 Description of parameters used in investigating the impact of gravity on flow using Kirya's structural model

Fixed parameter	Varying parameter	Calculated parameter
Outlet opening of the hopper a (m) = 0.1, Dimensionless coefficient $K_2 = 1$ Kinetic coefficient $k = 10$ Particle diameter $d = 100\mu\text{m}$ Friction coefficient $f = 0.3$	g (m^2/s) Varied from 20 – 200% of g_0 . $g_0 = 9.8$ (Earth gravity)	Granular flow rate Q (m^2/s), Dimensionless coefficient K_1 , Length of the channel $l = hc$ Loss coefficient ζ

As discussed earlier on understanding the impact of gravity on the granular flow rate, the effect of gravity has been observed for the materials with parameters shown in Table 5.2. The calculated flow rate was normalized with the flow rate under 1g (earth gravity at $9.8\text{m}^2/\text{s}$), Q_0 which gives a ratio(Q/Q_0). Same trend was carried out to normalize the gravity level where g_0 is the earth gravity giving a ratio (g/g_0). Hence, the normalized flow rate ratio Q/Q_0 was calculated for various cases of g/g_0 with constant values of other parameters as given in equation 5.15. The gravity level was varied from $0.2g_0$ to $2g_0$. In particular, the hopper outlet opening was fixed at a value of 0.1m, the particle diameter fixed at $100\mu\text{m}$ and the friction coefficient at 0.3 which is typical.

By applying equations 5.15 to 5.18, it can be concluded that the rate at which granular materials flow under low gravity is very low (Fig. 5.15). This is also evident in the experimental investigation using hourglass confirming the pertinence of the Beverloo equation studied by Le Penne et al. (1995) as shown in Fig. 5.14 in two situations i.e. the hourglass evacuated or filled by air.

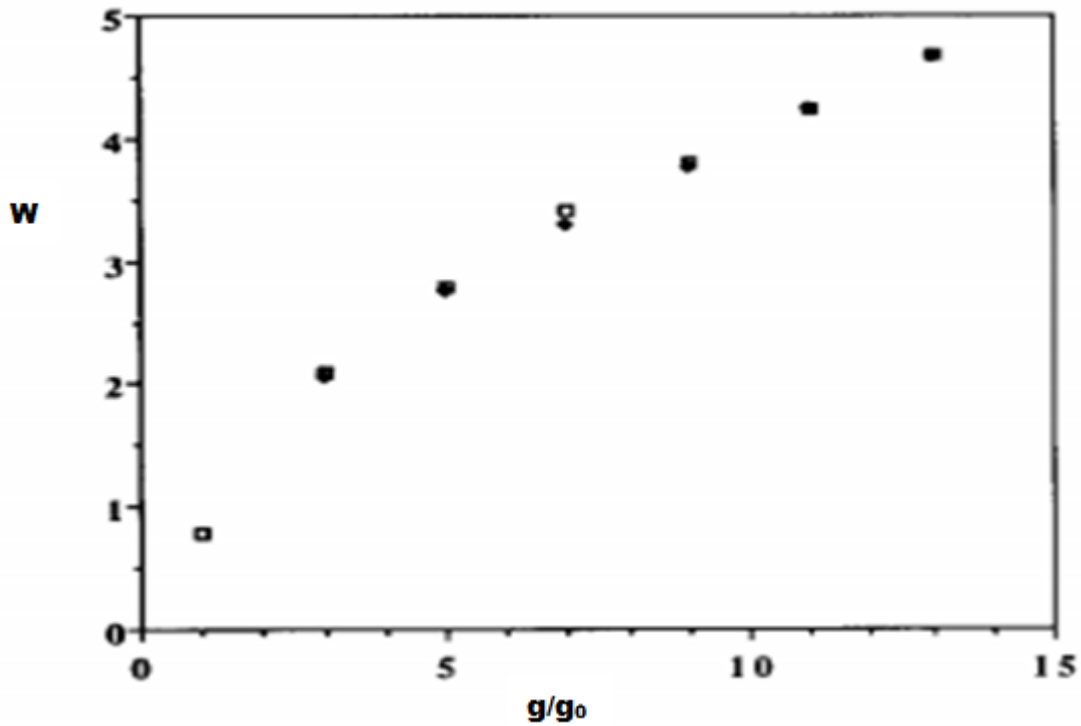


Fig. 5. 14 Variations of mass flow rate versus gravity g when hourglass is evacuated (\blacklozenge) or filled by air (\square) (Le Penne et al., 1995)

The predicted results for the effect of gravity examined in this study as shown in Fig 5.15 indicate that the granular flow rate varies non-linearly with gravity such that it can be predicted that granular flow rate increase with increase in gravity.

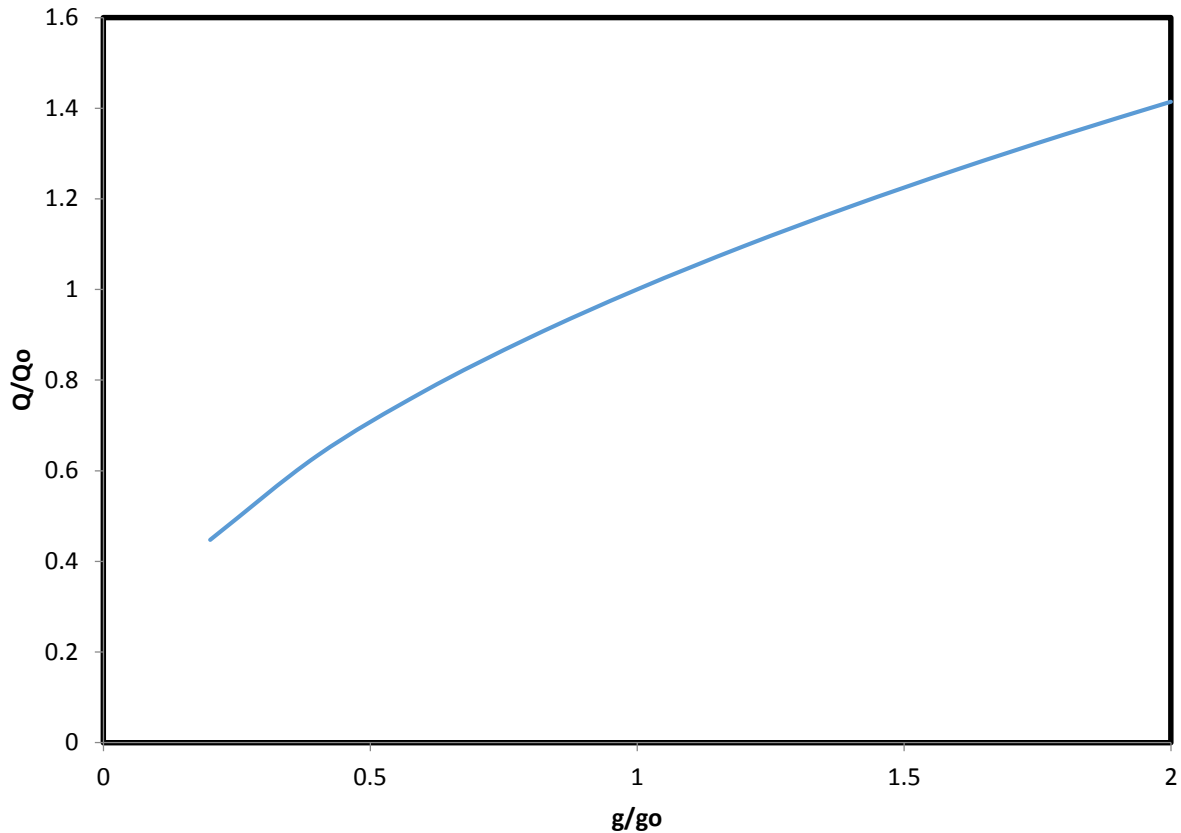


Fig. 5.15 Variations of gravity effect on flow rate using continuum theory

Overall, treating the granular material as a plastic continuum, based on the continuum approach adopted, the flow rate of non-cohesive granular material is predicted to be highly dependent on the gravitational field. The volume flow of the granular materials is perfectly constant over time and depends on gravity (Hofmeister et al., 2009). The overall mass throughput decreases with decreasing gravity level which implies that the decrease in gravity level leads to less acceleration (Brucks et al., 2008). It is to be noted that the continuum theory employed in this study did not consider the cohesive nature of the materials and the problem is for granular flow in hoppers only. Predicted results also indicate that it is expected to experience very high flow of granular materials at higher gravity levels above earth gravity.

5.2.2 Impact of particle size on granular flow under gravity level using Kirya's structural model

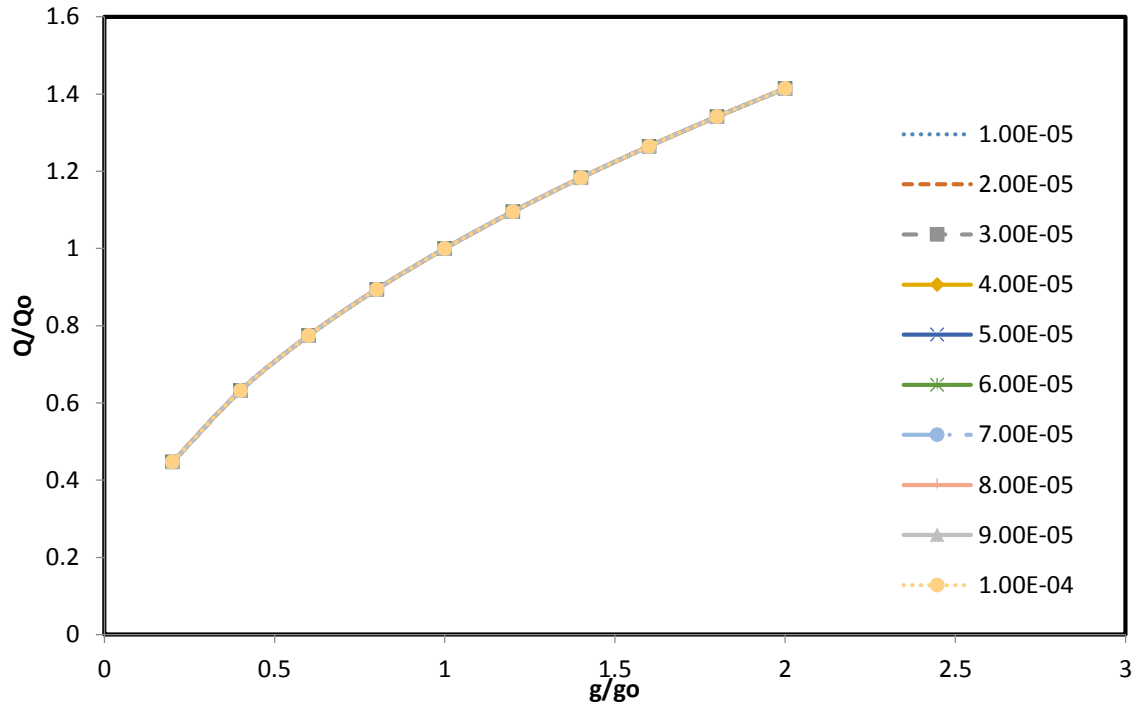
Further analysis was done on the impact of the particle size on granular flow rate under variable gravity levels by varying the diameter of the particle. Presented in Fig. 5.16, is the relationship between the particle size, the flow rate and gravity level using the Kirya's structural model.

The particle diameter studied for analysis in Fig. 5.16 was chosen to understand the effect of smaller particle sizes on granular flow under varying gravity level. Table 5.3 gives a summary of the parameters used in this investigation.

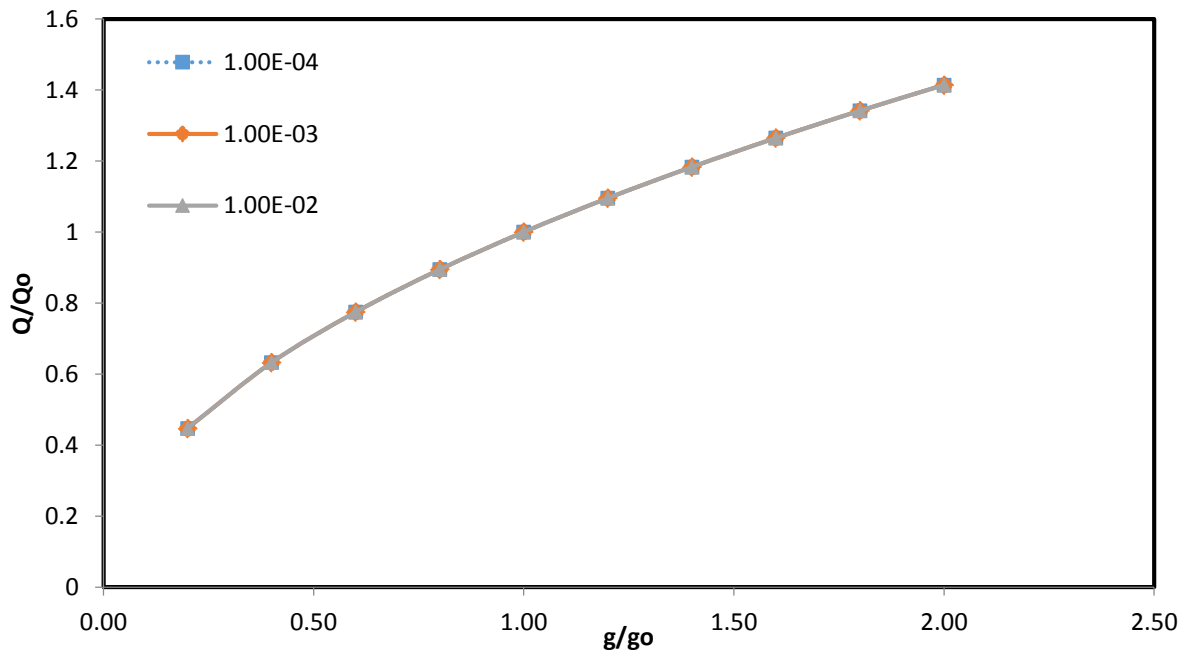
Table 5.3 Description of parameters used in investigating the impact of particle size on flow under varying gravity level using the Kirya's structural model

Fixed parameter	Varying parameter	Calculated parameter
Outlet opening of the hopper a (m) = 0.1, Dimensionless coefficient $K_2 = 1$ Kinetic coefficient $k = 10$ Friction coefficient $f = 0.3$	g (m ² /s) Varied from 20 – 200% of g_0 . $g_0 = 9.8$ (Earth gravity) Particle diameter $d = 10\mu\text{m} - 100\mu\text{m};$ $d = 100\mu\text{m} - 10^4\mu\text{m}$	Granular flow rate Q (m ² /s), Dimensionless coefficient $K_1,$ Length of the channel $l = hc$ Loss coefficient $\zeta,$

The investigation into the particle size was studied in two parts which was due to the results of the initial size range used. The initial analysis was varying the particle diameter between 10 μm – 100 μm and further analysis on varying from 100 μm – 10⁴ μm and the results are as indicated in Fig. 5.16.



(a)



(b)

Fig. 5. 16 Impact of particle diameter (a) $10\mu\text{m} - 100\mu\text{m}$ (b) $100\mu\text{m} - 10^4\mu\text{m}$ on the gravity effect on flow rate using Kriya's structural model

It was deduced from Fig. 5.16(a) and (b) that if the granular material is treated as a continuum, the particle size would have no effect on the granular flow rate of the materials. However, the gravity effect is relevant and for predictions at low gravity, low flow rate will exist and the granular flow rate will increase with gravity for various particle sizes with the sizes having no significant difference on the flow rate.

5.2.3 Impact of friction coefficient on granular flow under gravity level using Kirya's structural model

The effect of friction coefficient was estimated assuming that the actual contacts are continuous as a result of the assumed continuous distribution of the contact forces (Nedderman, 1992). Ideally, the contacts are not continuous but occur between the two contacting surfaces (Duran, 1999). With this understanding, the discrete nature of the material grains is neglected by assuming the length of the granular bed is sufficiently large. The Kirya's structural model was adopted to help in investigating the response of granular flow rate at different friction coefficient under variable gravity conditions. Equations 5.13 – 5.15 are used to relate the friction coefficient to the granular flow rate. Parameters used are presented in Table 5.4.

Table 5.4 Description of parameters used in investigating the impact of friction coefficient on flow under varying gravity level using Kirya's structural model

Fixed parameter	Varying parameter	Calculated parameter
Outlet opening of the hopper a (m) = 0.1, Dimensionless coefficient $K_2 = 1$ Kinetic coefficient $k = 10$ Particle diameter $d = 100\mu\text{m}$	g (m^2/s) Varied from 20 – 200% of g_0 . $g_0 = 9.8$ (Earth gravity) Friction coefficient $f = 0.1 - 0.5$	Granular flow rate Q (m^2/s), Dimensionless coefficient K_1 , Length of the channel $l = hc$ Loss coefficient ζ ,

From Table 5.4, the friction coefficient varied from 0.1 – 0.5 and gravity varied from 20% – 200% of earth gravity and the results obtained are further presented in Fig.5.17.

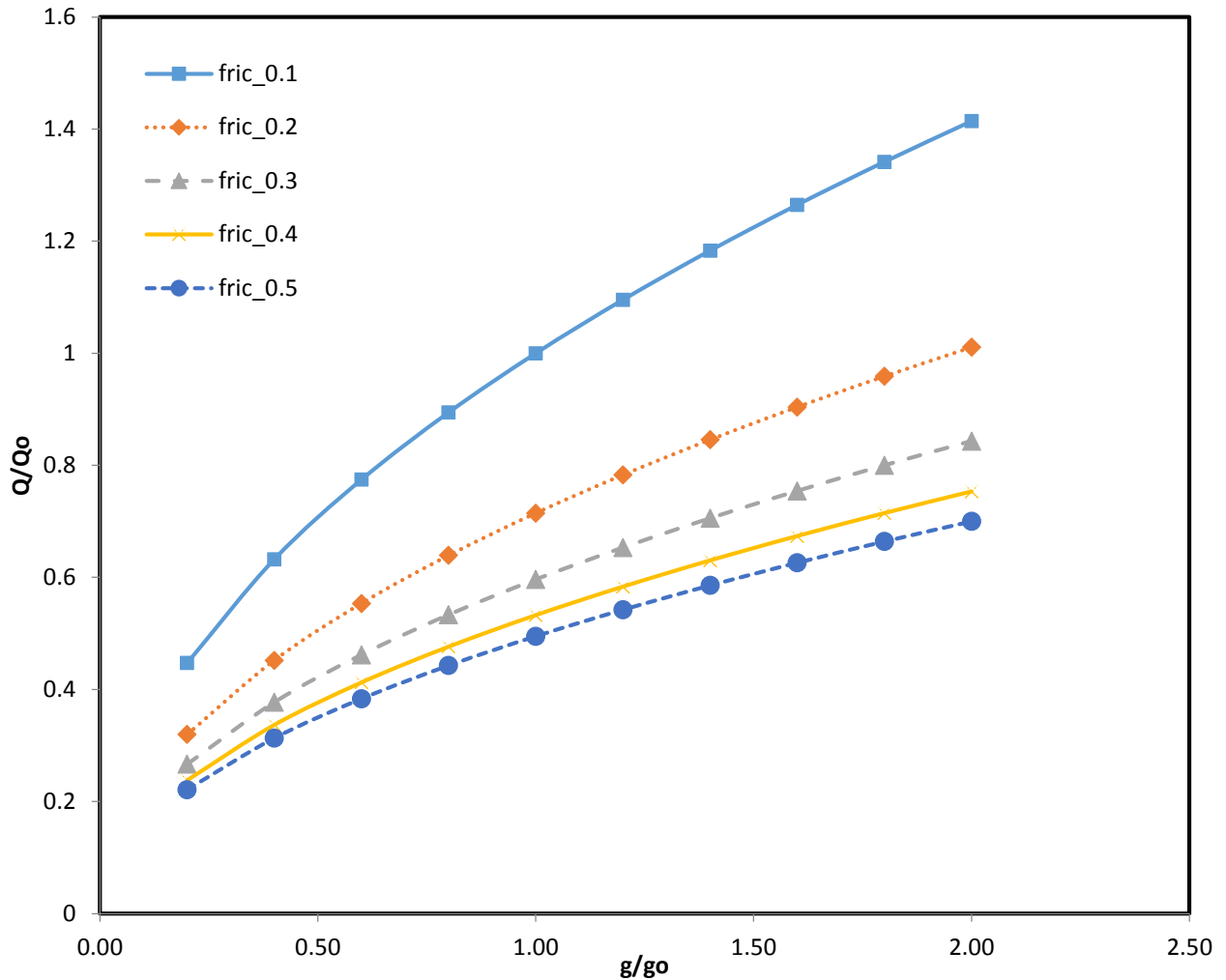


Fig. 5.17 Impact of friction coefficient on the gravity effect on flow rate using Kriya's structural model

From the result analysis as presented in Fig. 5.17, it was deduced that higher flow rates are required for a granular material having low coefficient of friction (Sun and Sankaran, 2012). This effect of friction coefficient on granular materials qualitatively matches practical experience. The difference in flow rate for different friction coefficient is observed to increase with increasing gravity. Granular materials with very low friction coefficient of 0.1 tend to have a very high flow rate as compared to higher friction coefficients of 0.2 and above. The difference between the friction coefficient of 0.1 and 0.2 was observed to be large compared with other values of friction coefficients. As with all the values of friction coefficient studied, the impact increased with increasing gravity. The model helps to predict how friction coefficient of granular materials will slow down granular flow at very low gravity. In the model, the interaction between the flowing

layer and the hopper medium is described by the friction predicted. Previous experiments on friction between solids (Heslot et al., 1994) or between a rough plate and a granular layer (Nasuno et al., 1997) have shown complex and rich dynamics which are not yet fully understood. Important point to be noted from the predictions from the Kriya's structural model is that the effect of increasing friction coefficient on granular flow slows down the grain with increasing gravity level. Also, effectively, friction coefficient has more impact in slowing down the grains at higher gravity than at very low gravity. The effect of the friction coefficient on flow rate at different gravity environment was then extended for different particle diameter. The results are shown in Fig. 5.18. The results presented in Fig. 5.18 further supports the already established predictions on the impact of particle size on granular flow under variable gravity in this report. The results indicate that even under variable friction coefficients between 0.1 and 0.5, particle size had no influence on granular flow under varying gravity level. Also, granular flow was still observed to increase with increasing gravity.

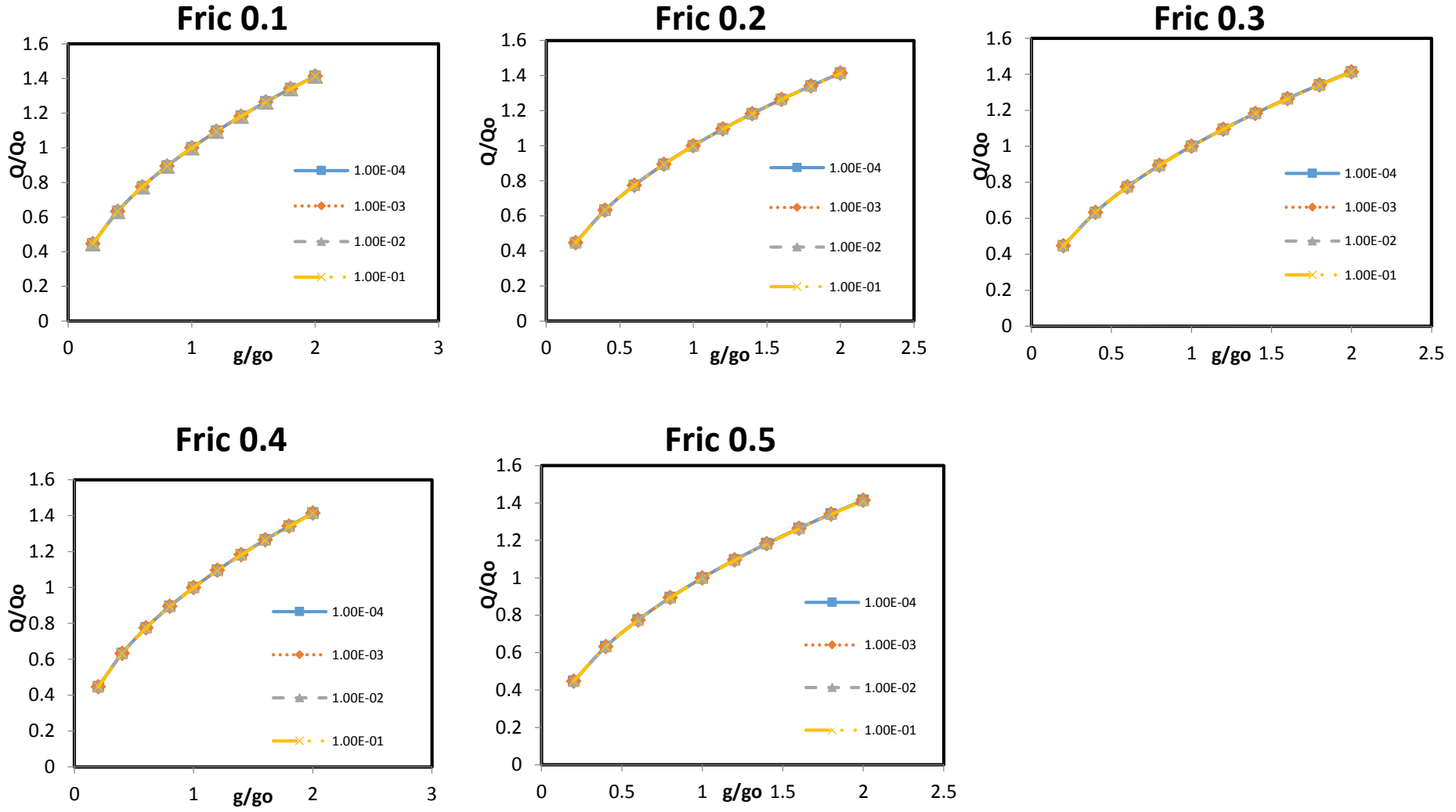


Fig. 5. 18 Variation of particle diameter and friction coefficient (a-e) on flow rate at different gravity level

5.3 Gravity Effect of Granular Flow using DEM Model

The objective of this section is to investigate the impact of varying gravitational environment on the discharge rate of granular materials from hoppers using DEM and compare with continuum and experimental studies. Following the results obtained from investigations using the Kirya structural model, the results obtained for predicting the gravity effect on granular flow using three dimensional DEM are provided and discussed in detail in this section.

To gain understanding of the surfaces of planets and small bodies in the solar system, DEM is used as a simulation tool to analyse the flow behaviour of granular material for various gravity levels. The fundamental principles in DEM are as explained in chapter three and this provides a platform to aid in investigating the effect of gravity levels on granular flow. DEM is modelled based on a finite number of discrete particles interacting with each other in which every particle in the system is defined and supported by the Newton's equations of motion (translational and rotational motion) (Zhu et al., 2005). For simplicity, this study considers the steady state granular flow in a three dimensional hopper and the discrete simulation is performed using DEM with the linear contact model as explained in appendix A. The behaviour of the granular analysis based on DEM is studied using the particle flow code in three dimension (PFC^{3D}). Through this method, it is easier to analyse the trajectory paths and velocities of all particles (Zhu et al., 2008). Two types of hoppers were initially considered in this study; wedged shaped hopper and conical hopper. The geometry of the wedged shaped hopper was created as represented in Fig. 5.19 considering the following constraints:

- All of the walls are planar.
- All of the plan sections are rectangular.
- The geometry is symmetrical in the yz- and xz-planes.

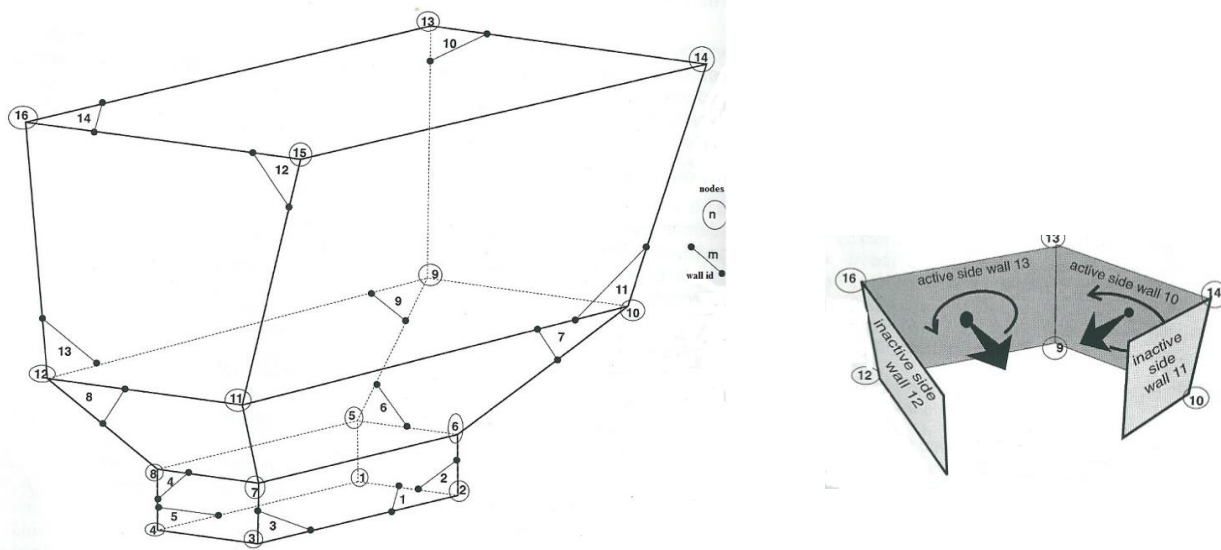


Fig. 5.19 Geometry arrangement of a wedge shaped hopper

The main substantial amount of work in creating the geometry is creating an arbitrary three-dimensional volume, generating the particles within the space, and then obtaining a specific compaction.

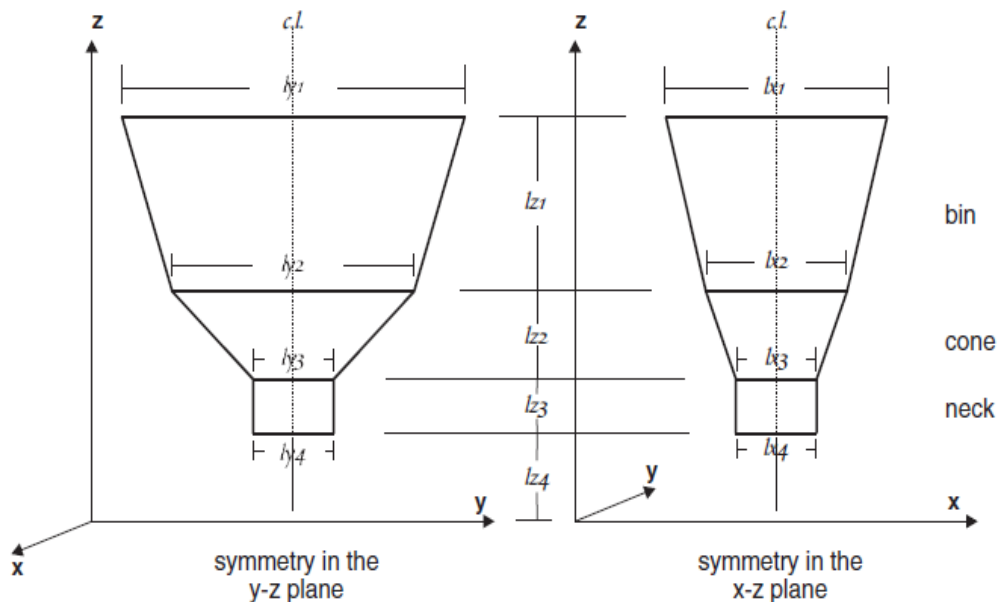


Fig. 5.20 Geometry constraint in a wedge shaped hopper

The effect of gravity was predicted from this model with the particles confined in the hopper initially. Confining particles within specific regions in space can be tedious and often difficult using PFC^{3D}. However, the walls were created enclosing the volumes and taking note of the active and inactive sides of the walls (Fig. 5.21). The particles were positioned in a defined space during the generation of randomly placed particles. This simulation makes use of optimum particle size using the size of the hopper and the required number of particles.

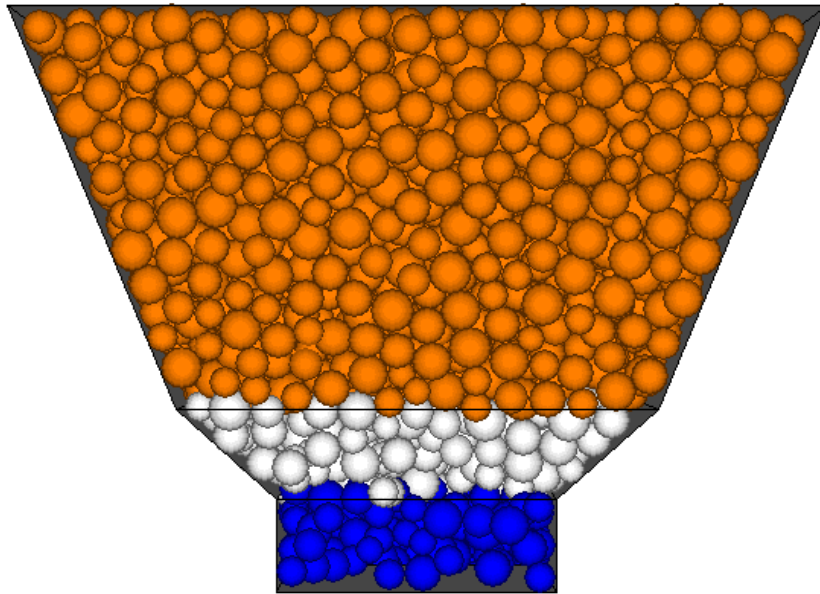


Fig. 5. 21 Particles confined in a wedged shaped hopper

Also, the conical shaped hopper was modelled to study flow behaviour in conical hoppers. The hopper is defined by two flat walls and a cone-shaped general wall that contain an initial compact assembly of particles as shown in Fig. 5.22.

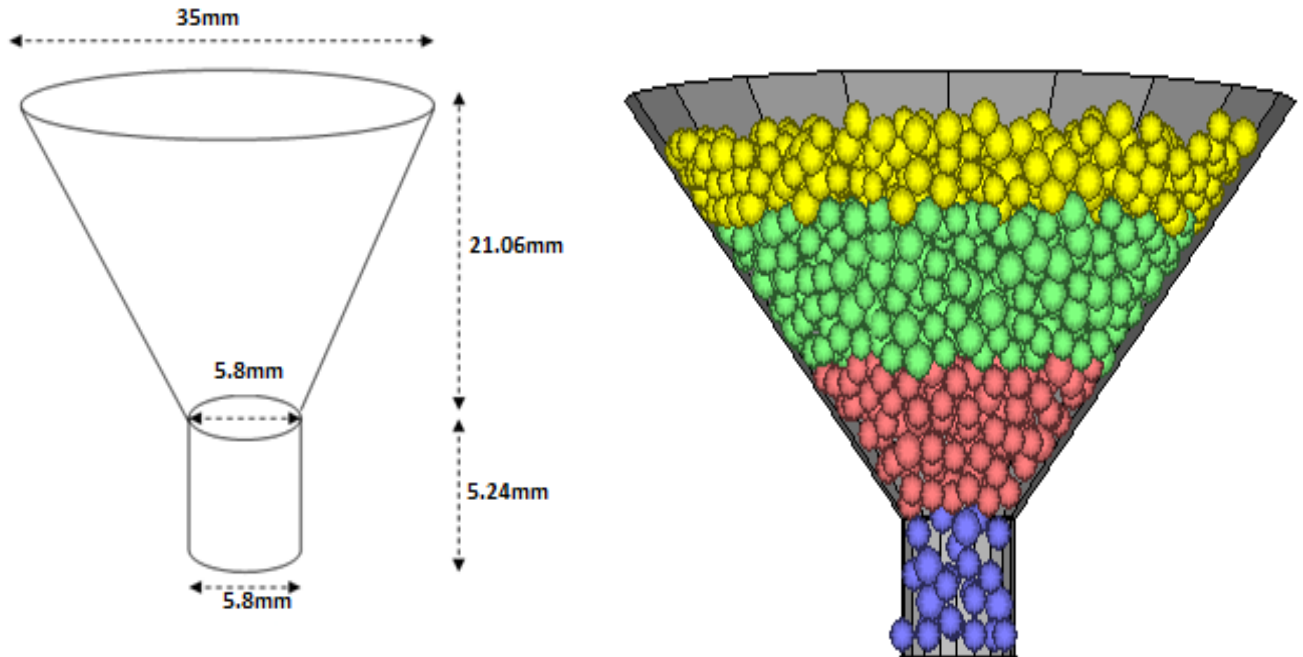


Fig. 5.22 Geometry arrangement of conical hopper and confined particles within the hopper

The particles were created considering the following assumptions;

- Smooth particles.
- Isotropic elasticity of particles.
- No influence of tangential components of contact force on normal component.
- No diffusion of the particles.

As regards both hopper models, a desired compaction was achieved by applying a multiplication factor and this assisted the restoration of the particles to the required radii with the particles randomly distributed. The model was created using developed fish functions and commands needed to create the hopper and the assemblies of particles were allowed to gradually settle into the hopper under gravity. During the falling and settling stages, the base of the hopper was left closed and cycled until near equilibrium conditions were met.

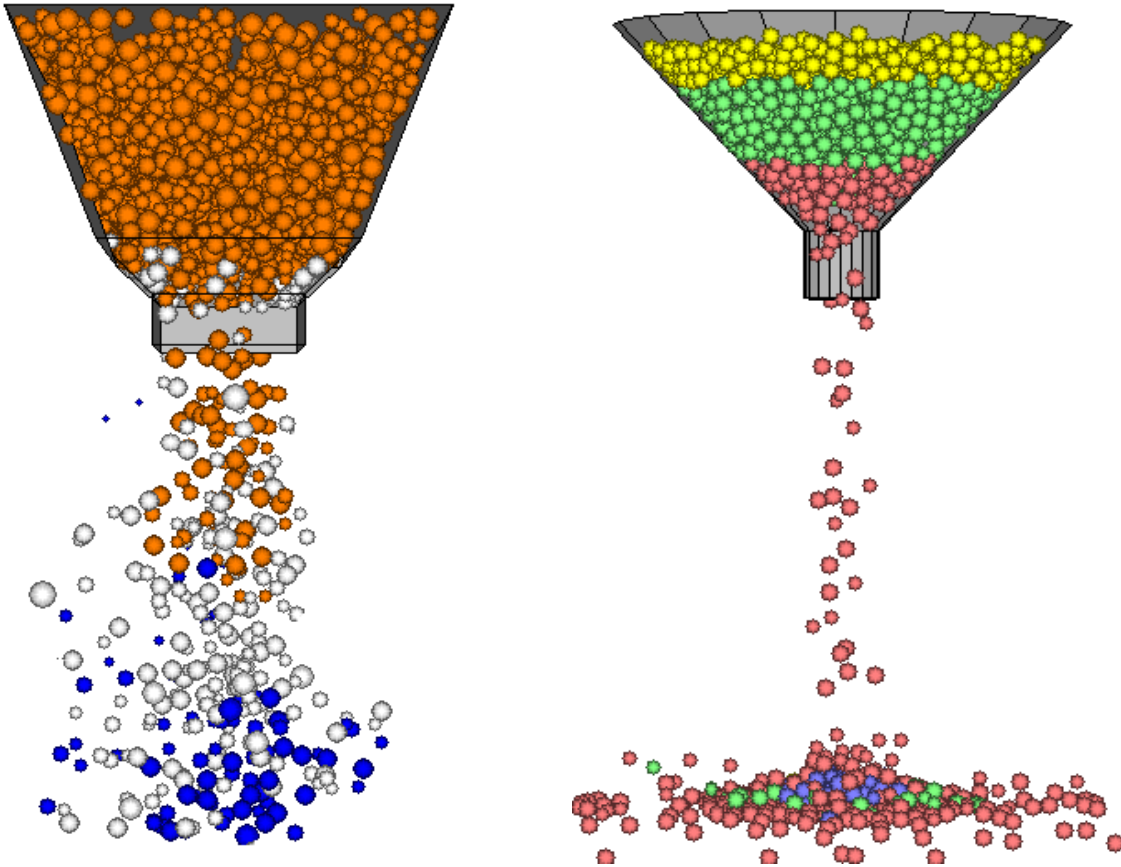


Fig. 5. 23 Flow of particles under gravity for both hopper model types

When these equilibrium conditions have been achieved, the base is opened and the particles were allowed to flow out of the hopper under gravity as seen in Fig. 5.23. The model was created in an initial compact state (Figs. 5.21 and 5.22) with the particles generated for specific target porosity, the minimum radius particle and the ratio of the maximum to minimum radii. The overall constants and parameters required for the investigation are defined and presented in Table 5.5.

Table 5.5 Constant values used in investigating gravity effect in 3D DEM simulation

Fixed parameter	Varying parameter	Calculated parameter
Wall normal stiffness $1 \times 10^8 Pa$,	g (m ³ /s) Varied from 20 – 100% of g_0 . $g_0 = 9.8$ (Earth gravity)	Volumetric flow rate Q (m ³ /s),
Wall shear stiffness $1 \times 10^8 Pa$,		Mass flow rate M (kg/s),
Wall friction coefficient 0.6		Time required to empty Accumulation time (s)
Ball contact friction coefficient 0.6		
Ball normal stiffness $1 \times 10^8 Pa$		
Ball shear stiffness $1 \times 10^8 Pa$		
Ball density 1600kg/m ³		
Radius multiplier 1.6		
Desired final porosity 0.36		

The effect of the various gravity levels on granular flow was analysed and predicted with the aid of the DEM simulations successfully. The time evolution which is the time required for the particles to be completely emptied from the hopper was investigated and shown in Fig. 5.24.

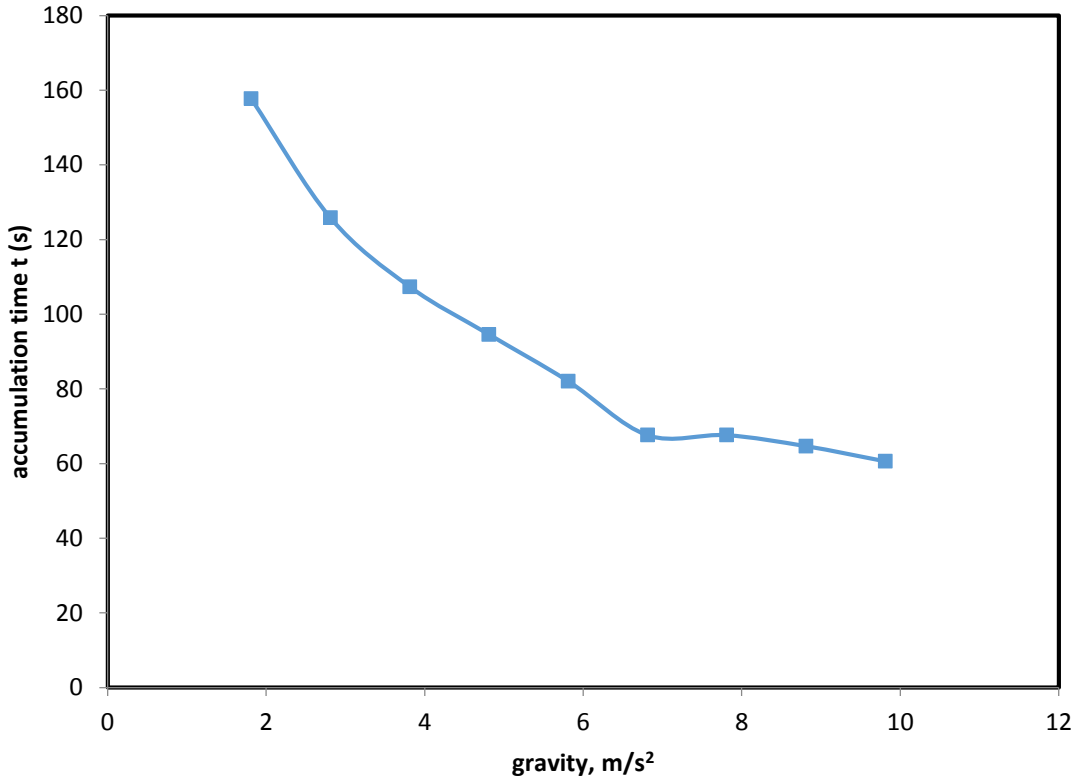


Fig. 5. 24 Time evolution of the effect of gravity

As discussed earlier in the section A of this chapter, the time required to empty the hopper is a function of the granular flow. This has been further established with three dimensional simulations using DEM technique. As represented in Fig. 5.24, the time required to empty the hopper decreases with increasing gravity levels. At lower gravity levels, the emptying time is very high which helps to give an insight on how low gravity levels can affect flow. The linear decrease is seen for low gravities lower than 7 m/s² while at gravities higher than 7 m/s², the accumulation time is relatively close and the difference in gravity levels between 7m/s and the earth gravity, 9.8 m/s² is minimal as compared with gravity levels less than 7 m/s².

This can then be related to the granular flow rate which is further predicted from DEM calculations and the results presented in Fig. 5.25.

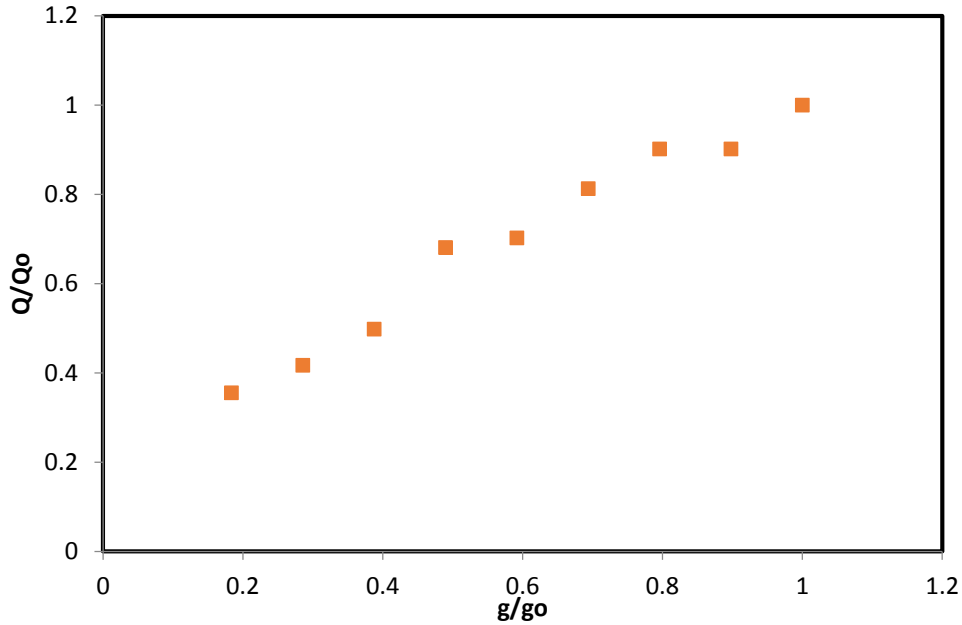


Fig. 5.25 Gravity effect on volumetric flow rate using DEM

In relating the flow rate with the gravity as presented in Fig. 5.25, similar hourglass experiment was carried out using basalt spheres hourglass by Hofmeister et al. (2009) to represent the effect of gravity on volume flow of grains as shown in Fig. 5.26.

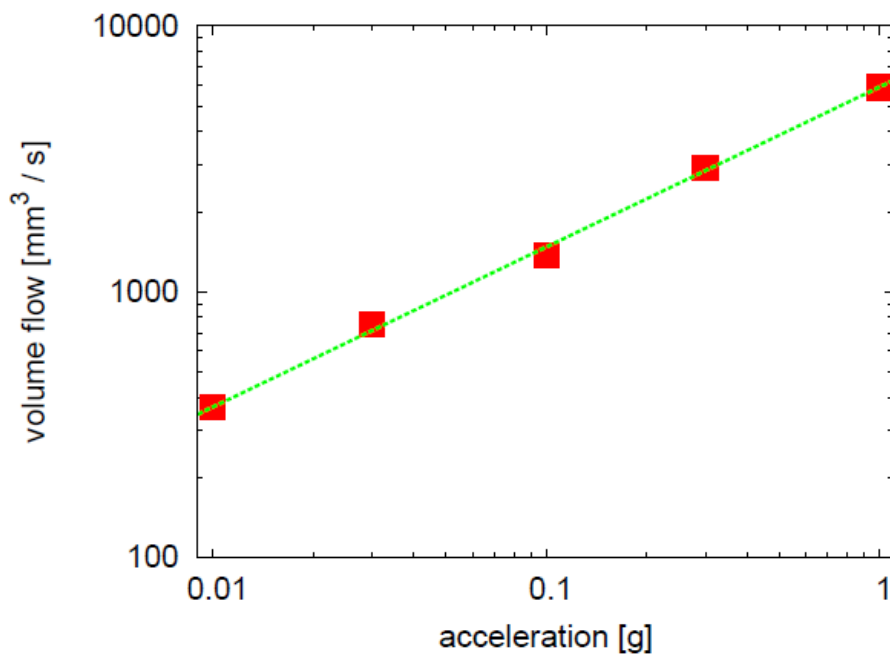


Fig. 5.26 Volume of basalt spheres in the hourglass experiment as a function of gravity level (Hofmeister et al., 2009)

Results obtained from DEM investigation (Fig. 5.25) agrees with previous predictions using the hourglass experiment (Fig 5.26) and it can be concluded that the volumetric flow rate is predicted to increase with increasing gravity level. It is evident that granular hoppers in relatively low gravity environments results in low flow rate as compared with earth gravity condition and vice versa. This analysis is done for both a wedge shaped hopper and a conical hopper. However, from observation, the wedge shaped hopper developed more arches and is seen to have more disadvantages as compared to a conical hopper (Schulze, 2006a). The gravity result obtained from DEM simulation gives a similar trend as seen in the continuum approach estimations.

In comparison, the gravity effects for both approaches – DEM and Continuum theories can be deduced to qualitatively agree by following the same trend. Both results are thus superimposed as seen in Fig. 5.27.

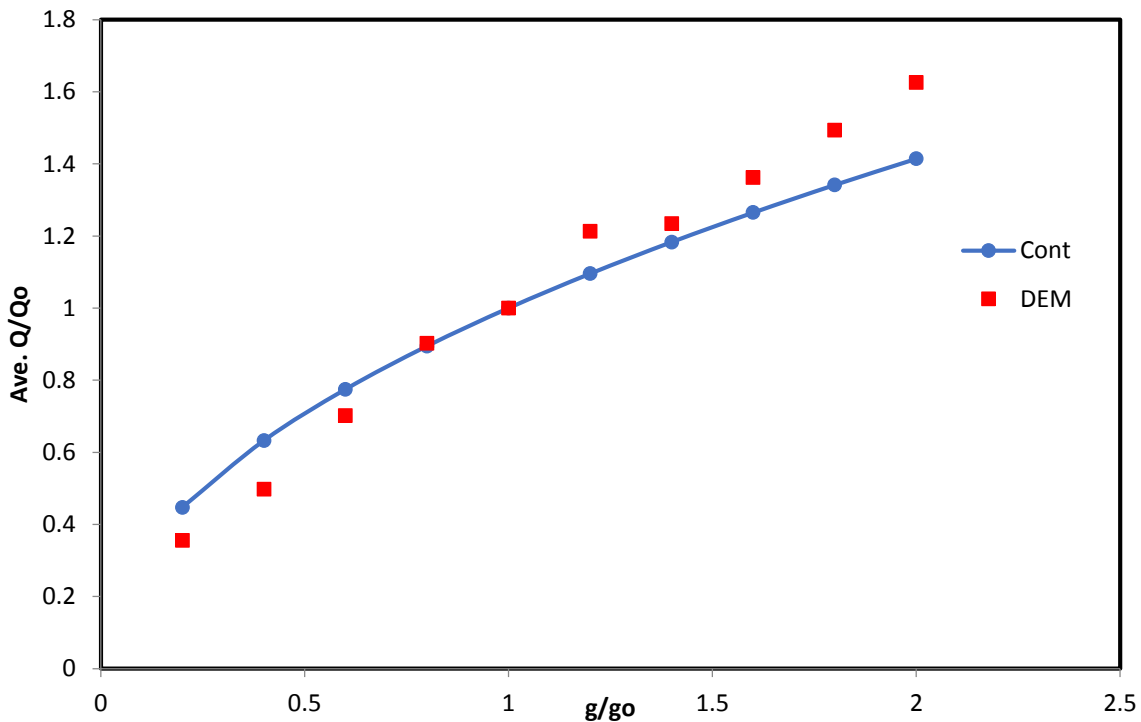


Fig. 5. 27 Validation of gravity effect between Kirya’s continuum theory and DEM

Results of the gravity effect on the volume flow of grains from both the continuum (Kirya’s structural model) and DEM approach agree qualitatively. Previous research indicate that the

volume flow is expected to depend on the square root of gravity (Hagen, 1852). This agrees qualitatively with predictions shown in Fig 5.27. A successful prediction of the flow behaviour of granular materials under various gravity levels has been achieved via both approaches of the continuum theory and DEM technique. Both approaches tend to agree qualitatively which implies the significant effect of gravity on flow properties of granular materials.

As reported in chapter three, the contact forces acting on individual particles and its trajectories are traced in a DEM simulation and as a result, information for the flow pattern, velocity field and force structure (Zhu et al., 2005) of the hopper flow can be readily established as shown in Fig. 5.28.

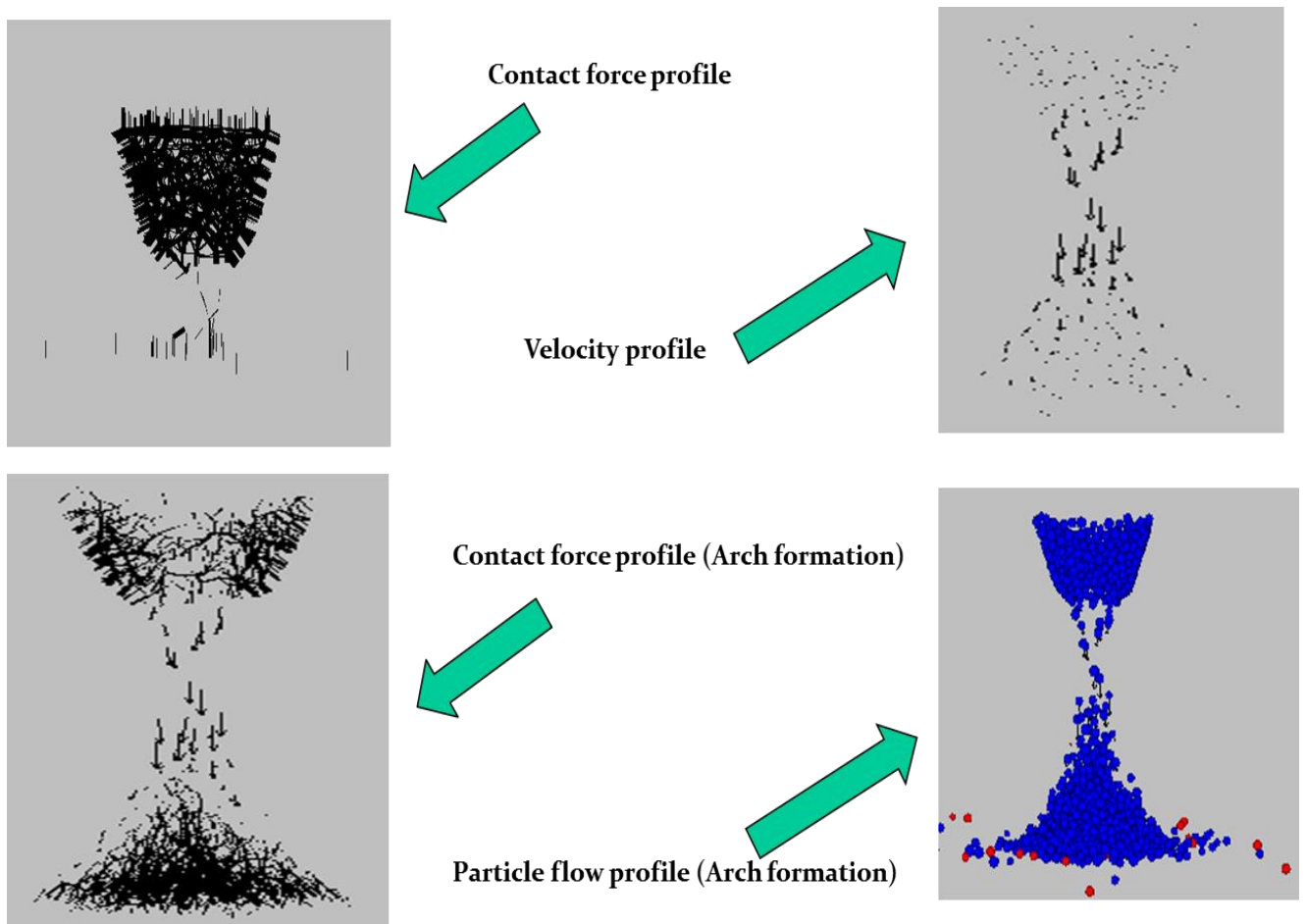


Fig. 5. 28 General information from DEM simulation profile during hopper flow

The profile information presented in Fig. 5.28 indicate that DEM simulation can generate micro-dynamic information which is difficult to obtain either experimentally, via the continuum approach or other mathematical models but plays a vital role in elucidating the fundamentals governing

granular flow. For example, arch formation was observed during flow within the hopper from the information presented in Fig. 5.28. This is a re-occurring problem within granular flow which is continuously been studied extensively by researchers Guo et al. (2012), Garcimartin et al. (2007), and Guo and Zhou (2013) to predict ways to overcome arch formation during flow.

5.3.1 Qualitative validation of gravity effect on granular flow with parabolic flight campaign

Understanding the discrete nature of granular materials with the aid of DEM simulations tend to allow a better understanding of the fundamental mechanics of granular flow. As a result, DEM is fully adopted considering granular material properties similar to sandstone which also helps represent the regolith materials. The sandstone grains adopted are as used in a recent parabolic flight campaign test (Hofmann et al., 2013) of the sample preparation and dosing station (SPDS) hoppers at simulated Mars and lunar gravity.

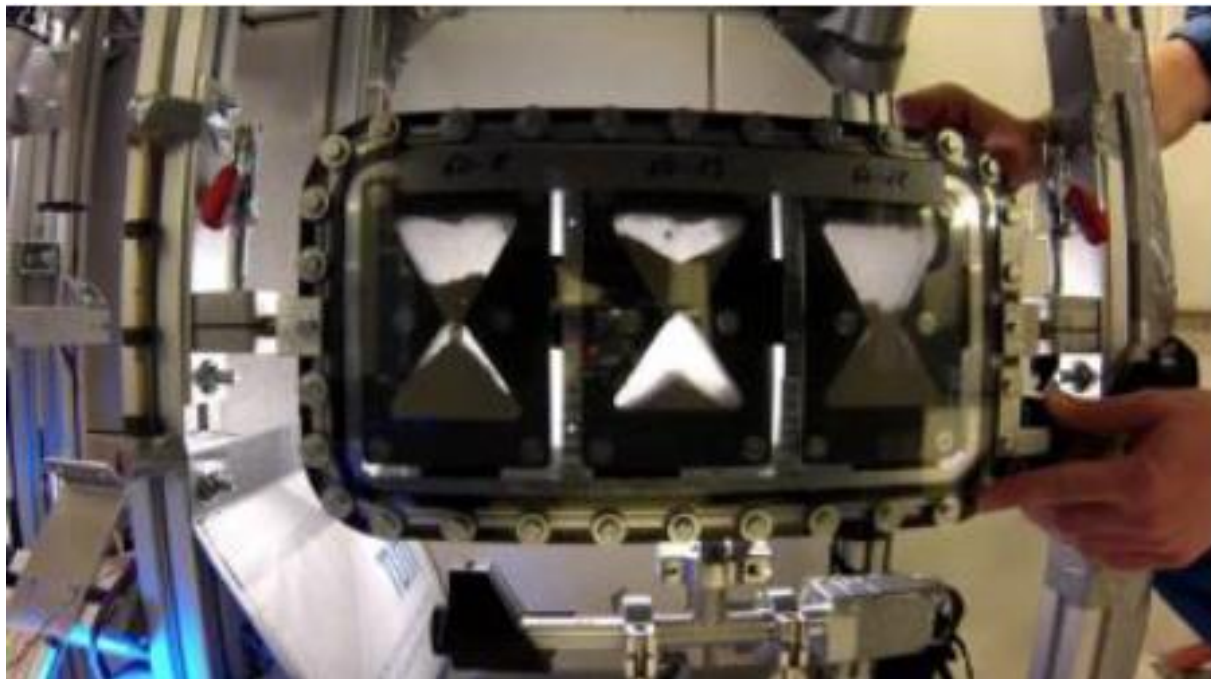


Fig. 5. 29 Still from December 2012 TUM/LRT parabolic flight experiment with 2D hoppers (set of 3 hoppers of different throat diameters (credit: P. Reiss TUM/LRT))

To gain a better understanding of the planets of interest; Earth, Mars and lunar, the flow behaviour of granular materials for various gravity levels is of utmost interest which is generally fairly unknown (Hofmeister et al., 2009).

The simulation was done to check for the effect of gravity on the flow of sandstone material as used in experiments performed in a parabolic test flight. The wedge shaped hopper material as related to the parabolic flight test campaign is assumed to be steel and the analysis was done by simulating flow of sandstone material under gravity conditions earth ($g_o = 9.8\text{m/s}^2$), Mars ($g = 0.38g_o$) and Lunar ($0.167g_o$). The hopper and sandstone properties used in the simulation are presented in Table 5.6:

Table 5. 6 Sandstone properties used in DEM simulation for granular flow under EML gravity

Sandstone Properties	Value
Wall stiffness	2.5×10^7 Pa
Ball stiffness	2.5×10^7 Pa
Ball density	2000 kg/m ³
Shear strength	25 MPa
Tensile strength	25 MPa
Friction Coefficient	0.6
Porosity	0.3

The first analysis was to simulate the granular flow under earth gravity conditions. The materials are allowed to flow out and the flow rate observed. Every material in the hopper was observed to flow out completely with time.

The second analysis was performed simulating granular flow under Mars gravity environment. Following same procedure, the materials were allowed to flow through but took a longer time as compared to earth gravity for all materials to flow through. As compared to the simulation under earth gravity level as explained earlier, this shows that lower flow rate is observed within the Mars gravity conditions.

Thirdly, the lunar environment was simulated, analysing the flow conditions using same properties of sandstone material as used in earlier analysis. It was observed here that even after the simulation run time, there were still some sandstone particles in the hopper as seen in Fig 5.30.

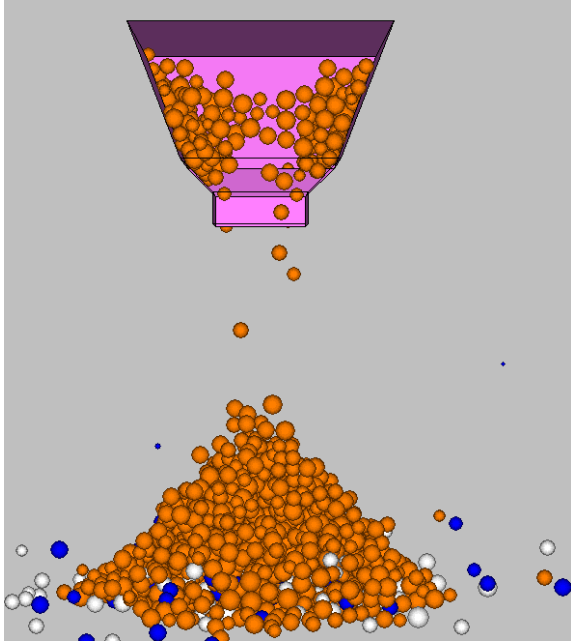


Fig. 5. 30 Flow of sandstone materials under lunar gravity conditions ceased

The predictions indicate that flow rate is very low and difficulties will be encountered during granular flow under lunar gravity environment. This was also observed in the parabolic flight test campaign as a result from recommendations from this study where sandstone materials became difficult to process under simulated lunar gravity environment. Further test was carried out by simulating a $2g_0$ gravity environment and transferring the hopper with the remaining stuck particles to the $2g_0$ gravity. The results from the parabolic flight test campaign support results from DEM simulations proposed which further strengthens the validation and use of the DEM approach and simulation developed for this research to study granular flow under varying gravity levels. The result is presented in Fig. 5.31.

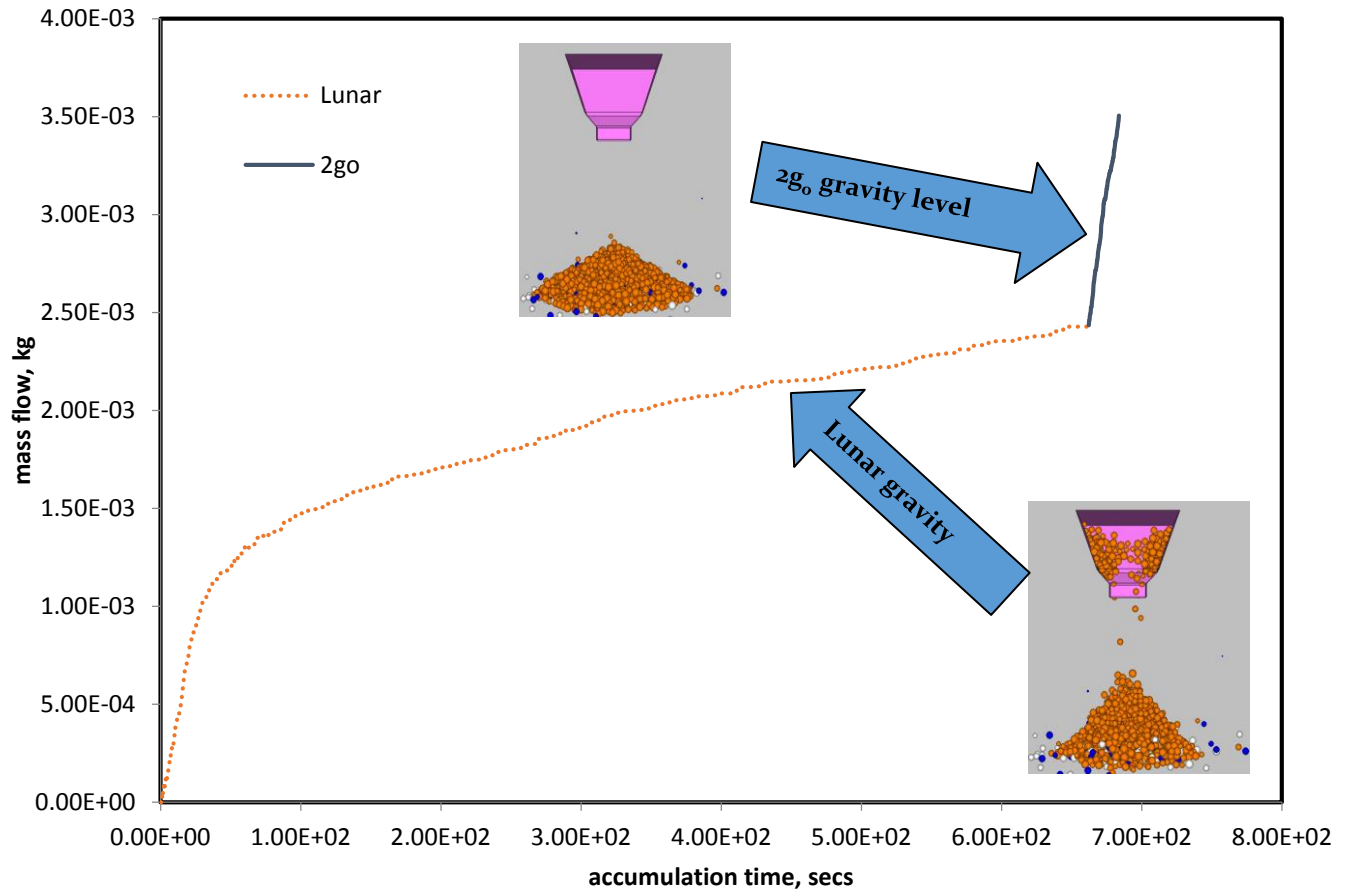
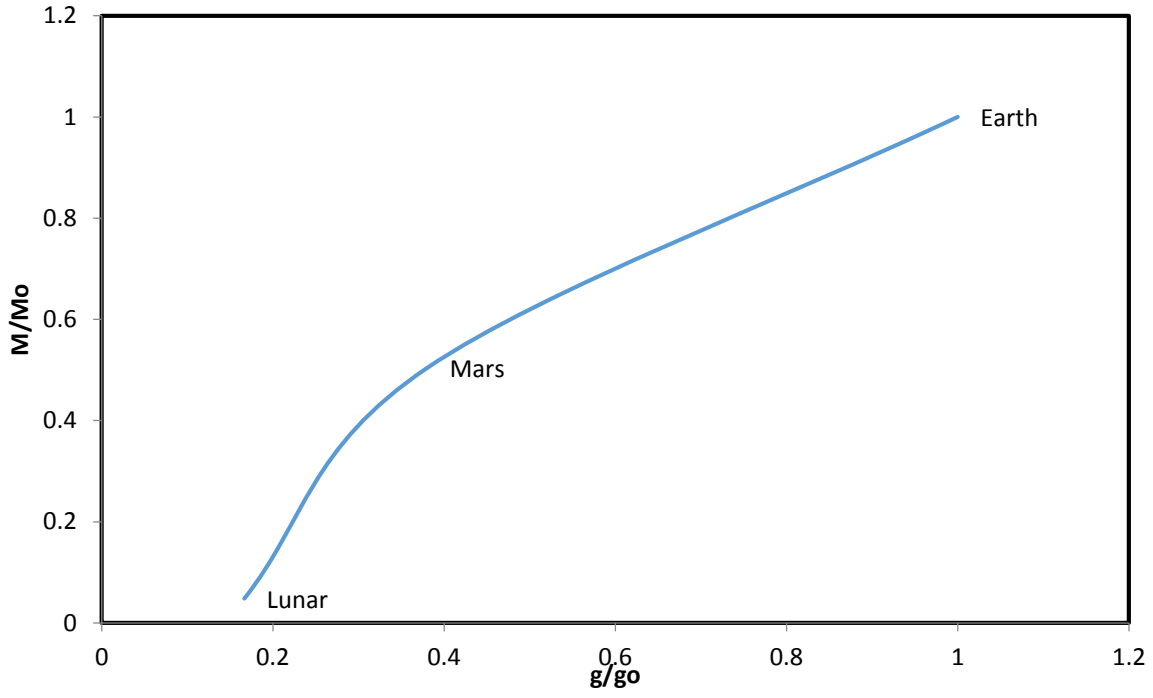


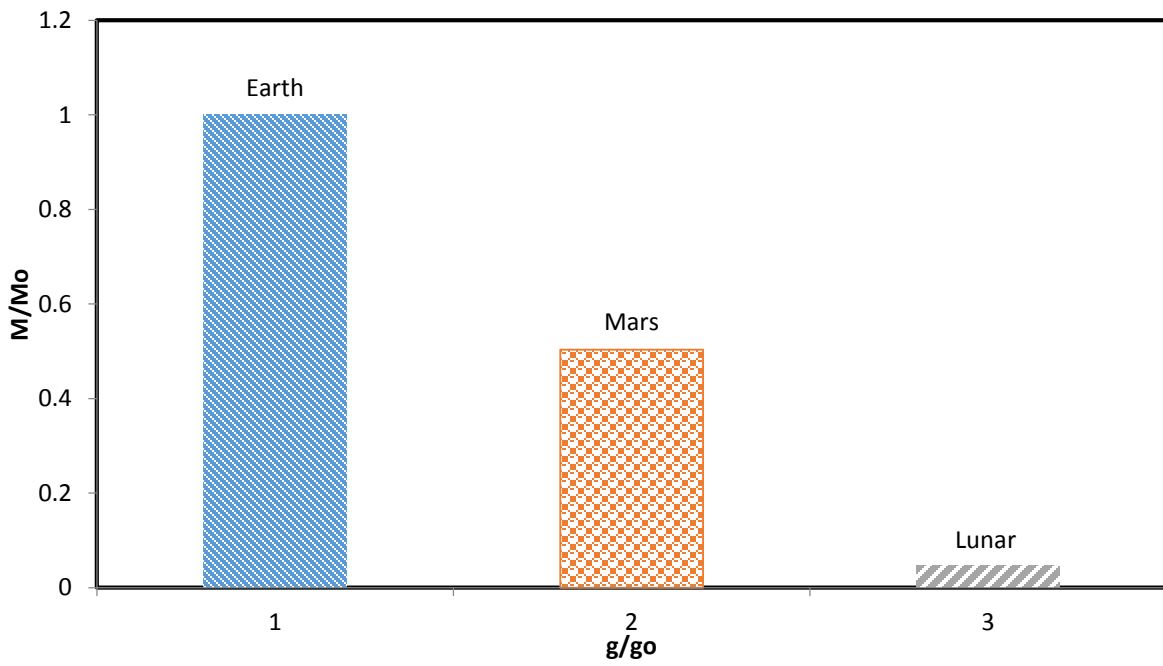
Fig. 5.31 Mass flow of sandstone materials under lunar gravity and $2g_0$ gravity levels

The effect of the $2g_0$ gravity level is seen such that the flow rate increased at a very high rate. The total mass flow was seen to increase drastically under the $2g_0$ gravity environment and within very little simulation time-steps, all the particles were discharged out of the hopper. The results then suggest difficulty in processing sandstone materials.

Further investigations were carried out under the EML gravity levels on granular flow in a conical hopper using material properties in Table 5.5 and the results presented in Fig. 5.32.



(a)



(b)

Fig. 5.32 Influence of EML gravity levels on mass flow

The EML gravity effect further clearly shows that at low gravity environments such as Lunar and Mars, the mass flow are much lower as compared to the earth gravity environment. As the gravity increases, the mass flow increases. A clearer view of the gravity influence is presented in Fig 5.32 (b) with the lunar gravity environment exhibiting very low mass flow as compared to the earth environment. The gravity dependence is also seen in volume flow and presented in Fig. 5.33.

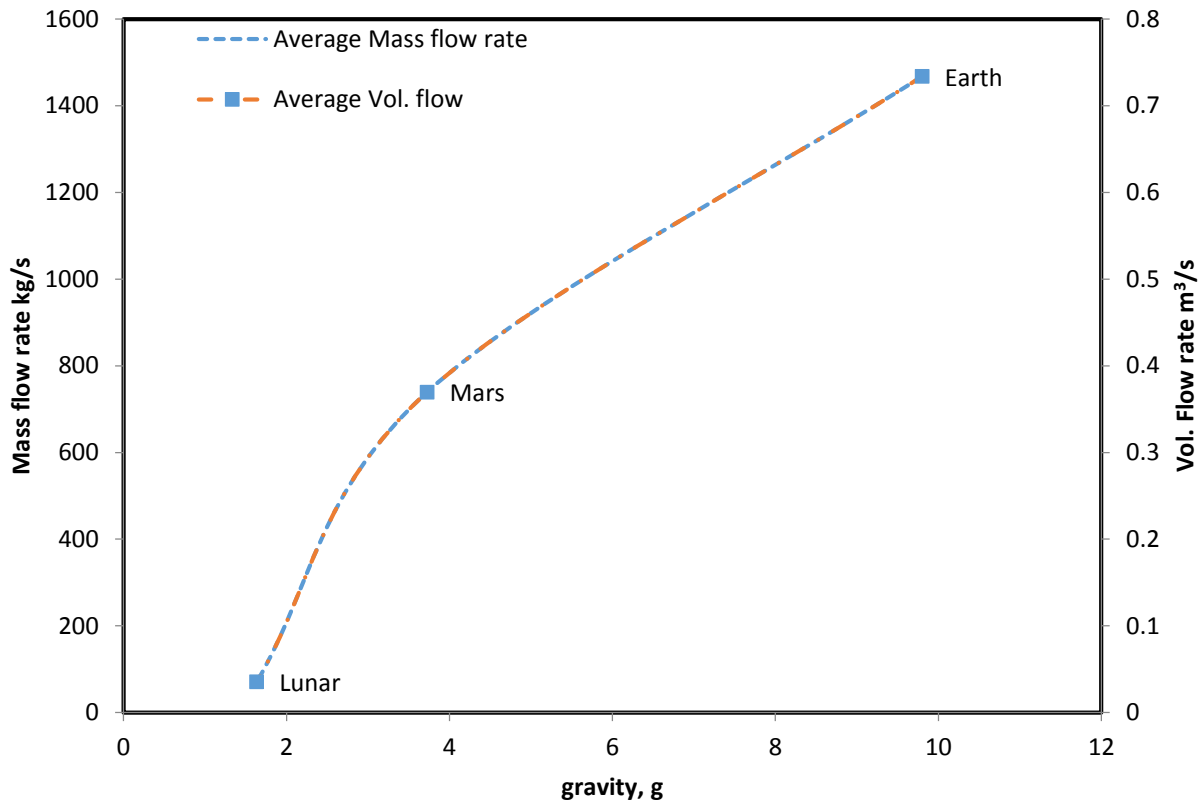


Fig. 5.33 Influence of EML gravity on mass and volume flow rate

As a result, it is then deduced that sandstone material can be a difficult material to process under the lunar gravity environment as it was observed earlier that even after the simulation run time, there were still some of the sandstone materials stuck in the hopper. Within the earth and the Mars gravity environment, all the particles went through the hopper but with less mass flow in the Mars environment.

Conclusively, in comparing this result with experimental data, it can be deduced that gravity has a very real impact and considerable influence on the functioning and cross-contamination levels of the dosing station. From the experimental data analysis, it was deduced that sandstone materials

which were easily processed under earth gravity conditions could be processed as well under Mars gravity conditions. However, under the lunar gravity conditions, they were problematic. This conclusion was easily observed with DEM simulations of the dosing station.

5.4 Conclusion

In the first part of this chapter, analysis has been done on the influence of some particle-scale properties using continuum analysis with the developed DLA model. Results generated from most of the studies show good agreement with studies reported in literature. Also, investigations into the hopper orifice gives contrary predictions to previous studies in literature and this gives an opportunity to investigate further reasons for this deviation. The various particle scale properties investigated macroscopically showed that all the properties investigated play a major role in granular flow except the particle height representing the granular layer. It is concluded that the granular layer will not reasonably affect granular flow in an ideal hopper

Further, the influence of gravity on granular flow in a conical hopper has been investigated using the Kirya's structural model and DEM simulations using PFC^{3D}. Results of the gravity dependence on granular flow under varying gravity have been obtained by simultaneously solving the continuity equations and simulating via DEM. It has been demonstrated using the Kirya's structural continuum model that various particle scale properties will have different response to granular flow under different gravity levels. Defining the particle media as a continuum, granular flow and its particle properties have been shown to depend on gravity level where the rate of flow reduces with reduced gravity. These results on the gravity dependence are supported qualitatively by experimental results obtained from literature, practical parabolic flight test operation as well as DEM simulations carried out within the scope of this study.

The significance of this chapter has been demonstrated to lie in connecting particle-scale properties with both the continuum-level computation and discrete-level simulations through macrostructure and microstructure evolution, obviating the need to specify bulk properties and enabling prediction of particle-property effects on granular flow under varying gravity.

Chapter 7 further intensifies the application of three dimensional DEM using PFC^{3D} to investigate the effect of particle-scale properties in its discrete nature on granular flow.

Chapter 6

INFLUENCES OF PARTICLE-SCALE PROPERTIES AND HOPPER GEOMETRY ON THE FLOW BEHAVIOUR OF GRANULAR MATERIALS UNDER EARTH, MARS AND LUNAR GRAVITIES: PARAMETRIC ANALYSIS USING THREE-DIMENSIONAL DEM SIMULATIONS

6 Influences of Particle-Scale Properties and Hopper Geometry on the Flow Behaviour of Granular Materials under Earth, Mars and Lunar Gravities: Parametric Analysis Using Three-Dimensional DEM Simulations

Investigations into the effect of particle-scale properties and hopper geometry on granular flow under earth, mars and lunar gravity are detailed in this chapter. The study is based on the application of three dimensional DEM simulations using PFC^{3D}. Predictions and further understanding of the complex behaviour of particles and its response under EML gravity levels are presented in this chapter.

6.1 Introduction

A collection of distinct macroscopic particles makes up granular materials and it becomes complex to handle with the existence of distinct macroscopic properties. As reported earlier in previous chapters, the behaviour of granular materials during handling is greatly influenced by the inherent characteristics of the materials and gravitational environment. A lot of interesting and complex physics needs to be understood by studying the effects of gravity on the flow properties of granular materials in hoppers. The particle-particle interaction plays an important role in determining the flow properties of granular materials and because of the lack of understanding of this, many processing plants operate inefficiently and sometimes experience catastrophic failures (Jaeger et al., 1996b). The flow properties of particulate solids are known to depend on physical properties as well as the microscopic properties of the materials. The properties and phenomena associated with an assembly of particles and its handling in a hopper are: particle size distribution, cohesion and strength, packing properties (bulk density and porosity), flowability properties, coefficient of friction, hopper orifice opening and hopper internal angle. In recent years, the development of better methods in characterizing inherent particle properties has resulted to improvements in particle modelling using discrete element modelling (DEM) applications. During granular handling, different flow properties are required at different stages of processing and this is required to be carefully taken into consideration. In this research, computational three dimensional DEM modelling is then used to simulate granular flow in a conical hopper (Fig. 6.1) by predicting the effect of key particle-scale properties on flow properties under earth, mars and lunar gravity levels.

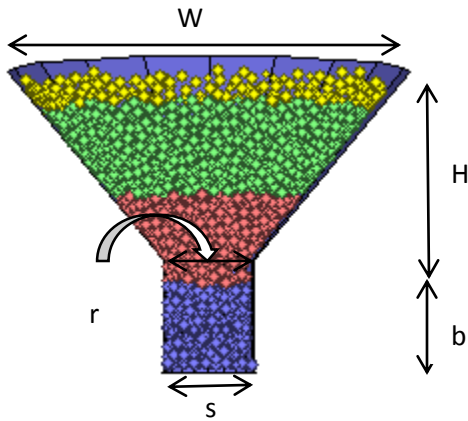


Fig. 6. 1 Conical hopper with confined grains for granular flow under EML gravity levels

The geometry of the conical hopper used in this investigation is presented in Table 6.1 with colour coded particles for presentation and tracing purposes only. The granular material used corresponds to the JS1 size distribution material defined in chapter four. Other material properties will be further emphasized in relevant sub-sections studying the various micro-scale properties. Discrete spherical particles were created randomly with the size distribution corresponding to JS1 simulant inside the hopper assembly with specifications of typical material properties of grains and hopper.

Table 6. 1 Standard values for the conical hopper geometry used in simulating granular flow under EML gravity levels

DESCRIPTION	VALUE
Upper Diameter (W)	Ø 35mm
Funnel Height (H)	21.06mm
Funnel lower diameter (r)	Ø 5.8mm
Throat Diameter (s)	Ø 5.8mm
Throat height (b)	5.24mm

After generating the initial random assembly with grains and the required packing density, they were allowed to flow through the opening of the hopper orifice. DEM thus helps to model the interaction between the contiguous particles as a dynamic process and the position of the particles are advanced using explicit finite difference scheme (Cundall and Strack, 1979). The motion of all the particles was carefully tracked down in exceedingly small time steps so as not to miss any natural behaviour under low gravity and the computations of flow parameters were performed under earth, mars and lunar (EML) gravity levels. For simplicity and in view of the large amount

of computational time required to simulate granular flow under low gravity levels, linear spring-dashpot model (Cundall and Strack, 1979) is used here, however with a bond strength added in the case of cohesive grains (Vermeer et al., 2007). The DEM model is applied to simulate the effects of different material properties associated with the granular materials under EML gravity levels.

6.2 DEM Model to Predict the Influence of Granular Packing on Granular Flow under EML Gravitational Field

It is well known that the characteristics of granular flow depend on the physical and mechanical properties of the single grains and also on the way the grains interact with each other. Recent development in DEM techniques has shown that more general materials can be simulated using packing of spheres and modelling the behaviour of the contacts between the particles as well as predicting the effect of granular packing on flow. A good understanding of the packing fraction, i.e. a ratio of the volume of the grains occupied per the total volume available is desirable to predict its effect on granular flow which has only been partially considered by the Beverloo's law (Mankoc et al., 2007, Dorbolo et al., 2013). Most of the existing knowledge on granular flow under low gravity is on the use of mono-disperse spheres with identical spheres (Hofmeister et al., 2009, Timounay et al., 2015, Delannay et al., 2007). However, this study is based on poly-dispersed spheres which are reported to be more of an advantage in replicating real systems. It is expected that flow rate may be induced by the changes in variations of packing fraction in horizontal silos, however, minimum or negligible effect is expected in vertical hoppers (Aguirre et al., 2014).

The impact of packing fraction on granular flow was then investigated under EML gravity levels to further understand its effect on flow at low gravity. DEM simulations were carried out using the hopper geometry in Table 6.1 and parameters in Table 6.2 under EML gravity levels.

Table 6.2 Parameters used to study the effect of packing fraction on granular flow under EML gravity.

Quantity	Value	Quantity	Value
Gravity m/s^2	1.67, 3.72, 9.8	Porosity	0.3 – 0.7
Density kg/m^3	2000	friction	0.6
Hopper wall Stiffness (Shear) N/m	2.0×10^{11}	Particle Stiffness (Shear) N/m	1.0×10^7
Hopper wall Stiffness (Normal) N/m	2.0×10^{11}	Particle Stiffness (Normal) N/m	1.0×10^7
Particle radius ratio	1.5		

The discharge process was analysed as the grains flow out of the hopper orifice. The mass of the grains as a function of time was investigated for various packings of the granular bed under EML gravity levels. Snapshots of the granular material at mid flow are presented in Fig 6.3 for highly dense and loose packed systems under EML gravity levels.

The rate at which the grains flow out of the hopper was studied and under earth gravity and presented in Fig. 6.2. It was observed that granular flow decreased with decreasing porosity. This implies that the grains tend to have easier flow in highly dense systems than in loosely packed systems with an increasing rate with gravity.

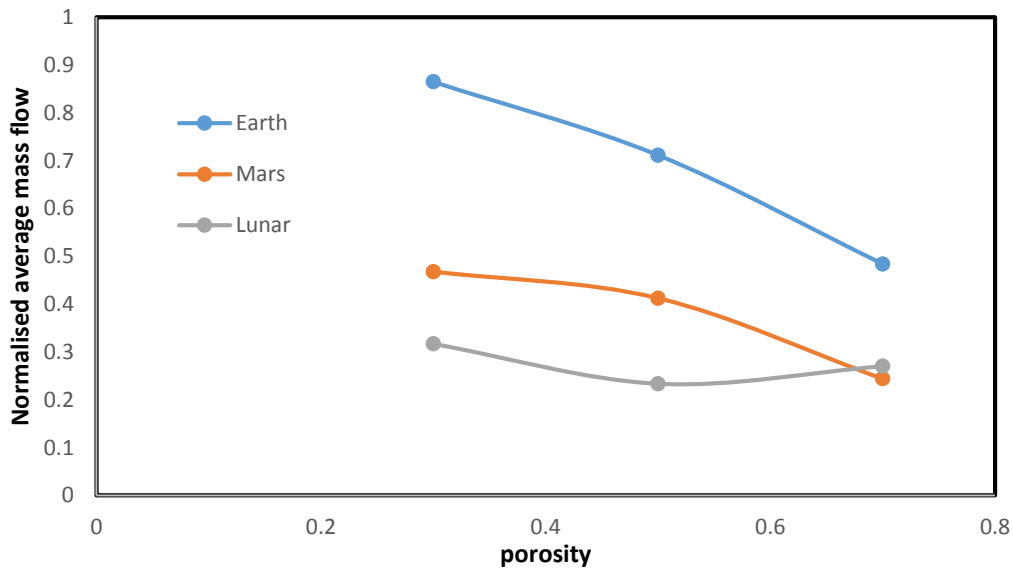


Fig. 6.2 Influence of packing fraction on granular flow under EML gravity

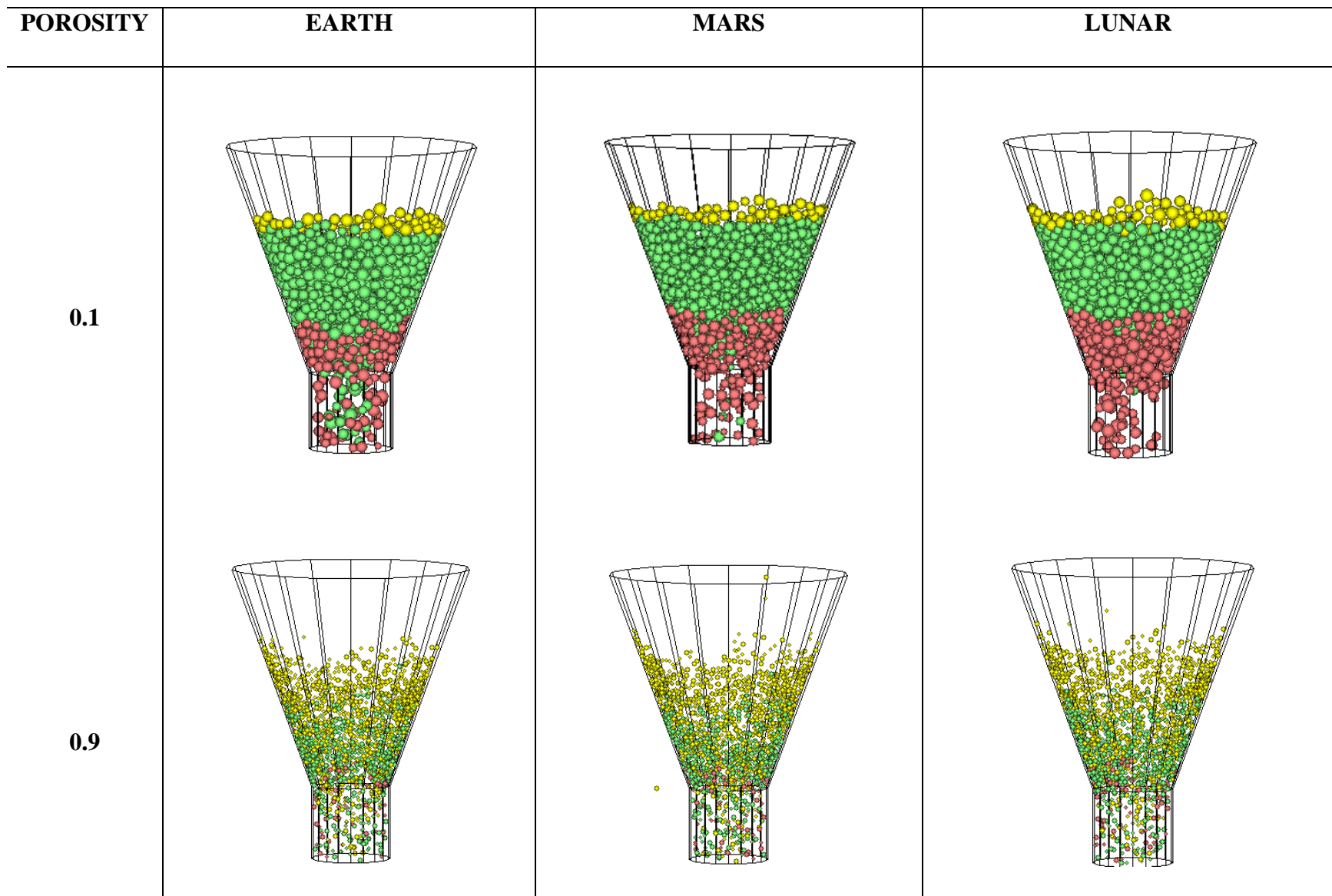


Fig. 6.3 Snapshots of the system during discharge process at mid flow for loose and dense packed grains under EML gravity levels

Results also show that under lunar gravity, the difference in the granular discharge rate for different packings is small compared to other gravities. This shows that the influence of granular packing is more notable and significant under earth and mars gravity compared to lunar gravity. For a loose granular packing with porosity 0.7 under mars and lunar gravity, the rate at which the grains flow out of the hopper tend to be similar.

6.3 Effect of Cohesion (Granular Bond Strength) on Granular Flow under EML Gravitational Field

6.3.1 Constant slit opening size of hopper

The study of cohesive granular media is necessary in the study of the behaviour of granular material and its applications. This work further extends this study to granular behaviour under lower gravity levels i.e. mars and lunar gravity levels. Cohesion in particles is as a result of adhesive forces formed as explained in section 2.4.6. The adhesive forces can either be as a result of a small aqueous wetting layer which forms menisci at the inter-particle contacts or due to the van der Waals interaction between the particles at close contact.

Extensive level of investigations for granular flow characteristics in hopper under three core gravity levels viz., Earth, Martian and Lunar conditions is carried out using DEM models on dry granular materials in view of getting a coherent and collective picture. The hopper geometry is as presented in Fig. 6.1 with the dimensions in Table 6.1. A range of bond strength values has been considered to investigate the effect of cohesion as presented in Table 6.3. The details of the inter-particle interaction with bond strength is provided in section A.3.3 in the appendix. The constitutive relation properties for this simulation set-up is that the bonds are created by specifying a non-zero value for any of the bond properties. In this case, the bonds are installed at real contacts (with non-zero overlap) and virtual contacts (between two particles with a separation less than 10^6 times the mean radius of the two particles) that lie within the range.

Table 6.3 Material properties used in DEM simulations for cohesion effect with constant hopper slit opening size

Quantity	Value	Quantity	Value
Gravity m/s^2	1.67, 3.72, 9.8	Particle radius ratio	1.5
Density kg/m^3	2000	Particle bond strength (Shear) N	1 – 5
Porosity	0.36	Particle bond strength (Normal) N	1 – 5
Particle friction	0.6	Wall friction	0.6
Hopper wall Stiffness (Shear) N/m	2.0×10^{11}	Particle Stiffness (Shear) N/m	1.0×10^7
Hopper wall Stiffness (Normal) N/m	2.0×10^{11}	Particle Stiffness (Normal) N/m	1.0×10^7

DEM simulations were performed to understand the inter-particle cohesion which was represented in terms of bond strength along the normal and tangential direction of individual grains on flow rate of grains in a systematic manner. Conical hopper geometry with dimensions shown in Fig. 6.1 containing granular material was simulated for flow properties under three dimensional conditions.

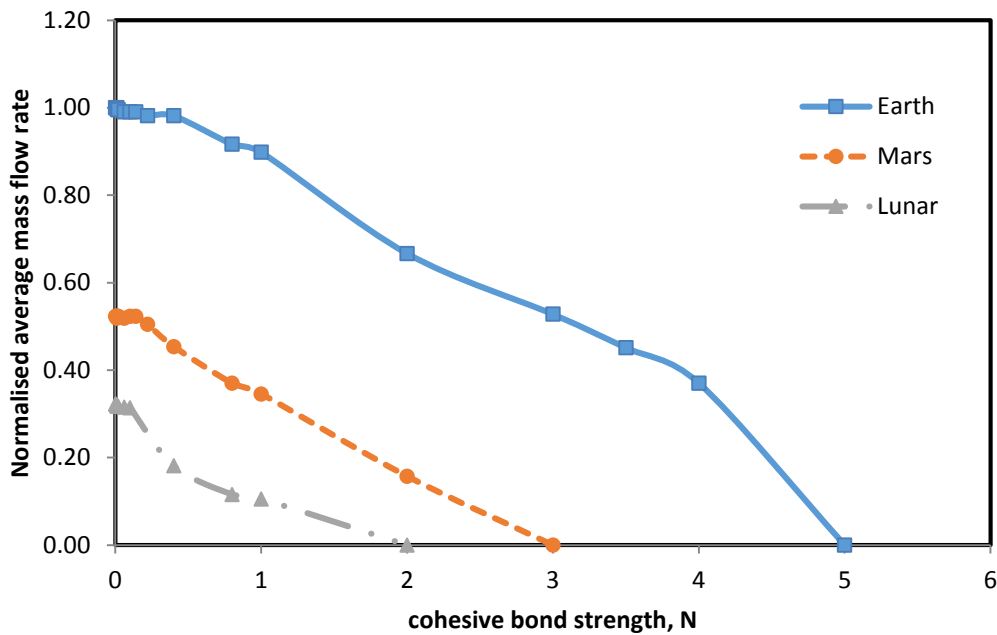


Fig. 6.4 Effect of cohesion on granular flow using three dimensional DEM under EML gravity

Fig. 6.4 shows the variation of normalized mass flow rate (with respect to that of earth gravity) as a function of cohesive bond strength between the individual grains.

The results presented in Fig. 6.4 show that inter-particle cohesion could have a strong influence on the flow behaviour of grains, especially under low gravity environments because the cohesion forces between the particles become more important under low gravity (Güttler et al., 2013). With increase in cohesion, it becomes more difficult for particles to flow from the hopper under all gravity conditions. It is also evident that, some cohesive particles which can still flow under earth gravity environment could potentially be more difficult to process under mars and lunar gravity environment as cohesion could promote particles to form clusters, which in turn is not conducive for free flow as illustrated in Fig. 6.5.

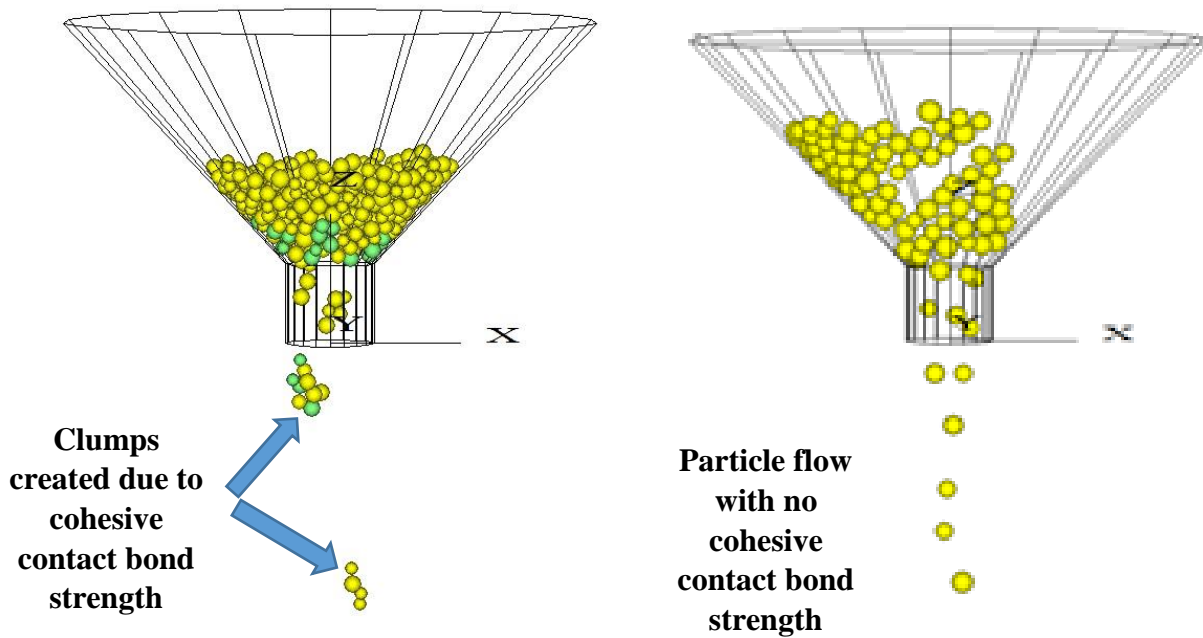


Fig. 6.5 DEM snapshots of clumps created due to cohesive bonds (3N) and particles with no cohesive bonds during granular flow

It is deduced from the simulation results predicting the cohesion effect that a limit can exist at which the flow behaviour of very low cohesive materials is likely to be similar to that of cohesionless materials. Thus, a magnification of Fig. 6.4 to see and understand the effects of low values of cohesive bond strength from 0 to 0.5N under EML gravity environment is presented in Fig. 6.6. It is clear that, though low cohesion may not affect the flow of the studied grains under earth gravity conditions, it could have a significant effect under lunar gravity environment. At low cohesion, the effect on flow more responsive under the lunar gravity level.

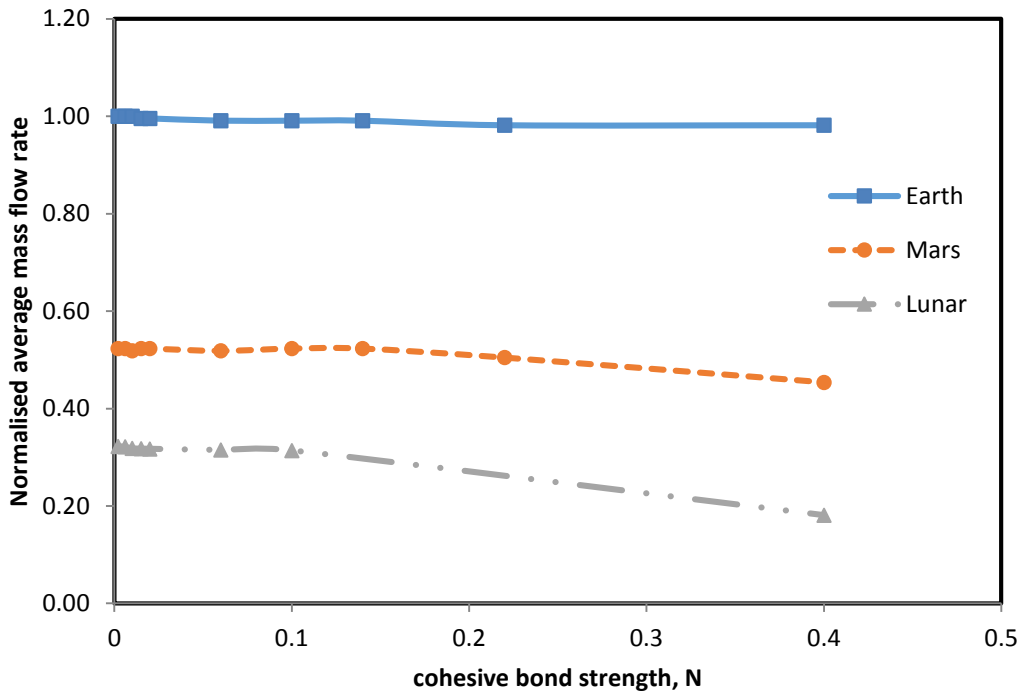


Fig. 6.6 Cohesion effect on particle flow at low bond strength under EML gravity using DEM

Simulation results presented in Fig. 6.4 and Fig. 6.6 help to understand the gravity environment under which cohesion effects are more detrimental to flow of grains.

6.3.2 Varying slit opening sizes of hopper

The hopper slit opening also known as the aperture or orifice opening has been reported to naturally have a critical size D_{min} below which flow is jammed. It is required that the hopper slit opening be significantly larger than the size of a single particle (Geiger et al., 2007). The hopper slit opening is a very important parameter which can impact the hopper discharge rate and as

discussed earlier in previous chapters, the Beverloo equation has shown that the discharge rate increases exponentially with increasing hopper width opening (Mankoc et al., 2007).

This section focus on applying three dimensional DEM simulations to investigate the effect of the hopper slit opening on granular flow for cohesive grains. In previous section, the importance of inter-particle cohesion has been established in which it was predicted that the inter-particle cohesion is less sensitive at low cohesion values. The cohesive nature was characterized in relation to the inter-particle contact bonds. This concept is applied to investigate the effect of slit opening on granular flow for cohesive particles under EML gravity levels. In order to compare the effect of the slit opening in all three gravity levels studied, cohesive material that has been reported earlier to flow in all gravity environments was applied by assigning a cohesive force value suitable for all gravity environments. As a result, the hopper geometry used are presented in Table 6.1. Additionally, the DEM simulation parameters used are as presented in Table 6.4 with a lower limit and upper limit values of the cohesive bond strength, viz., 1N (low cohesive grains) and 5N, (high cohesive grains) respectively used to represent the cohesion in the particles.

Table 6.4 Material properties used in DEM simulations for cohesion effect with varying hopper slit opening size

Quantity	Value	Quantity	Value
Gravity m/s^2	1.67, 3.72, 9.8	Hopper slit opening (mm)	4 – 6.4
Density kg/m^3	2000	Particle bond strength (Shear) N	1 & 5
Porosity	0.36	Particle bond strength (Normal) N	1 & 5
Particle friction	0.6	Wall friction	0.6
Hopper wall Stiffness (Shear) N/m	2.0×10^{11}	Particle Stiffness (Shear) N/m	1.0×10^7
Hopper wall Stiffness (Normal) N/m	2.0×10^{11}	Particle Stiffness (Normal) N/m	1.0×10^7

Considering that practical limitations of the SPDS would not allow increasing the height of the hopper funnel, sensitivity analysis was performed to study the effects of the hopper slit size on flow characteristics of grains. A range of hopper slit opening was considered from 4 mm to 6.4 mm under all three EML gravity levels and the results are normalized in relation to flow properties of the maximum hopper slit opening under earth gravity as presented in Fig. 6.7.

It is evident from results using low cohesive grains presented in Fig. 6.7 that the size of the hopper slit opening significantly influences flow behaviour of grains under all gravity levels considered, viz., earth, mars and lunar gravity levels. Increase in size of the hopper slit opening increases the average granular flow though at a decreasing rate for reduction in gravity level. For example, the results suggest that a 10% increase in hopper slit opening would result in an increase in the average mass flow rate of grains through the funnel by 6% for lunar gravity, 20% for mars gravity and 25% for earth gravity. The results indicate that for lower hopper slit opening (< 5.3mm) under lunar gravity, there will be a cease in granular flow and the grains tend not to flow out of the hopper. Also, for a higher hopper slit opening (> 5.3mm), the flow rate under lunar gravity is very low as compared to mars and earth gravity levels.

Further analysis was performed to understand the effect of hopper slit opening on granular flow for grains with higher cohesion strength of 5N considering the same range of the hopper slit opening and other conditions used above.

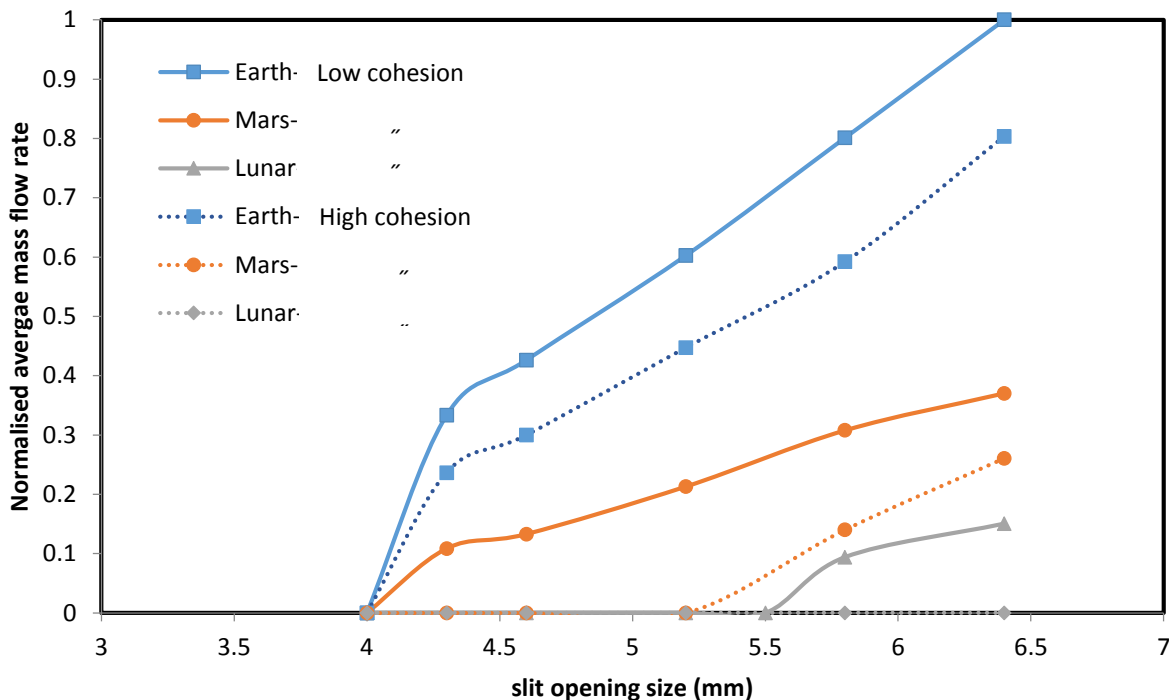


Fig. 6.7 Superimposed gravity effect of hopper slit opening on granular flow of low and high cohesive particles using DEM

Using high cohesive grains, the results presented in Fig 6.7 indicate that under earth and mars gravity levels, granular flow tends to increase with opening slit size. However, gravity is observed to be hindering the flow for higher cohesive grains under lunar gravity. Deductions from the result indicate that flow was not experienced under lunar gravity for all hopper slit opening ranges for higher cohesive grains investigated as shown in Fig. 6.8. Under Mars gravity, it was observed that grains will only start to flow at hopper slit opening size $> 5.3\text{mm}$ and tend to increase with increasing slit opening.

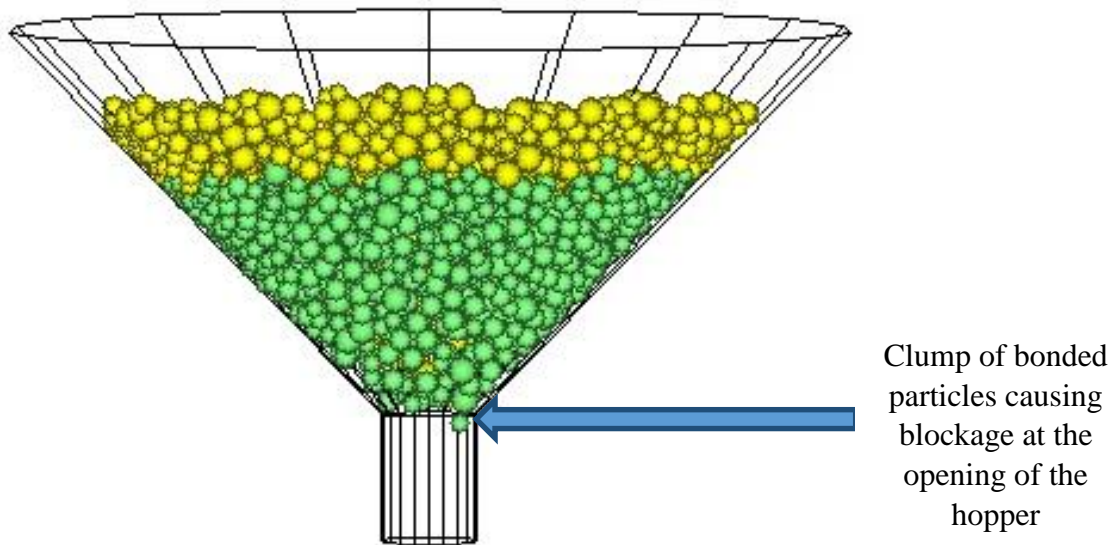


Fig. 6.8 DEM profile showing ceased flow of grains under lunar gravity

The result also further intensifies the predictions made earlier regarding the difficulty in processing granular materials under lower gravity. It can then be predicted that cohesive particles will be very difficult to process under lunar gravity with most cohesive particles not able to be processed under lunar gravity irrespective of the hopper slit opening size. Also under mars gravity, the slit size opening at which the grains began to flow differ to that under earth gravity for higher cohesive particles while for lower cohesive particles, flow will occur at the minimum hopper slit opening under both earth and mars gravity levels. Finally, predictions are that cohesive nature of grains will affect the hopper slit opening width at which flow will occur under earth, mars and lunar gravity levels.

6.4 Effect of Contact Stiffness on Granular Flow under EML Gravitational Field

A further approach is to vary the stiffness of the particle and also understand its effect on granular flow under EML gravity conditions.

Investigations were done on predicting the effect of different stiffness of particle from soft to hard particles. In this simulation, same parameters in Table 6.5 were used with a constant bond strength value of $1N$ in order to have reasonable flow under the EML gravity levels.

Table 6.5 Material properties used in DEM simulations for particle stiffness effect

Quantity	Value	Quantity	Value
Gravity m/s^2	1.67, 3.72, 9.8	Particle radius ratio	1.5
Density kg/m^3	2000	Particle bond strength (Shear) N	1
Porosity	0.36	Particle bond strength (Normal) N	1
Particle friction	0.6	Wall friction	0.6
Hopper wall Stiffness (Shear) N/m	2.0×10^{11}	Particle Stiffness (Shear) N/m	$1.0 \times 10^6 - 1.0 \times 10^8$
Hopper wall Stiffness (Normal) N/m	2.0×10^{11}	Particle Stiffness (Normal) N/m	$1.0 \times 10^6 - 1.0 \times 10^8$

The stiffness of the particle was varied broadly between $1 \times 10^6 N/m$ and $1 \times 10^8 N/m$ to understand and predict the effect of particle stiffness within different ranges on granular flow.

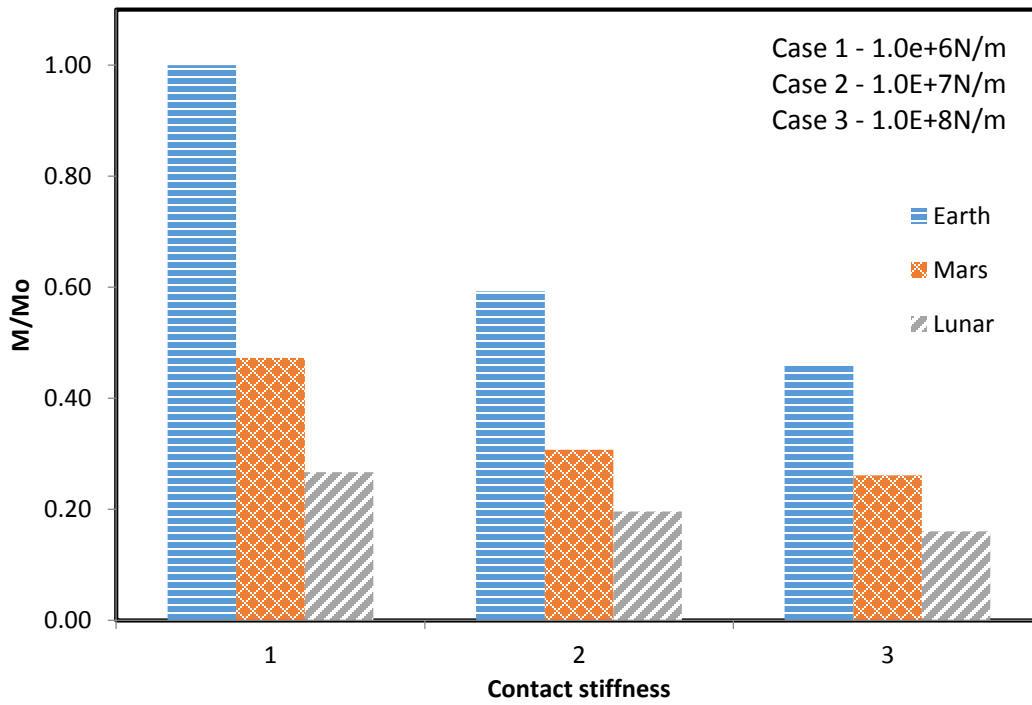
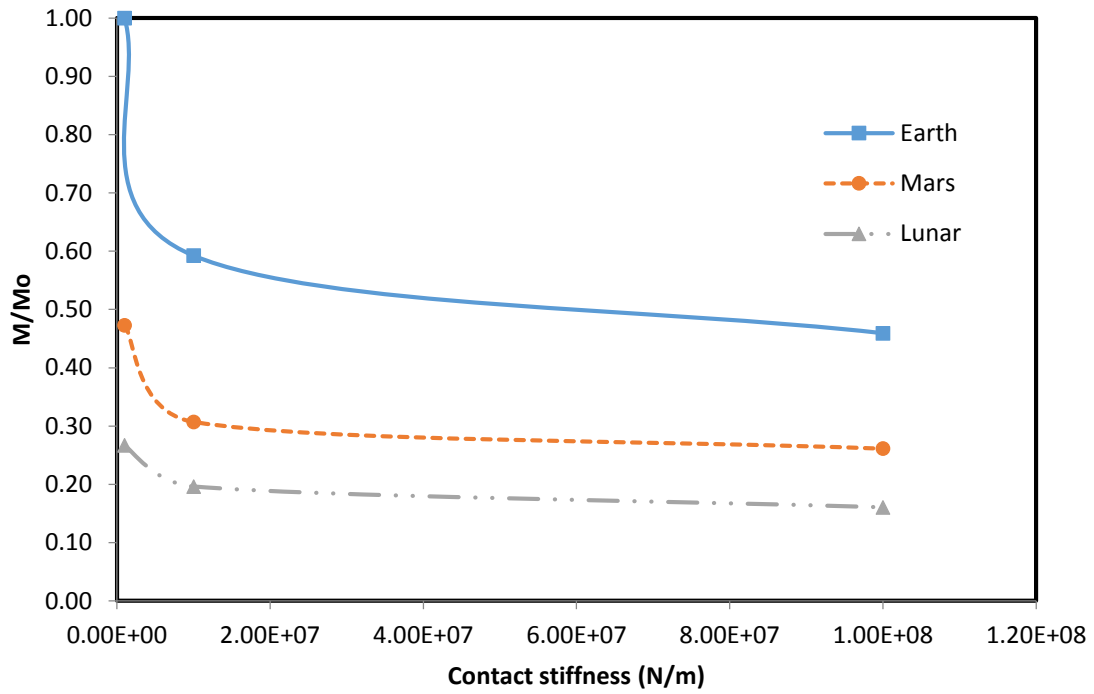


Fig. 6.9 Effect of particle stiffness on granular flow in hopper under EML gravity level using DEM

The results as shown in Fig. 6.9 indicate that an increase in particle stiffness leads to reduced granular flow which simply implies hard spheres will have low flow rate and soft spheres will flow quicker. In a related experiment by Peng et al. (2014), it was reported that soft spheres are more easily to deform and dissipate contact energy. Also, a similar phenomenon was found in a study by Kulkarni and Ochoa (2012). In that study, it was found that greater forces occurred in the hard particles and maximum deformation occurred in the soft particles.

From Fig. 6.9, as particle stiffness increases, the granular flow reduces with decreasing gravity level. Predictions are that at lower gravity levels, hard particles are likely to be difficult to process as compared to earth gravity. As the gravity reduces further, greater difficulty will be encountered in processing the hard spheres relative to the soft spheres. For increased stiffness, the cluster formation is much more.

6.5 Effect of Density of Particles on Granular Flow under EML Gravitational Field

The density of granular materials is not an intrinsic property and can change depending on the handling of the materials. The Beverloo law, and particularly the 5/2 power dependence of the flow rate on the diameter of the orifice, has been reported to be robust for different kinds of non-cohesive particles, independently of their density (Hirshfeld and Rapaport, 2001). Investigations are performed in this research to determine the effect of grain-scale density of particulate packing on granular flow in hoppers with different slit opening sizes under earth, mars and lunar gravity. For examining the effects of density of particles, two cases of grains: sandstone (density 2000 kg/m³) and basaltic grains (3000 kg/m³) were considered as given in Table 6.6

Table 6.6 Material properties used in DEM simulations for density effect

Quantity	Value	Quantity	Value
Gravity m/s^2	1.67, 3.72, 9.8	Particle radius ratio	1.5
Density kg/m^3	2000, 3000	Particle bond strength (Shear) N	1
Normal size distribution parameter	1.6	Particle bond strength (Normal) N	1
Porosity	0.36	Friction coefficient	0.6
Hopper wall Stiffness (Shear) N/m	2.0×10^{11}	Particle Stiffness (Shear) N/m	1.0×10^7
Hopper wall Stiffness (Normal) N/m	2.0×10^{11}	Particle Stiffness (Normal) N/m	1.0×10^7

Using the parameters given in Table 6.6 and the hopper geometry shown in Fig. 6.1, density effects were simulated for particles with different densities under all three EML gravity levels and slit opening sizes. Hence, many simulations were run and the results presented in Fig. 6.10.

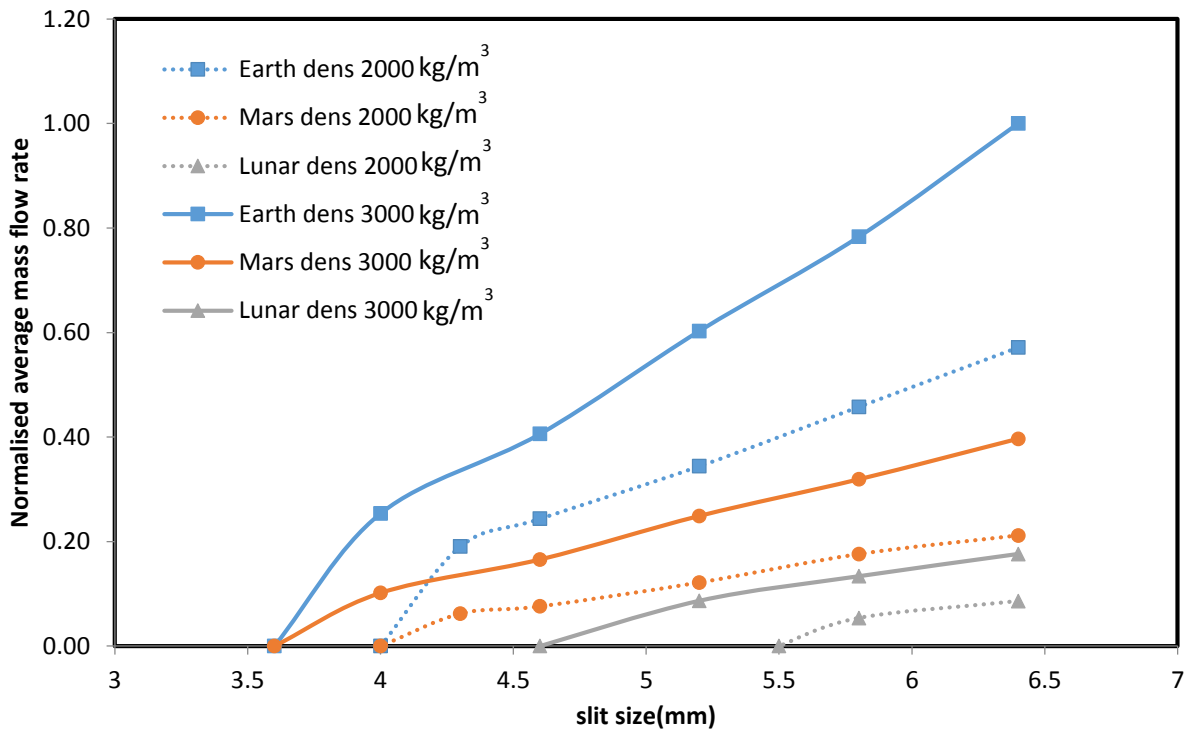


Fig. 6.10 Density effects on granular flow rate through hopper under EML gravity levels using DEM

From Fig. 6.10, it is evident that increase in density of particles resulted to an increase in the average granular flow rate of the particles through the hopper flow chamber under all three gravity environments considered, viz., earth, mars and lunar gravities. For the particulate system considered, 1000kg/m^3 increase in density results to an increase in flow rate of about 100% under mars and lunar gravity levels and 75% under earth gravity levels. Density was seen to make a significant impact on the minimum hopper slit opening size at which flow can occur. As represented in Fig.6.10, it was observed that the minimum slit opening size at which flow can occur for all gravity levels reduced for an increase in the density of the particles. It shows that the higher the density, the lower the minimum slit opening required at which flow will occur. The level of impact of the density effect was greater under the lunar gravity environment as compared to the other two gravity environment in terms of the slit opening flow occurrence.

6.6 Effects of Hopper Internal Angle on the Granular Flow under EML Gravity Level

As reported earlier with the analyses of stresses in static assemblies of granular media inside hopper geometries, the internal angle of the hopper orifice has been reported to have a strong influence on the spatial and temporal distribution of maximum stress inside hoppers (Albaraki and Antony, 2014). Further analysis on the influence of this internal angle on granular flow is carried out under EML gravity levels. In general as discussed in chapter two, gravity flow of granular materials can be broadly classified into mass flow, funnel flow and sometimes intermediate flow (Rhodes, 2008a, Tüzün et al., 1982, Johanson and Jenike, 1962). Though, a number of studies have been performed in the past to probe the flow properties of granular materials, a systematic level of investigations to provide a thorough understanding of the effect of hopper internal angles on granular flow is still lacking.

Three dimensional DEM has been applied to probe the influence of hopper angles between 30° and 90° and complemented with results from theoretical model using continuum theory and experimental results. Investigations were carried out using the hopper geometry as given in Fig. 6.1 and material properties in Table 6.7.

Table 6.7 Material properties used in DEM simulations for density effect

Quantity	Value	Quantity	Value
Gravity m/s ²	1.67, 3.72, 9.8	Hopper internal angle	30°, 45°, 60°, 90°
Density kg/m ³	2000	Particle bond strength (Shear) N	1
Porosity	0.36	Particle bond strength (Normal) N	1
Wall friction	0.6	Particle friction	0.6
Hopper wall Stiffness (Shear) N/m	2.0×10^{11}	Particle Stiffness (Shear) N/m	1.0×10^7
Hopper wall Stiffness (Normal) N/m	2.0×10^{11}	Particle Stiffness (Normal) N/m	1.0×10^7

Simulations were carried out for internal angles of 30, 45 60 and 90 degrees under EML gravity levels and the result presented in Fig. 6.11.

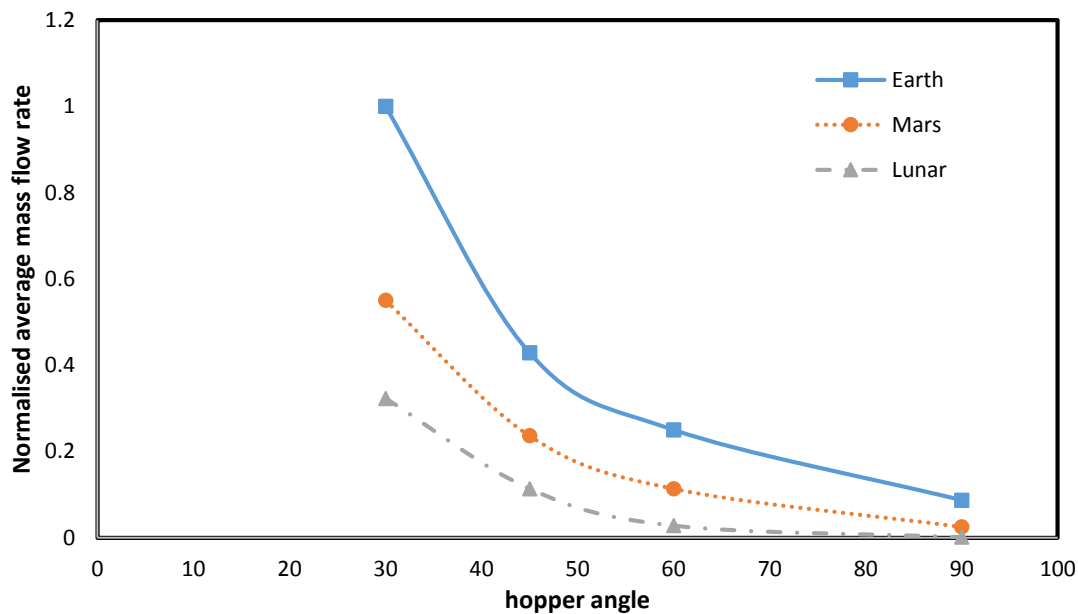


Fig. 6.11 Influence of hopper angle on granular flow under earth, mars and lunar gravity

Results presented in Fig. 6.11 indicates that as the internal angle increases, granular flow rate decreases. This simply implies that hoppers designed to have higher internal angles are likely to slow down the rate of flow of the grains from the hopper. During simulations, it was observed that hoppers with higher angles have the tendencies to form arches (Fig. 6.12) which have the capability

to hinder flow. Similar trend was observed under different gravity levels investigated, however, results show that as gravity reduces, the effect of the hopper angles becomes more significant.

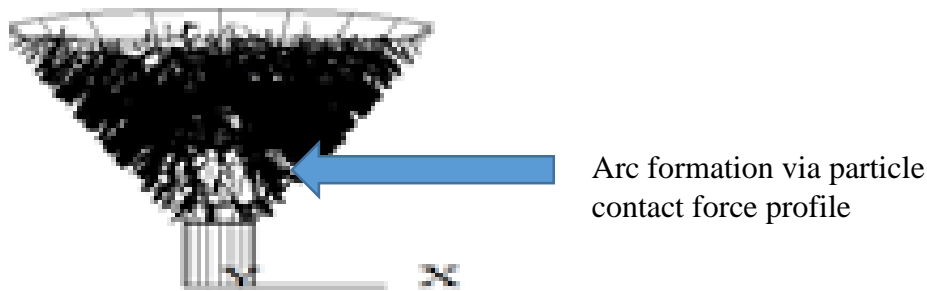


Fig. 6.12 Formation of arc during granular flow at high internal angle in DEM simulation

DEM results obtained agree with earlier investigations carried out using continuum model (Fig. 5.7) and the experimental investigations (Fig. 5.6) reported by Albaraki et al. (2013) and Albaraki and Antony (2014) using PSAT and DPIV technique under earth gravity. Also, comparing with the conclusions reached earlier in the stress analysis across the hopper width, the influence of the internal angle on the max stress of the particles can be said to have an effect on the dynamic nature of the granular materials. For lower hopper angles such as 30° as investigated, the flow rate is high. Additionally, the particle displacement aligned in the same direction with gravity for hopper angles at 30° while for hopper angles at 90° , the particle displacement are towards the hopper walls as shown in Fig. 6.13.

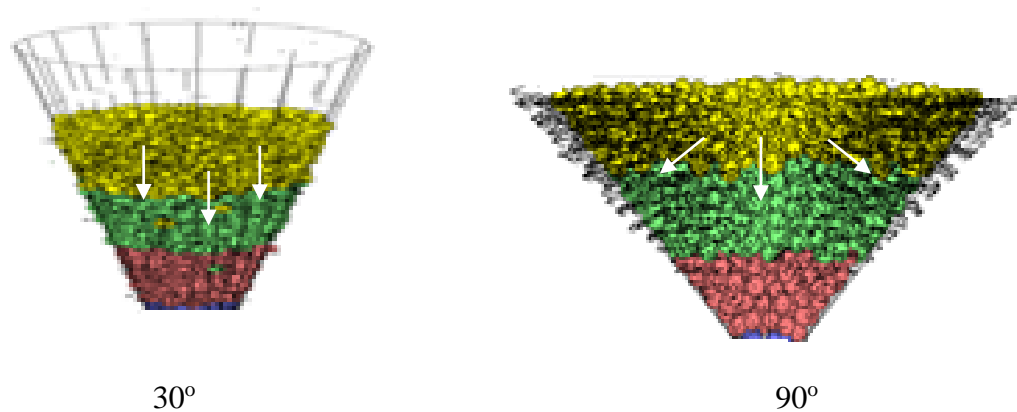


Fig. 6.13 Typical DEM simulation profiles showing the displacement of particles at 30° and 90° hopper internal angle

Also, this gives an indication on the type of flow that can exist due to the hopper internal angle. It shows that flow within 30° hoppers are in continuous motion and exhibit a mass flow profile. On the other hand, hoppers designed with higher internal angles tend to exhibit funnel flow and grains are mostly displaced towards the hopper walls apart from around the orifice.

Such observations are also found in experimental studies reported by Albaraki et al. (2013) and Albaraki and Antony (2014) as shown in Fig. 6.14. It was concluded that even granules which are generally classified as free flowing could experience difficulty in flow through hopper orifices depending on the hopper internal angle.

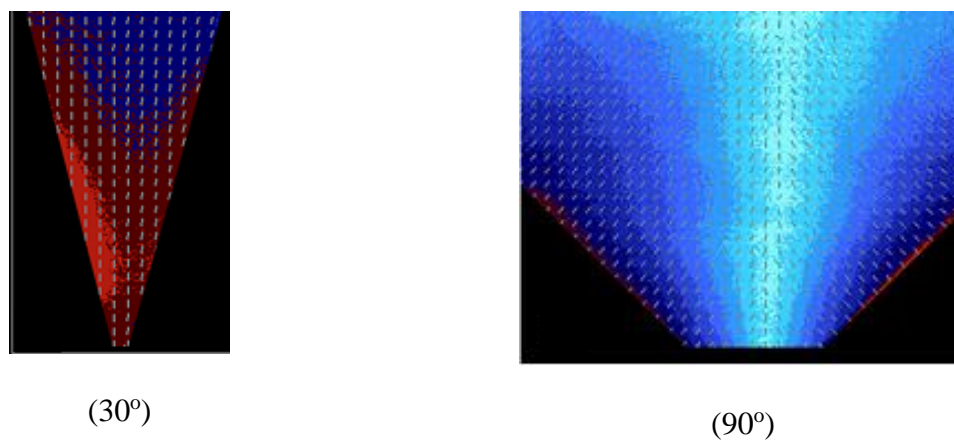


Fig. 6.14 Experimental results showing major stress principal directions inside stress responsive granules at 30° and 90° internal angle hopper geometry (Albaraki and Antony, 2014)

The influence of the hopper internal angle is also seen to increase with decreasing gravity and at lunar gravity, the design of hoppers should be limited to a maximum of 60° where reasonable flow rate can be obtained.

6.7 Influences of Friction Coefficient on Granular Flow under EML Gravitational Field

Friction can be seen as how the particles interact inside granular materials and is the resistance of flow of granular materials. The coefficient of friction μ is seen as the ratio of friction force friction between two bodies (particle-particle or particle-wall) and the interacting force. The understanding of the impact of friction coefficient on granular flow has been studied by many researchers (Thornton et al., 2012, Langston et al., 1995, To et al., 2001), however, no fully established research has been done to analyse the effect of inter-particle friction as well as wall-particle friction independently under low gravitational environments. A number of researches focus on the measurement technique of friction coefficient, for example using AFM (Attard et al., 2007, Breakspear et al., 2004). The friction effect in filling as well as unsteady/steady discharge in a three dimensional wedge-shaped hopper was investigated numerically using DEM by Cundall and Strack (1979). The friction effect was analysed by varying inter-particle friction coefficient over the range 0 – 0.6 and compared with available continuum based predictions. Cox and Hill (2005) studied the friction effect on discharge velocities under earth gravity and that the velocity profiles predicted do not depend much on the friction angle. These studies do not consider the individual effects of particle–particle as well as particle–wall friction.

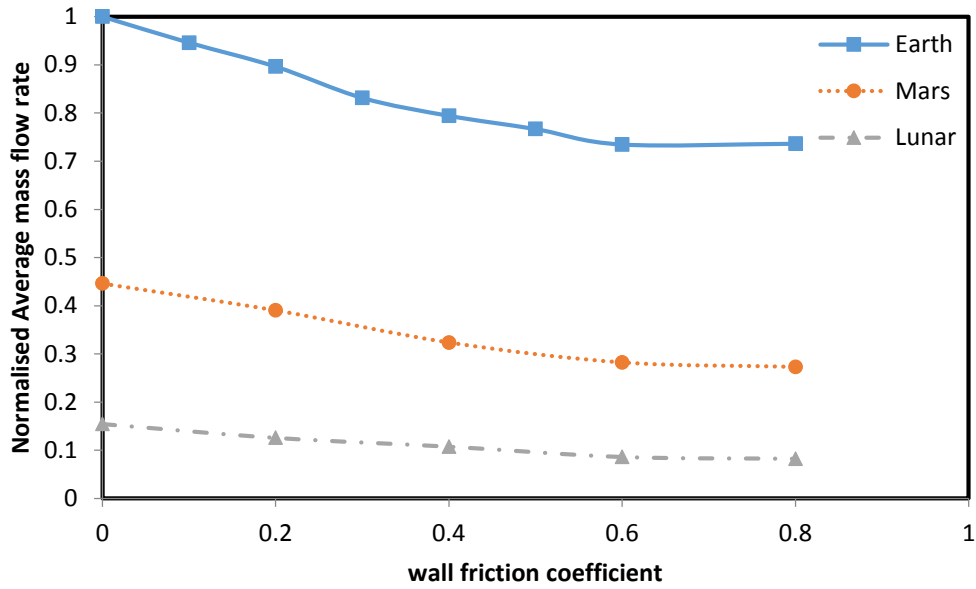
Three dimensional DEM is applied using the parameters listed in Table 6.8 and hopper geometry provided in Fig. 6.1 to extensively simulate the effect of particle and wall friction on granular flow.

Table 6.8 Material properties used in DEM simulations for friction effect

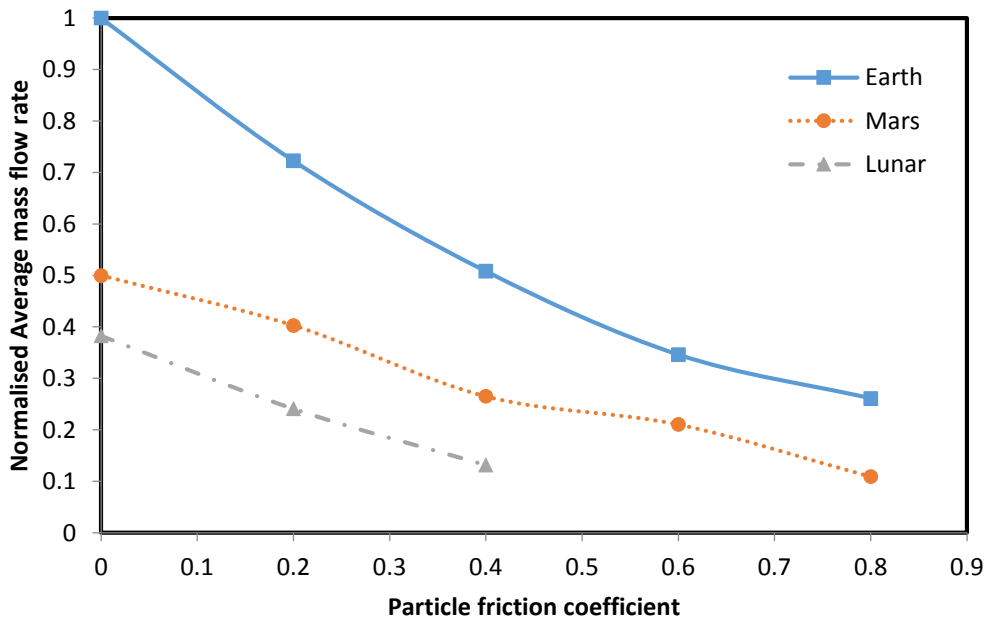
Quantity	Value	Quantity	Value
Gravity m/s ²	1.67, 3.72, 9.8	Particle bond strength (Shear) N	1
Wall friction	0-0.7	Particle bond strength (Normal) N	1
Particle friction	0-0.7	Density kg/m ³	2000
Porosity	0.36	Particle Stiffness (Shear) N/m	1.0×10^7
Hopper wall Stiffness (Shear) N/m	2.0×10^{11}	Particle Stiffness (Normal) N/m	1.0×10^7
Hopper wall Stiffness (Normal) N/m	2.0×10^{11}	Particle radius ratio	1.5

The effect of friction coefficient is analysed under the EML gravity levels. The friction effects considered for analysis in this study are for both particle-particle (particle friction) and particle-wall (wall friction) of the hopper granular flow independently. The effect is considered numerically using the DEM and results presented in Fig. 6.15. Varying wall friction effect was simulated at a constant particle friction coefficient of 0.3 and vice versa where the wall friction was constant at 0.3 for different cases of inter-particle friction under EML gravity levels.

Results presented in Fig.6.15 indicate that increase in both wall and particle friction independently leads to a decrease in granular flow. Thus, at no/low friction, high flow is experienced within the hopper and as the friction coefficient is increased, the flow rate decreases with decreasing gravity. It is evident that wall friction results decrease in average mass flow rate of grains from the chamber especially under earth gravity environment – however, the level of this influence decreases with decrease in gravity. It is interesting to note that for Lunar gravitational environment, the effect of wall friction is minimal. For example, a reduction of friction coefficient by 0.4 is required to achieve an increase in average mass flow rate of grains only by about 20% under lunar gravity environment and 25-30% for Martian and Earth gravity environments. It was also observed that friction coefficients (both particle and wall) have greater effects on flow rate within the hopper under earth gravity environment as compared to mars and lunar gravity environments.



(a) Wall Friction Effect



(b) Particle Friction Effect

Fig. 6.15 Effect of (a) wall friction and (b) particle friction on granular flow in hopper under EML gravity levels

DEM simulations can also help to develop virtual platforms to assess the effect of material behaviour under low-gravity conditions. The effect of Wall friction is less sensitive to flow than particle friction. The sensitivity of particle friction increased with reducing gravity and as a result, particle friction influences granular flow far more dominantly than wall friction under low gravity. Under lunar gravity, particle friction is expected to play a dominant role during granular flow.

6.8 Effects of Angle of Repose Formed by Grains of Granular Flow under EML Gravity Levels

Angle of repose is a method used to characterize the flowability of granular materials / powders (Zhou et al., 2002, Ileleji and Zhou, 2008). It gives information about the static properties of the granular assembly. To illustrate the effect of gravity levels on the angle of repose, three dimensional DEM is employed to simulate granular flow. Grains that are discharged from the hopper forms a heap on a flat surface at a near distance from the hopper orifice. It has been reported that the angle of repose is a function of grain properties and its shape is dependent on the material properties (Lumay et al., 2012). The angle of repose is a basic property of non-cohesive granular materials which is as applied in this study. In this study, the angle of repose is measured after complete discharge of the particles from the hopper under different gravity levels. The same process of modelling granular flow in the hopper has been explained in chapter 5. The properties used during the study of the angle of repose are given in Table 6.9. The particles in the hopper are allowed to reach equilibrium and the base of the hopper orifice is opened for the particles to discharge. The particles form a heap on the flat surface and the angle of repose is measured.

Table 6.9 Parameters used in DEM simulation of gravity effect of angle of repose

Quantity	Value	Quantity	Value
Gravity m/s^2	1.67, 3.72, 9.8	Porosity	0.36
Wall friction	0.6	Particle friction	0.6
Density kg/m^3	2000		
Hopper wall Stiffness (Shear) N/m	2.0×10^{11}	Particle Stiffness (Shear) N/m	1.0×10^7
Hopper wall Stiffness (Normal) N/m	2.0×10^{11}	Particle Stiffness (Normal) N/m	1.0×10^7

Overtime, there have been conflicting predictions regarding the role of gravity on the angle of repose of cohesionless particles. It is however assumed in planetary morphology and geology that the angle of repose of a non-cohesive granular material is independent of gravity. This hypothesis has hardly been tested and proven, though; so many experimental studies have been carried out to test the angle of repose. For example, experiments have been carried out to test the angle of repose as a function of material properties (Brucks et al., 2007), discharge time and dynamics (Mangeney et al., 2010).

Results obtained from this study are surprising and indicate that for decreasing gravity, the angle of repose decreases with a small margin from earth gravity to lunar gravity (Fig. 6.16).

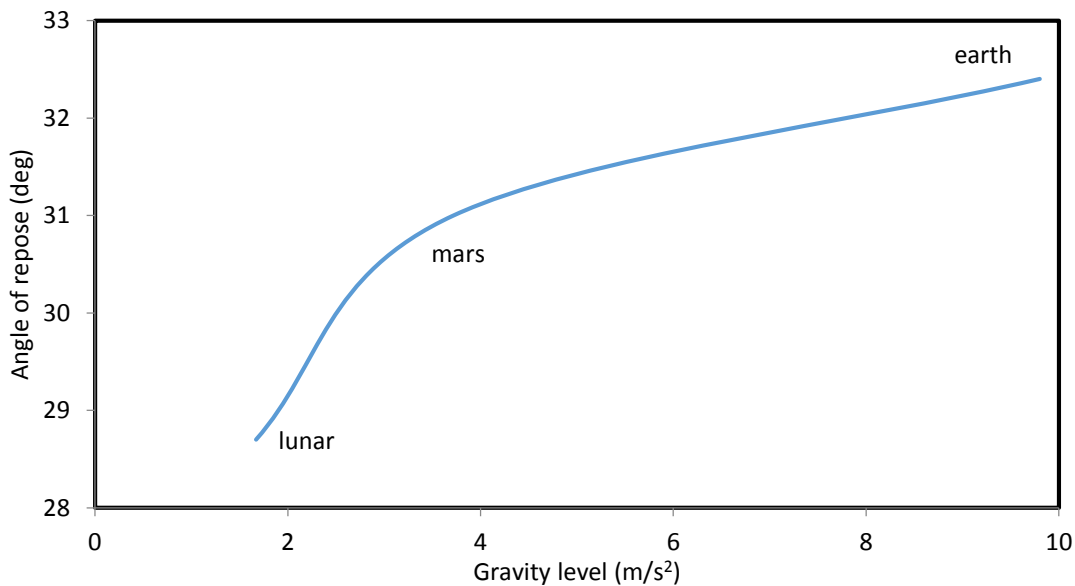


Fig. 6. 16 EML gravity effect on angle of repose of cohesionless granular material

The result obtained is in disagreement with a large body of work that assumes the independency of gravity on angle of repose. Similar experimental investigations by Nakashima et al. (2011) showed that both dense and loose sand displays little change in angle of repose under varying gravity. It was concluded that the change in angle of repose is not significant and the shape of the pile formed under low and high gravity levels in relation to earth gravity with the angle of repose obtained during the experiments was averaging 30.1°. DEM simulation profiles of the angles of repose under earth, mars and lunar gravity from this study are given in Fig. 6.17.

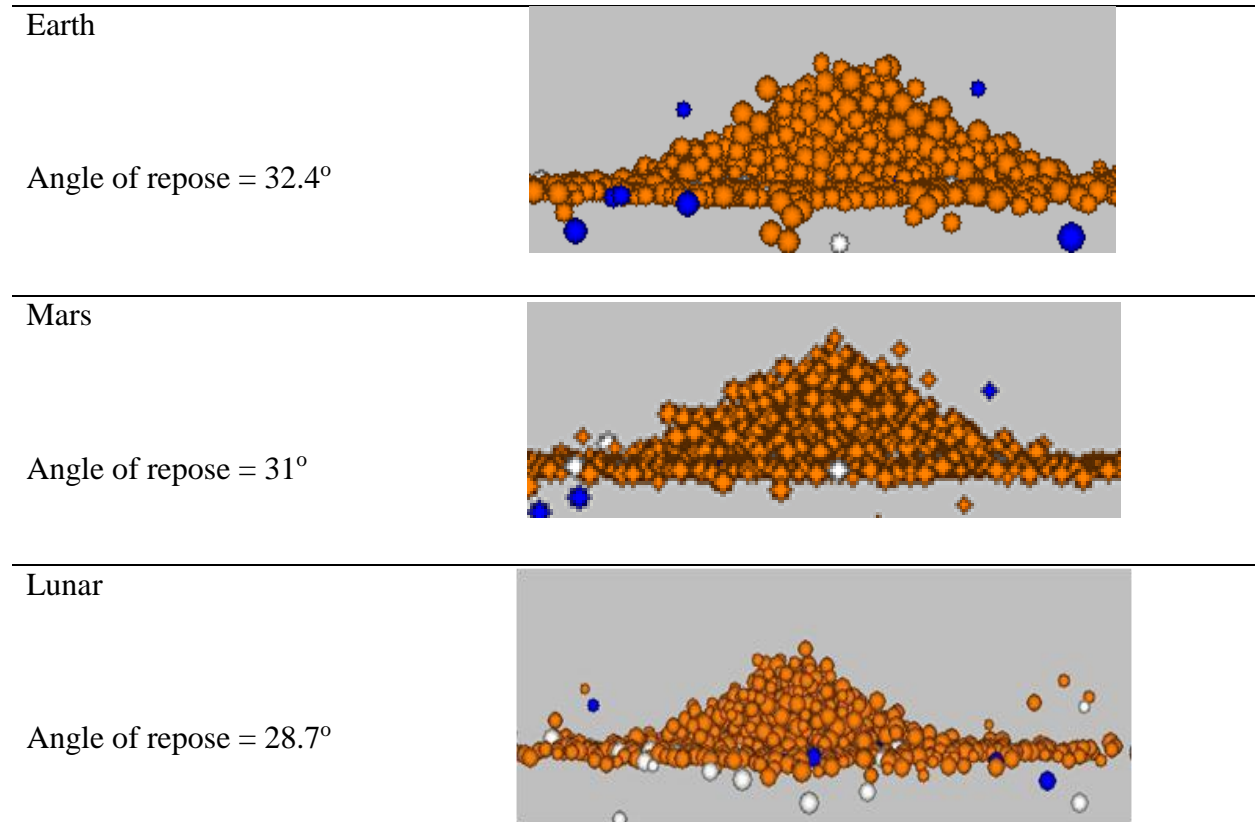


Fig. 6. 17 Angle of repose predictions from DEM simulations using cohesionless granular materials

Predictions from this three dimensional DEM simulation gives an angle of repose ranging from 28.7 to 32.4 degrees between lunar and earth gravity. This indicates the angle of repose will depend on gravity as against the general assumption of its independence. This effect is however predicted to be relatively marginal as validated with results obtained from a parabolic flight test experiment reported by Kleinhans et al. (2011) and Dorbolo et al. (2013) with the dynamic angle of repose predicted to decrease with decreasing gravity with about 10°. It is however worth noting that the sample size used in investigating the angle of repose in this study is limited. The predictions from this study could be related to the dilatancy effect as granular flow is more dilated in lower gravity.

6.9 Influence of Combined Effects of Particle Size Distribution (PSD) and Adhesion Strength of Grains on Granular Flow

In relation to evaluating the combined effects of particle size distribution (PSD) and adhesion force properties, simulations correspond to real samples for which their characteristics are given in chapter 3. The method of measurement of the adhesion force is based on colloidal force microscopy (CFM) which is a modified atomic force microscopy. PSD describes a population of particles which can be expressed with the aid of frequency distribution or cumulative curves. The distribution curve which is depicted by a histogram has the distribution divided into different size ranges.

The combined effects of PSD and adhesion force on granular flow was studied for different samples of granular materials, viz., JS1, JS2, JS3, JS4, JB1, JB2, JB3, and JB4. The distinct measurement procedure of particle size distribution and adhesion force for the different samples obtained from experiment are explained in sections 3.1 and 3.2. The particle size distribution for each sample corresponds to the images in Fig. 3.2 and the adhesion force measurements are summarised in table 3.1. It has been reported that for granular materials having narrow size distributions, the flowability increases significantly with increase in particle size while, wider particle size distributions allow better particle packing, thereby increasing inter-particle friction (Liu et al., 2008).

A conical hopper was modelled as previously used with the geometry parameters in Table 6.10 and other particle-scale properties given in Table 6.11.

Table 6. 10 Standard values for the conical hopper geometry used in simulating granular flow under EML gravity levels for different particle size distribution

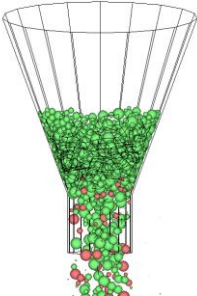
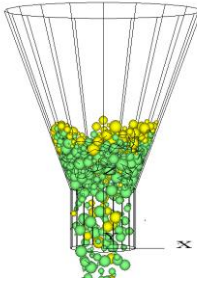
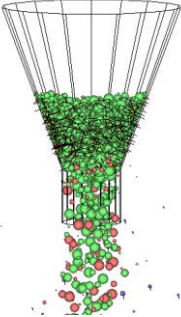
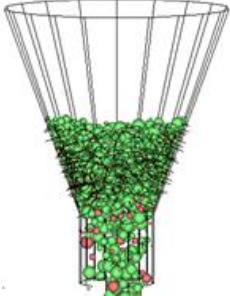
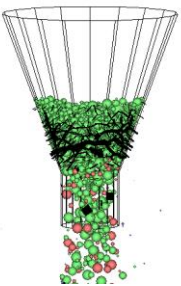
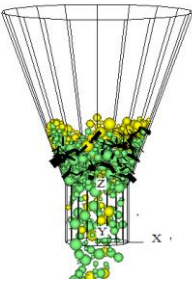
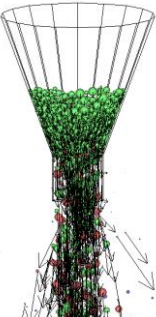
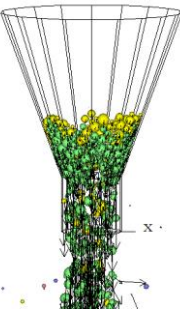
DESCRIPTION	VALUE
Upper Diameter (W)	Ø 26.8mm
Funnel Height (H)	27.5mm
Throat Diameter (s)	Ø 6.1mm
Throat height (b)	7.5mm
Funnel angle (β)	56 degree

Table 6. 11 Parameters used in DEM simulation on the effect of combined particle size distribution and adhesion force on granular flow under EML gravity levels

Quantity	Value	Quantity	Value
Gravity m/s^2	1.67, 3.72, 9.8	Porosity	0.36
Wall friction	0.6	Particle friction	0.6
Density kg/m^3	2000	Particle radius ratio	
Hopper wall Stiffness (Shear) N/m	2.0×10^{11}	Particle Stiffness (Shear) N/m	1.0×10^7
Hopper wall Stiffness (Normal) N/m	2.0×10^{11}	Particle Stiffness (Normal) N/m	1.0×10^7
Particle size distribution	JS1 – JB4		

The simulation was carried out using DEM following same procedure as explained earlier under EML gravity levels. Discrete spherical particles were created randomly with different size distributions inside the hopper assembly with specifications of typical material properties of grains and hopper.

Typical flow profiles are extracted for samples JS1 and JB1 for the contact bond, particle contact, force contacts, velocity and displacement at third quarter of flow under gravity flow as shown in Fig.6.18.

	JS1	JB1	Scale
Contact bond			Bonding that exist between the particles.
Particle Contact			Contact between particles in the bulk assembly
Contact forces			The forces are both normal and shear forces. The black lines denote normal forces while red lines denote shear forces. The thickness of the line denotes the magnitude of the forces
Maximum contact force chain is 1.156e2N			
Velocity profile			This is denoted with arrows and the length of the arrow shows the magnitude of the velocity. Long arrow length shows high velocity
Maximum velocity profile is 2.84e-2m/s			

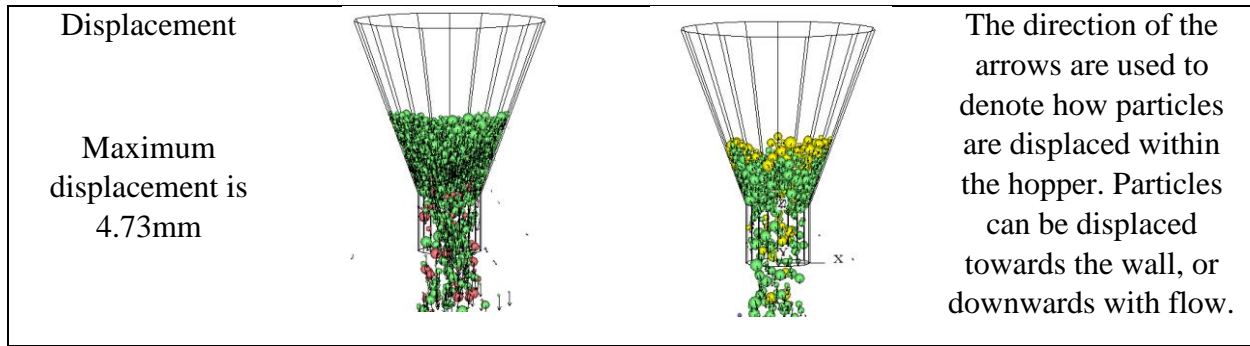
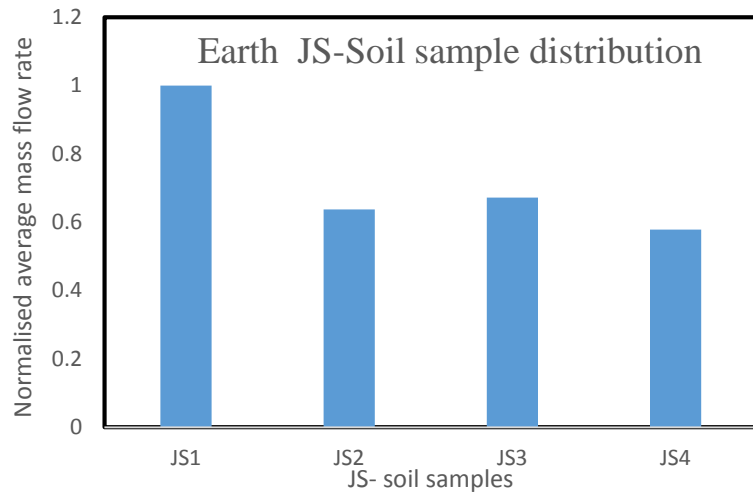


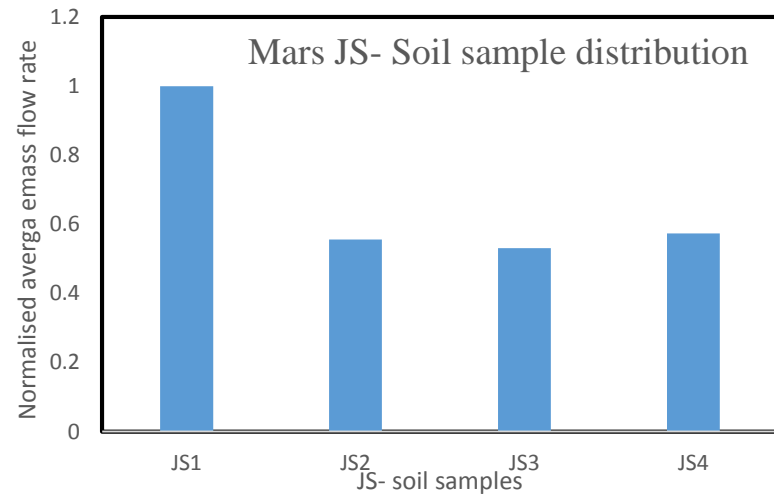
Fig. 6. 18 Typical flow profile for PSD of soil samples JS1 and JB1 at $\frac{3}{4}$ flow under gravity flow

The macroscopic flow rate was investigated for all the various soil samples with different size distribution. Having established the dependence of granular flow on gravity in previous chapters, the effect of gravity on the samples with different size distributions and adhesion values are reported under EML gravity levels.

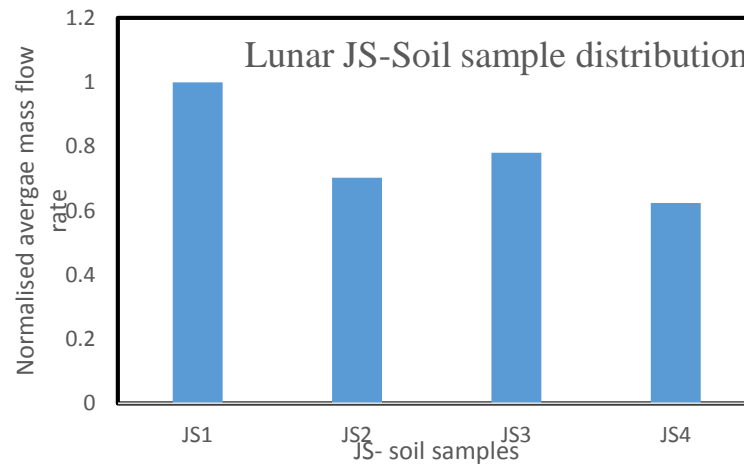
The results of the granular flow of JS soil simulants and JB soil simulants are presented in Figs. 6.19 and 6.20 respectively under EML gravity levels. The JS and JB flow rates are normalised with the flow rate of the JS1 soil sample under similar gravity conditions (for example, Fig. 6.20(b) is normalised w.r.t JS1 of Fig. 6.19(b) etc.).



(a)

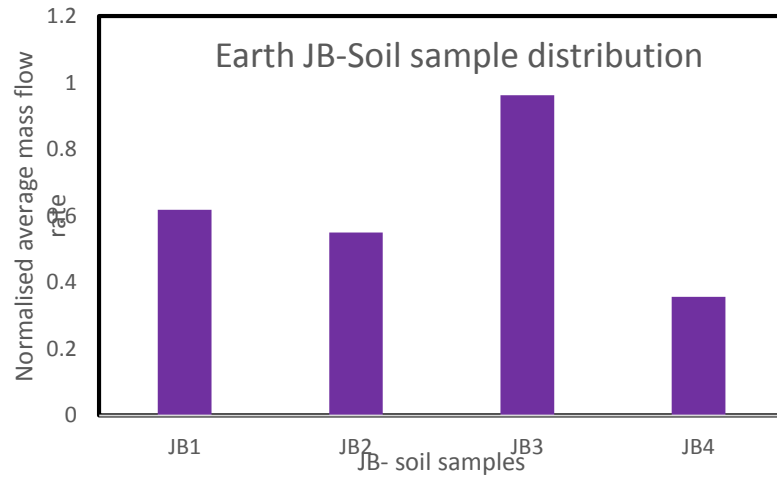


(b)

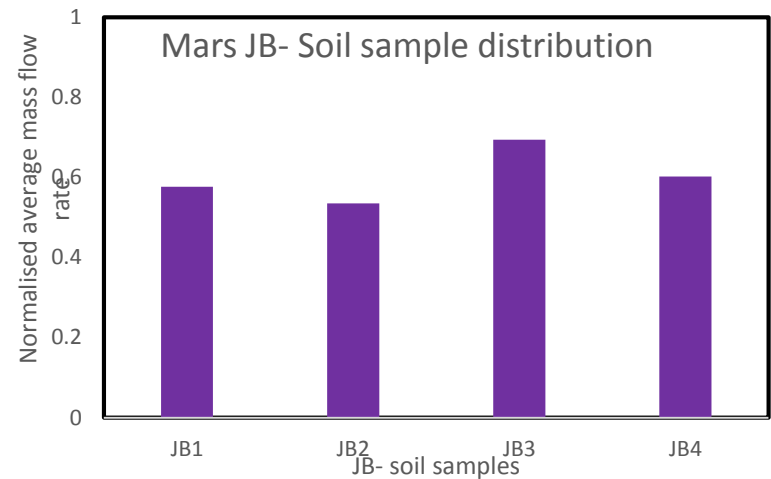


(c)

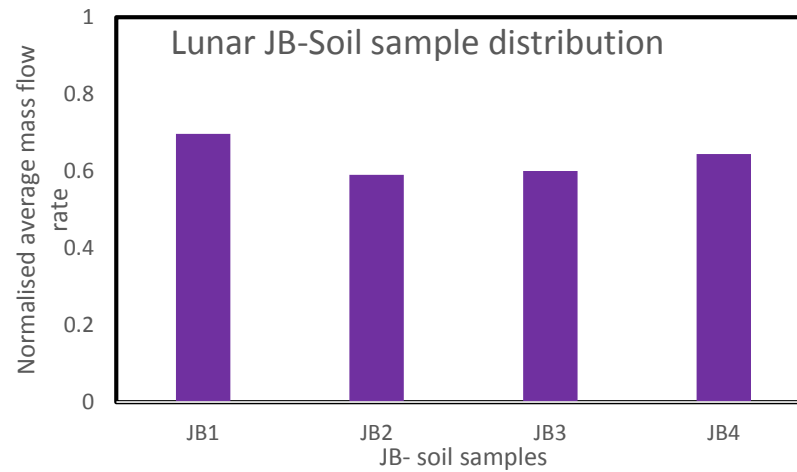
Fig. 6. 19 Particle size distribution dependence on granular flow for JS1 to JS4 soil simulants under EML gravity levels



(a)



(b)



(c)

Fig. 6.20 Particle size distribution dependence on granular flow for JB1 to JB4 soil simulants under EML gravity levels

Results presented in Figs. 6.19 and 6.20 indicate that grains with different size distributions and adhesion forces tend to behave and flow differently under varying gravity environment. Although it is generally accepted that granular flowability increases with increase in particle size, comprehensive insights and quantitative studies on the particle effects of real samples are still lacking (Liu et al., 2008). Results of the JS samples (Fig. 6.19) indicates that JS1 grains are the easiest free flowing grains and also has the lowest adhesion force. The order of granular flow for JS samples from the easy flowing grains is such that under earth gravity, JS1 > JS3 > JS2 > JS4; under mars gravity, JS1 > JS4 > JS2 > JS3 while under lunar gravity, JS1 > JS3 > JS2 > JS4. The macroscopic flow of the JB samples presented in Fig. 6.20 indicate that JB3 grains are the easiest free flowing grains under earth and mars gravity. Though, JB3 grains have higher adhesive forces, they also have very big particle sizes. The trend is such that under earth gravity, JB3 > JB1 > JB2 > JB4 and under mars gravity, JB3 > JB4 > JB1 > JB2. JB3 soil samples have bigger particles as compared to other soil samples and the large particle sizes have an effect on the flow rate. However, under lunar gravity, same cannot be said for the bigger particles with the trend indicating that JB1 is the easiest free flowing materials and the order is such that JB1 > JB4 > JB3 > JB2 with very little difference in their granular flow rates.

It is expected that as particle size decreases, the ratio of the surface area to mass increases. Inter-particle surface forces such as cohesion and friction are related to the total surface area and since mass is proportional to volume, the surface area to the volume ratio gives good indication of granular flow (Frisch, 1989, Liu et al., 2008). Thus, granular materials have the propensity to cling to each other at higher surface area to volume ratio rather than flow under the influence of gravity thereby reducing the ability to flow freely (Stanford et al., 2003). Also, particles with narrow size distributions and wider size distributions tend to affect flowability (Liu et al., 2008) under gravitational flow.

Results obtained under EML gravity levels also indicate that granular flowability is a multifunctional parameter (Mullarney and Leyva, 2009, Hart, 2015) which not only depend on size distribution but also on gravity, inter-particle forces and particle interactions. Simulation results also gives indication of great dependency on gravity levels as the flow of the materials vary for different size distributions under earth, mars and lunar gravity. This also suggests that, when

the gravity levels are relatively small such as under the lunar gravity, individual effects of particle-scale properties of larger size particles negate the differences on the net bulk flow rate.

6.10 Conclusions

Three dimensional DEM simulations using PFC^{3D} have been used to successfully analyse and predict the effect of micro-properties on granular flow under earth, mars and lunar gravity. The effect of gravity on granular flow was generally observed in analysing individual granular properties and characteristics. DEM simulation models were developed in aiding the prediction on the influence of granular packing, granular bed density, cohesion, hopper geometry (orifice and internal angle), friction effect, angle of repose and combined adhesion strength and size distribution (for real samples) of the granular materials. It was found that grains tend to have higher flow rate in highly dense systems than in loosely packed systems with an increasing rate with gravity. Also, the dependence on gravity was established such that the impact of granular packing was more significant under earth gravity as compared to mars and lunar gravity and this impact was decreasing with decreasing gravity. Reduced flow was predicted for grains at low cohesion with decreasing gravity level. The results obtained from the simulation indicate that inter-particle cohesion can have a strong influence on the flow behaviour of grains, especially in low gravity environments. As a result, at low cohesion, the effect on flow is more responsive under lunar gravity level. The hopper orifice was also investigated and results predict a significant influence of the hopper orifice on flow behaviour of grains under all gravity levels considered, viz., earth, mars and lunar gravity. The influence of gravity was more pronounced under lunar gravity such that there was a cease in flow at low hopper orifices in which at same low hopper orifices, granular flow still exist under higher gravity levels. A granular bed with higher density resulted in a high rate of granular flow of the particles through the hopper flow chamber under all three gravity environments considered, viz., earth, mars and lunar gravities. Compared to other gravity levels, density was observed to have more impact on the flow of grains under lunar gravity levels in terms of the hopper orifice opening. In a related approach, the hopper internal angle investigated also indicate a strong influence on granular flow. Conclusions are that hoppers designed to have higher internal angles are likely to slow down the rate of flow of the grains from the hopper. Friction effect was investigated for both particle – particle friction and particle – wall friction independently. Simulation results obtained indicate the influence both have independently on

granular flow under earth, mars and lunar gravity. The influence of these friction coefficients independently has not been fully explored in the literature under low gravity and simulation results indicate the independent influence of both friction coefficients under earth, mars and lunar gravity. The effect of wall friction on flow is smaller than particle friction and the sensitivity to particle friction increased with reducing gravity. Particle friction influences granular flow far more dominantly than wall friction under low gravity and as such, under lunar gravity, particle friction plays a dominant role during granular flow. Angle of repose was also reported to marginally depend on gravity and the reduced angle of repose under low gravity further implies the difficulty in the movement of granular materials under lower gravity as compared to earth gravity. The results obtained in this report are in disagreement with a large body of work that assumes the angle of repose is independent of gravity. This contrasting result may be due to the limited sample size used in this study. However, recent parabolic flight test investigations agree with simulation results from this study showing slight differences in the angle of repose under low gravity levels. Finally, the combined effect of adhesion force and size distribution of real samples was also investigated. Simulation results show that samples with different adhesion forces and size distributions behave differently under a low gravity environment and have different influences on flow as compared to earth gravity. Additionally, the differences in particle scale properties don't seem to affect far strongly for larger particles. Thus, the combined effect of adhesion force and PSD for the real samples seems to reduce with decreasing gravity.

In general, the aim of this work is to have intimate good understanding of granular materials in the application of future robot propagation and processing plants of granular material on the moon (lunar) and mars. Thus, from the simulation results and few experimental/theoretical support from earth gravity obtained, the work has not only successfully added insight to granular handling and possible problems that may be encountered in the manufacturing operations in a variety of disciplines but gives a profound view to similar granular handling and possible problems that may be encountered regarding flow in moon and mars exploration.

Chapter 7

DEM SIMULATIONS FOR ENHANCING GRANULAR FLOW UNDER EML GRAVITIES

7 Granular Flow Aids and Flow Improvement

This chapter focuses on improving gravity driven granular flow through a hopper under earth, mars and lunar (EML) gravity environments. The study considers the effect of horizontal vibration on gravity driven granular flow without considering the damping effect. Also in this chapter, three dimensional DEM simulations are performed to understand the differences in filling a collection chamber with continuous granular flow and staggered (intermittent) granular flow. Three dimensional DEM model is applied to investigate possible ways flow can be improved under EML gravity levels. The first part of the chapter is focused on the application of vibration horizontally to improve flow while the second part is focused on the introduction of staggering on a gravity driven flow under EML gravity levels.

7.1 Introduction

Understanding granular flow driven by gravity in the discharge of granular materials from bins and hoppers is essential to solve material handling challenges. However, not all materials flow well under the influence of gravity alone leading to flow problems that can adversely affect the process (Lumay et al., 2009, Forterre and Pouliquen, 2006, Hilton and Cleary, 2011). The addition of flow aids can help to improve the granular flow such as turning cohesive granular materials to an improved flowing material (Antony et al., 2004). As a result, ranges of flow aid approaches which have been discussed in chapter two have been studied overtime to try to overcome the problem. The flow aid adopted in this study is one of the mechanical active devices known as vibrating dischargers. Application of vibration in industries involves the disposal of granular materials and improving granular flow using horizontal vibration devices (Wu and Sun, 2008).

Horizontal vibrating discharger aids are intended to shake the throat of the hopper horizontally and periodically (Kollmann and Tomas, 2002, Hunt et al., 1999). The transmission of vibration is through the outer shell of the hopper medium and a cohesive/non-flowing bulk can be broken up and induced to flow depending on the amplitude of the vibration applied (Jaeger et al., 1996b). Vibrators are usually mounted on the side of a bin or hopper to help initiate or induce flow and can be air or electrically operated (Marinelli, 2014). In this chapter, DEM simulations are employed to model vibrational induced gravity flow in a hopper under EML gravity levels.

This chapter further introduces the effect of staggering gravity flow as against continuous flow of granular materials. This is to study the possibility of improving flow using a stop-flow system by staggering flow at intervals under EML gravity levels which is similar to the study previously carried out on continuous granular flow (Chapter 5).

7.2 Horizontal Vibration Induced Hopper Flow under EML Gravity Levels

Extensive levels of examinations were performed to understand both the microscopic (internal characteristics) and macroscopic (bulk) flow characteristics of grains under the influence of horizontal vibrational induced gravity flow under EML gravity levels. The microscopic properties investigated include particle contacts, contact force chains, velocity profile and displacement profile. JS1 type particles are considered here and placed into a hopper (Fig. 6.1) of given dimension summarised in Table 7.1.

Table 7.1 Hopper parameters and Microscopic material properties used in simulating vibrational induced gravity flow under EML gravity levels

Hopper Inlet Funnel		Micro properties	
Description	Value	Description	Value
Upper Diameter (W)	Ø 26.8 mm	Porosity	0.36
Funnel Height (H)	27.5 mm	Particle Stiffness N/m	1.0×10^7
Throat Diameter (s)	Ø 6.1 mm	Particle Friction	0.6
Throat Height (b)	7.5 mm	Wall Friction	0.6
Funnel angle (β)	56deg	Wall Stiffness N/m	2.0×10^{11}
		Density kg/m^3	3000
		Bond Strength	JS1 type (Table 3.1)
		Size Distribution	JS1 type (Fig. 3.2)

Particles are allowed to flow under gravity with the aid of a horizontal vibrator modelled using DEM. Simulations were carried out for gravity flow with vibrations at different frequencies and compared with gravity flow without vibration under EML gravity levels. The model is allowed to reach equilibrium under specified gravity loading and the gate wall is opened to allow flow. The piezo-vibrator technique is employed in which the walls of the hopper shake horizontally at specified sinusoidal velocity. This velocity depends on the frequency and amplitude which is the

displacement specified horizontally in the x-direction. The vibrator technique is governed by the mathematical derivatives given in equations 7.1 to 7.3

$$Wvx = D * \omega * \text{Cos}(\omega * \text{time}) \quad (7.1)$$

$$D = k * hw \quad (7.2)$$

$$\omega = 2 * \pi * f \quad (7.3)$$

Where,

Wvx = Wall velocity,

D = Displacement induced horizontally in the x-direction (Amplitude)

k = a constant (in percent) to multiply the width

hw = Hopper width (bottom width)

ω = angular frequency

f = normal frequency

time = time-step in secs

With the aid of the vibrator technique, the frequency at which the hopper wall vibrates was initially varied between 0 – 10Hz at a constant k of 5%. Microscopic properties were monitored during flow and a typical profile of the microscopic properties is reported for vibration induced granular flow under mars gravity. The quantities described in the profiles were taken at different durations of the flow: the initial state and three further stages of the flow viz., quarter, half and three-quarters of the total flow duration. The particle contacts show a plot of line connecting the contacts between neighbouring particles (centre to centre of spheres) in the bulk assembly. The contact force chains provides the plot of normal and tangential contact force between the grains. The velocity profile provides the plot of resultant velocity component of the grains while the displacement profile provides the profile of relative displacement of the particles. In the plots presented in Figs 7.1 – 7.5, the thickness of the lines is scaled proportional to the magnitude of the quantities presented. The following observations reported under the mars gravity level, which is the focus of the current

investigations. However, at later stages, corresponding macroscopic flow parameters are presented for all the three cases of gravity (EML) levels.

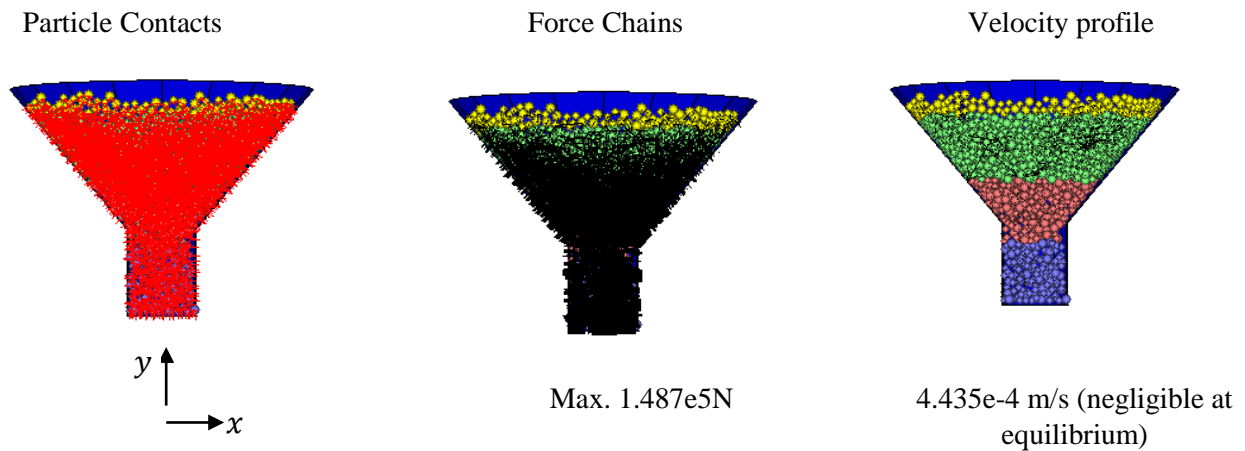
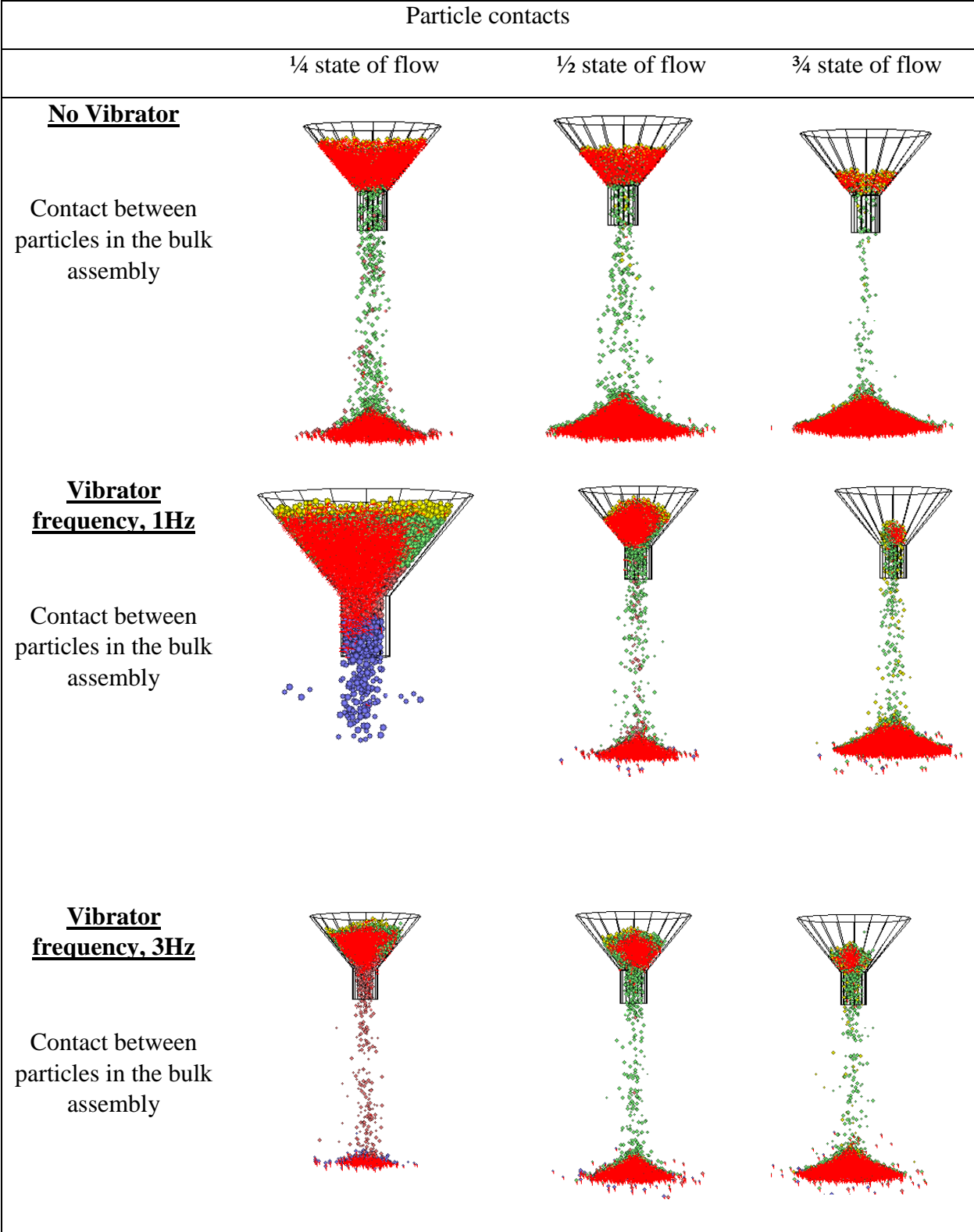


Fig. 7. 1 Initial position of grains just after samples attained equilibrium

The observations indicated in Fig. 7.1 further emphasized the fact that force distribution and contact features of granular media are non-homogenous even in a random packing (Antony, 2007). The colour coding of the grain layers are with respect to their elevation for easy presentation at later stages. The profile of the particle contact at different vibration frequencies during flow is presented in Fig 7.2.



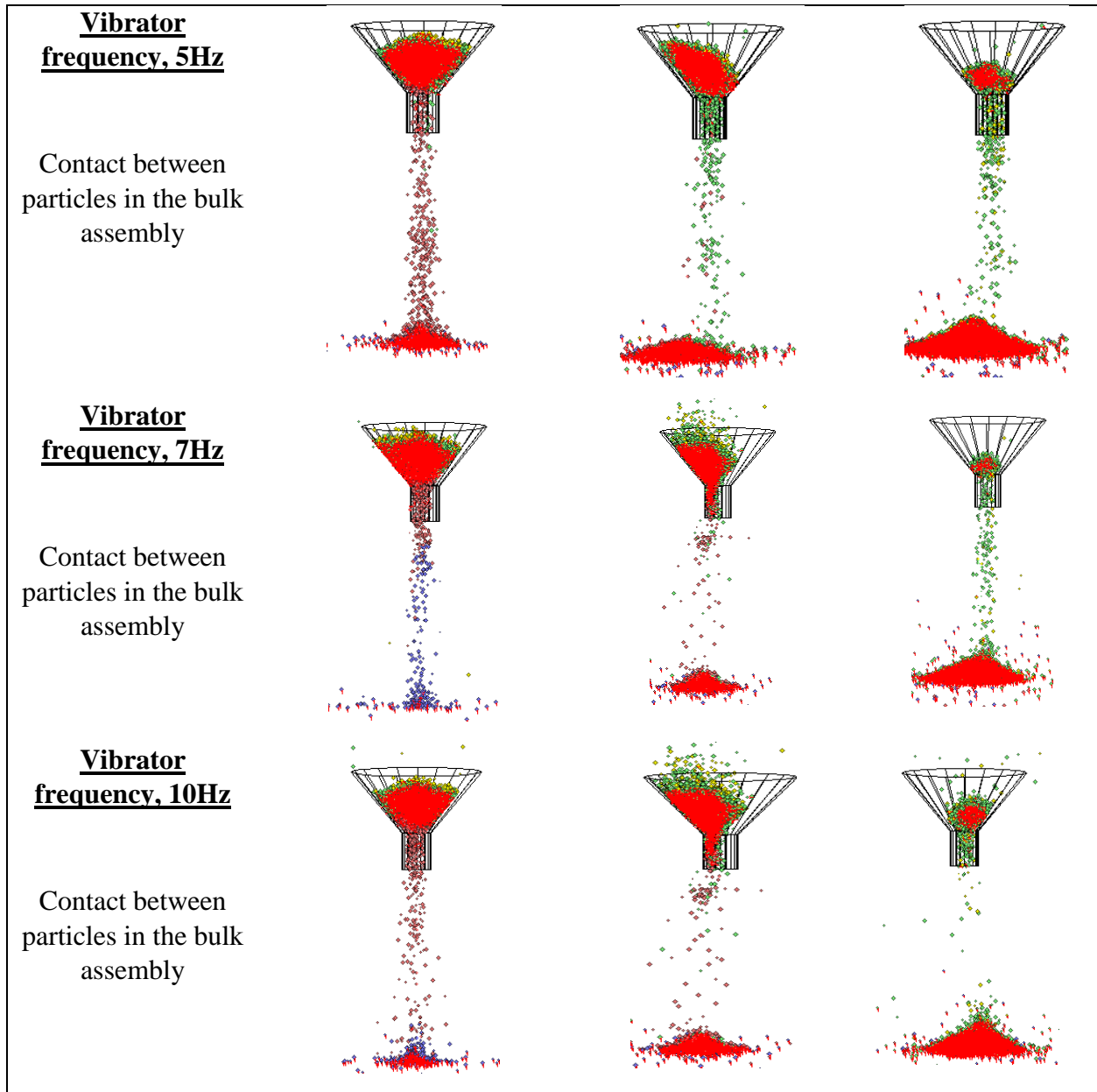
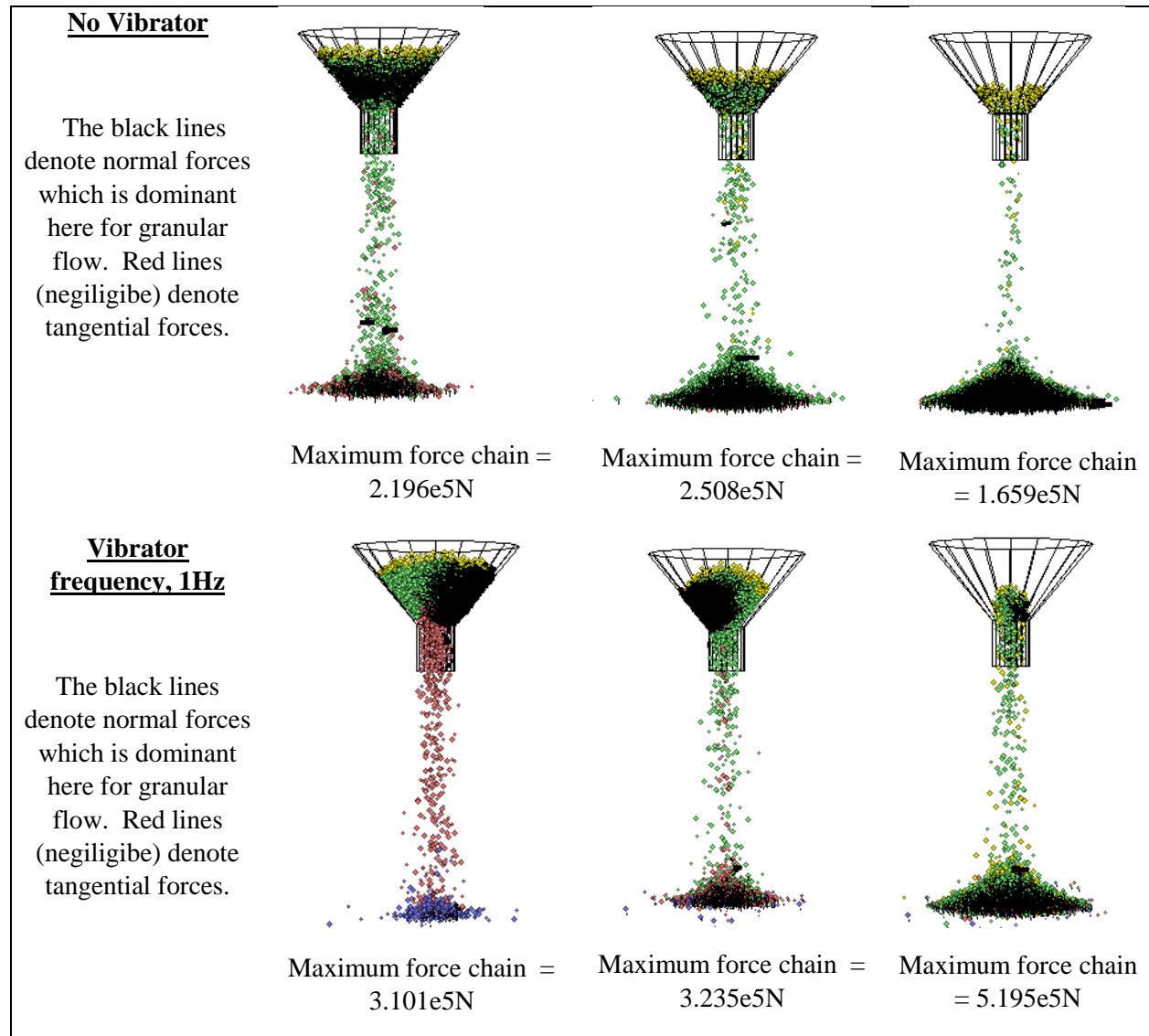


Fig. 7. 2 Profiles of particle contacts at different stages of flow: for the cases of no vibrator and vibrator with sinusoidal frequency 1Hz, 3Hz, 5Hz, 7Hz, and 10Hz under gravity flow (Mars gravity)

The results from Fig. 7.2 indicate that when vibrator was not activated, the contact bonds of the particles tend to be symmetrical with respect to the vertical axis, whereas the symmetry breaks down in the case of grains under vibratory motion. This break down occurs especially at the early and mid-flow durations. Also, relatively more dominant contact bonds are observed at a vibration frequency of 1Hz. This suggests for a potentially better macroscopic flow rate of grains at a slow vibration with a relatively low frequency.

The contact force distribution was also observed and the profile at various vibration frequencies during flow is presented in Fig 7.3.

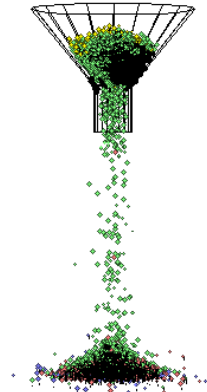


Vibrator frequency, 3Hz

The black lines denote normal forces which is dominant here for granular flow. Red lines (negligible) denote tangential forces.



Maximum force = $9.804e5N$



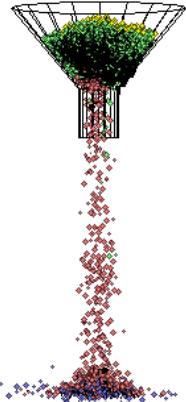
Maximum force = $3.831e5N$



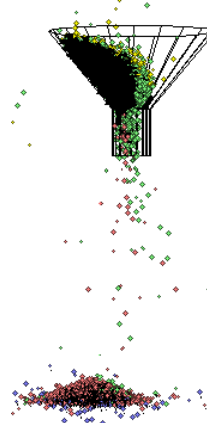
Maximum force = $3.919e5N$

Vibrator frequency, 5Hz

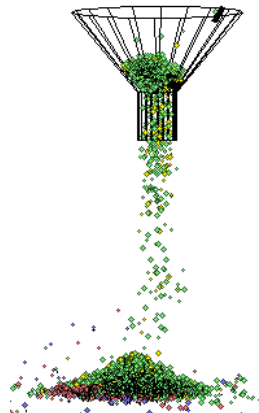
The black lines denote normal forces which is dominant here for granular flow. Red lines (negligible) denote tangential forces.



Maximum force = $6.931e5N$



Maximum force = $1.385e6N$



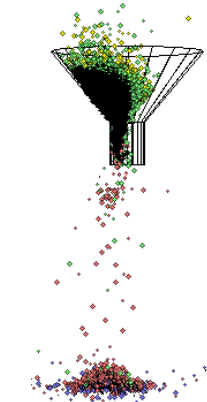
Maximum force = $1.054e6N$

Vibrator frequency, 7Hz

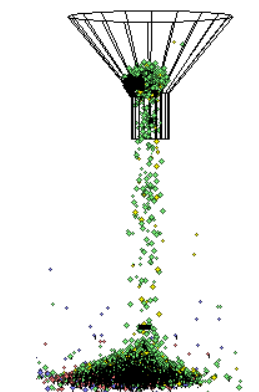
The black lines denote normal forces which is dominant here for granular flow. Red lines (negligible) denote tangential forces.



Maximum force = $7.746e5N$



Maximum force = $9.545e5N$



Maximum force = $3.695e5N$

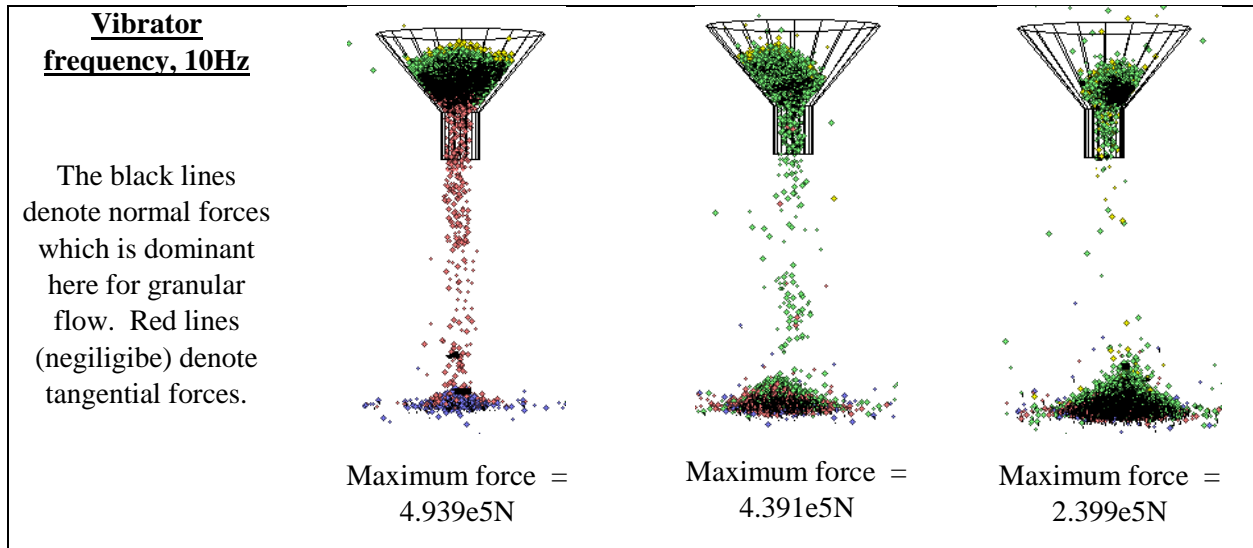
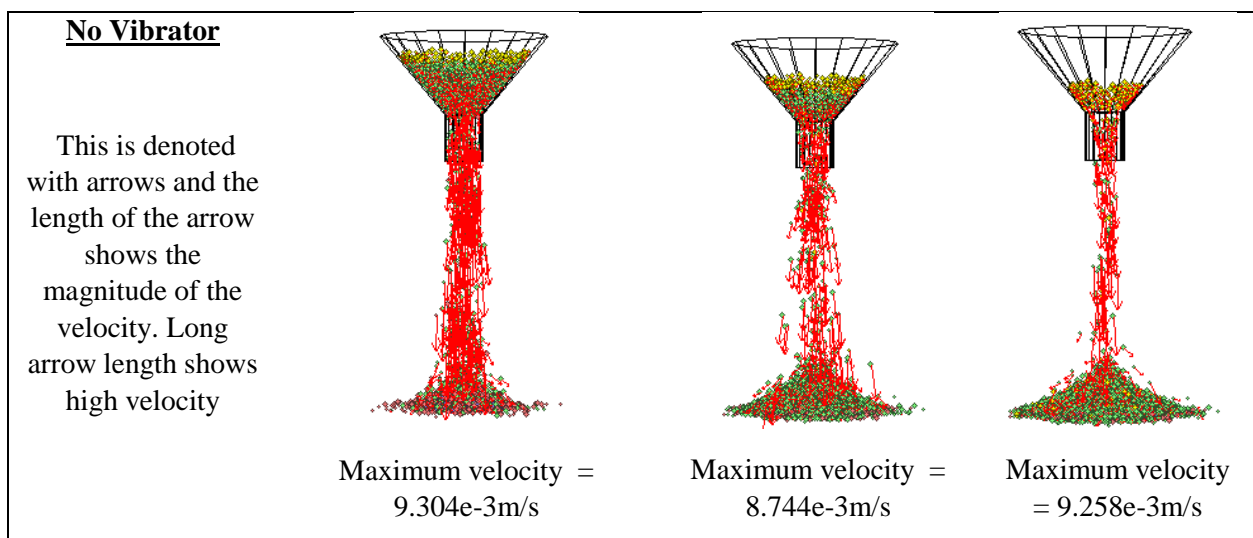


Fig. 7.3 Profiles of contact force distribution at different stages of flow: for the cases of no vibrator and vibrator with sinusoidal frequency 1Hz, 3Hz, 5Hz, 7Hz, and 10Hz under gravity flow (Mars gravity)

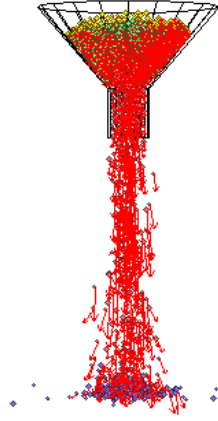
The contact force distribution profile of the grains also tend to be symmetrical with respect to the vertical axis when the vibrator was not activated as shown in Fig. 7.3. When the grains were under vibratory motion, the symmetry was also seen to break down. At frequencies greater than 3Hz, some grains were seen to escape from the top of the funnel and this effect increases with the frequency of the vibrator. This suggests that for Martian gravitational flow devices, it may be advantageous to operate at low frequencies to avoid flow of grains in the opposite direction to the desired vertical direction of the granular flow.

The velocity distribution was also monitored and the profiles observed are presented in Fig. 7.4.

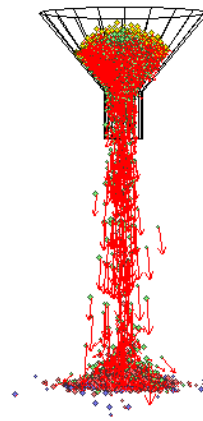


Vibrator
frequency, 1Hz

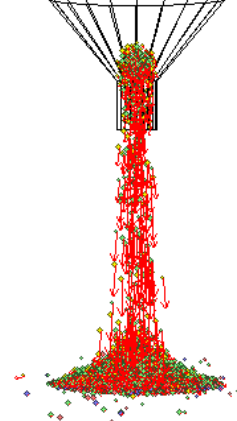
This is denoted with arrows and the length of the arrow shows the magnitude of the velocity. Long arrow length shows high velocity



Maximum velocity =
 $9.436e-3m/s$



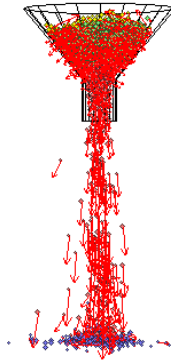
Maximum velocity =
 $9.110e-3m/s$



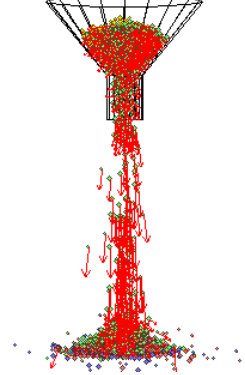
Maximum velocity =
 $9.421e-3m/s$

Vibrator
frequency, 3Hz

This is denoted with arrows and the length of the arrow shows the magnitude of the velocity. Long arrow length shows high velocity



Maximum velocity =
 $9.319e-3m/s$



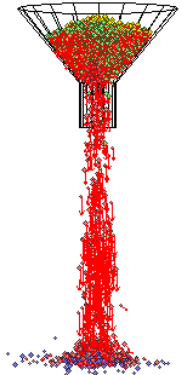
Maximum velocity =
 $9.360e-3m/s$



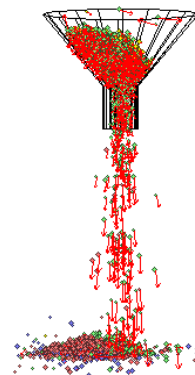
Maximum velocity =
 $9.519e-3m/s$

Vibrator
frequency, 5Hz

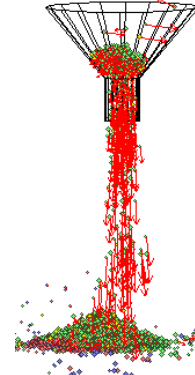
This is denoted with arrows and the length of the arrow shows the magnitude of the velocity. Long arrow length shows high velocity



Maximum velocity =
 $1.442e-2m/s$



Maximum velocity =
 $1.573e-2m/s$



Maximum velocity =
 $9.737e-3m/s$

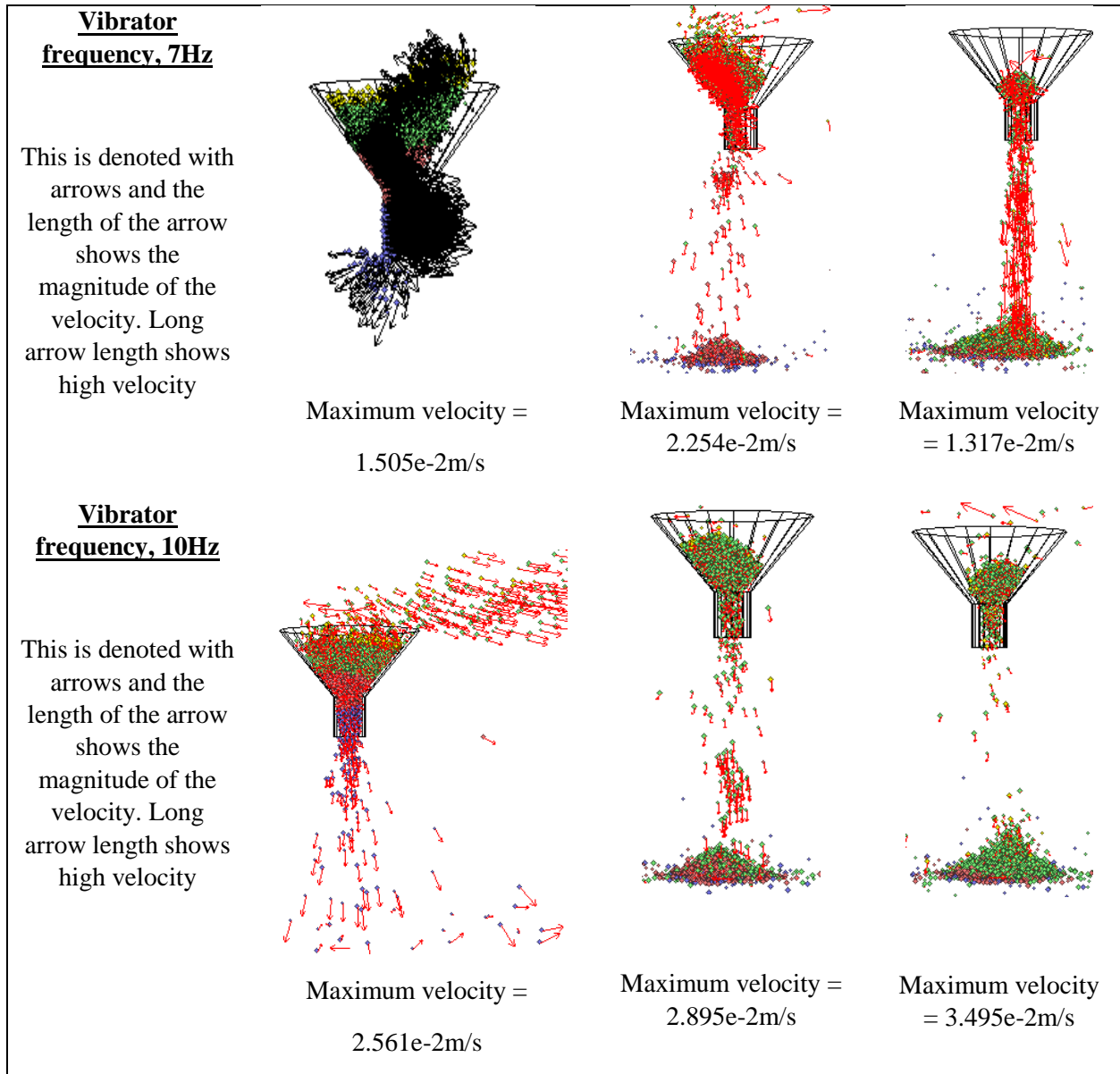
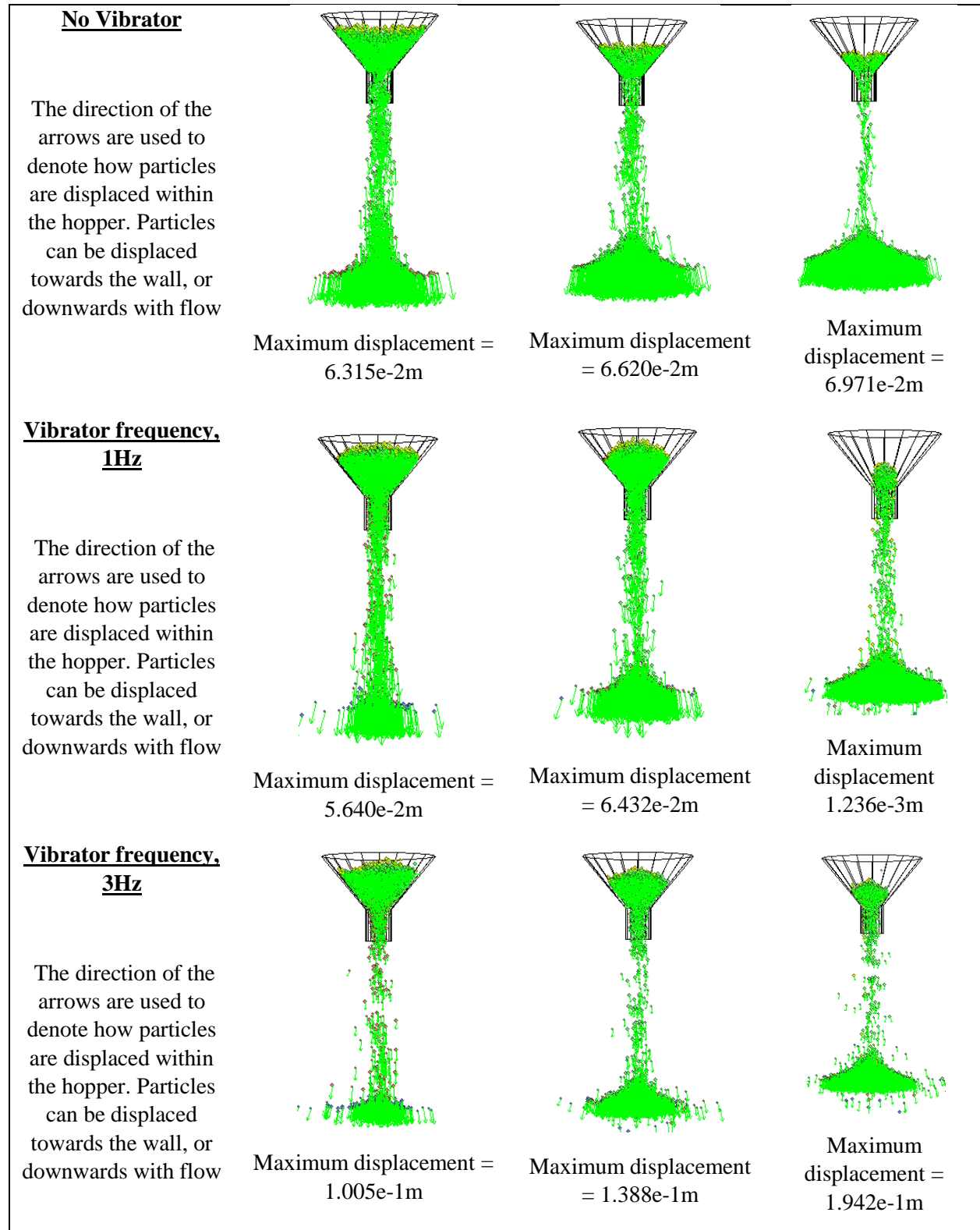


Fig. 7. 4 Velocity distribution profiles at different stages of flow: for the cases of no vibrator and vibrator with sinusoidal frequency 1Hz, 3Hz, 5Hz, 7Hz, and 10Hz under gravity flow (Mars gravity)

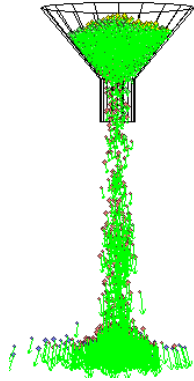
As with previous microscopic properties observed, results shown in Fig. 7.4 also indicate that when the vibrator was not activated, the velocity profile of the grains remained symmetrical with respect to the vertical axis whereas the symmetry breaks down when the grains were under vibration motion. Also similar to previous observation for the contact force distribution, at vibratory frequencies greater than 3Hz, grains escaped from the top of the funnel and the effect increased with the frequency of the vibrator.

Lastly, the way at which the grains are displaced is also presented in Fig. 7.5.

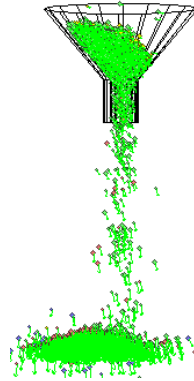


Vibrator frequency, 5Hz

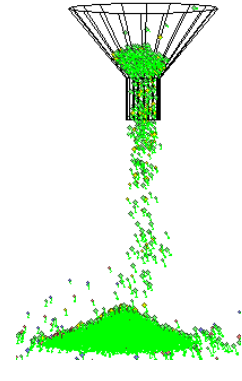
The direction of the arrows are used to denote how particles are displaced within the hopper. Particles can be displaced towards the wall, or downwards with flow



Maximum displacement = $1.335e-1m$



Maximum displacement = $1.747e-1m$



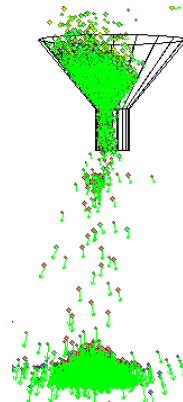
Maximum displacement = $3.422e-1m$

Vibrator frequency, 7Hz

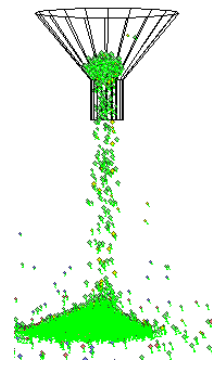
The direction of the arrows are used to denote how particles are displaced within the hopper. Particles can be displaced towards the wall, or downwards with flow



Maximum displacement = $1.276e-1m$



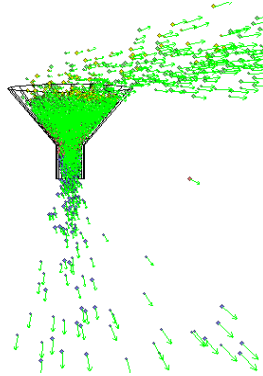
Maximum displacement = $1.276e-1m$



Maximum displacement = $3.833e-1m$

Vibrator frequency, 10Hz

The direction of the arrows are used to denote how particles are displaced within the hopper. Particles can be displaced towards the wall, or downwards with flow



Maximum displacement = $1.325e-1m$



Maximum displacement = $3.296e-1m$



Maximum displacement = $4.601e-1m$

Fig. 7. 5 Displacement profiles at different stages of flow: for the cases of no vibrator and vibrator with sinusoidal frequency 1Hz, 3Hz, 5Hz, 7Hz, and 10Hz under gravity flow (mars gravity)

Results in Fig. 7.5 show that without the vibrator, the displacement profile of the grains also tend to be symmetrical with respect to the vertical axis and upon granular vibration motion, the symmetry breaks down. Analysis of the granular displacement profiles after they pass out of the flow chamber (granular stream) suggests a better and continuous flow of grains for the case of maintaining the vibration frequency at 1Hz. Beyond this frequency, non-continuous and intermittent flow profiles are observed which is not necessarily good for the design of smooth flow devices to operate under gravity loading.

The macroscopic flow rate was also investigated and the average flow rate of the chambers under different sinusoidal vibrations of the chambers with 0Hz corresponding to switching off the vibrator. By studying the microscopic features of the granular flow characteristics presented earlier, it is evident that employing the vibration frequency at 1Hz results in more favourable microscopic features from the point of view of designing granular flow devices. Hence the macroscopic flow rate results are normalized with respect to a frequency of 1Hz under mars gravity and the results presented in Fig 7.6. The results show that at a low frequency of 1Hz, the rate of flow peaks when compared with that of no vibrator and vibrator operating at higher frequencies.

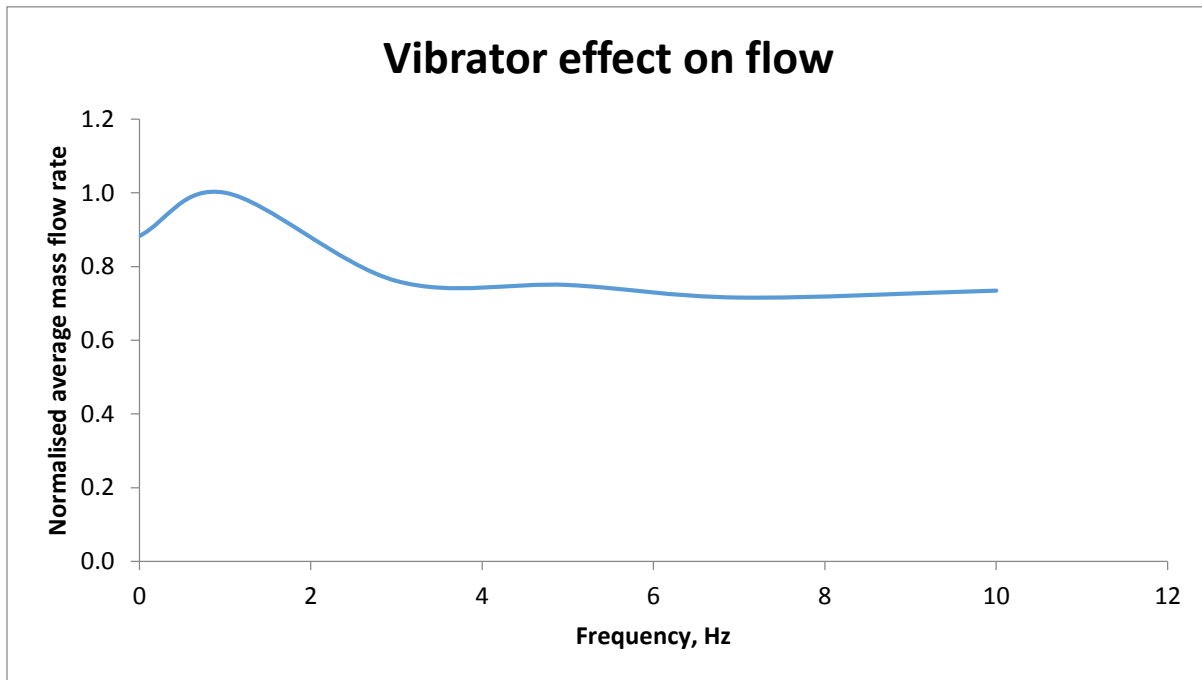
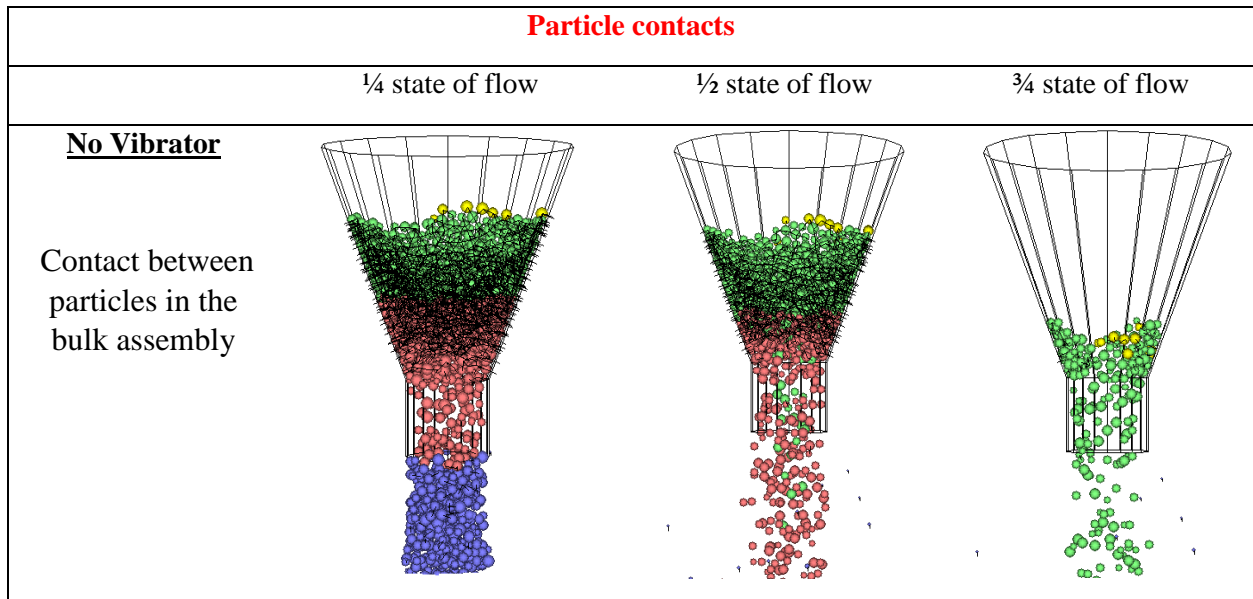


Fig. 7.6 Average bulk flow rate at different stages of flow: for cases of no vibrator and vibrator with sinusoidal frequency 1Hz – 10Hz under Mars gravity

The results reported so far show the vibratory effect of frequency 0 – 10Hz under mars gravity level on granular flow in a hopper. This investigation is however further extended for higher frequencies which helps avoid overhead spillage. Consequently, it was observed that the wall velocity (Wvx) greatly depends on the magnitude in the x-direction as well as the frequency which is shown in equation 7.1. Results (Fig. 7.5) show high rate of head loss at frequencies between 7Hz and 10Hz and to investigate higher frequencies, the head loss have to be avoided or minimized.

High frequency or low frequency vibration can be desired depending on the amplitude, nature of the product and the design of the hopper. Depending on the design of the hopper, vibration frequency can range from 1Hz to around 1300 Hz and amplitude from about zero to over 60mm (Woodcock and Mason, 1987). The reduction of the displacement level at higher frequencies ($> 10\text{Hz}$) helps to reduce/eliminate head loss. In view of this, investigations were carried out at reduced displacement level ($k = 0.05\%$) for all the frequencies and under no vibration ($f=0$) condition.



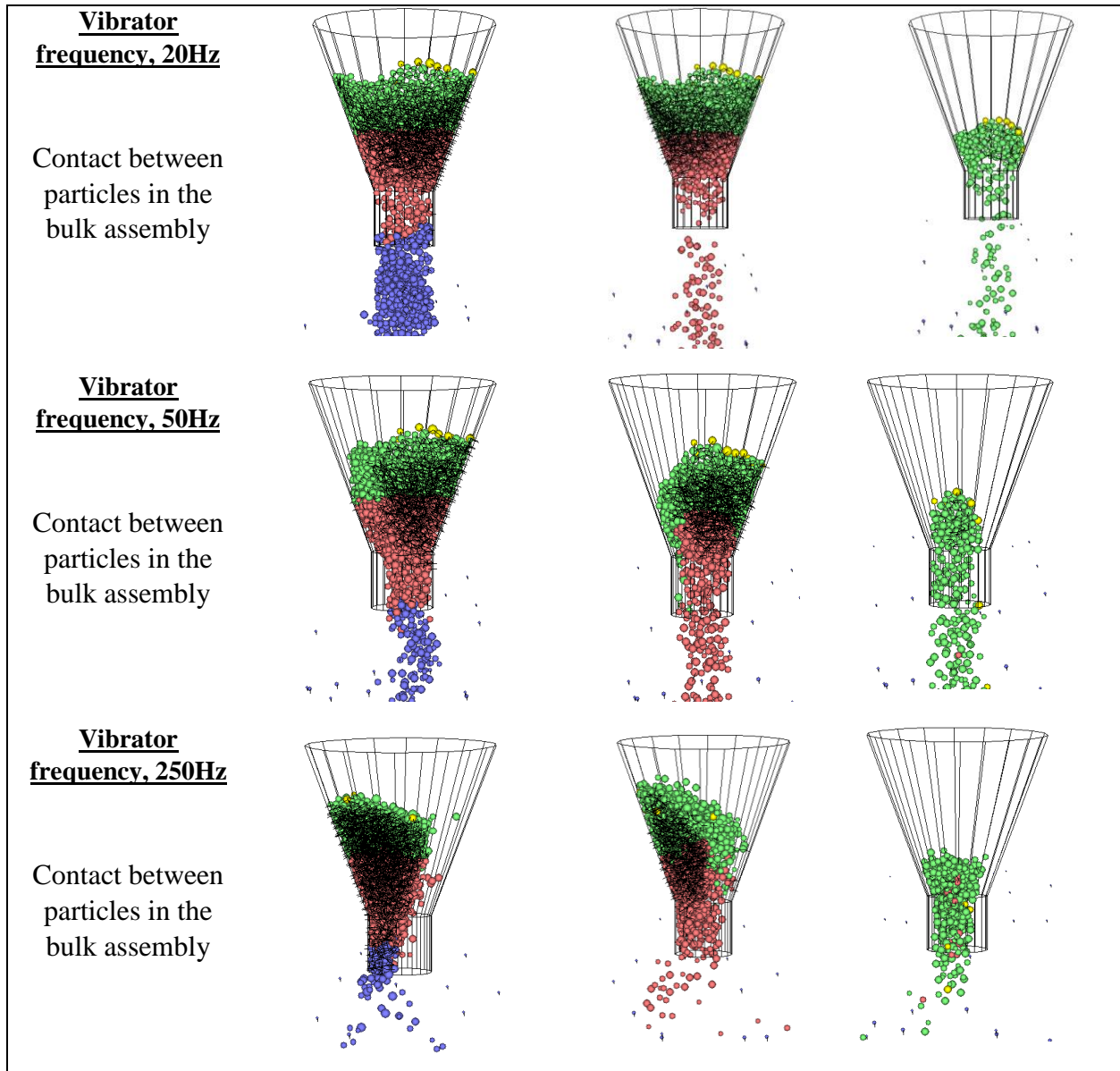
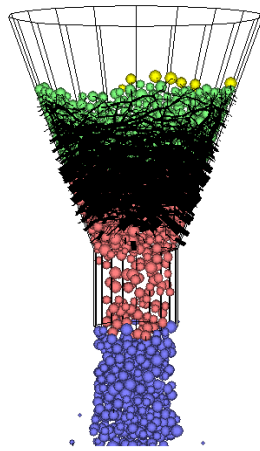


Fig. 7. 7 Profiles of particle contacts at different stages of flow: for the cases of no vibrator and vibrator with sinusoidal frequency 20Hz, 50Hz and 250Hz under gravity flow (Mars gravity)

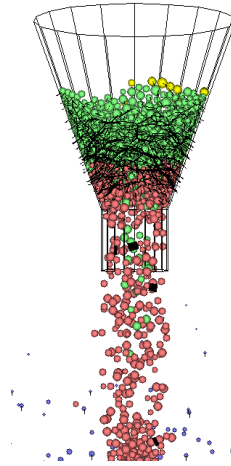
Contact force chains

No Vibrator

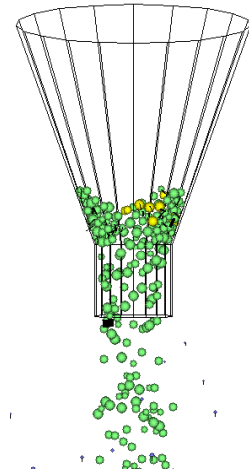
The black lines denote normal forces which is dominant here for granular flow. Red lines (negligible) denote tangential forces.



Maximum force = $8.326e4N$



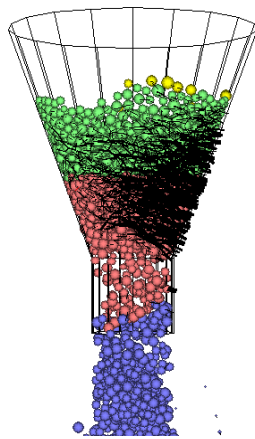
Maximum force = $1.130e5N$



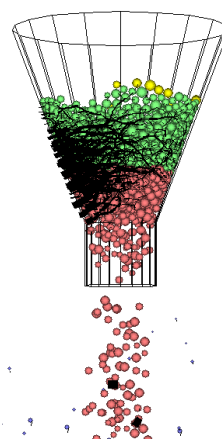
Maximum force = $7.641e4N$

Vibrator frequency, 20Hz

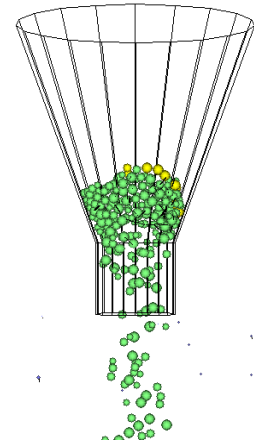
The black lines denote normal forces which is dominant here for granular flow. Red lines (negligible) denote tangential forces.



Maximum force = $1.387e5N$



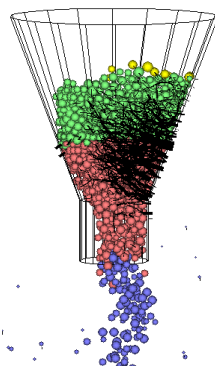
Maximum force = $7.901e4N$



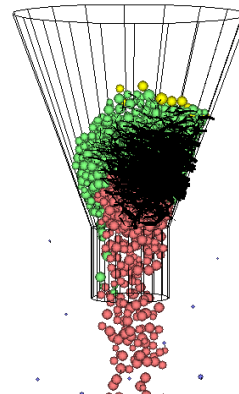
Maximum force = $9.718e4N$

Vibrator frequency, 50Hz

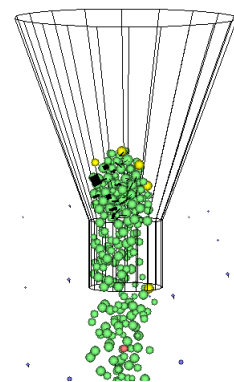
The black lines denote normal forces which is dominant here for granular flow. Red lines (negligible) denote tangential forces.



Maximum force = $1.457e5N$



Maximum force = $1.675e5N$



Maximum force = $1.441e5N$

Vibrator frequency,
250Hz

The black lines denote normal forces which is dominant here for granular flow. Red lines (negligible) denote tangential forces.

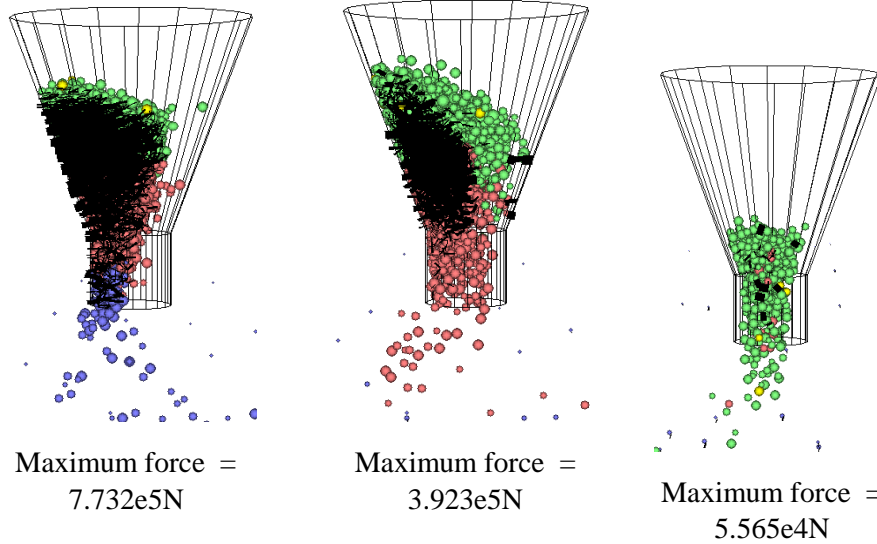
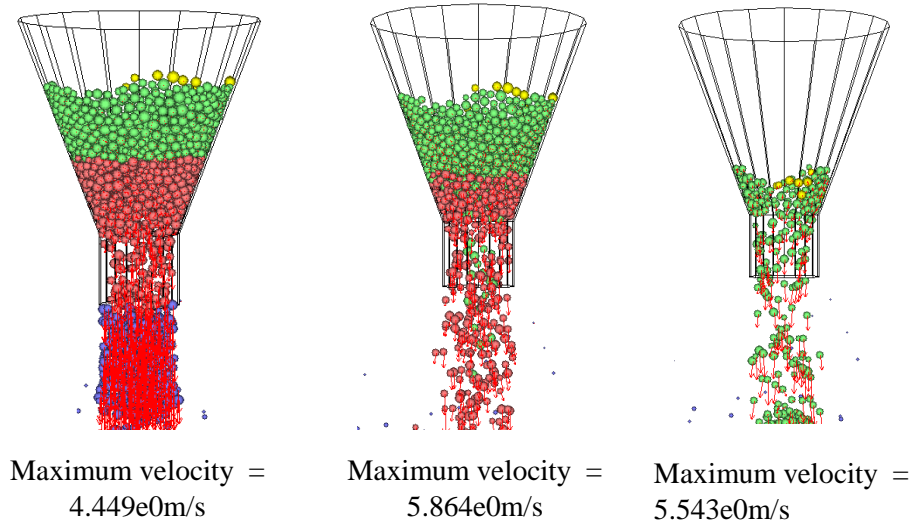


Fig. 7. 8 Profiles of contact force distribution at different stages of flow: for the cases of no vibrator and vibrator with sinusoidal frequency 20Hz, 50Hz, and 250Hz under gravity flow (Mars gravity)

Velocity profiles

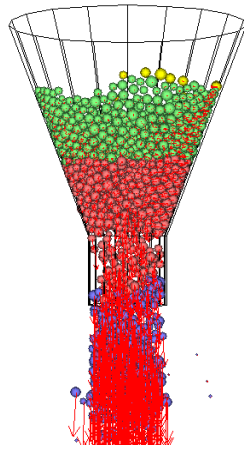
No Vibrator

This is denoted with arrows and the length of the arrow shows the magnitude of the velocity. Long arrow length shows high velocity

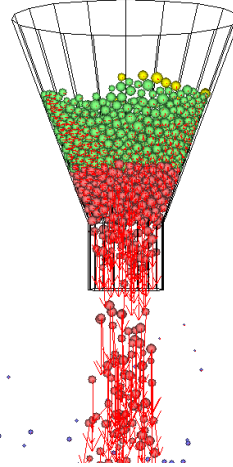


Vibrator frequency,
20Hz

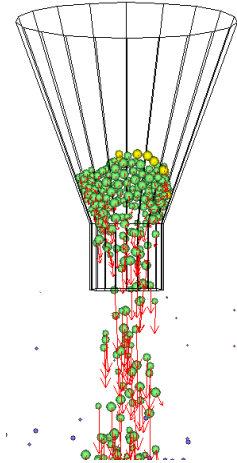
This is denoted with arrows and the length of the arrow shows the magnitude of the velocity. Long arrow length shows high velocity



Maximum velocity =
4.915e0m/s



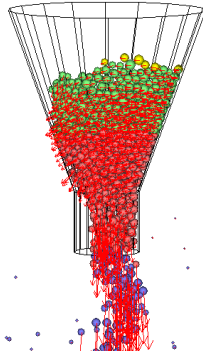
Maximum velocity =
5.949e0m/s



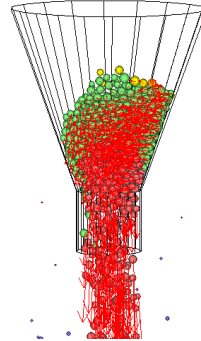
Maximum velocity =
6.449e0m/s

Vibrator frequency,
50Hz

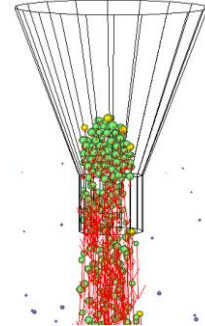
This is denoted with arrows and the length of the arrow shows the magnitude of the velocity. Long arrow length shows high velocity



Maximum velocity
4.514e0m/s



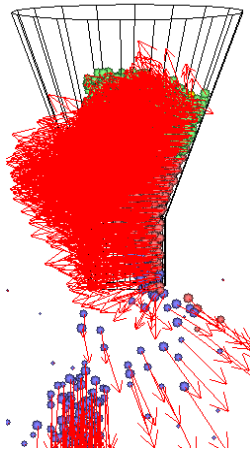
Maximum velocity
5.180e0m/s



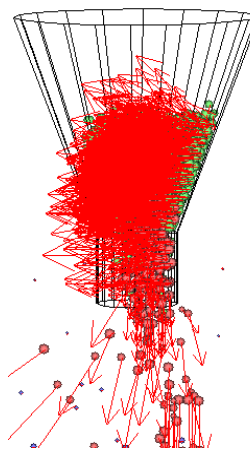
Maximum velocity
5.083m/s

Vibrator frequency,
250Hz

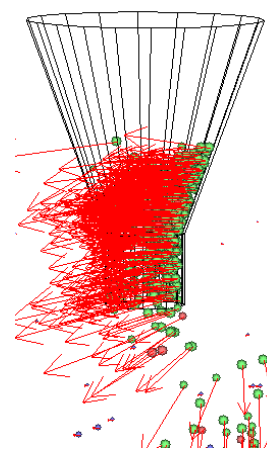
This is denoted with arrows and the length of the arrow shows the magnitude of the velocity. Long arrow length shows high velocity



Maximum velocity
7.394e0m/s



Maximum velocity
7.683e0m/s



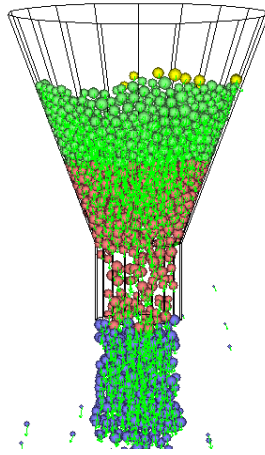
Maximum velocity =
8.799e0m/s

Fig. 7. 9 Velocity distribution profiles at different stages of flow: for the cases of no vibrator and vibrator with sinusoidal frequency 20Hz, 50Hz, and 250Hz under gravity flow (Mars gravity)

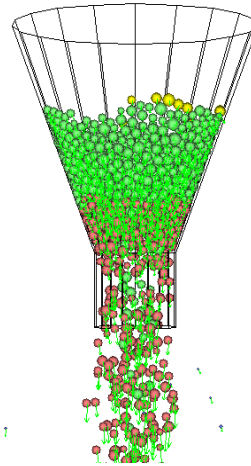
Displacement profile

No Vibrator

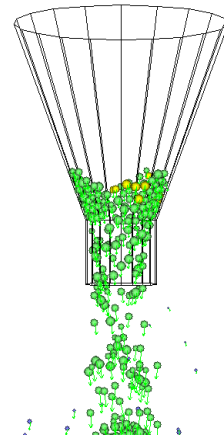
The direction of the arrows are used to denote how particles are displaced within the hopper. Particles can be displaced towards the wall, or downwards with flow



Maximum displacement = $2.818e-1m$



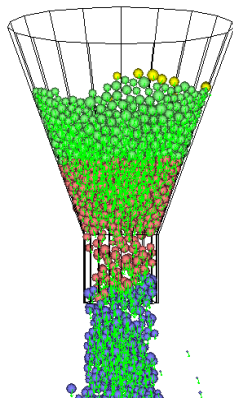
Maximum displacement = $3.106e-1m$



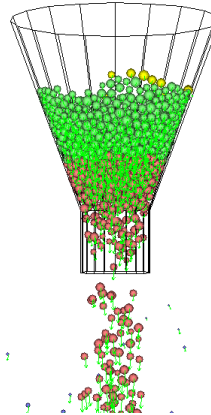
Maximum displacement = $3.757e-1m$

Vibrator frequency, 20Hz

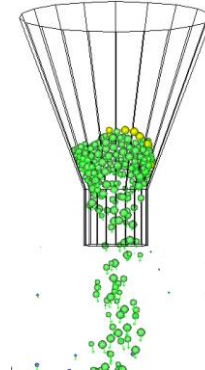
The direction of the arrows are used to denote how particles are displaced within the hopper. Particles can be displaced towards the wall, or downwards with flow



Maximum displacement = $2.845e-1m$



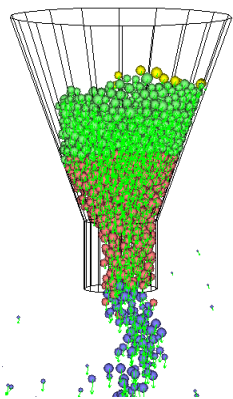
Maximum displacement = $3.289e-1m$



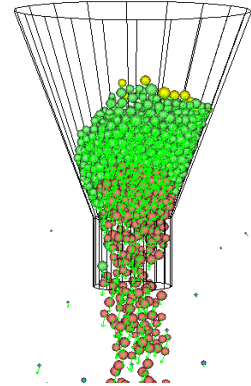
Maximum displacement = $5.677e-1m$

Vibrator frequency, 50Hz

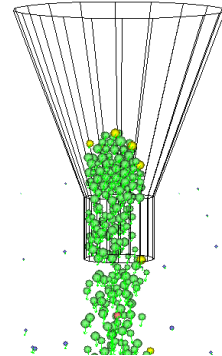
The direction of the arrows are used to denote how particles are displaced within the hopper. Particles can be displaced towards the wall, or downwards with flow



Maximum displacement = $3.026e-1m$



Maximum displacement = $3.579e-1m$



Maximum displacement = $5.128e-1m$

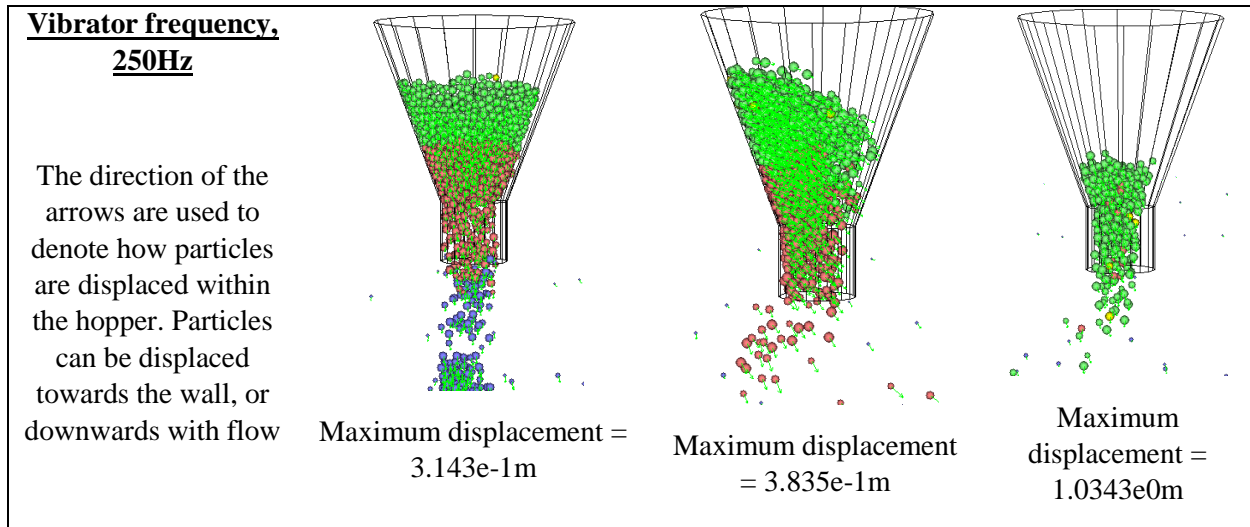


Fig. 7. 10 Displacement profiles at different stages of flow: for the cases of no vibrator and vibrator with sinusoidal frequency 20Hz, 50Hz, and 250Hz under gravity flow (mars gravity)

The profile observed for all the plots indicate reducing the magnitude of the displacement in x-direction helped to minimize or overcome the head loss. The symmetry breaks down when the grains were under vibratory motion as observed in Figs. 7.7 – 7.10. As presented in Fig. 7.7, more dominant contact bonds exist at lower frequencies and as suggested in the initial study at low frequencies 0Hz – 10Hz, potentially better macroscopic flow rate is expected at slow vibrations. In general, the average flow rate of the chambers at different vibrating frequencies under EML gravities is presented in Fig. 7.11.

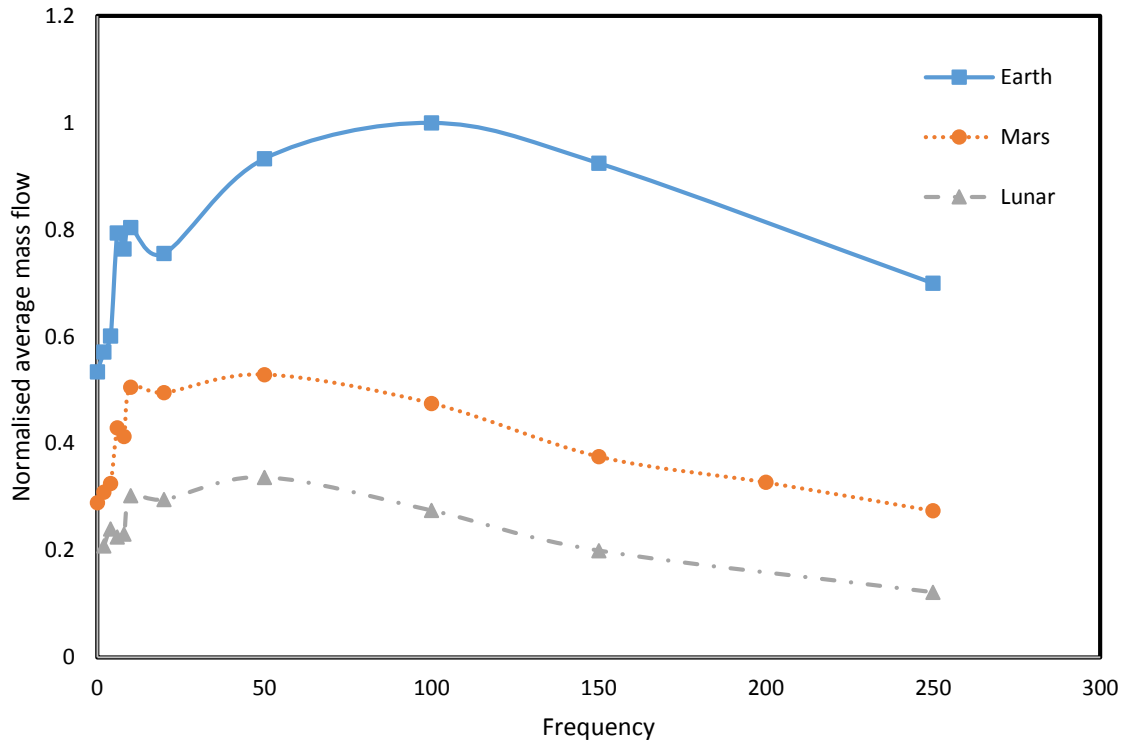


Fig. 7.11 Average bulk flow rate for cases of vibrator with sinusoidal frequency 1Hz – 250Hz under EML gravity

Results obtained as shown in Fig. 7.11 indicate that a critical frequency exist under earth, mars and lunar gravity levels at which flow rate is high. It was observed that the flow rate initially increased at lower flow rate until it peaked at a frequency of 100Hz for JS1 soil under earth gravity. At frequencies > 100Hz, the flow rate began to decrease with increasing frequency. For Mars and Lunar gravity level simulations, results show that flow also increased with increasing vibration frequency to a peak at a frequency of 50Hz for same JS1 soil used under earth gravity. Flow rate was also observed to decrease with increasing frequency beyond 50Hz.

Experimental investigations under earth gravity on the effects of horizontal vibration on hopper flows of granular materials done by Hunt et al. (1999) indicate that granular flow increased with increase in velocity of the vibration as compared with the no vibration conditions. However, their investigation was limited to maximum frequency of 20 – 35 Hz. It was also reported that for low frequencies, (5 Hz and 10 Hz), the discharge rate in the hopper was relatively uniform. In comparison with DEM simulations reported in Fig. 7.11, uniform flow rate seem to exist at low frequencies. With limited study under lower gravity levels, DEM simulation results obtained in

this investigation further improves the understanding of the vibrational induced hopper flow under earth, mars and lunar gravity levels.

Additionally, In comparison with investigations by Kollmann and Tomas (2002) and Roberts and Scott (1978), it was observed that increase in frequency aided the reduction of particle interlocking and arch formation during flow.

7.3 Staggered Vs Continuous Granular Flow in a Hopper under EML Gravity Levels

The effect of gravity on the Continuous flow of granular materials in a hopper has been studied in the previous sections. The current section introduced a stop-flow effect known as staggered flow to understand if the staggering of flow can have any impact on the grains gathered in a collection chamber. The hopper and a cylindrical collection chamber are modelled. After the hopper, collection chamber and particles are generated, gravity loading is applied. As the base is removed, there is variation in the measure of different quantities and the grains flow into a collection chamber. This schematic is represented in Fig. 7.12 and the dimensions of the hopper, collection chamber and parameters used in the simulation are given in Table 7.2.

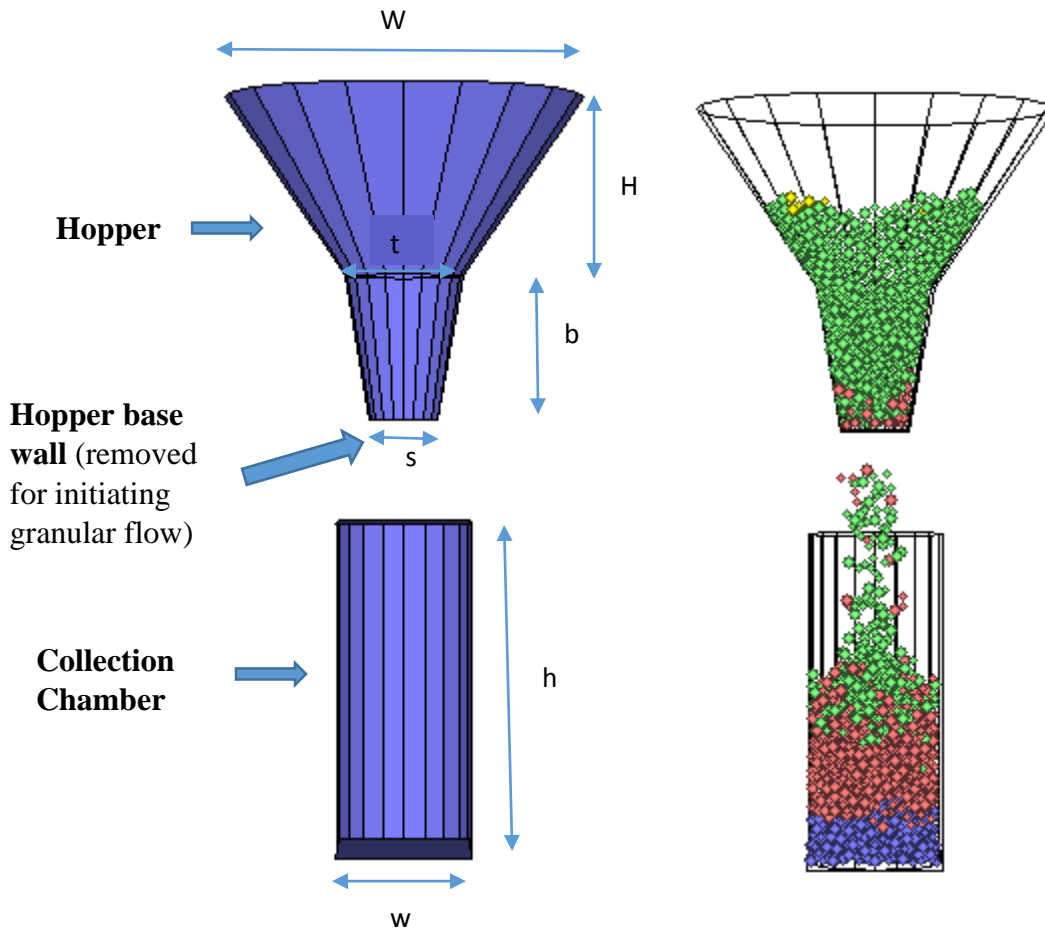
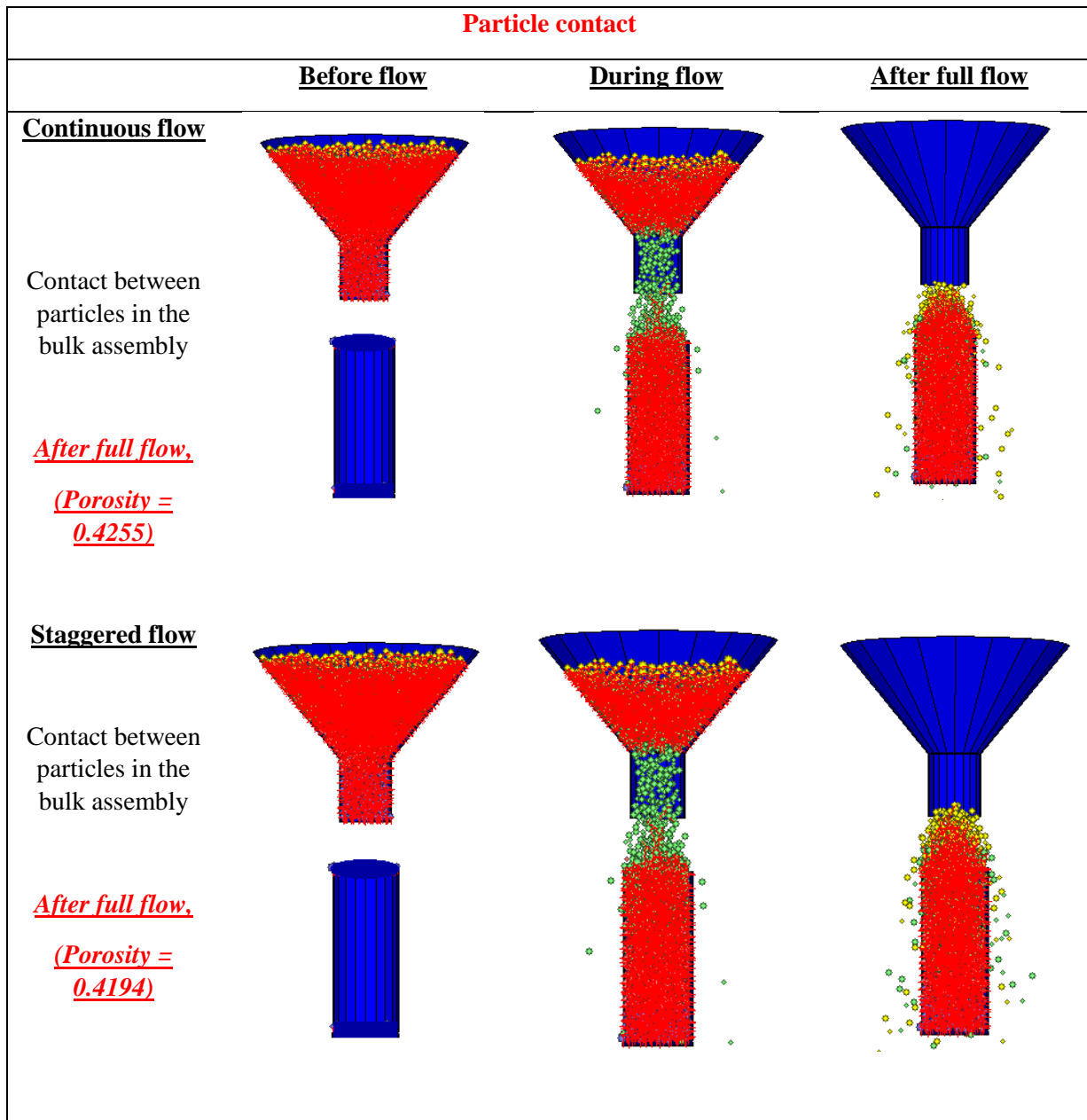


Fig. 7. 12 Pictorial view of a hopper and collection chamber designed using DEM simulations

Table 7. 2 Hopper parameters and Microscopic material properties used to simulate the stop-flow system under EML gravity levels

Hopper Outlet Funnel		Collector (Oven)	
Description	Value		
Upper Diameter (W)	Ø 20.9 mm	Upper Diameter (w)	Ø 6 mm
Funnel Height (H)	18.8 mm	Funnel Height (h)	18 mm
Base Diameter (s)	Ø 4.0 mm	Micro properties	
Base Height (b)	8.4 mm	Density	3000 kg/m ³
Hopper angle (β)	70 degree	Porosity	0.36
Mid Diameter (t)	Ø 6.9 mm	Particle Stiffness	1.0×10^7 N/m
Wall Friction	0.6	Particle Friction	0.6
Wall Stiffness	2.0×10^{11} N/m	Bond Strength	JS1 type (Table 3.1)
		Size Distribution	JS1 type (Fig. 3.2)

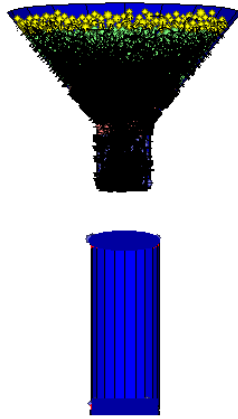
The effect of staggered flow was monitored during granular flow under earth, mars and lunar gravity levels. To investigate the effect of the staggered nature of granular flow, the grains were allowed to flow for 30s and induced the blockage for a duration of 30s. This process is continued until the whole hopper is empty. The mass flow rate was then calculated from the simulation result data obtained and compared with continuous granular flow. The velocity, particle contact, contact force, displacement were tracked during simulation.



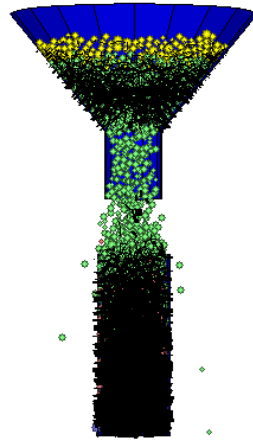
Contact force chain

Continuous flow

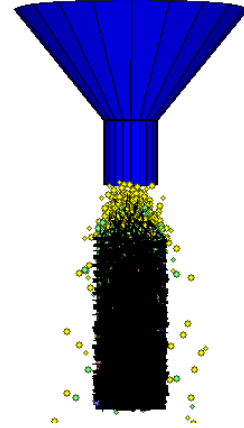
The forces are both normal and shear forces. The black lines denote normal forces which is dominant here. The thickness of the line denotes the magnitude of the forces



Maximum force chain = $1.233e5N$



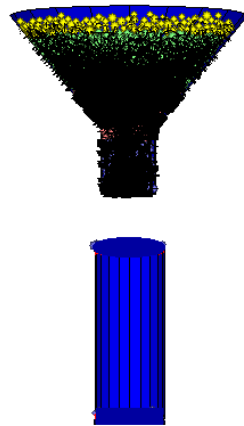
Maximum force chain = $1.233e5N$



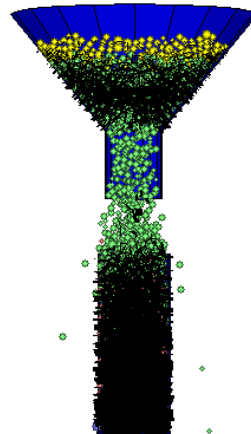
Maximum force chain = $5.806e5N$

Staggered flow

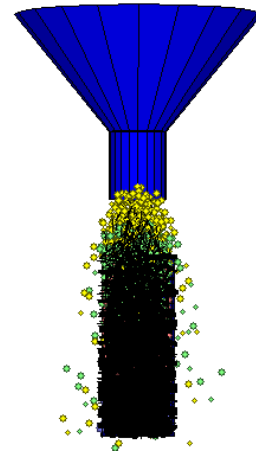
The forces are both normal and shear forces. The black lines denote normal forces which is dominant here. The thickness of the line denotes the magnitude of the forces



Maximum force chain = $1.233e5N$



Maximum force chain = $1.233e5N$

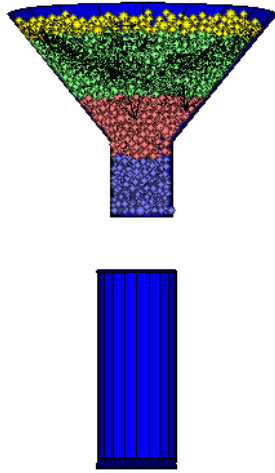


Maximum force chain = $1.665e5N$

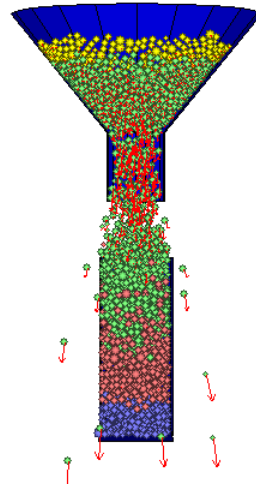
Velocity profile

Continuous flow

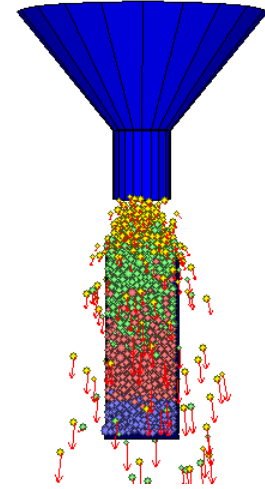
This is denoted with arrows and the length of the arrow shows the magnitude of the velocity. Long arrow length shows high velocity



Maximum velocity profile = $8.451e-3m/s$



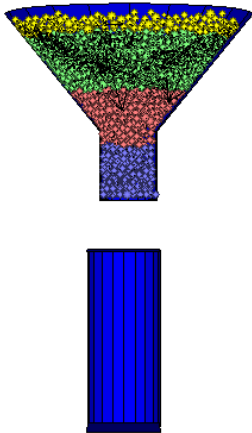
Maximum velocity profile = $9.313e-3m/s$



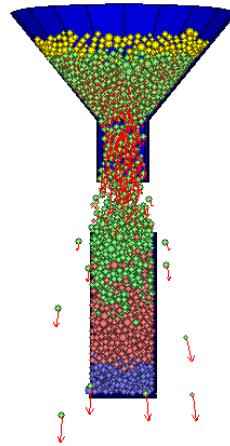
Maximum velocity profile = $8.871e-3m/s$

Staggered flow

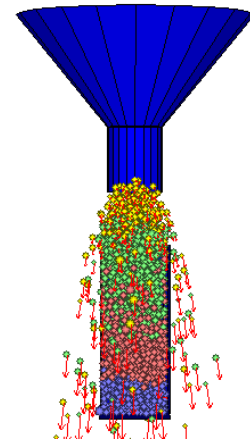
This is denoted with arrows and the length of the arrow shows the magnitude of the velocity. Long arrow length shows high velocity



Maximum velocity profile $8.451e-3m/s$



Maximum velocity profile = $9.313e-3m/s$



Maximum velocity profile = $8.914e-3m/s$

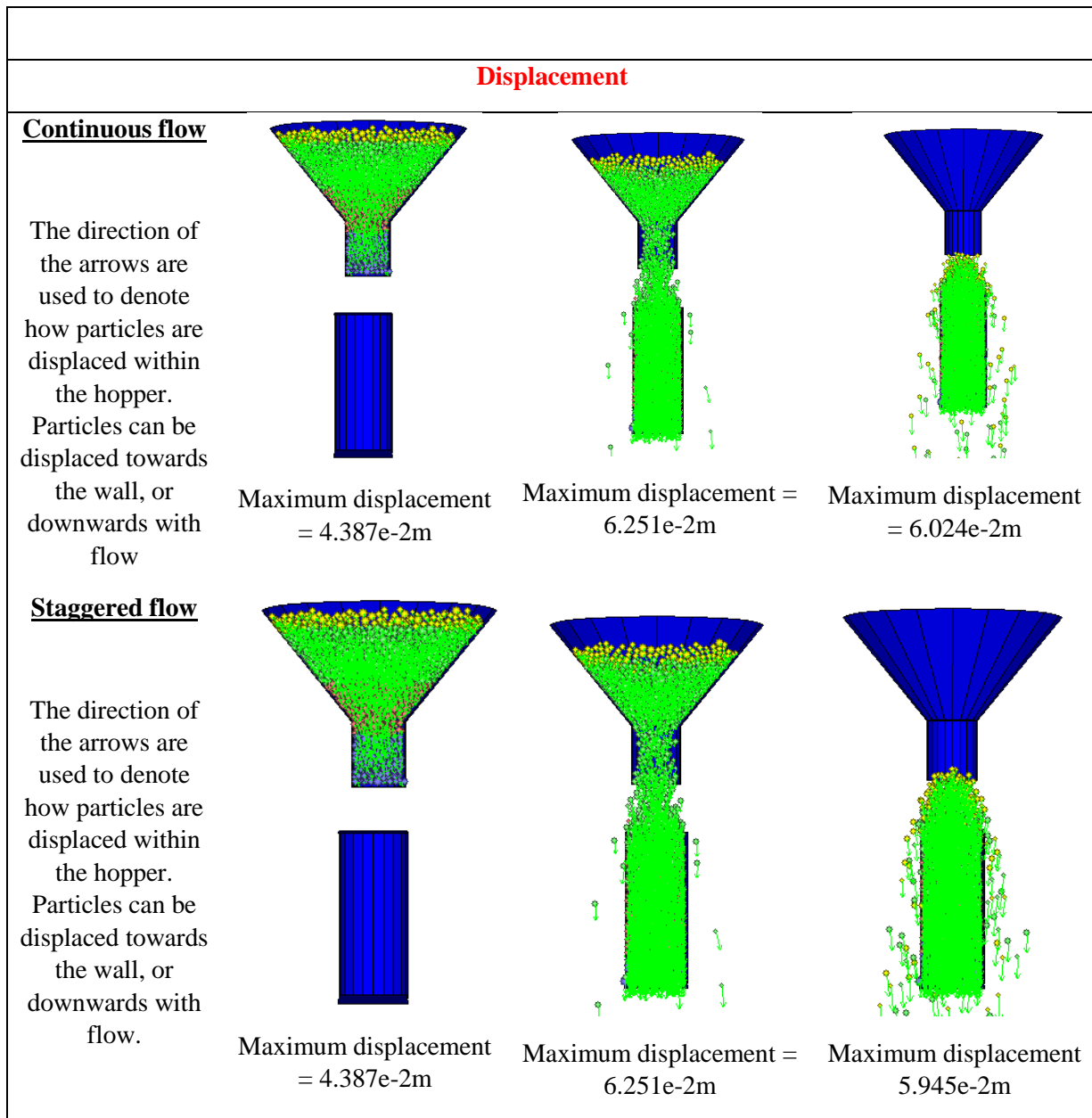
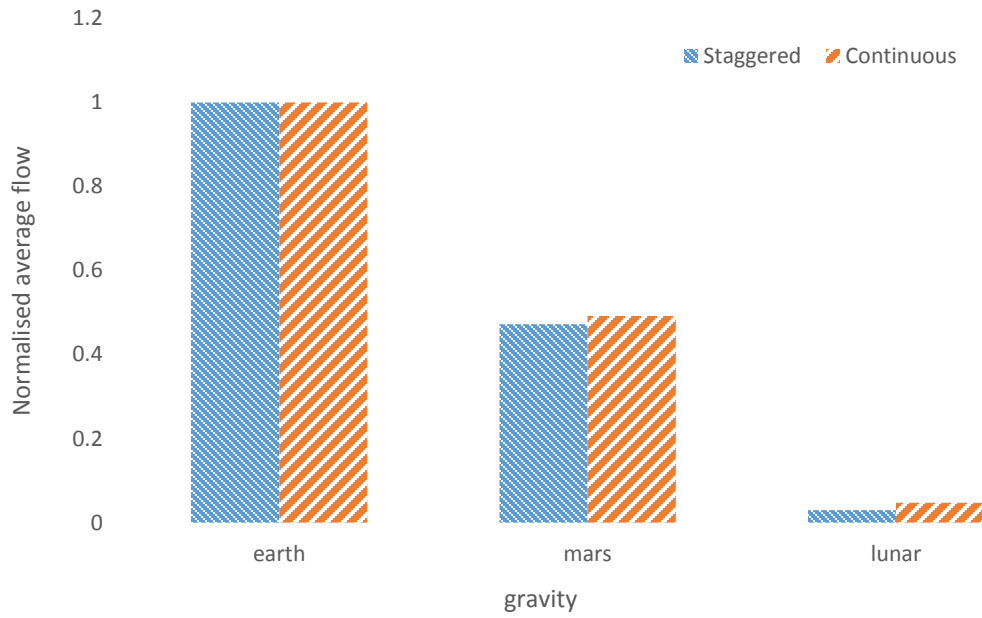
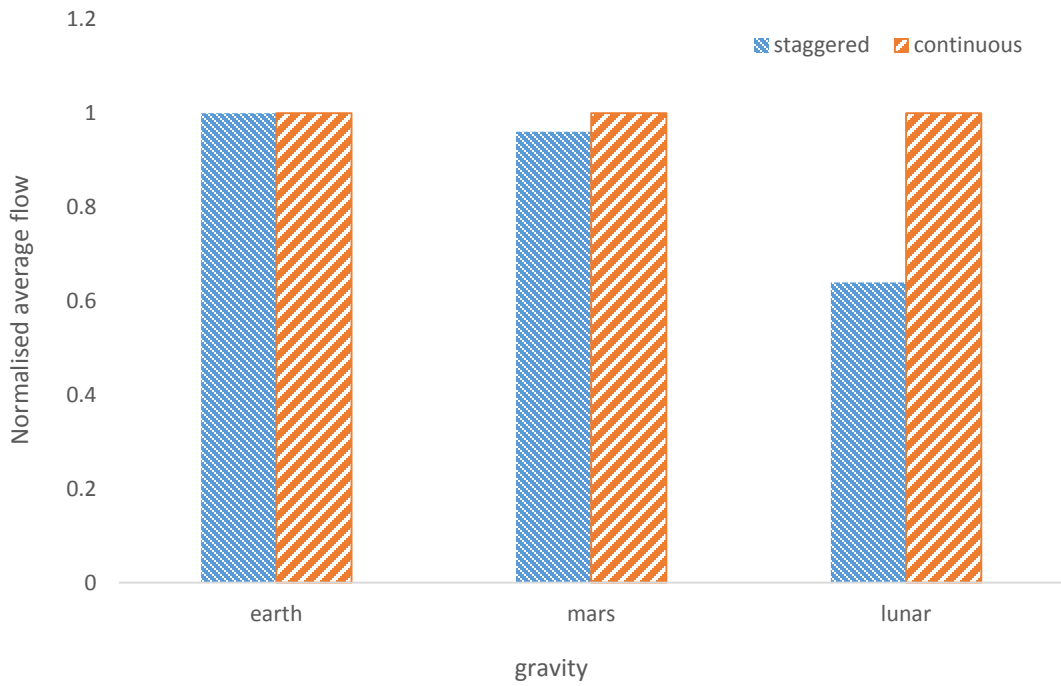


Fig. 7.13 Flow profiles obtained from staggered and continuous flow of grains from hopper using DEM simulation

The microscopic profile suggests that there is no significant difference in the profiles of the contact force, particle contact, velocity, and displacement profile between the continuous flow and the staggered flow. The macroscopic flow results (Fig. 7.14) indicate that there is a marginal difference in the flow rate during continuous flow and staggered flow under earth gravity.



(a)



(b)

Fig. 7. 14 Effect of staggered flow against continuous flow system (a) normalized with earth gravity (b) normalized with continuous flow under each gravity level

The simulation results show that for grains having a continuous discharge under earth gravity, the flow rate was typically similar to that of the staggered flow. However, the impact of the staggered flow increased with reducing gravity. As presented in Fig. 7.14, grains with staggered flow tend to have lower flow rate as compared to continuous flow under mars and lunar gravity levels. Fig. 7.15 gives a better representation of the difference in flow rate under each gravity with reference to the continuous flow. When the flow is staggered, the flow rate reduced with decreasing gravity. Thus, the stop-flow system will rather decrease the rate of flow of the grains under low gravity with decreasing gravity levels. The difference in the flow rate between the continuous flow and staggered flow is much more distinctive under lunar gravity with a 34% difference as compared to that of mars gravity with a 4% difference. This suggest that even for staggered flow, it will be a lot more difficult for grains to flow as compared to continuous flow under lunar gravity.

7.4 Conclusion

The piezo-vibrator technique on granular flow has been shown to have a significant impact on flow of grains from the hopper. From the simulation results, it was found that vibrating the hopper could aid granular flow up to a peak frequency after which the flow rate began to decrease. This effect was also observed to decrease with gravity in which a lower peak frequency value was observed for mars and lunar gravity. This showed that gravity has a big influence on flow even when a discharge aid such as a vibrator is used. The simulation results also helped to show the dependence of the effect of the vibrator on the hopper wall velocity which in turn greatly depends on the magnitude (in the x-direction) and the frequency (Equation 7. 1). This suggests that in the design of a hopper with a piezo-vibrator as its discharge aid, a peak frequency exist for any displacement magnitude chosen for horizontal oscillation.

Another concept known as the stop-flow system where the flow of grains were staggered intermittently was introduced. Simulation results indicate that staggering the flow under earth gravity had no major/negligible impact on the rate of flow of the grains from the hopper. However, the impact of the staggered flow had a different response under low gravity. Gravity was more influential in the flow of the grains during staggered flow as compared to continuous flow of the grains. The staggering of the flow decreased the rate at which the grains flow under low gravity with a distinct percentage observed under lunar gravity.

Variations of the horizontal magnitude, angular velocity and frequency can aid the design of a vibrator to operate at its optimum with maximum efficiency in space as well as in most industrial applications of granular flows through hoppers. Additionally, especially for space/low gravity exploration, it is recommended to have continuous flow of grains during processing where possible during the granular filling operations.

Chapter 8

COMPACTION PROPERTIES OF GRANULAR MEDIA WITH ICE CONTENTS

8. Compaction Properties of Granular Media with Ice Content

Planetary surface exploration is an area that is generating much interest around the globe as space researchers prepare to send humans to the lunar surface (also termed as the moon) as an alternative to living on earth in the future. The success or failure of this mission depends greatly on the design, use of local resources and implementation of systems that can effectively process materials under lunar gravity. As researchers prepare for this mission, available knowledge on the strength of lunar materials is still limited and mostly based on the study of the lunar samples returned by the Apollo missions (Sibille et al., 2005). Recent data from remote sensing reported by Metzger et al. (2011) indicate the existence of enormous quantities of water/ice in the lunar regolith, frozen into the permanently shadowed craters near the pole.

This is an important scientific discovery because of the magnitude and importance of such a resource outside Earth's gravity. This has led to the focus of this chapter in understanding the response of lunar materials with ice content under mechanical compaction. Here, the concept of ice-bonding with granular particles is introduced to model the lunar ground and investigated using three dimensional DEM simulations.

Although the primary focus of this chapter is on understanding the compaction properties of Lunar granular media, for the purpose of comparison, the simulations are also presented for the earth and mars gravity levels for the same properties of the granular assemblies tested for lunar gravity.

8.1 Brief Background on Lunar Explorations

The moon also regarded as an alien environment is one of the first body beyond Earth that has been systematically sampled (Vaniman et al., 1991). Samples were collected in cores by the Apollo and Luna mission from known locations on the lunar surface. Analysis of rocks and soils from these sites served as “ground-truth” points for remotely-sensed physical and geochemical maps (Fig. 8.1) of the Moon (Vaniman et al., 1991). Historically, emphasis on lunar science has been on geological interpretations in order to understand the evolution of the Moon with its comparison with earth (Sibille et al., 2005).

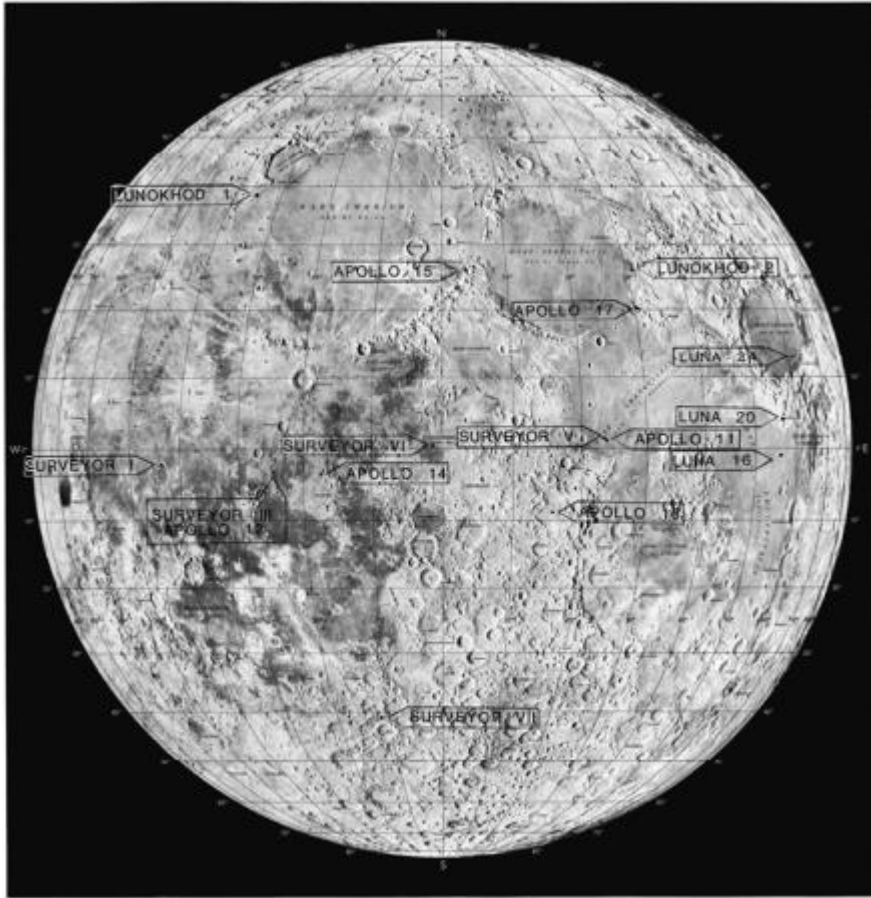


Fig. 8.1 Lunar landing Site Chart – Nearside of the Moon with locations of Apollo, Surveyor and Lunar (Sibille et al., 2005)

A layer of unconsolidated debris called the lunar regolith (Fig. 8.2) covers the lunar surface with varying thickness from the mare surfaces to the highland surfaces (Meyer, 2003). The bulk of the regolith is composed of fine particles which contain breccia and rock fragments. Past lunar landings and existing photographic investigations (Fig. 8.1) indicate that the entire lunar surface consists of a regolith layer except for a few crater walls and lava channels. The lunar regolith results from unique processes given as the continuous impact of large and small meteoroids and the constant bombardment of the lunar surface by charged atomic particles from the sun and stars (McKay et al., 1991).



Fig. 8. 2 Footprint in lunar soil with few rocks on the regolith (NASA photo AS11-40-5877)

At any given spot, the nature and history of the regolith is determined by two completely random mechanisms (McKay et al., 1991). The first one is a destructive process which is the excavation of existing regolith by impact craters while the second is a constructive process which is as a result of addition of layers of new material either from older regolith or the bedrock (McKay and Blacic, 1991).

8.2 Lunar Soil and Simulants

Soil samples obtained during missions to the moon are limited and not readily available for testing purposes in space exploration research. As a result, lunar simulants have been developed as terrestrial materials based on the matches of the bulk chemistry and physical properties of the regolith. Some other materials may be added to the simulants to provide representative properties of lunar regolith (Sibille et al., 2005). Lunar simulants are usually not readily available to meet the growing needs of lunar research projects (Mantovani et al., 2014). Hence, three dimensional computational simulations using DEM are employed here using the specifications of the simulant material properties of the regolith.

The ability to use locally available resources in the moon will however boost a successful human colonisation on the moon in the future decades. Reliable exploration such as excavation and material processing is crucial for all lunar surface activity and other gravitational fields to come. There are however challenges in characterizing the regolith properties due to the existence of low temperature on the lunar regolith. Thus to plan a mission to the lunar planetary surface, characterization of the physical properties and strength of the lunar soil samples is important. In view of this, the impact on mechanical properties due to the introduction of icy deposits must also be explored so as to devise effective and robust excavation technologies. The Lunar Prospector orbiter detected two resources indicated by the hydrogen signal near both lunar poles (Feldman et al., 1998). The readings provided useful materials for lunar activities which could be due either to ice from cometary impacts, or to solar wind protons implanted in regolith grains (Vondrak and Crider, 2003). Ice regolith is believed to exist in the subsurface of some areas near the lunar South Pole and as such interest is growing in obtaining such samples from that region (Pitcher et al., 2015). Concentrations of water ice at this impact region has been reported to be $5.6 \pm 2.9\%$ by mass as indicated by the LCROSS mission (Colaprete et al., 2010, Mitrofanov et al., 2010). It is also believed that ice reported in this regolith may be in form of ice-cemented particles, ice blocks (Gertsch et al., 2006) or absorbed to the surface (Hegde et al., 2012).

The discovery of these volatiles would be of a beneficial value for future lunar activities and exploration. Still, experimental support by investigating the lunar regolith in situ is far-fetched and a major goal of future lunar exploration. Studies on excavation, soil/granular handling and processing have been intensively developed and successful on earth ($g = 9.81 \text{ m/s}^2$). However, it is not certain what is expected when such analytical techniques are applied to model soil handling and processing on the lunar surface ($g = 1.67 \text{ m/s}^2$) due to its soil properties, environmental conditions, and gravity which are completely different from those of Earth.

Thus, in such circumstance, before such a mission can be embarked on, numerical tools such as DEM becomes a useful tool to study the mechanisms of the lunar surface operations which thereafter provides basic knowledge to improve its applicability for lunar explorations. Currently, there appears to be no standard preparation method for creating icy regolith simulants as demonstrated via techniques applied by Pitcher et al. (2015), Cooper et al. (2011), and Mantovani et al. (2014). Due to the lack of quantitative information on the extent and distribution of ice in the

lunar regolith, everything from fully saturated or over-saturated ice lenses to strongly under-saturated or completely dry regolith may be possible. Thus, the properties of the regolith considered by future lunar explorations or missions could vary considerably depending on the water content and degree of saturation.

As a step towards the design of equipment to be used in the exploration of lunar regolith, investigations are made in this section to focus on one of the resources (ice regolith mixtures) detected near the lunar poles. The effective design therefore relies on accurate characterization of the ice regolith mixture seen to exist on the lunar surface. Property data or estimates for the properties of dry lunar regolith are readily available (Bui et al., 2009), but very little knowledge exists for the ice-regolith mixtures under lunar gravity conditions. This is further discussed with the introduction of ice bonded materials that is reported to exist in lunar regolith.

8.3 Compaction on Ice-Bonded Lunar Soil using Three Dimensional DEM

Water, including ice has been reported to exist on the surface of the moon in which one of the possible ways of formation is by ice cementing the particles together under lunar gravity (Gertsch et al., 2006). The ice-bonded granular particles are represented by generating an ensemble of granular particles describing the individual grains and ice bonds. The developed inter-granular bond models are of three types (Gertsch et al., 2006) as shown in Fig. 8.3.



Fig. 8.3 Relative effects of three (3) common modes of ice contents on lunar soil strength

The developed algorithm used in this research helps to predict the effect of ice bonding of individual grains. The strategy used in different modes presented in Fig. 8.3 is defined as:

Mode 1: Simulating ice bonds at particle interface (contact bonds)

Mode 2: Mode 1 + Uniform spread strength of ice bonds (parallel bonds)

Mode 3: Uniform spread strength of ice (parallel bonds)

The concept of the contact and parallel bond has been explained in chapter three. The advantage in representing the ice bonds using the contact and parallel bond concept is for simplicity in which the contact bond acts only at the contact point of the particles while the parallel bond is of a finite size that acts over a circular cross-section lying between the particles. This bonding concept is however limited to spherical particles and more complex models can be applied to irregular shaped particles.

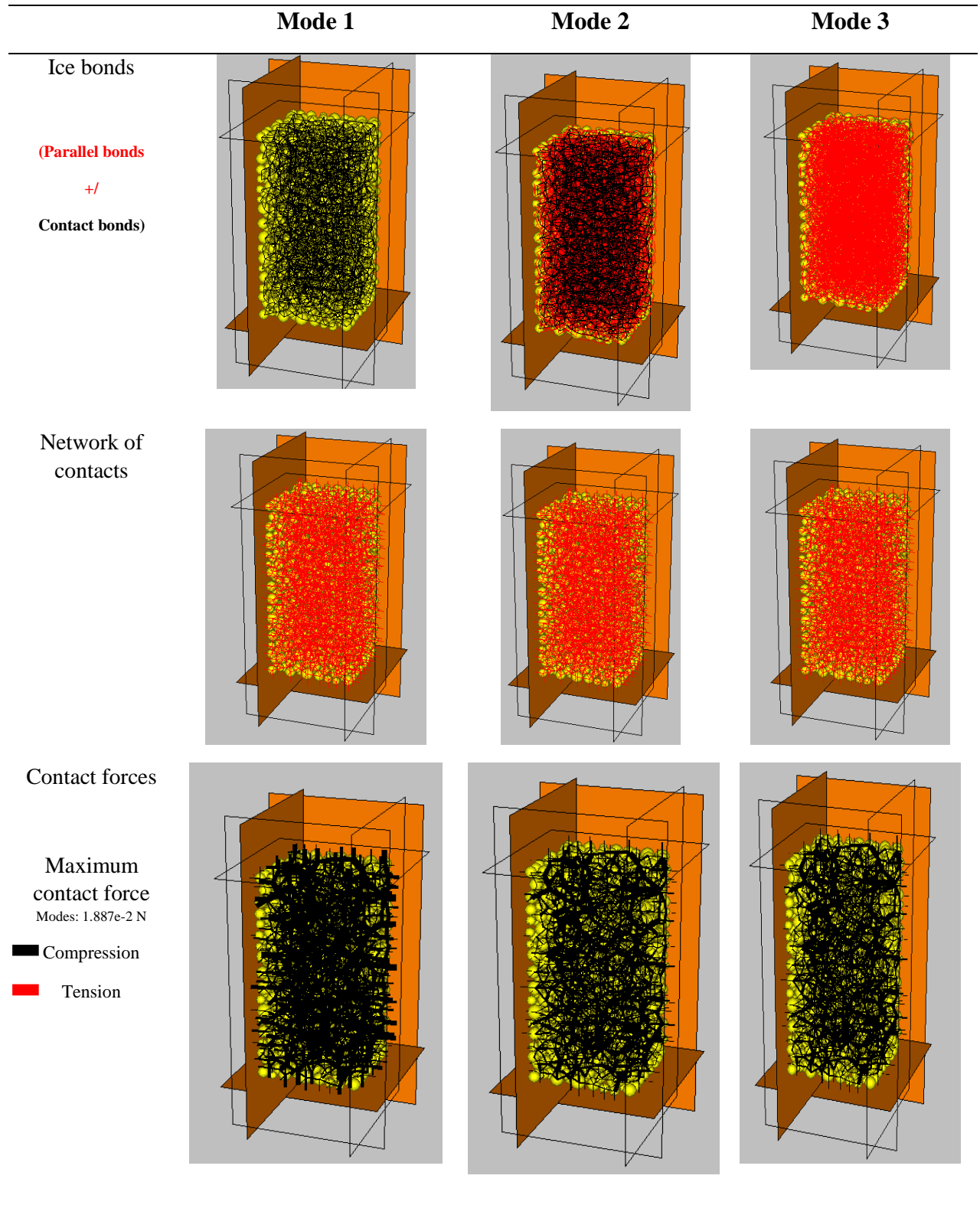
Lunar simulant has been defined as any material manufactured from natural or synthetic terrestrial or meteoritic components for the purpose of simulating one or more physical and/or chemical properties of a lunar rock or soil (McKay and Blacic, 1991). Materials chosen to simulate the lunar regolith need to replicate the critical physical and chemical parameters of the regolith. As a result, A synthetic material consisting of grains and cement (contact or/and parallel bonds) is produced such that it forms an isotropic and well-connected system by specifying the target stress. The initially specified isotropic strength (which is defined as the mean of the three principal stresses) is usually set to a low value relative to the material strength (which is less than 1% of the uniaxial compressive strength). After the initial isotropic samples are generated, the ice bond strength between the grains are introduced and the samples attained equilibrium. This helps in the simulation to manage the locked-in-stresses that develop after subsequent bond installation. The parameters used in the DEM simulation of the compression test are given in Table 8.1.

Table 8.1 Micro-properties and compression conditions used in the DEM simulation for compression of ice-bonded lunar regolith

Micro-properties and compression conditions		
Density kg/m ³	Ice Bond mean strength	Compression loading rate
2000	35KN/m ²	1.0×10^{-3} /s
Young's Modulus	Standard deviation	Target axial stress
20GPa	8.75KN/m ²	0.001MPa
Porosity	Particle average radius	Particle Friction
0.36	1.838×10^{-3} m	0.1

The compression loading has an axial strain of 0.1% and the bond (contact/parallel) mean strength replicates the mean strength of ice. Also, the standard deviation used is the standard deviation of the mean strength of ice bond (Tremblay and Hakakian, 2006, Mantovani et al., 2014, Allan, 2008, Izumi et al., 1997).

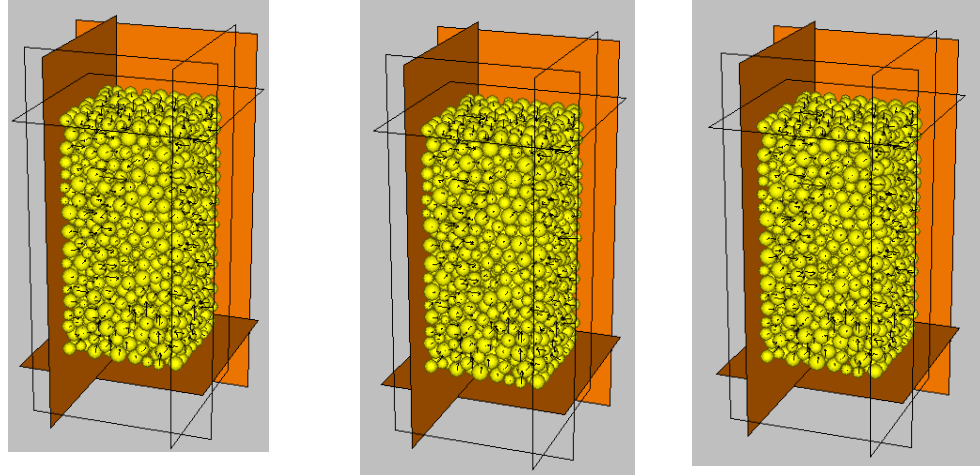
Results are obtained from the DEM simulations under lunar gravity and the profiles are provided in the isotropic state and at the post-peak state after failure as follows:



Velocity profile

Maximum velocity is

Modes: 1.064×10^{-10} m/s



Displacement

Maximum displacement is

Modes: 5.846×10^{-3} m

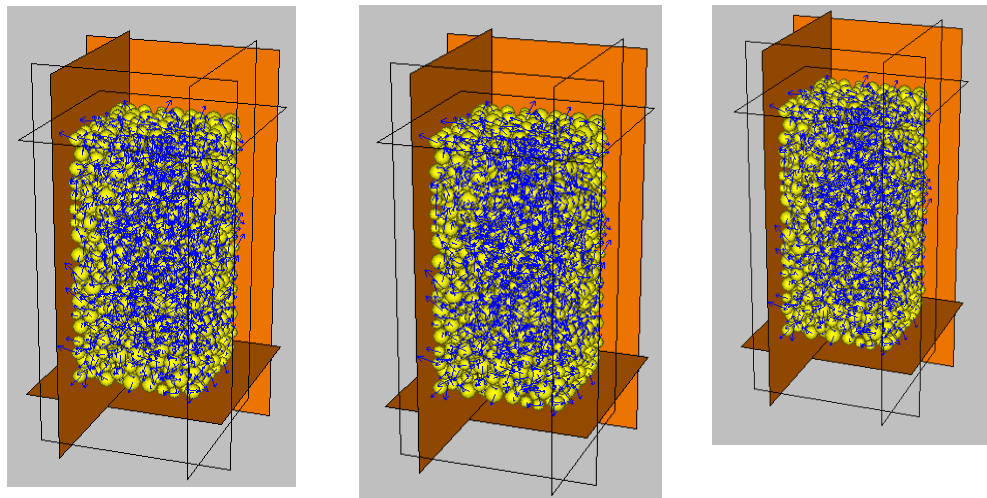
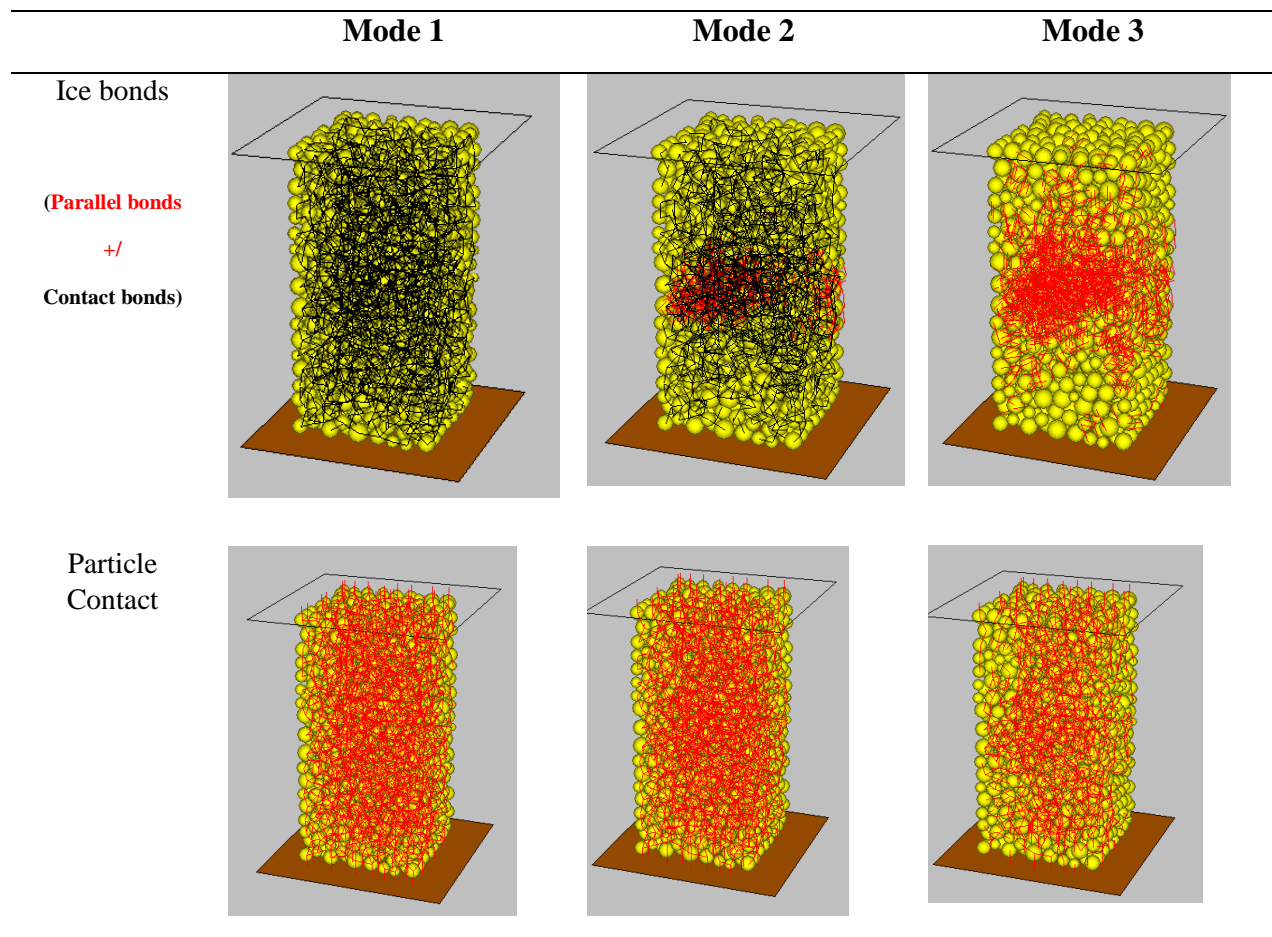


Fig. 8.4 DEM profile for ice-bonded simulated lunar regoliths at isotropic state before applying axial compaction under lunar gravity

The initial assembly characteristics of the three types of lunar samples are presented in Fig. 8.4. From Fig 8.4, the ice bonding existing between the grains are initially spread without much bias, but more dominantly in modes 2 and 3. The images representing the contact network shows the network connecting grains in the bulk assembly. This confirms the proportion of particle content identical in the samples but the ice content in different modes. The contact forces presented have a maximum contact force value of 1.887×10^{-2} N for all modes investigated (Pre-compaction stage). The contact force is colour coded to differentiate between the compression tension and forces. The thickness of the line is proportional to the magnitude of the contact force. For the initial assembly at isotropic state, the contact forces are dominantly compressive in nature. The contact forces of the grains are relatively more dominant in mode 1. The maximum value for the velocity for all modes in the initial assembly is 1.064×10^{-10} m/s. The velocity profile is denoted

with arrows and the length of the arrow is scaled to the magnitude of the velocity vector. The displacement of the particles was also monitored and observed to have a maximum value of 5.846×10^{-3} m. The directions of the arrows as presented in Fig 8.4 are used to denote the particles that move within the assembly. Axial load is further applied at a loading rate of 1×10^{-3} /s with axial strain 0.1%. The loading rate is slow enough to ensure the system has time to adjust to the force redistribution. The profiles obtained at the post-peak steady state are presented in Fig. 8.5.



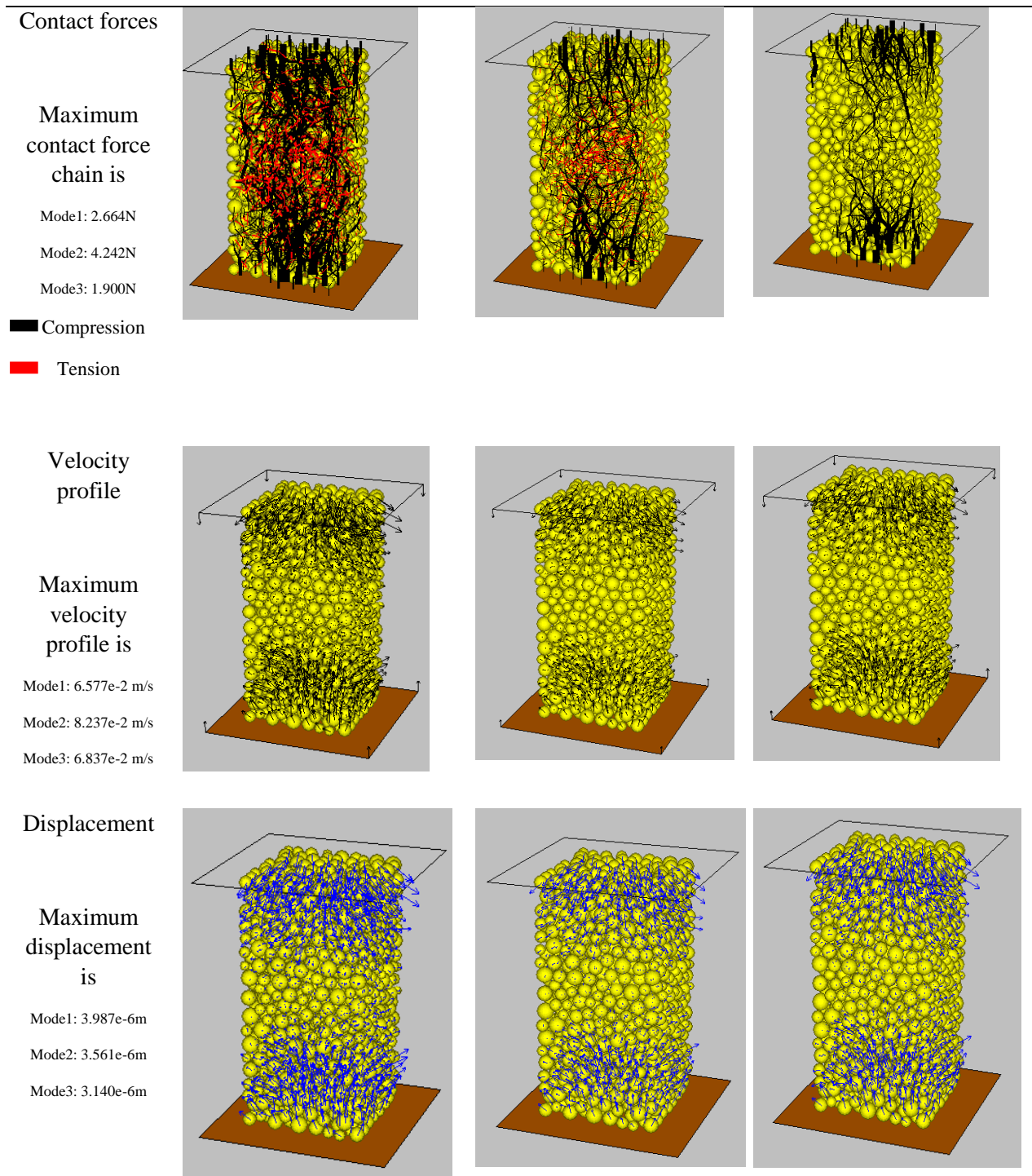


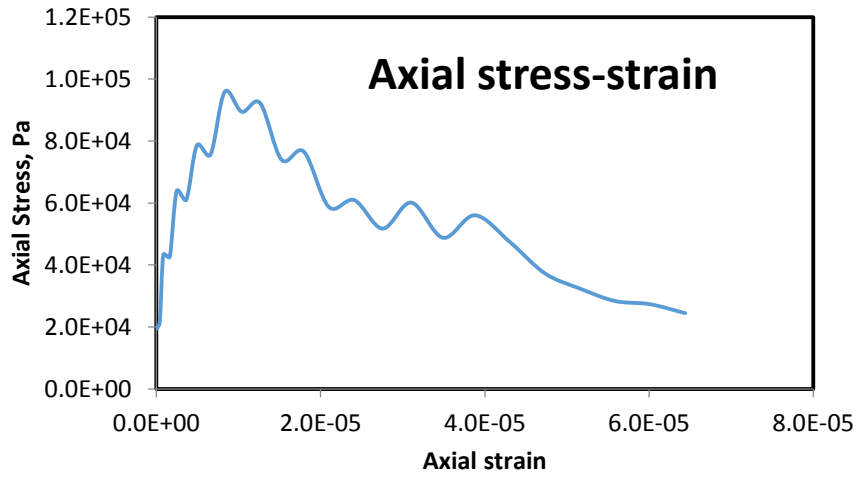
Fig. 8.5 DEM profile for ice-bonded simulated lunar regoliths at steady state (post-peak)

The profiles presented in Fig 8.5 show the tracked contact bonds of grains which help to understand the migration of grains in developing contacts during loading. They are concentrated more at the mid region of the samples in modes 2 and 3 during compression with the highest in mid region of

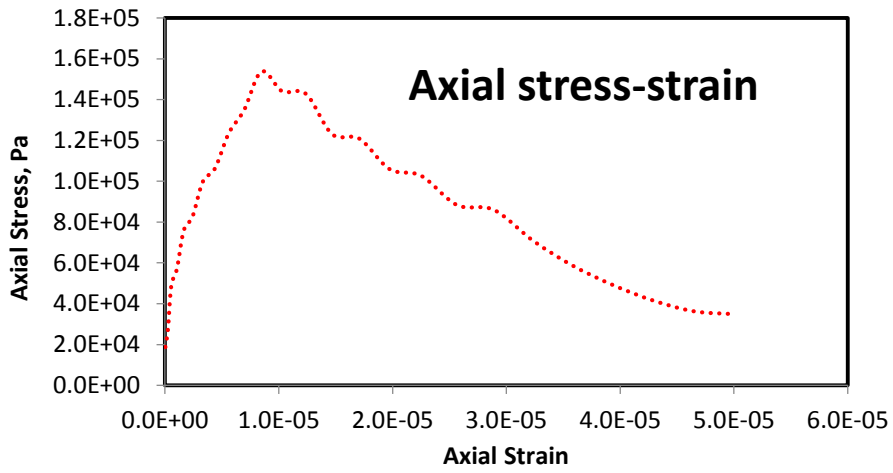
mode 3. As seen in the previous profile before loading, the contact network shows the grains connecting in different proportion with the ice content in different modes. The contact force chain at the post-peak state is predicted to have different maximum values for different modes. The maximum contact force chain for mode 1, mode 2 and mode 3 are 2.664N, 4.242N, and 1.900N respectively. With the colour codes applied to differentiate between compression and tension, grains in mode 1 sustain more tension when compared with other cases and the weakest in tension is the sample of mode 3. The velocity profile was observed to have a maximum value for mode 1, mode 2 and mode 3 as 6.577×10^{-2} m/s, 8.237×10^{-2} m/s and 6.837×10^{-2} m/s respectively. Also, the maximum displacement is predicted to be 3.987×10^{-6} m, 3.561×10^{-6} m, and 3.140×10^{-6} m for modes 1, 2 and 3 respectively. The results for the stress-strain curves obtained from the compression tests on the ice-bonded granular material under lunar gravity are presented in Fig 8.6 and 8.7 for modes 1, 2, and 3.

The axial stress (Fig. 8.6), the mean stress (Fig. 8.7), the frictional energy (Fig.8.8) and the kinetic energy (Fig 8.9) are measured against the axial strain to identify the effect of ice bonding of different modes on these key variables.

Mode 1



Mode 2



Mode 3

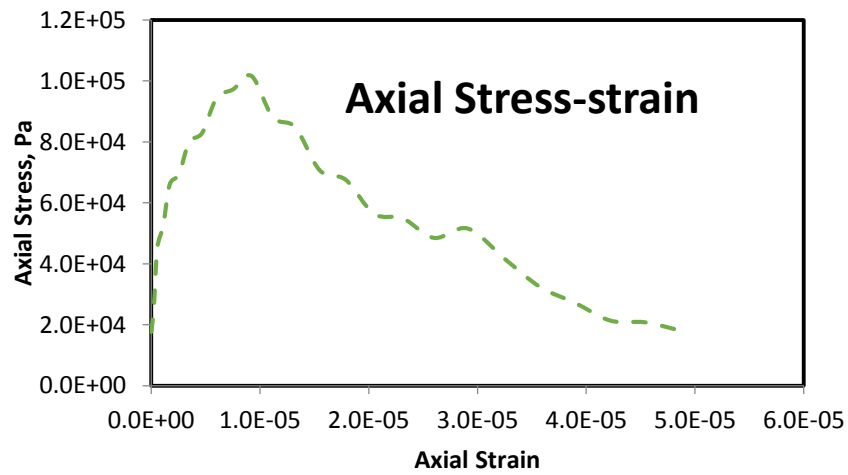
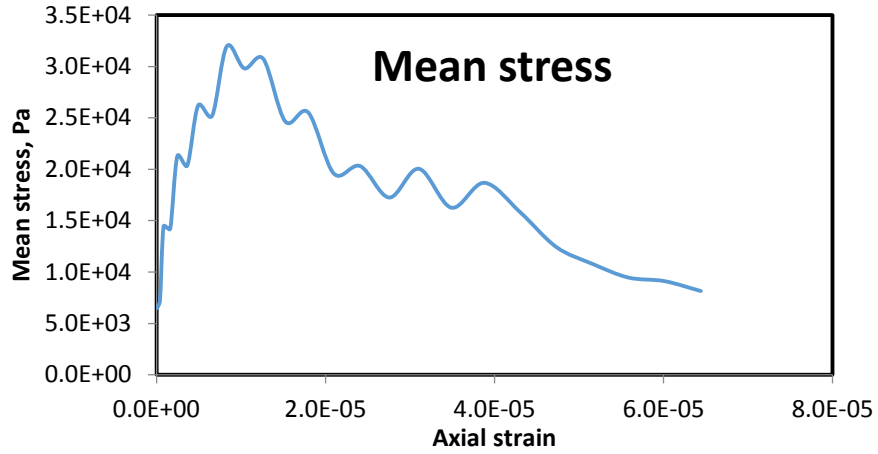
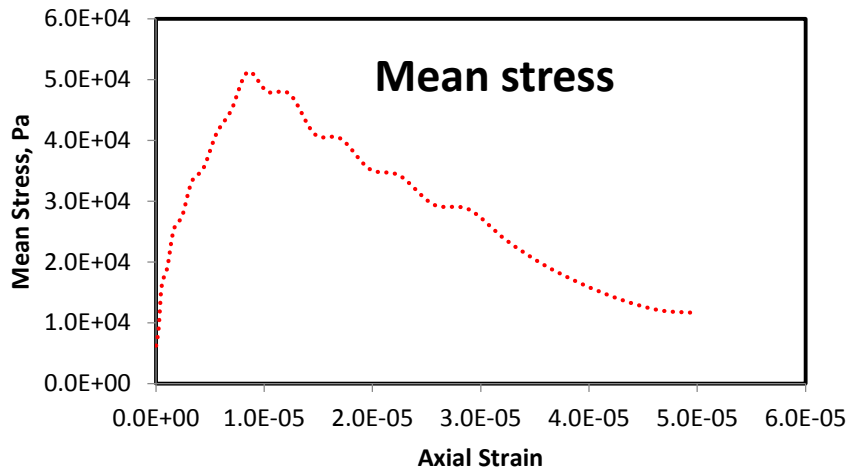


Fig. 8. 6 DEM simulation results of axial stress measured against the axial strain for ice bonded grains of modes 1, 2 and 3 under lunar gravity

Mode 1



Mode 2



Mode 3

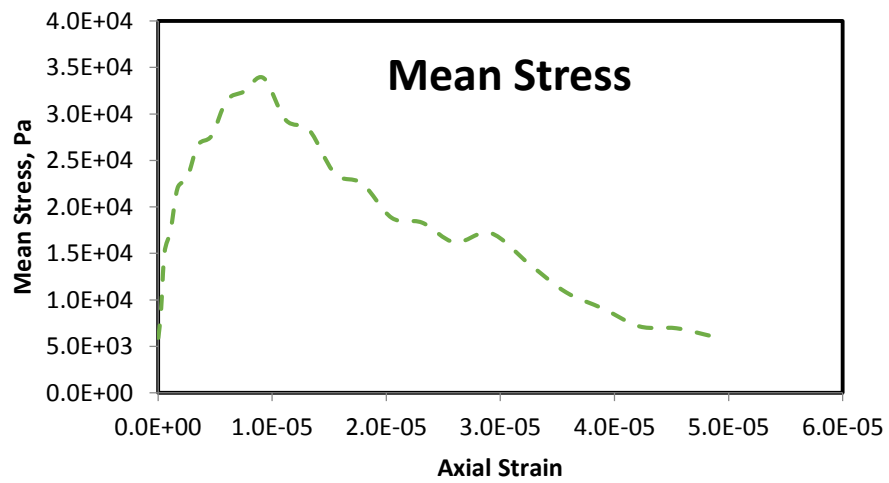
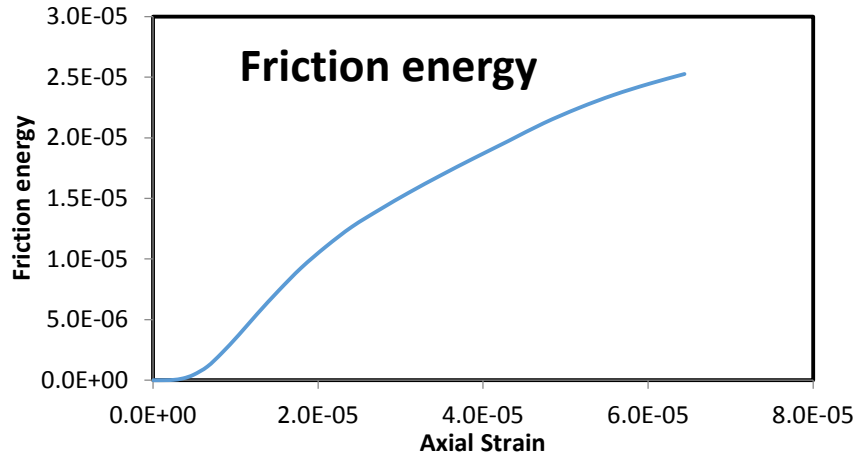
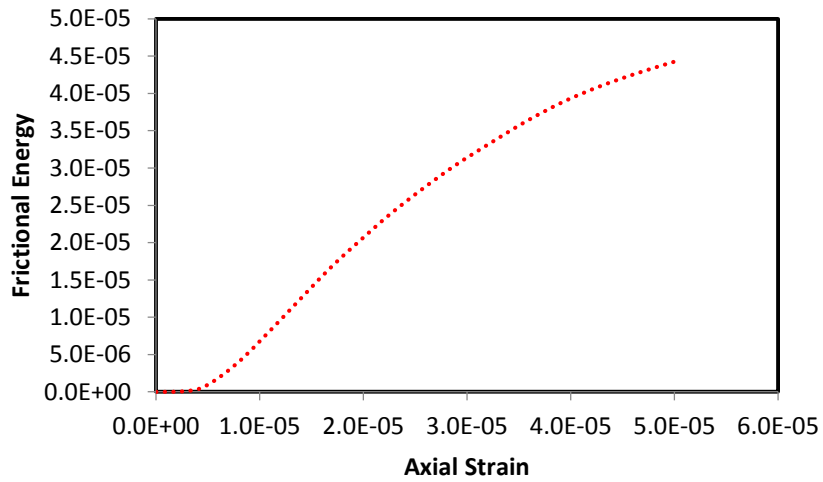


Fig. 8.7 DEM simulation results of mean stress measured against the axial strain for ice bonded grains of modes 1, 2 and 3 under lunar gravity

Mode 1



Mode 2



Mode 3

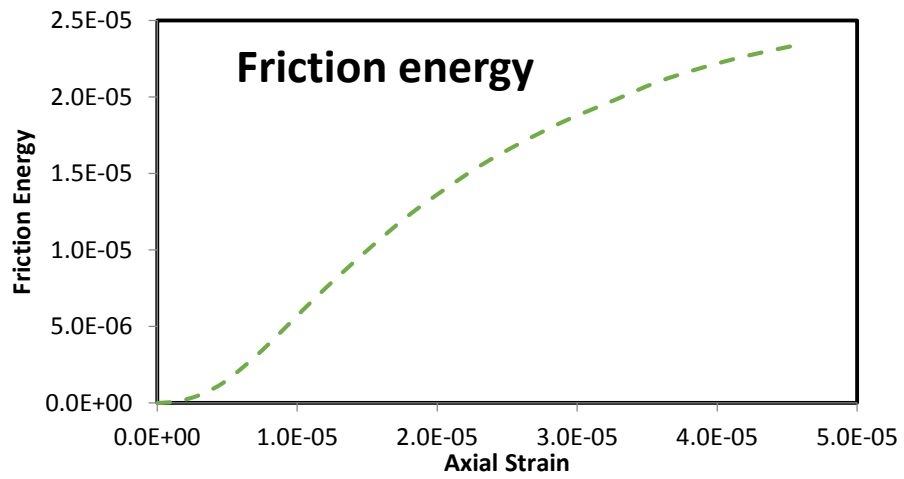
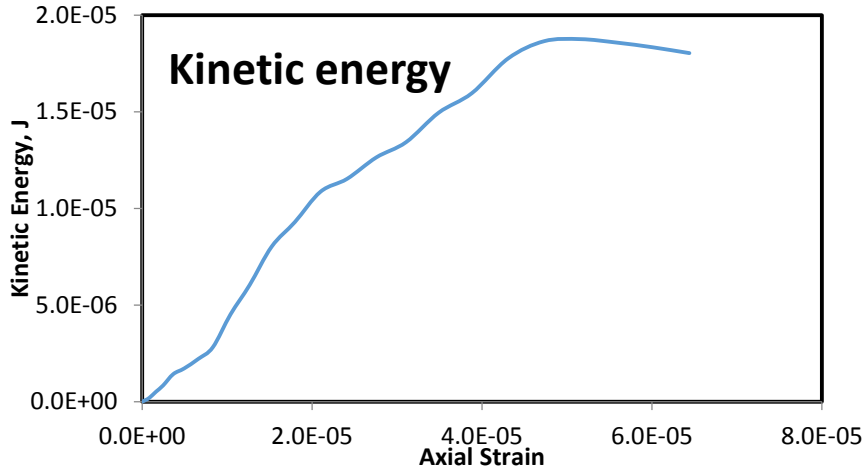
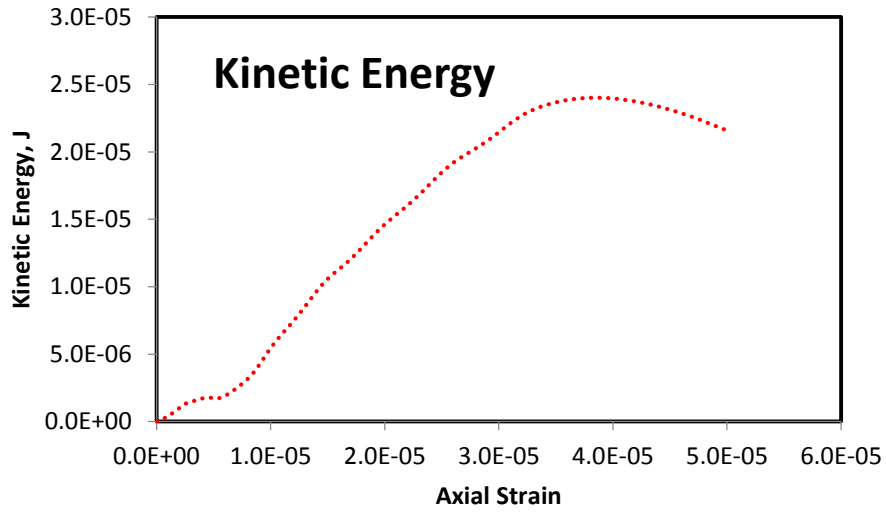


Fig. 8. 8 DEM simulation results of friction energy measured against the axial strain for ice bonded grains of modes 1, 2 and 3 under lunar gravity

Mode 1



Mode 2



Mode 3

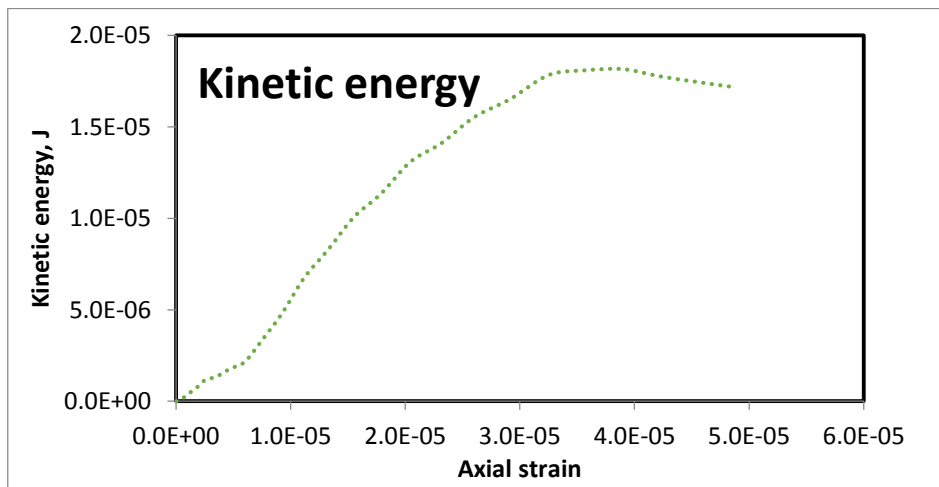


Fig. 8. 9 DEM simulation results of kinetic energy measured against the axial strain for ice bonded grains of modes 1, 2 and 3 under lunar gravity

The stress-strain curves reach a near steady state plateau denoted as the strength. The friction energy is also monitored and predicted to increase with the axial strain. The kinetic energy also increased with the applied axial strain to a peak value after which the kinetic energy tends to be steady at a maximum with increasing strain post-peak. Comparing the results for the 3 modes of the ice-bonded grains and un-bonded grains under compression as presented in Fig. 8.10, it is concluded that under lunar gravity, the peak strength values obtained in simulations for mode 1 and mode 3 are similar, though mode 3 has slightly higher peak strength in magnitude. Also, when both bonds (contact and parallel bonds) are present as in the case of mode 2, there is an increase in the peak strength of the ice-bonded granular material. The presence of both contact and parallel bonds (mode 2) also gives higher frictional and kinetic energy as against mode 1 and mode 3. Additionally, the peak strength of the un-bonded grains is the lowest.

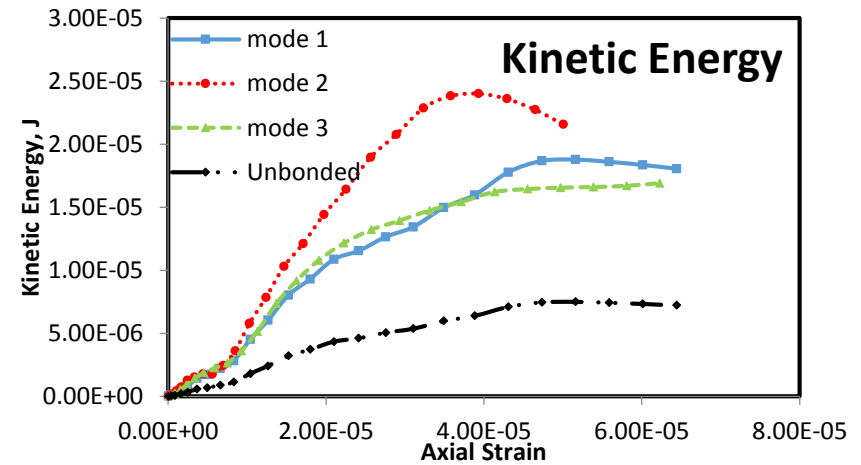
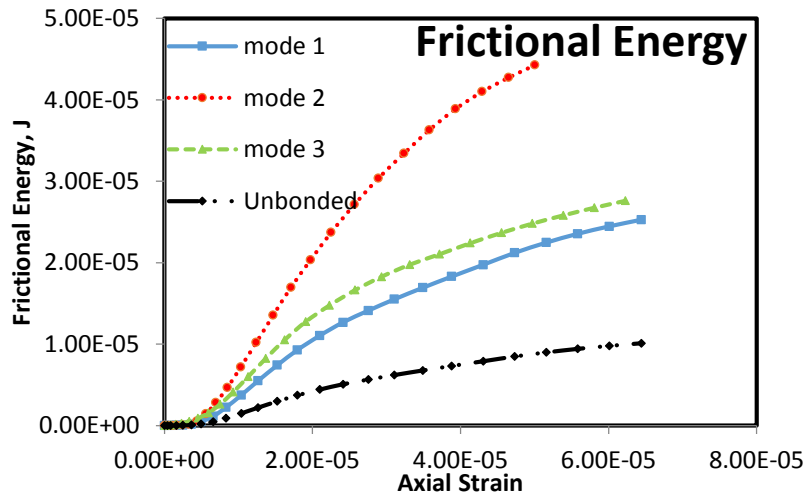
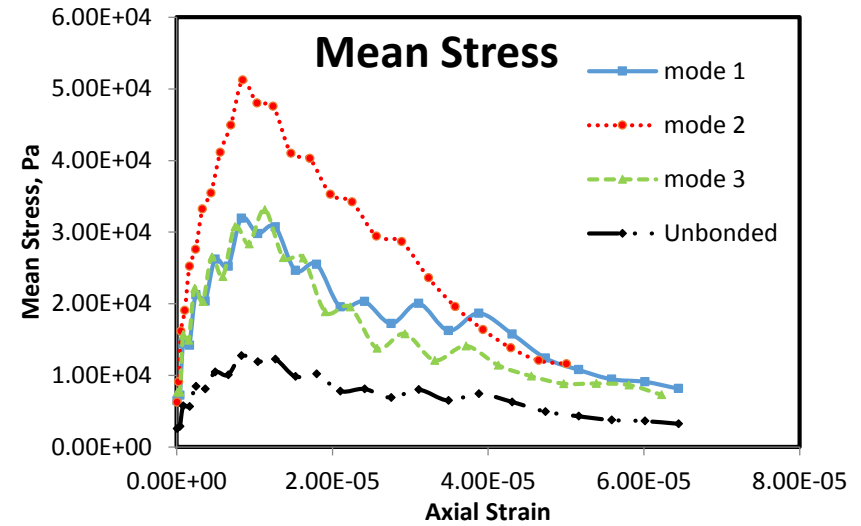
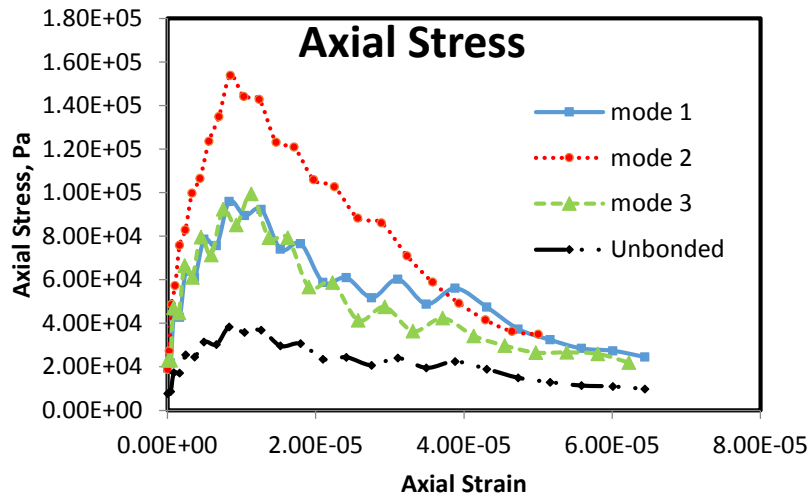


Fig. 8.10 DEM simulation results of axial stress, mean stress, frictional and kinetic energy measured against the axial strain for ice-bonded grains of modes 1, 2 and 3 under lunar gravity

The results obtained and presented in Fig 8.10 helps to predict and understand the effect of different modes of ice-bonded and un-bonded granular materials on lunar regolith such that when the contact bond and parallel bonds exist separately in grains, they tend to behave differently under compression load but with similar peak strength. However, when both contact and parallel bonds are present in the regolith (mode 2), the strength is expected to be higher. The un-bonded grains has the lowest peak strength as expected. Mantovani et al. (2014) reported that the increase in ice mix bonded with planetary regolith is likely to increase the strength of the material. Thus, regolith with contact bonds (mode 1) and parallel bond (mode 3) existing will readily be excavated compared with regolith with both contact and parallel bonds (mode 2) present. This response is further investigated under earth and mars gravity in the next section.

8.4 Compaction of Ice-Bonded Granular materials for Earth and Mars Gravity Levels

For the purpose of completeness and comparison, the previous simulations are presented here with change from lunar gravity to earth and mars gravity levels. The results are presented in Figs. 8.11 and 8.12 for earth and mars gravity levels respectively.

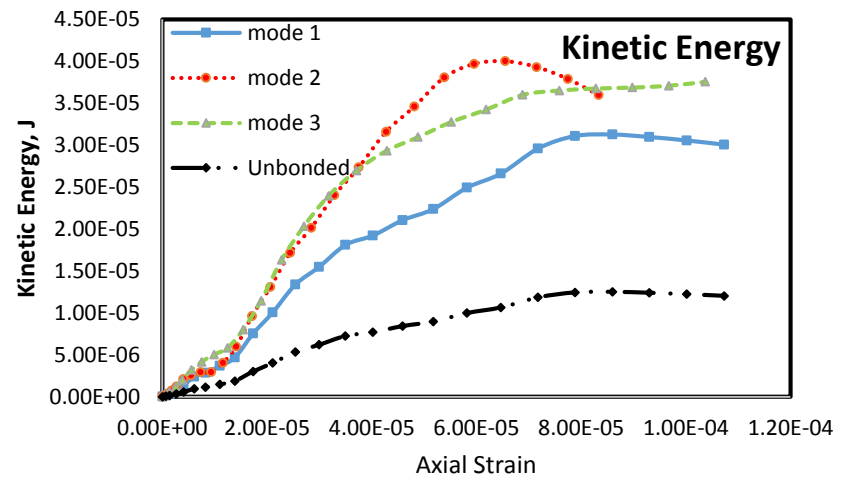
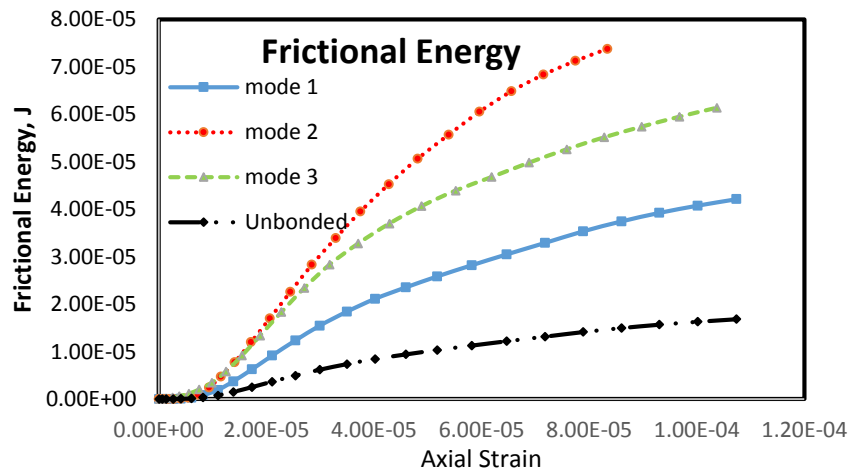
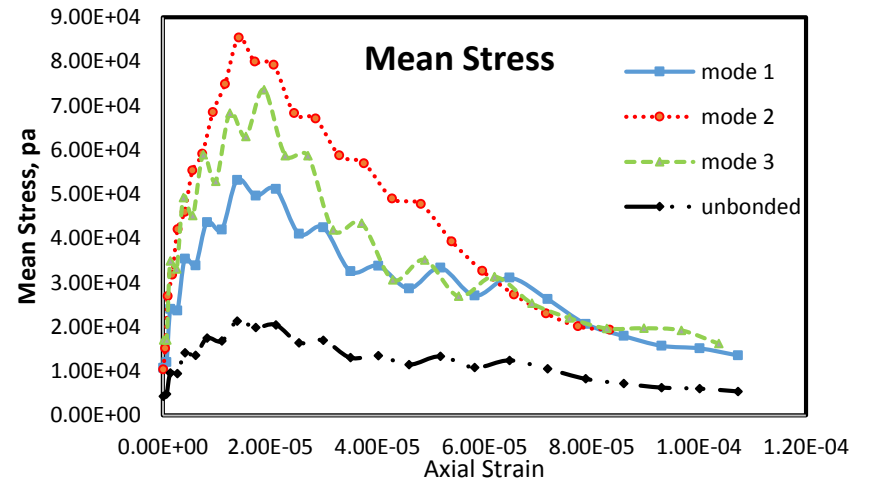
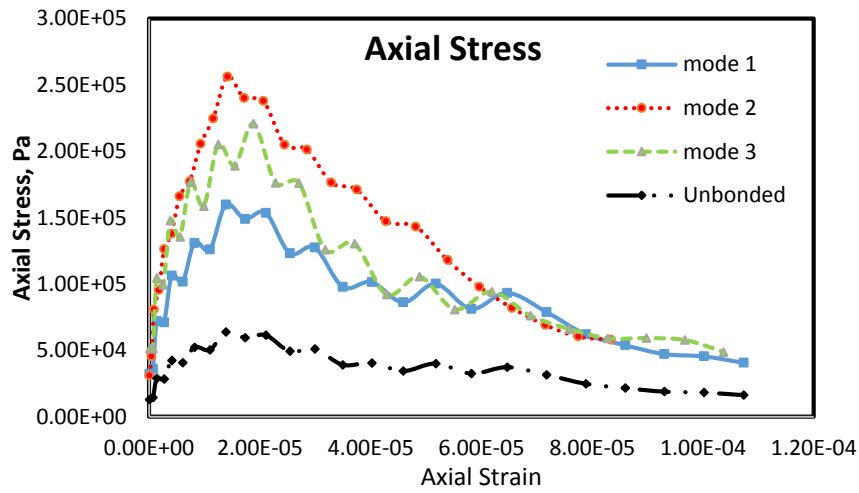


Fig. 8.11 DEM simulation results of axial stress, mean stress, frictional and kinetic energy measured against the axial strain for ice-bonded grains of modes 1, 2 and 3 under earth gravity

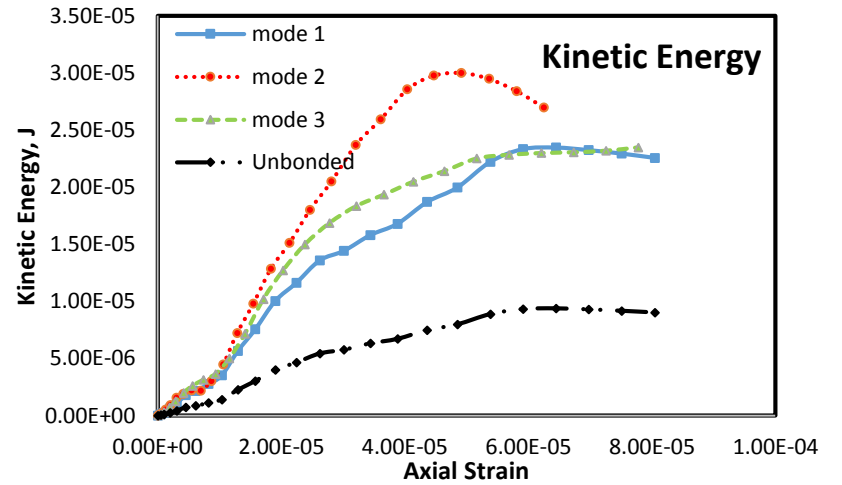
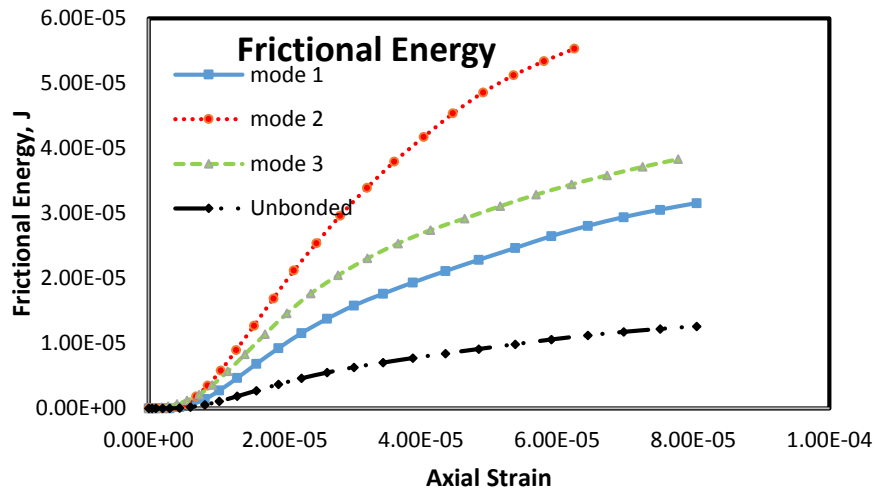
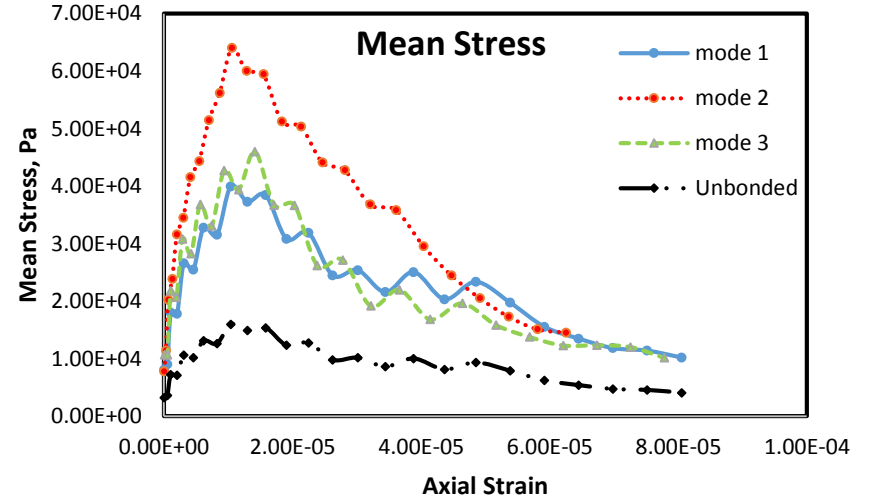
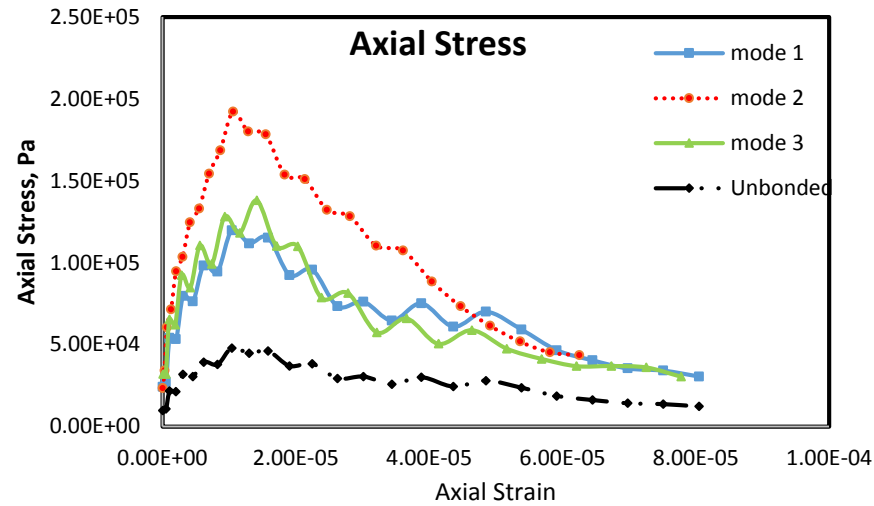


Fig. 8.12 DEM simulation results of axial stress, mean stress, frictional and kinetic energy measured against the axial strain for ice-bonded grains of modes 1, 2 and 3 under mars gravity

From Figs. 8.11 and 8.12, the response of the ice-bonded particles of different modes behave differently under earth gravity and mars gravity. Granular materials with ice bonds of mode 1 (contact bond) tend to have the lowest peak stress followed by grains with ice bonds of mode 3 (parallel bond). Ice-bonded grains with mode 2 still have the highest peak stress. However, under mars gravity, the sensitivity reduced with reducing gravity and the peak stress of grains with only parallel bonds (mode 3) reduced with reducing gravity. Again, under earth and mars gravity, the un-bonded grains had the lowest peak stress. It has however been shown experimentally under earth gravity (Yu et al., 2007, Cuccovillo and Coop, 1999) that the presence of cohesion inhibits dilatancy such that grains having cement bonds exhibits less dilatancy. Also, suggestions are that cohesion arising from the parallel bonds inhibits dilatancy (Marri et al., 2012) which as a result is related to higher peak stress of the grains. However, with three dimensional DEM simulations, this pattern was only observed under earth gravity and to some extent under lower gravities for ice-bonded materials. At lower gravities, the sensitivity of the ice cement bonds (parallel bonds) reduced with gravity as observed with the reduction in the peak stress of mode 3 (parallel bonds) with reducing gravity.

The results of terrestrial experiments on lunar regolith simulant have shown the importance of testing lunar regolith containing different types of ice bonding and the necessity of designing and testing excavators that are flexible yet robust (Gertsch et al., 2006). This is evident that the introduction of ice bonds (parallel bonds in addition to the contact bonds) causes a larger peak to appear compared to other types of ice bonded grains and eventually approach the stress state of the other modes under the EML gravity levels.

8.5 Conclusions

The present study explored an approach to DEM simulation to further investigate the compaction strength of different modes of ice-bonded materials and un-bonded materials reported to exist in the lunar regolith under earth, mars and lunar (EML) gravity levels.

A novel concept of applying three dimensional DEM simulation to evaluate three different modes of ice-bonded simulated materials representing lunar regolith was reported. Compression tests were carried out on all three modes of ice bonded granular materials simulated under EML gravity. The results show that the peak strength values for mode 1 with ice bonds at particle interface and

mode 3 with uniform spread strength of ice exhibit no significant difference, while mode 2 with both particle interface ice bonds and uniform strength of ice has higher peak strength in magnitude under lunar gravity environment. However, under earth gravity the peak stress of mode 3 is higher than that of mode 1 with mode 2 having the highest peak stress values. The presence of both ice-bonding modes (mode 2) also gives higher frictional and kinetic energy as against mode 1 and mode 3 under EML gravity levels. Under the EML gravity levels, the un-bonded materials have the lowest strength as expected. This suggest that grains with both contact and parallel bonds (mode 2) hold high strength of the granular assemblies, especially under reduced gravities.

Chapter 9

CONCLUSIONS AND FUTURE RECOMMENDATIONS

9 Conclusions and Future Recommendations

9.1 Conclusions

This work investigated the role of particle-scale properties on granular flow under varying gravity conditions viz., earth, mars and lunar (EML) gravity. The motivation to carry out this research was derived from the challenges in achieving smooth and reliable flow from hoppers in the process and handling of bulk particulate in industries as well as the challenges faced in space exploration industries dealing with particulate materials, e.g. exploration of mars and moon. Flow behaviour of granular materials has been regarded to be exceedingly complex and not yet well established, however very much needed in the design of operating capabilities in the industry and in recent development such as of space explorers as EXOMARS where gravity effects could strongly influence granular flow. Particle scale properties and hopper design play a major part in processing earth gravitational granular flows and this aspect is extended to different low gravity levels. In this research, investigations were carried out to study the gravity effect on the influence of particle-scale properties and hopper geometry on flow of granular materials. Three different approaches have been used in this study to understand the flow characteristics of granular materials through flow geometries under different gravitational environments. Though the DLA approach is the simplest of all, it helps to evaluate the dynamic nature of the grains such as the completion time of the flow under different gravitational conditions. Furthermore, even a simple continuum approach such as Kirya's model could help to estimate the three dimensional flow behaviour of grains more quickly unlike DEM simulations which involve a significantly greater amount of computational time and resources, especially for studying the low gravitational behaviour of granular materials. These approaches provided well captured understandings of the dominant role which gravity plays with results from the approaches agreeing qualitatively very well. Further investigations on the effect of hopper design, the force field indicating the stress and strain within the granular assembly and the particle scale properties affecting the rheology under earth gravity (1g) was validated with available literature and extended for low gravity studies. Additionally, two parameters (PSD and adhesion force) were characterized experimentally, in addition with other grain scale properties which served as input parameters in the DEM simulations. DEM provides a clearer understanding of the effects of particle scale properties and interactions on their flow and compaction

characteristics under EML gravities. The main conclusions from this research are summarised in the following sections.

9.1.1 Investigations on the stress analysis and shear deformation of granular materials under EML gravity

Investigations were conducted to study the maximum shear stress that develops in hoppers across the granular bed and along the hopper walls under earth mars and lunar (EML) gravities using three dimensional DEM simulations. The DEM results were qualitatively compared with experimental results (PSAT) and existing Walker's theoretical predictions under earth gravity and further estimations made under mars and lunar gravities. Results indicate that a good level of agreement is obtained between the experimental (PSAT) and DEM simulations. Furthermore, grains close to the hopper walls are more stressed compared to those at the middle of the hopper. The stresses were measured at hopper height, $H/2$ under static conditions and reduced from both sides of the hopper walls towards the middle of the hopper. Results also show that the distribution of the stresses greatly depends on the hopper internal angle with different stress profiles obtained under different angles between 30° and 90° . The stress towards the middle of the hopper was observed to decrease with increasing internal angle under earth gravity. For the 30° hopper internal angle, DEM simulations show near uniform stresses across the granular bed horizontally. These results agreed with PSAT experimental results at least under earth gravity levels. The gravity effect was investigated with the DEM simulations carried out under mars and lunar gravity levels. Results show that gravity plays no significant role in the way stresses are distributed across the hopper bed under static condition. Different angles investigated had similar stress distributions under EML gravity levels.

Further estimations were carried out to predict the stresses along the hopper walls under static filling under the EML gravity levels. The results predicted using DEM simulations here also showed good comparative agreement with existing Walkers' theoretical model. Results showed how the stresses are distributed along the walls for different hopper internal angles between 30° and 60° . DEM simulations predicted that the maximum stress on the wall was at maximum at an intermediate height along the walls and not at each ends of the hopper. Again, further investigations showed that gravity did not play a significant role in estimating the stresses that develop along the walls of the hopper. In view of the complexities of predicting and evaluating

stresses in granular materials, the investigations carried out on evaluating these stress distributions in granular materials has shown the usefulness, reliability and excellence of feeding characterized materials as key inputs into DEM modelling.

Following the findings from these investigations, the study provides a framework using three dimensional DEM within which larger spectrum of behaviours exhibited by granular materials can be captured under different gravity levels which cannot yet be encompassed by existing experimental or continuum theories.

9.1.2 Gravity effects on granular flow using theoretical approaches and DEM simulations

In this thesis, two types of theoretical continuum approaches, (DLA and Kirya's structural model) were adopted and DEM simulations performed to evaluate the influence of particle-scale properties and hopper geometry on the flow characteristics of grains. Investigations carried out using the DLA approach did not explicitly account for gravity but gave an implicit qualitative evaluation of the flow characteristics of granular flow inside hoppers under various discharge regimes. Results obtained from predictions made from Kirya's model were compared with three dimensional DEM simulations.

Results obtained from the DLA approach indicate that particle-scale properties as well as hopper geometry have significant effect on granular flow. Most of the results obtained using this approach agree well with existing literature except in the case of the hopper orifice opening which was further investigated using DEM simulations in later sections.

Both Kirya's structural model and three dimensional DEM were further used to investigate the influence of gravity on granular flow in a hopper. Results show strong effects of gravity on granular flow qualitatively using both models. Kirya's model further estimates the response of various particle scale properties on granular flow under different gravity levels. Investigations defining the particle media as a continuum as well as discrete particles both indicate that granular flow and its particle properties depend greatly on gravity levels. The gravity dependence of granular flow was supported and validated with experimental results obtained from literature and practical parabolic flight test operation.

The successful predictions from this investigation gives an understanding of the connections existing in the particle scale properties with both the continuum approaches and DEM simulations through microstructure evolution.

9.1.3 Influences of particle-scale properties and hopper geometry on granular flow behaviour under earth, mars and lunar gravity levels using DEM simulation

Individual properties have particular effects on granular flow and the combined effect makes the study of granular flow complex. Three dimensional DEM simulations have been used to understand the individual properties affecting granular flow under earth, mars and lunar (EML) gravity levels. Properties such as granular packing, granular bed density, cohesion, coefficient of friction, angle of repose, hopper geometry (orifice and internal angle) and the combined adhesion strength and size distribution (for real samples) of the granular materials were investigated using DEM simulations.

Results indicate that loosely packed grains will flow slower than highly dense granular bed under earth gravity. The dependence of the packing fraction on granular flow reduced with reducing gravity levels and at lunar gravity, the effect of packing fraction of the granular bed on granular flow was much less significant. Also, results show that particle cohesion plays a significant role on granular flow under EML gravity levels. This cohesion dependence is more pronounced under lunar gravity which implies that at low cohesion, the effect of flow is more responsive with decreasing gravity levels. The hopper orifice also showed significant influence on granular flow under the EML gravity levels. The influence was much more sensitive under lunar gravity where grains ceased to flow at low orifice opening compared to higher gravity levels and this influence increased with increase in cohesion. Results further showed the dependence of granular flow on the stiffness of the particles in which soft spheres flow quicker than hard spheres under EML gravity levels. With decreasing gravity, it becomes more difficult for hard spheres to flow and this could be as a result of more cluster formation at increased stiffness. Also, in hopper design, hoppers with higher internal angles are likely to slow down the rate of flow of grains from the hopper. This agrees qualitatively with results obtained from the continuum approach and other experimental results from literature under earth gravity levels. The effect of the internal angles also showed strong dependence on gravity with the effect becoming more significant with decreasing gravity. DEM simulations also gave an indication on the way the particles are displaced at lower and higher

internal angles. This supported the dependence of flow types on hopper angles as reported in literature. Friction effect was studied for both particle-particle and particle-wall friction coefficients and the simulation result indicate the influence both have independently on granular flow under earth, mars and lunar gravity levels. Results obtained indicate the less sensitivity of the wall friction on flow than particle friction with the sensitivity of particle friction increasing with increasing gravity levels. This shows that particle friction plays a more dominant role during granular flow with the dominance increasing with decreasing gravity levels. This results further provides an understanding on the influence of these friction coefficients independently which has not been fully explored in literature under low gravity levels. Simulation results on angle of repose was also observed to marginally depend on gravity and the reduced angle of repose under low gravity further suggests the difficulty in particle movements under low gravity. Though the dependence of the angle of repose on gravity is in disagreement with a large body of work in the literature, recent investigations including parabolic flight test simulations agree with the results presented in this thesis. Further simulations carried out on the selected granular samples show that samples with different adhesion forces and size distributions behave differently under low gravity environment and have different influence on flow as compared to earth gravity. Results indicate that, for the sample types that had relatively bigger size particles (with their corresponding inter-particle adhesion) i.e., JB1-4 samples, the bulk flow rate under the lunar gravity was fairly similar, though much lesser in magnitude than that of earth and mars gravities. This suggests that, when the gravity levels are relatively small such as under the lunar gravity, individual effects of particle-scale properties of larger size particles negate the differences on the net bulk flow rate.

Successful investigations carried out here coupled with the few experimental and theoretical support under earth gravity has added an insight into granular handling and its complexities with a profound view regarding granular flow in Moon and Mars exploration.

9.1.4 Enhancing granular flow under EML gravity

To improve gravity driven granular flow through a hopper, horizontal vibration on the hopper was investigated using three dimensional DEM. Further simulations were carried out to understand the differences in continuous and staggered (intermittent) granular flow. Simulation results show that vibrating the hopper could increase granular flow up to peak frequency after which flow rate began to decrease. This effect was observed to reduce with reducing gravity levels with the peak

frequency reducing with decreasing gravity levels. Results obtained further indicate the dependence of the vibrator effect on the magnitude and frequency and a peak frequency will exist for any displacement amplitude chosen for horizontal vibrations under EML gravity levels. Variations of the amplitude, angular velocity and frequency can aid the design of a vibrator to operate at its optimum with maximum efficiency in space and most industrial applications of granular flows through hoppers.

It was also observed using DEM simulations that staggering flow under earth gravity had negligible or no major impact on the rate of flow of grains. However, the staggered effect is more sensitive to gravity with the effect increasing with reduced gravity and at a distinct percentage under lunar gravity. It is thus recommended to maintain continuous flow of grains during processing especially for space/low gravity exploration.

9.1.5 Compaction properties of ice-bonded granular media

Three dimensional DEM simulations is used to model the lunar ground with the concept of ice-bonding within granular materials. Results on compression tests carried out on the three modes of the ice-bonded granular materials and un-bonded grains shows different peak strength of the modes with mode two having the highest peak strength under EML gravity levels. The un-bonded granular materials was observed to have the lowest strength as expected. The parallel-bonded grains however responded differently under low gravity conditions with its strength effects more significant with increasing gravity compared to the contact bond grains. Simulation results obtained suggests that grains with both contact and parallel bonds (mode 2) hold high strength.

The results obtained generally in this work shows that studying the gravity effect is an important issue not only for the low gravity environment (space) applications but also for earth gravity conditions or normal day to day processing of powder grains in the process industry. The primary subject of the study described in this study, decreasing gravity decreases the major driving force acting materials in many processing operations, thus leading to the assemblies of particles to appear to be more cohesive in their bulk behaviour than they would on earth.

9.2 Future Recommendations

This research study has provided valuable information on the role of particle scale properties and gravity on the behaviour of granular flow characteristics. These properties are known to influence granular flow under earth gravity but limited knowledge exists under low gravity. The aim of investigating these properties is to fully understand the complexities behind its individual role and hopper geometry on granular flow under varying gravity conditions with special focus in earth, mars and moon (EML) gravities. This has led to the observed strong gravity dependence on flow. Further studies are required to evaluate more complex conditions as mentioned below. This could help scientists, engineers and astronomers in future to develop clearer understanding of multi-scale functional properties of grains on flow characteristics under varying gravity conditions beyond the ranges considered in this study. Also, future research needs to be done in the following:

1. There is need to develop further experimental stress sensing methodologies for the dynamic flow state characteristics as against the static state investigated in this work under varying gravity levels.
2. To further evaluate the particle scale properties for different shapes of particles for example, non-spherical particles for packing densities and other characteristics beyond the range considered in this study. This will aid in further getting the complete control of the complexities in granular materials even under low gravity environments.
3. More real samples from planetary regolith can be characterized fully beyond the characterizations carried out in this study to obtain realistic and complete key input parameters to be used in DEM simulations in investigating the flow characteristics.
4. Carrying out realistic or more rigorous parabolic flight simulations to compare the simulation predictions with experiments more comprehensively.

References

- ABDULLAH, E. C. & GELDART, D. 1999. The use of bulk density measurements as flowability indicators. *Powder Technology*, 102, 151-165.
- ACTON, Q. A. 2012. *Issues in Engineering Research and Application: 2011 Edition*, ScholarlyEditions.
- AGUIRRE, M. A., DE SCHANT, R. & GÉMINARD, J. C. 2014. Granular flow through an aperture: Influence of the packing fraction. *Physical Review E*, 90, 012203.
- ALBARAKI, S. & ANTONY, S. J. 2014. How does internal angle of hoppers affect granular flow. Experimental studies using Digital Particle Image Velocimetry. *Powder Technology (Submitted)*.
- ALBARAKI, S., ANTONY, S. J. & AROWOSOLA, C. B. Visualising shear stress distribution inside flow geometries containing pharmaceutical powder excipients using photo stress analysis tomography and DEM simulations. *Powders and Grains*, 2013 Sydney, Australia. AIP Conference Proceedings, 706-709.
- ALLAN, M. 2008. The coefficient of friction, particularly of ice. *Physics Education*, 43, 392.
- ANAND, A., CURTIS, J. S., WASSGREN, C. R., HANCOCK, B. C. & KETTERHAGEN, W. R. 2008. Predicting discharge dynamics from a rectangular hopper using the discrete element method (DEM). *Chemical Engineering Science*, 63, 5821-5830.
- ANTONY, S. J. 2001. Evolution of force distribution in three-dimensional granular media. *Phys Rev E Stat Nonlin Soft Matter Phys*, 63, 18.
- ANTONY, S. J. 2007. Link between single-particle properties and macroscopic properties in particulate assemblies: role of structures within structures. *Philosophical Transactions of the Royal Society of London Series A*, 365, 2879-2891.
- ANTONY, S. J. & AMANBAYER, T. 2011. Technical report on Discrete and Continuous modelling of granular flows. *Personal Communication*.
- ANTONY, S. J. & CHAPMAN, D. 2010. Probing shear stress distribution within single particle scale inside particulate packing. *KONA Powder and Particle Journal*, 28.

- ANTONY, S. J., CHAPMAN, D., SUJATHA, S. J. & BARAKAT, T. 2015a. Interplay between the inclusions of different sizes and their proximity to the wall boundaries on the nature of their stress distribution within the inclusions inside particulate packing. *Powder Technology*, 286, 98-106.
- ANTONY, S. J. & GHADIRI, M. 2006. Size effects in a slowly sheared granular media. *Journal of Applied Mechanics, American society of mechanical engineers*, 68(5), 772-775.
- ANTONY, S. J., HOYLE, W. & DING, Y. 2004. *Granular materials: fundamentals and applications*, Royal Society of Chemistry.
- ANTONY, S. J., IMAFIDON, O. & BARAKAT, T. 2015b. Micromechanical analysis of inclusions in particulate media using photo-stress analysis tomography. *Optical Engineering*, 54, 081202.
- ANTONY, S. J. & KRUYT, N. P. 2009. Role of Interparticle friction and particle-scale elasticity in the shear strength mechanism of three-dimensional granular media. *Physical Review E*, 79, 031308, 9.
- ANTONY, S. J., KUHN, M. R., BARTON, D. C. & BLAND, R. 2005. Strength and signature of force networks in axially compacted sphere and non-sphere granular media: micromechanical investigations. *Journal of Physics D: Applied Physics*, 38, 3944.
- ANTONY, S. J. & SARANGI, F. 2006. Computational Study Investigating the Influence of Long-Range Repulsive Forces on the Collective Behaviour of Particulate Media. *Journal of Computational and Theoretical Nanoscience*, 3, 487-496.
- ARÉVALO, R., GARCIMARTÍN, A. & MAZA, D. 2007. A non-standard statistical approach to the silo discharge. *The European Physical Journal Special Topics*, 143, 191-197.
- ARNOLD, P. C., MCLEAN, A. G. & ROBERTS, A. W. 1978. *Bulk Solids: Flow and Handling*. TUNRA Limited, The University of Newcastle, NSW, Australia.
- ATTARD, P., STIERNSTEDT, J. & RUTLAND, M. W. Measurement of friction coefficients with the atomic force microscope. *Journal of Physics: Conference Series*, 2007. IOP Publishing, 51.

- BABIC, M., SHEN, H. H. & SHEN, H. T. 1990. The stress tensor in granular shear flows of uniform, deformable disks at high solids concentrations. *J. Fluid Mech*, 219: 81-118.
- BAGNOLD, R. A. 1941. The physics of blown sand and desert dunes. London: Methuen. *Progress in Physical Geography*, 18, 91-96.
- BAGNOLD, R. A. 1966. An Approach to the sediment transport problem from general physics. *Geological Survey Professional Paper Proc. Roy. Soc. London*, 295, 219.
- BAKER, A. J. 1998. Numerical solution of the equations of fluid dynamics: Finite Element Method. In: JOHNSON, R. W. (ed.) *The handbook of fluid dynamics*. Florida, USA: CRC Press LLC
- Springer-Verlag GmbH & Co. KG.
- BALEVIČIUS, R., SIELAMOWICZ, I., MRÓZ, Z. & KAČIANAUSKAS, R. 2011. Investigation of wall stress and outflow rate in a flat-bottomed bin: A comparison of the DEM model results with the experimental measurements. *Powder Technology*, 214, 322-336.
- BARANAU, V. & TALLAREK, U. 2014. Random-close packing limits for monodisperse and polydisperse hard spheres. *Soft Matter*, 10, 3826-3841.
- BARBOSA-CÁNOVAS, G. V. & JULIANO, P. 2005. Compression and Compaction Characteristics of Selected Food Powders. *Advances in Food and Nutrition Research*. Academic Press.
- BATES, L., DHODAPKAR, S. & KLINZING, G. 2007. Discharge Aids. *SHAPA Technical Bulletin*, 12, 1-34.
- BATHE, K.-J. & WILSON, E. L. 1976. *Numerical methods in finite element analysis*, Englewood Cliffs: Prentice-Hall.
- BATHURST, R. J. & ROTHENBURG, L. 1988. Micromechanical Aspects of Isotropic Granular Assemblies with Linear Contact Interactions. *Journal of Applied Mechanics, ASME*, 55, 17 - 23.

- BAXTER, G. W. Stress distributions in a two dimensional granular material. *In: BEHRINGER, R. P. & JENKINS, J. T., eds. Powders and Grains, 1997 Balkema, Rotterdam. APS, 345 - 348.*
- BEHRINGER, R., HOWELL, D., KONDIC, L., TENNAKOON, S. & VEJE, C. 1999. Predictability and granular materials. *Physica D: Nonlinear Phenomena*, 133, 1-17.
- BELL, T. A. 2001. Solids flowability measurement and interpretation in industry. *In: LEVY, A. & KALMAN, H. (eds.) Handbook of Conveying and Handling of Particulate Solids.*
- BELL, T. A., CATALANO, E. J., ZHONG, Z., OOI, J. Y. & ROTTER, J. M. Evaluation of the Edinburgh powder tester. *Proceedings of PARTEC, 2007. 2-6.*
- BENTZ, D. P., GARBOCZI, E. J., HAECKER, C. J. & JENSEN, O. M. 1999. Effects of cement particle size distribution on performance properties of Portland cement-based materials. *Cement and Concrete Research*, 29, 1663-1671.
- BERNARDIN, A. M. 2009. The influence of particle size distribution on the surface appearance of glazed tiles. *Dyes and Pigments*, 80, 121-124.
- BEVERLOO, W. A., LENIGER, H. A. & VAN DE VELDE, J. 1961. The flow of granular solids through orifices. *Chemical Engineering Science*, 15, 260-269.
- BODHMAGE, A. 2006. *Correlation between physical properties and flowability indicators for fine powders.* Master of Science, University of Saskatchewan.
- BORKOVEC, M., SZILAGYI, I., POPA, I., FINESSI, M., SINHA, P., MARONI, P. & PAPASTAVROU, G. 2012. Investigating forces between charged particles in the presence of oppositely charged polyelectrolytes with the multi-particle colloidal probe technique. *Advances in Colloid and Interface Science*, 179, 85-98.
- BRADLEY, M. 1998. Strategy for selecting the solution, Paper 13. *Hopper and Silo Discharge: Successful Solution.* IMechE.
- BRATBERG, I., MÅLØY, K. & HANSEN, A. Validity of the Janssen law in narrow granular columns. *The European Physical Journal E*, 18, 245-252.

- BREAKSPEAR, S., SMITH, J., NEVELL, T. & TSIBOUKLIS, J. 2004. Friction coefficient mapping using the atomic force microscope. *Surface and interface analysis*, 36, 1330-1334.
- BREITUNG-FAES, S. & KWADE, A. 2011. Production of transparent suspensions by real grinding of fused corundum. *Powder Technology*, 212, 383-389.
- BROWN, R. L. 1961. Minimum energy theorem for flow of dry granular through apertures. *Nature*, 191, 458.
- BRUCKS, A., ARNDT, T., OTTINO, J. M. & LUEPTOW, R. M. 2007. Behavior of flowing granular materials under variable g . *Physical Review E*, 75, 032301.
- BRUCKS, A., RICHTER, L., VINCENT, J. & BLUM, J. Effect of Reduced-Gravity Conditions on the Flowability of Granular Media. In: BINIENDA, K. W., ed. Earth & Space 2008, 2008 California, USA. American Society of Civil Engineers, 1-8.
- BUI, H. H., KOBAYASHI, T., FUKAGAWA, R. & WELLS, J. C. 2009. Numerical and experimental studies of gravity effect on the mechanism of lunar excavations. *Journal of Terramechanics*, 46, 115-124.
- BURNFIELD, J. M. & POWERS, C. M. 2006. Prediction of slips: an evaluation of utilized coefficient of friction and available slip resistance. *Ergonomics*, 49, 982-995.
- BUTT, H.-J., CAPPELLA, B. & KAPPL, M. 2005. Force measurements with the atomic force microscope: Technique, interpretation and applications. *Surface Science Reports*, 59, 1-152.
- BUTT, H.-J. & KAPPL, M. 2009. Normal capillary forces. *Advances in Colloid and Interface Science*, 146, 48-60.
- CAGNOLI, B. & ROMANO, G. P. 2010. Effect of grain size on mobility of dry granular flows of angular rock fragments: An experimental determination. *Journal of Volcanology and Geothermal Research*, 193, 18-24.
- CAI, W., MCDOWELL, G. R. & AIREY, G. D. 2013. Discrete element modelling of uniaxial constant strain rate tests on asphalt mixtures. *Granular matter*, 15, 163-174.

- CAIN, J. 2002. An alternative technique for determining ANSI/CEMA standard 550 flowability ratings for granular materials. *Powder handling and processing*, 14, 218-221.
- CALVERT, G., GHADIRI, M. & TWEEDIE, R. 2009. Aerodynamic dispersion of cohesive powders: A review of understanding and technology. *Advanced Powder Technology*, 20, 4-16.
- CARR 1965. Evaluating flow properties of solids. *Chemical Engineering Journal*, 72, 163-168.
- CARR, J. F. & WALKER, D. M. 1968. An annular shear cell for granular materials. *Powder Technology*, 1, 369-373.
- CARROLL, P. J. & COLIJN, H. 1975. Vibrations in Solids Flow. *Chemical Engineering Progress*, 71, 53-65.
- CARSON, J. W. 2000. *Silo Failures: Case histories and lessons learned* [Online]. Jenike & Johanson, Inc. Available: <http://www.jenike.com/TechPapers/>.
- CAWTHORN, C. J. 2008. *A Constitutive Law for Granular Flows: Predicting the Appearance of Static Zones*. University of Cambridge.
- CHANG, C. S., KABIR, M. & CHANG, Y. 1992. Micromechanics modelling for the stress-strain behaviour of granular soil - II. *Evaluation. J. Geotech. Engrg Div*, 118.
- CHANG, C. S. & LIAO, C. 1989. Constitutive Relations for Particulate Medium with the Effect of Particle Rotation. *International Journal of Solids and Structures*, 26, 437-453.
- CHANG, C. S., MISRA, A., LIANG, R. Y. & BABIC, M. 1997. Mechanics of deformation and flow of particulate materials. In: ODA, M. (ed.) *A micro-deformation model for dilatancy of granular materials*. ASCE.
- CHEN, J.-F., ROTTER, M. J. & OOI, J. Y. 1998. Statistical Inference of Unsymmetrical Silo Pressures from Comprehensive Wall Strain Measurements. *Thin-Walled Structures*, 31, 117-136.
- CHEN, J. F., ROTTER, J. M., OOI, J. Y. & ZHONG, Z. 2005. Flow pattern measurement in a full scale silo containing iron ore. *Chemical Engineering Science*, 60, 3029-3041.

- CHEN, Y., ZHAO, Y., GAO, H. & ZHENG, J. 2011. Liquid bridge force between two unequal-sized spheres or a sphere and a plane. *Particuology*, 9, 374-380.
- CHOI, J., KUDROLLI, A. & BAZANT, M. Z. 2005. Velocity profile of granular flows inside silos and hoppers. *Journal of Physics: Condensed Matter*, 17, S2533.
- CHOI, J., KUDROLLI, A., ROSALES, R. R. & BAZANT, M. Z. 2004. Diffusion and mixing in gravity driven dense granular flow. *Physics Review letters*, 92, 174301.
- CHOU, C. S. & CHEN, R. Y. 2003. The static and dynamic wall stresses in a circulatory two-dimensional wedge hopper. *Advanced Powder Technology*, 14, 195-213.
- CHRISTOFFERSEN, J., MEHRABADI, H. M. & NEMAT-NASSER, S. 1981. A Micromechanical Description of Granular Material Behavior. *Journal of Applied Mechanics, ASME*, 48, 339-344.
- CHUNG, Y.-C. & OOI, J. Y. 2008. A study of influence of gravity on bulk behaviour of particulate solid. *Particuology* [Online], 6. Available: <http://www.sciencedirect.com/science/article/B8JJD-4TY91CT-4/2/a1c1fedcde16b3d590de62d129724740> [Accessed 18-2-2011].
- CLAUDIN, P. & BOUCHAUD, J.-P. 1997. Static Avalanches and Giant Stress Fluctuations in Silos. *Physical Review Letters*, 78, 231-234.
- CLEARLY, P. W. 2004. Large scale industrial modelling. *Engineering computations*, 21 (2-4), 169-204.
- CLEARLY, P. W. & SAWLEY, M. L. 2002. DEM modelling of industrial granular flows: 3D case studies and the effect of particle shape on hopper discharge. *Applied Mathematical Modelling* [Online], 26. Available: www.elsevier.com/locate/apm [Accessed 28-02-2011].
- CLEARY, P. W. & CAMPBELL, C. S. 1993. Self-lubrication for Long Runout Landslides: Examination by computer simulation. *Journal of Geophysical Research: Solid Earth*, 98, 21911-21924.

- COLAPRETE, A., SCHULTZ, P., HELDMANN, J., WOODEN, D., SHIRLEY, M., ENNICO, K., HERMALYN, B., MARSHALL, W., RICCO, A. & ELPHIC, R. C. 2010. Detection of water in the LCROSS ejecta plume. *Science*, 330, 463-468.
- COOPER, B., PAZ, A. & SMITH, M. Preparation and Testing of Ice-Enriched Lunar Regolith Simulant for RESOLVE OVEN. Planetary and Terrestrial Mining Sciences Symposium, 2011 Ottawa, Canada.
- CORWIN, E. I., JAEGER, H. M. & NAGEL, S. R. 2005. Structural signature of jamming in granular media. *Nature*, 435, 1075-1078.
- COULOMB, C. A. 1773. Essai sur une application des règles de maximis et minimis à quelques problèmes de statique, relatifs à l'architecture. *In English translation: Heyman J.*, 7, 343-382.
- COX, G. M. & HILL, J. M. 2005. Some Exact Velocity Profiles For Granular Flow in Converging Hoppers. *Zeitschrift für Angewandte Mathematik und Physik (ZAMP)*, 56, 92-106.
- CRAIG, K., BUCKHOLZ, R. & DOMOTO, G. 1986. An Experimental study of the rapid flow of dry cohesionless metal powders. *ASME J.Appl. Mech*, 53, 935 - 942.
- CRAIG, K., BUCKHOLZ, R. H. & DOMOTO, G. 1987. The effects of shear surface boundaries on stresses for the rapid shear of dry powders. *ASME Journal of Tribology*, 109, 232.
- CREWDSON, B. J., ORMOND, A. L. & NEDDERMAN, R. M. 1977. Air-impeded discharge of fine particles from a hopper. *Powder Technology*, 16, 197-207.
- CROWE, C. T. 2005. *Multiphase Flow Handbook*, CRC Press.
- CUCCOVILLO, T. & COOP, M. 1999. On the mechanics of structured sands. *Geotechnique*, 49, 741-760.
- CUNDALL, P. A. 1971. A computer model for simulating progressive, large-scale movements in blocky rock systems. *Proc. Symp. Int. Soc. Rock Mech*, Nancy 2, No. 8.
- CUNDALL, P. A. 1988. Computer Simulations of Dense Sphere Assemblies. *In: SATAKE, M. & JENKINS, J. T. (eds.) Micromechanics of Granular Materials*. Amsterdam: Elsevier Science Publishers B.V.

- CUNDALL, P. A. & STRACK, O. D. L. 1979. A Discrete Numerical Model for Granular Assemblies. *Geotechnique*, 1, 47-65.
- DABROWSKI, A. 1957. Parcie Materialow Sypkich w Leju (Pressures from Bulk Solids in Hoppers). *Archiwum Inzynierii Ladowej*. Warszawa.
- DALLY, J. W., RILEY, W. F. & KOBAYASHI, A. 1978. Experimental stress analysis. *Journal of Applied Mechanics*, 45, 968.
- DANIEL, J. S. & KIM, Y. R. 2002. Development of a simplified fatigue test and analysis procedure using a viscoelastic, continuum damage model (with discussion). *Journal of the Association of Asphalt Paving Technologists*, 71.
- DATTA, A., MISHRA, B., DAS, S. & SAHU, A. 2008. A DEM analysis of flow characteristics of noncohesive particles in hopper. *Materials and Manufacturing Processes*, 23, 195-202.
- DAVIDSON, J. & NEDDERMAN, R. M. 1973. The hour-glass theory of hopper flow. *Trans. Int. Inst. Chem. Eng.*, 51, 29-35.
- DE-GENNES, P. G. 1999. Granular Matter: A Tentative View. *Rev. Mod. Phys.*, 71, S374 - S382.
- DELANNAY, R., LOUGE, M., RICHARD, P., TABERLET, N. & VALANCE, A. 2007. Towards a theoretical picture of dense granular flows down inclines. *Nat Mater*, 6, 99-108.
- DERESIEWICZ, H. 1958. Stress-Strain Relations for a Simple Model of a Granular Medium. *Journal of Applied Mechanics, Transactions ASME*, 25, 402 -406.
- DERESIEWICZ, H. & MINDLIN, R. D. 1952. *Elastic Spheres in Contact Under Varying Oblique Forces*, Columbia University. Department of Civil Engineering.
- DERJAGUIN, B. V., MULLER, V. M. & TOPOROV, Y. P. 1975. Effect of contact deformations on the adhesion of particles. *Journal of Colloid and Interface Science*, 53, 314-326.
- DIMEMMO, L., HUBERT, M., SARFIELD, B. & SHEKUNOV, B. 2011. Role of Microscopy as the Reference Method for Particle Size Analysis in Drug Development. *Microscopy and Microanalysis*, 17, 1146-1147.

- DING, S., ROTTER, J., OOI, J., ENSTAD, G. & XU, D. 2013. Normal pressures and frictional tractions on shallow conical hopper walls after concentric filling: predictions and experiments. *Chemical Engineering Science*, 89, 264-272.
- DISHMAN, K. L. 2006. Sieving in particle size analysis. *Encyclopedia of Analytical Chemistry*.
- DORBOLO, S., MAQUET, L., BRANDENBOURGER, M., LUDEWIG, F., LUMAY, G., CAPS, H., VANDEWALLE, N., RONDIA, S., MÉLARD, M., VAN LOON, J., DOWSON, A. & VINCENT-BONNIEU, S. 2013. Influence of the gravity on the discharge of a silo. *Granular matter*, 15, 263-273.
- DRESCHER, A. 1992. On the criteria for mass flow in hoppers. *Powder Technology* [Online], 73. [Accessed 15-06-2011].
- DRESCHER, A. & DE JONG, G. D. J. 1972. Photoelastic verification of a mechanical model for the flow of a granular material. *Journal of the Mechanics and Physics of Solids*, 20, 337-340.
- DRESCHER, A., WATERS, A. J. & RHOADES, C. A. 1995. Arching in hoppers: I. Arching theories and bulk material flow properties. *Powder Technology*, 84, 165-176.
- DUFFY, J. & MINDLIN, R. D. 1957. Stress-Strain Relations and Vibrations of a Granular Media. *Journal of Applied Mechanics, Transactions ASME*, X, 585 - 593.
- DUNKIN, J. E. & KIM, D. E. 1996. Measurement of static friction coefficient between flat surfaces. *Wear*, 193, 186-192.
- DURAN, J. 1999. *Sands, Powders, and Grains: An Introduction to the Physics of Granular Materials*, Berlin, Springer.
- DURAN, J., REISINGER, A. & DE GENNES, P. G. 2012. *Sands, Powders, and Grains: An Introduction to the Physics of Granular Materials*, Springer New York.
- EDEM 2012. EDEM Technical Overview. *DEM Solutions*.
- EMERIAULT, F. & CHANGH, C. S. 1997. Interparticle Forces and Displacements in Granular Materials. *Computers and Geotechnics*, 20, 223 - 224.

- ENIOLA-ADEFESO, O. & CHAROENPHOL, P. Effect of Particle Size and Shape In Prescribing the Efficacy of Vascular-Targeted Drug Delivery Vehicles. AICHe 2008 Annual Meeting, 2008.
- ENSTAD, G. 1975. On the theory of arching in mass flow hoppers. *Chemical Engineering Science*, 30, 1273-1283.
- FAMOYE, F. 1995. Continuous Univariate Distributions, Volume 1. *Technometrics*, 37, 466-466.
- FAN, L. S. & ZHU, C. 1998. *Principles of Gas-Solid Flows*, New York, Cambridge University Press.
- FARADAY, M. 1857. The Bakerian Lecture: Experimental Relations of Gold (and Other Metals) to Light. *Philosophical Transactions of the Royal Society of London*, 147, 145-181.
- FELDMAN, W. C., MAURICE, S., BINDER, A. B., BARRACLOUGH, B. L., ELPHIC, R. C. & LAWRENCE, D. J. 1998. Fluxes of Fast and Epithermal Neutrons from Lunar Prospector: Evidence for Water Ice at the Lunar Poles. *Science*, 281, 1496-1500.
- FENISTEIN, D., VAN DE MEENT, J. W. & VAN HECKE, M. 2004. Universal and wide shear zones in granular bulk flow. *Physical Review Letters*, 92, 094301.
- FIGUEROA, I., LI, H. & MCCARTHY, J. 2009. Predicting the impact of adhesive forces on particle mixing and segregation. *Powder Technology*, 195, 203-212.
- FORTERRE, Y. & POULIQUEN, O. 2006. Granular Flows. In: DAMOUR, T. (ed.) *Séminaire Poincaré IX*. CNRS-Université de Provence.
- FRANKLIN, S. V. & SHATTUCK, M. D. 2015. *Handbook of Granular Materials*, Taylor & Francis.
- FRANZEN, M. A., ROE, L. A., BUFFINGTON, J. A. & SEARS, D. W. G. 2008. A sample collector for robotic sample return missions I: Temperature effect on collected mass. *Advances in Space Research*, 42, 20-24.
- FREEMAN, R. & FU, X. W. The Development of a Compact Uniaxial Tester. Particulate Science Analysis, 2011 Edinburgh, UK. 1-6.

- FRISCH, B. 1989. Characterization of Powder and Pressings Based on Geometric Fundamentals. *Particle & Particle Systems Characterization*, 6, 39-47.
- FU, S.-Y., FENG, X.-Q., LAUKE, B. & MAI, Y.-W. 2008. Effects of particle size, particle/matrix interface adhesion and particle loading on mechanical properties of particulate–polymer composites. *Composites Part B: Engineering*, 39, 933-961.
- GALLEGO, E., GONZÁLEZ-MONTELLANO, C., RAMÍREZ, A. & AYUGA, F. 2011. A simplified analytical procedure for assessing the worst patch load location on circular steel silos with corrugated walls. *Engineering Structures*, 33, 1940-1954.
- GANESAN, V., ROSENTRATER, K. A. & MUTHUKUMARAPPAN, K. 2008. Flowability and handling characteristics of bulk solids and powders – a review with implications for DDGS. *Biosystems Engineering*, 101, 425-435.
- GARCIMARTIN, A., MANKOC, C., JANDA, A., AREVALO, R., PASTOR, J. M., ZURIGUEL, I. & MAZA, D. 2007. Flow and Jamming of Granular Matter through an Orifice. *Eur. Phys. J. Special Topics*, 143, 191.
- GEIGER, D., WANDSTRAT, M. & MORT, P. Granular flow through an orifice – effect of granule properties on the onset of jamming. Proceedings of AIChE Annual Meeting, 2007 Salt Lake City. Procter and Gamble Co.
- GENG, J., LONGHI, E., BEHRINGER, R. P. & HOWELL, D. W. 2001. Memory in two-dimensional heap experiments. *Physical Review E*, 64, 060301.
- GERTSCH, L., GUSTAFSON, R. & GERTSCH, R. Effect Of Water Ice Content on the Excavatability of Lunar Regolith. In: EL-GENK, M. S., ed. Space Technology and Applications International Forum (STAIF), 2006. American Institute of Physics.
- GONZÁLEZ-MONTELLANO, C., AYUGA, F. & OOI, J. Y. 2011. Discrete element modelling of grain flow in a planar silo: influence of simulation parameters. *Granular matter*, 13, 149-158.
- GONZÁLEZ-MONTELLANO, C., GALLEGO, E., RAMÍREZ-GÓMEZ, Á. & AYUGA, F. 2012. Three dimensional discrete element models for simulating the filling and emptying of silos: Analysis of numerical results. *Computers & Chemical Engineering*, 40, 22-32.

- GOODEY, R. J., BROWN, C. J. & ROTTER, J. M. 2006. Predicted patterns of filling pressures in thin-walled square silos. *Engineering Structures*, 28, 109-119.
- GOODMAN, M. A. & COWIN, S. C. 1971. Two problems in the gravity flow of granular materials. *Journal of fluid mechanics*, 45, 487.
- GOODMAN, M. A. & COWIN, S. C. 1972. A continuum theory for granular materials. *Archive for Rational Mechanics and Analysis*, 44, 249-266.
- GOSENS, I., POST, J. A., DE LA FONTEYNE, L., JANSEN, E., GEUS, J. W., CASSEE, F. R. & DE JONG, W. H. 2010. Impact of agglomeration state of nano-and submicron sized gold particles on pulmonary inflammation.
- GRIFFITH, E. J. 1991. *Cake formation in Particulate Systems*, New York, VCH Publishers.
- GUO, J., ROBERTS, A. W. & PRIGGE, J. D. 2012. Investigation of Arch Model Acting in Mass-Flow Hoppers. *Advanced Materials Research*, 508, 135 - 140.
- GUO, P. & ZHOU, S. 2013. Arch in granular materials as a free surface problem. *International Journal for Numerical and Analytical Methods in Geomechanics*, 37, 1048-1065.
- GUPTA, A. K. 1959. Particle size analysis by sedimentation in a long-arm centrifuge. *Journal of Applied Chemistry*, 9, 487-489.
- GÜTTLER, C., VON BORSTEL, I., SCHRÄPLER, R. & BLUM, J. 2013. Granular convection and the Brazil nut effect in reduced gravity. *Physical Review E*, 87, 044201.
- HAGEN, G. 1852. Druck und Bewegung des Trockenem Sandes. *Berliner Monatsberichte, Akademie der Wissenschaften*, 35 - 42.
- HALEBLIAN, J. K. 1975. Characterization of habits and crystalline modification of solids and their pharmaceutical applications. *Journal of Pharmaceutical Sciences*, 64, 1269-1288.
- HAMAKER, H. C. 1937. The London - van der Waals attraction between spherical particles. *Physica*, 4, 1058-1072.
- HAQUE, E. 2013. Estimating bulk density of compacted grains in storage bins and modifications of Janssen's load equations as affected by bulk density. *Food Science & Nutrition*, 1, 150-156.

- HARE, C., GHADIRI, M. & DENNEHY, R. 2011. Prediction of attrition in agitated particle beds. *Chemical Engineering Science*, 66, 4757-4770.
- HART, A. 2015. Effect of Particle Size on Detergent Powders Flowability and Tabletability. *Journal of Chemical Engineering & Process Technology*, 6, 1.
- HART, R., CUNDALL, P. A. & LEMOS, J. 1988. Formulation of a three-dimensional distinct element model—Part II. Mechanical calculations for motion and interaction of a system composed of many polyhedral blocks. *International Journal of Rock Mechanics and Mining Sciences & Geomechanics Abstracts*, 25, 117-125.
- HAUSSLER, U. & EIBL, J. 1984. Numerical Investigations on Discharging Silos. *Journal of Engineering Mechanics*, 110, 957-971.
- HEGDE, U., BALASUBRAMANIAM, R. & GOKOGLU, S. A. 2012. *Analysis of Water Extraction from Lunar Regolith*, National Aeronautics and Space Administration, Glenn Research Center.
- HESLOT, F., BAUMBERGER, T., PERRIN, B., CAROLI, B. & CAROLI, C. 1994. Creep, stick-slip, and dry-friction dynamics: Experiments and a heuristic model. *Physical Review E*, 49, 4973-4988.
- HIHINASHVILI, R. & BLUMENFELD, R. Structural Characterization of Porous and Granular Materials. IOR 2011, 2011.
- HILAL, N., JOHNSON, D., BOWEN, W. R. & WILLIAMS, P. M. 2009. Chapter 2 - Measurement of Particle and Surface Interactions Using Force Microscopy. In: BOWEN, W. R. & HILAL, N. (eds.) *Atomic Force Microscopy in Process Engineering*. Oxford: Butterworth-Heinemann.
- HILL, J. M. & WU, Y. H. 1991. Kinematically determined axially symmetric plastic flows of metals and granular materials. *Quart J. Mech Appl Math*, 85, 51-69.
- HILTON, J. E. & CLEARY, P. W. 2011. Granular flow during hopper discharge. *Physical Review E*, 84, 011307.

- HIRSHFELD, D. & RAPAPORT, D. C. 2001. Granular flow from a silo: Discrete-particle simulations in three dimensions. *The European Physical Journal E*, 4, 193-199.
- HOFMANN, P., RICHTER, L., MUHLBAUER, Q., SCHULTE, W. & PAUL, R. 2013. The ExoMars Sample Handling and Distribution Subsystem and Instruments under Developments. In: KAYSER-THREDE (ed.) *64th IAC*. Beijing.
- HOFMEISTER, P. G., BLUM, J. & HEIßELMANN, D. 2009. The Flow Of Granular Matter Under Reduced-Gravity Conditions. *TU Braunschweig, Institut für Geophysik und extraterrestrische Physik, Mendelssohnstr, 3*.
- HOLLENBACH, A. M., PELEG, M. & RUFNER, R. 1983. Interparticle surface affinity and the bulk properties of conditioned powders. *Powder Technology*, 35, 51-62.
- HOPKINS, M., JENKINS, J. T. & LOUGE, M. 1991. On the structure of 3D shear flows. *Advances in Micromechanics of Granular Materials, Studies in Applied Mechanics*, 31, 271 - 279.
- HORIBA 2014. A Guidebook to Particle Size Analysis. In: INC, H. I. (ed.). Irvine, USA: Horiba Instruments Inc.
- HOWELL, D., BEHRINGER, R. P. & VEJE, C. 1999. Stress Fluctuations in a 2D Granular Couette Experiment: A Continuous Transition. *Physical Review Letters*, 82, 5241-5244.
- HU, L., ZHANG, Z., XIE, S., LIU, S. & XU, L. 2009. Effect of grain size of zeolite Y on its catalytic performance in olefin alkylation thiophenic sulfur process. *Catalysis Communications*, 10, 900-904.
- HUNT, M. L., WEATHERS, R. C., LEE, A. T., BRENNEN, C. E. & WASSGREN, C. R. 1999. Effects of horizontal vibration on hopper flows of granular materials. *Physics of Fluids (1994-present)*, 11, 68-75.
- HUTTER, K. & JÖHNK, K. 2013. *Continuum Methods of Physical Modeling: Continuum Mechanics, Dimensional Analysis, Turbulence*, Springer Berlin Heidelberg.
- HYODO, M., MURATA, H. & NAKATA, Y. 2006. *Geomechanics and Geotechnics of Particulate Media: Proceedings of the International Symposium on Geomechanics and Geotechnics of Particulate Media, Ube, Japan, 12-14 September 2006*, Taylor & Francis.

- ILELEJI, K. E. & ZHOU, B. 2008. The angle of repose of bulk corn stover particles. *Powder Technology*, 187, 110-118.
- IQBAL, T. & FITZPATRICK, J. J. 2006. Effect of storage conditions on the wall friction characteristics of three food powders. *Journal of Food Engineering*, 72, 273-280.
- ITASCA 2004. *ITASCA Manual - UDEC (Universal Distinct Element Code)*, Minneapolis, ICG.
- IZUMI, I., NAKAMURA, T. & SACK, R. L. 1997. *Snow Engineering: Recent Advances: Proceedings of the third international conference, Sendai, Japan, 26-31 May 1996*, Taylor & Francis.
- JAEGER, H., NAGEL, S. & BEHRINGER, R. 1996a. Granular solids, liquids, and gases. *Rev. Mod. Phys.*, 68, 1259-1262.
- JAEGER, H. M. & NAGEL, S. R. 1992. Physics of the granular state. *Science*, 255, 1523 - 1531.
- JAEGER, H. M., NAGEL, S. R. & BEHRINGER, R. P. 1996b. The Physics of Granular Materials. *Physics Today*, 49, 32-38.
- JAEGER, J. 2005. *New solutions in contact mechanics*, Wit Pr/Computational Mechanics.
- JANSSEN, H. A. 1895. Getreidedruck in Silozellen. *Ztg. Ver. dt. Ing.*, 39, 1045-1049 [in German].
- JENIKE, A., JOHANSON, J. & CARSON, J. 1973. Bin loads—Part 2: concepts. *Journal of Manufacturing Science and Engineering*, 95, 1-5.
- JENIKE, A. W. 1961. Gravity flow of bulk solids. Salt lake City: University of Utah.
- JENIKE, A. W. 1964a. Steady gravity flow of frictional cohesive solids in converging channels. *ASME J.Appl. Mech.*, 31, 5.
- JENIKE, A. W. 1964b. Storage and flow of Solids. *Utah Engineering Experimental Station, University of Utah*, Bulletin 123.
- JENIKE, A. W. & JOHANSON, J. 1969. On the theory of bin loads. *Journal of Manufacturing Science and Engineering*, 91, 339-344.
- JENKINS, J. & RICHMAN, M. W. 1985. Kinetic theory for plane flows of a dense gas of identical, rough, inelastic, circular disks. *Physics of Fluids*, 28, 3485-3495.

- JENKINS, J. & SAVAGE, S. 1983. A theory for the rapid flow of identical, smooth, nearly elastic, spherical particles. *Journal of Fluid Mechanics*, 130, 187-202.
- JENKINS, J. T. 1987a. *Rapid Flows of Granular Materials*
Non-Classical Continuum Mechanics, Cambridge University Press.
- JENKINS, J. T. 1987b. Volume Change in Small Strain Axisymmetric Deformations of a Granular Material. In: SATAKE, M. & JENKINS, J. T. (eds.) *Micromechanics of Granular Materials*. Elsevier, Amsterdam.
- JIAN, G., FU, Q. & ZHOU, D. 2012. Particles size effects of single domain CoFe₂O₄ on suspensions stability. *Journal of Magnetism and Magnetic Materials*, 324, 671-676.
- JIAN, N., OTTINO, J. M. & LUEPTOW, R. M. 2002. An experimental study of the flowing granular layer in a rotating tumbler. *Physics of Fluids*, 14.
- JOEKAR NIASAR, V., HASSANIZADEH, S. M., PYRAK-NOLTE, L. J. & BERENTSEN, C. 2009. Simulating drainage and imbibition experiments in a high-porosity micromodel using an unstructured pore network model. *Water Resources Research*, 45, n/a-n/a.
- JOHANSON, J. 1995. Flow indices in the prediction of powder behaviour. *Pharmaceutical Manufacturing International*, 159-164.
- JOHANSON, J. R. & JENIKE, A. W. 1962. Stress and Velocity fields in gravity flow of bulk solids. USA: Univeristy of Uttah Engineering Experiment Station.
- JOHNSON, D., HILAL, N. & BOWEN, W. R. 2009. Chapter 1 - Basic Principles of Atomic Force Microscopy. In: BOWEN, W. R. & HILAL, N. (eds.) *Atomic Force Microscopy in Process Engineering*. Oxford: Butterworth-Heinemann.
- JOHNSON, J. B. & HOPKINS, M. A. 2005. Identifying microstructural deformation mechanisms in snow using discrete-element modeling. *Journal of Glaciology*, 51, 432-442.
- JOHNSON, K. L., KENDALL, K. & ROBERTS, A. D. 1971. *Surface Energy and the Contact of Elastic Solids*.
- JOHNSON, R. W. 1998. *The Handbook of Fluid Dynamics*, Springer Berlin Heidelberg.

- JOHNSON, S. W., PYRZ, A. P. & LEE, D. G. 1970. Simulating the effect of gravitational field and atmosphere on behaviour of granular media. *J. Spacecraft*, 7, 1311-1317.
- JULIANO, P. & BARBOSA-CÁNOVAS, G. V. 2010. Food Powders Flowability Characterization: Theory, Methods, and Applications. *Annual Review of Food Science and Technology*, 1, 211-239.
- KACHANOV, M. 1980. Continuum model of medium with cracks. *J. Engng Mech Div.*, 106 (EM5).
- KADANOFF, L. P. 1999. Built Upon Sand: Theoretical Ideas inspired by Granular Flows. *Rev. Mod. Phys. B*, 71, 435 - 444.
- KALSON, P. A. & RESNICK, W. 1985. Angles of Repose and Drainage for Granular materials in a Wedge-Shaped Hopper. *Powder Technology* [Online], 43. [Accessed 16-06-2011].
- KAMATH, S. & PURI, V. M. 1999. Finite element model development and validation for incipient flow analysis of cohesive powders from hopper bins. *Powder Technology*, 102, 184-193.
- KAMRIN, K. & BAZANT, M. Z. 2007. Stochastic flow rule for granular materials. *Physical Review E*, 75, 041301.
- KANDALA, R. N. & PURI, V. M. 2000. MEASUREMENT OF COHESION AND ANGLE OF INTERNAL FRICTION USING CUBICAL TRIAXIAL TESTER AND COMPARISON WITH COMPUTER CONTROLLED SHEAR CELL. *Particulate Science and Technology*, 18, 71-88.
- KAYE, B. H., GRATTON-LIIMATAINEN, J. & FADDIS, N. 1995. Studying the Avalanching Behaviour of a Powder in a Rotating Disc. *Particle & Particle Systems Characterization*, 12, 232-236.
- KETTERHAGEN, W. R., AM ENDE, M. T. & HANCOCK, B. C. 2009a. Process modeling in the pharmaceutical industry using the discrete element method. *Journal of Pharmaceutical Sciences*, 98, 442-470.

- KETTERHAGEN, W. R., CURTIS, J. S., WASSGREN, C. R. & HANCOCK, B. C. 2009b. Predicting the flow mode from hoppers using the discrete element method. *Powder Technology*, 195, 1-10.
- KIRYA, R. V. 2009. The Description of process of flow out of granular material from tank by structural-mechanical models. *System technology*, 3, 3-19 (in Russian).
- KISHINO, Y. 2001. *Powder and Grains 2001*, Taylor & Francis.
- KLEIN, S. P. & WHITE, B. R. 1990. Dynamic shear of granular material under variable gravity conditions. *American Institute of Aeronautics and Astronautics journal*, 28, 1701-1702.
- KLEINHANS, M. G., MARKIES, H., DE VET, S. J., IN 'T VELD, A. C. & POSTEMA, F. N. 2011. Static and dynamic angles of repose in loose granular materials under reduced gravity. *Journal of Geophysical Research: Planets*, 116, E11.
- KLINZING, G. E., RIZK, F., MARCUS, R. & LEUNG, L. S. 2013. *Pneumatic Conveying of Solids: A theoretical and practical approach*, Springer Netherlands.
- KOJIMA, T. & ELLIOTT, J. A. 2012. Incipient flow properties of two-component fine powder systems and their relationships with bulk density and particle contacts. *Powder Technology*, 228, 359-370.
- KOLLMANN, T. H. & TOMAS, J. 2002. Effect of Applied Vibration on Silo Hopper Design. *Particulate Science and Technology*, 20, 15-31.
- KOZICKI, J. & DONZÉ, F. V. 2008. A new open-source software developed for numerical simulations using discrete modeling methods. *Computer Methods in Applied Mechanics and Engineering*, 197, 4429-4443.
- KRUGGEL-EMDEN, H., RICKELT, S., WIRTZ, S. & SCHERER, V. 2008. A study on the validity of the multi-sphere Discrete Element Method. *Powder Technology*, 188, 153-165.
- KRUGGEL-EMDEN, H., STEPANEK, F. & MUNJIZA, A. 2010. A study on adjusted contact force laws for accelerated large scale discrete element simulations. *Particuology*, 8, 161-175.
- KRUPP, H. 1967. *Particle adhesion theory and experiment*, Amsterdam, Elsevier.

- KRUYT, N. P. & ANTONY, S. J. 2007. Force, relative-displacement, and work networks in granular materials subjected to quasistatic deformation. *Physical Review E*, 75, 051308.
- KUHN, M. R. 2003. Heterogeneity and patterning in the quasi-static behavior of granular materials. *Granular matter*, 4, 155-166.
- KUHN, M. R. & ANTONY, J. 2004. Rate of Stress in Dense Unbonded Frictional Materials During Slow Loading. In: ANTONY, S. J., HOYLE, W. & DING, Y. (eds.) *Granular Materials - Fundamentals and Applications*. Leeds: The Royal Society of Chemistry.
- KUILA, U., MCCARTY, D. K., DERKOWSKI, A., FISCHER, T. B. & PRASAD, M. 2014. Total porosity measurement in gas shales by the water immersion porosimetry (WIP) method. *Fuel*, 117, Part B, 1115-1129.
- KULKARNI, M. C. & OCHOA, O. O. 2012. Mechanics of light weight proppants: A discrete approach. *Composites Science and Technology*, 72, 879-885.
- KULKARNI, P., BERRY, R. & BRADLEY, M. 2010. Review of the flowability measuring techniques for powder metallurgy industry. *Proceedings of the Institution of Mechanical Engineers, Part E: Journal of Process Mechanical Engineering*, 224, 159-168.
- KURZ, H. P. & RUMPF, H. 1975. Flow processes in aerated silos. *Powder Technology*, 11, 147-156.
- LAMARCHE, K. R., MUZZIO, F. J., SHINBROT, T. & GLASSER, B. J. 2010. Granular flow and dielectrophoresis: The effect of electrostatic forces on adhesion and flow of dielectric granular materials. *Powder Technology*, 199, 180-188.
- LAMBERT, C. & COLL, C. 2014. Discrete modeling of rock joints with a smooth-joint contact model. *Journal of Rock Mechanics and Geotechnical Engineering*, 6, 1-12.
- LANDRY, J. 2004. Granular packing and Hopper flow. *American Physical Society*.
- LANDRY, J. W., GREY, G. S. & PLIMPTON, S. J. 2004. Discrete element simulations of stress distributions in silos: crossover from two to three dimensions. *Powder Technology*, 139, 233-239.

- LANGSTON, P. A., AL-AWAMLEH, M. A., FRAIGE, F. Y. & ASMAR, B. N. 2004. Distinct element modelling of non-spherical frictionless particle flow. *Chemical Engineering Science* [Online], 59. Available: www.elsevier.com/locate/ces [Accessed 15-06-2011].
- LANGSTON, P. A., TUZUN, U. & HEYES, D. M. 1995. Discrete element simulation of internal stress and flow fields in funnel flow hoppers. *Powder Technology* [Online], 85. [Accessed 15-06-2011].
- LAYMAN, J. M. 2004. *Porosity Characterization Utilizing Petrographic Image Analysis: Implications for Identifying and Ranking Reservoir Flow Units, Happy Spraberry Field, Garza County, Texas*. Texas A&M University.
- LE PENNEC, T., AMMI, M., MESSENGER, J. C., TRUFFIN, B., BIDEAU, D. & GARNIER, J. 1995. Effect of gravity on mass flow rate in an hour glass. *Powder Technology*, 85, 279-281.
- LI, J., LANGSTON, P. A., WEBB, C. & DYAKOWSKI, T. 2004. Flow of sphero-disc particles in rectangular hoppers—a DEM and experimental comparison in 3D. *Chemical Engineering Science*, 59, 5917-5929.
- LI, X. & YU, H.-S. 2010. Numerical investigation of granular material behaviour under rotational shear. *Geotechnique*, 60, 381-394.
- LI, X., YU, H. S. & LI, X. S. 2009. Macro–micro relations in granular mechanics. *International Journal of Solids and Structures*, 46, 4331-4341.
- LIAO, C.-L., CHANG, T.-P., YOUNG, D.-H. & CHANG, C. S. 1997. Stress-Strain Relationship for Granular Materials Based on the Hypothesis of Best Fit. 34. [Accessed 20/03/2011].
- LINDBERG, N. O., PALSSON, M., PHIL, A. C., FREEMAN, T., ZETZENER, H. & ENSTAD, G. 2004. Flowability measurements of pharmaceutical powder mixtures with poor flow using five different techniques. *Drug. Dev. Ind. Pharm*, 30, 785-791.
- LIU, C.-H., NAGEL, S. R., SCHECTER, D. A., COPPERSMITH, S. N., MAJUMDAR, S., NARAYAN, O. & WITTEN, T. A. 1995. Force Fluctuations in Bead Packs. *Science*, 269, 513-515.

- LIU, L. X., MARZIANO, I., BENTHAM, A. C., LITSTER, J. D., E.T.WHITE & HOWES, T. 2008. Effect of particle properties on the flowability of ibuprofen powders. *International Journal of Pharmaceutics*, 362, 109-117.
- LIU, Y., LI, G.-H. & JIANG, L.-X. 2010. Hydrodynamic behavior of dense gas-particle flows under the reduced gravity conditions. *Acta Astronautica*, 67, 417-423.
- LIU, Y. & LI, G. 2010. Numerical prediction of particle dispersions in downer under different gravity environments. *Chemical Engineering Journal*, 158, 281-289.
- LUEPTOW, R. M., AKONUR, A. & SHINBROT, T. 2000. PIV for granular flows. *Experiments in Fluids*, 28, 183-186.
- LUMAY, G., BOSCHINI, F., TRAINA, K., BONTEMPI, S., REMY, J. C., CLOOTS, R. & VANDEWALLE, N. 2012. Measuring the flowing properties of powders and grains. *Powder Technology*, 224, 19-27.
- LUMAY, G., DORBOLO, S. & VANDEWALLE, N. 2009. Compaction dynamics of a magnetized powder. *Physical Review E*, 80, 041302.
- MAIA, N. 2009. Reflections on the hysteretic damping model. *Shock and Vibration*, 16, 529-542.
- MAJMUDAR, T. S. & BEHRINGER, R. P. 2005. Contact force measurements and stress-induced anisotropy in granular materials. *Nature*, 435, 1079-1082.
- MAJMUDAR, T. S., SPERL, M., LUDING, S. & BEHRINGER, R. P. 2007. Jamming Transition in Granular Systems. *Physical Review Letters*, 98, 058001.
- MALONE, K. F. & XU, B. H. 2008. Determination of contact parameters for discrete element method simulations of granular systems. *Particuology*, 6, 521-528.
- MANGENEY, A., ROCHE, O., HUNGR, O., MANGOLD, N., FACCANONI, G. & LUCAS, A. 2010. Erosion and mobility in granular collapse over sloping beds. *Journal of Geophysical Research: Earth Surface*, 115, F3.
- MANKOC, C., JANDA, A., ARÉVALO, R., PASTOR, J. M., ZURIGUEL, I., GARCIMARTÍN, A. & MAZA, D. 2007. The flow rate of granular materials through an orifice. *Granular matter*, 9, 407-414.

- MANTOVANI, J. G., SWANGER, A., TOWNSEND III, I. I., SIBILLE, L. & GALLOWAY, G. 2014. Characterizing the Physical and Thermal Properties of Planetary Regolith at Low Temperatures. *ACE International Conference on Engineering Science, Construction and Operations in Challenging Environments*. St. Louis, USA.
- MARINELLI, J. 2014. Overcoming Solids Caking with Flow Aids. *Solids Handling Technologies Inc. Chemical Engineering*.
- MARKOWICH, P. 2007. *Applied Partial Differential Equations:: A Visual Approach*, Springer Berlin Heidelberg.
- MARRI, A., WANATOWSKI, D. & YU, H. S. 2012. Drained behaviour of cemented sand in high pressure triaxial compression tests. *Geomechanics and Geoengineering*, 7, 159-174.
- MARTÍNEZ, M. A., ALFARO, I. & DOBLARÉ, M. 2002. Simulation of axisymmetric discharging in metallic silos. Analysis of the induced pressure distribution and comparison with different standards. *Engineering Structures*, 24, 1561-1574.
- MASSOUDI, M. 2004. Constitutive modelling of flowing granular materials: a continuum approach. *Granular Materials: Fundamentals and Applications*, 63.
- MATCHETT, A. J. 2004. A theoretical model of vibrationally induced flow in a conical hopper system. *Chemical Engineering Research and Design*, 82, 85-98.
- MATHER, I. 1998. External vibrators, Paper 2. *Hopper and Silo Discharge: Successful Solutions, Paper 2*. IMechE.
- MATSUOKA, H. & SUN, D. A. 1995. Extension of spatially mobilized plane (SMP) to frictional and cohesive materials and its application to cemented sands. *Soils & Foundations*, 35(4).
- MATUTTIS, H. G., LUDING, S. & HERRMANN, H. J. 2000. Discrete element simulations of dense packings and heaps made of spherical and non-spherical particles. *Powder Technology*, 109, 278-292.
- MAUGIS, D. & POLLOCK, H. 1984. Surface forces, deformation and adherence at metal microcontacts. *Acta Metallurgica*, 32, 1323-1334.

- MAYNARD, E. 2013. Ten Steps to an Effective Bin Design. *Chemical Engineering Progress*, 109, 25-32.
- MAZUMDER, B., RAJAN, R., KHANAM, J. & NANDA, A. 2008. Flow of Formulation Granules through a Conical Hopper. *Indian Journal of Pharmaceutical Sciences*, 70, 816-821.
- MCGLINCHEY, D. (ed.) 2005. *Characterisation of Bulk Solids*, Oxford: Blackwell Publishing Ltd.
- MCKAY, D. S., HEIKEN, G., BASU, A., BLANFORD, G., SIMON, S., REEDY, R., FRENCH, B. M. & PAPIKE, J. 1991. The lunar regolith. *Lunar Sourcebook*, 285-356.
- MCKAY, S. D. & BLACIC, D. J. 1991. Workshop on Production and Uses of Simulated Lunar Materials. *A Lunar and Planetary Institute Workshop, sponsored by NASA Johnson Space Center*. The Lunar and Planetary Institute, in Houston, Texas: Lunar and Planetary Institute, 3303 NASA Road 1, Houston, TX 77058.
- MEDINA, A., CORDOVA, J. A., LUNA, E. & TREVINO, C. 1998. Velocity field measurements in granular gravity flow in a near 2D silo. *Phys. Lett. A*, 220, 111-116.
- MEGIAS-ALGUACIL, D. & GAUCKLER, L. J. 2009. Capillary forces between two solid spheres linked by a concave liquid bridge: Regions of existence and forces mapping. *AIChE Journal*, 55, 1103-1109.
- MENARDO, S., AIROLDI, G. & BALSARI, P. 2012. The effect of particle size and thermal pre-treatment on the methane yield of four agricultural by-products. *Bioresource technology*, 104, 708-714.
- MERKUS, H. 2014. Pigments and Paint Dispersions. *In: MERKUS, H. G. & MEESTERS, G. M. H. (eds.) Particulate Products*. Springer International Publishing.
- MERROW, E. W. 1988. Estimating startup times for solids-processing plants. *Chem. Eng. Prog.*, 89(10):89.
- METZGER, P. T., GALLOWAY, G. M., MANTOVANI, J. G., ZACNY, K. & CRAFT, J. 2011. Low Force Icy Regolith Penetration Technology. NASA, NASA/TM - 2011-216302.

- MEYER, C. 2003. Lunar Regolith. *NASA Lunar Petrographic Educational Thin Section Set*, 46.
- MIDI, G. D. R. 2004. On Dense Granular Flows. *Groupement De Recherche Milieux Divis'és*.
- MINIFIE, B. 2012. *Chocolate, Cocoa and Confectionery: Science and Technology*, Springer Netherlands.
- MIO, H., AKASHI, M., SHIMOSAKA, A., SHIRAKAWA, Y., HIDAKA, J. & MATSUZAKI, S. 2009. Speed-up of computing time for numerical analysis of particle charging process by using discrete element method. *Chemical Engineering Science*, 64, 1019-1026.
- MIRONOV, V. L. 2004. Fundamentals of scanning probe microscopy. *Moscow: Technosfera*, 144.
- MITROFANOV, I., SANIN, A., BOYNTON, W., CHIN, G., GARVIN, J., GOLOVIN, D., EVANS, L., HARSHMAN, K., KOZYREV, A. & LITVAK, M. 2010. Hydrogen mapping of the lunar south pole using the LRO neutron detector experiment LEND. *Science*, 330, 483-486.
- MOLLON, G. & ZHAO, J. 2013. The influence of particle shape on granular Hopper flow. *AIP Conference Proceedings*, 1542, 690-693.
- MOREEA, S. B. M. & NEDDERMAN, R. M. 1996. Exact stress and velocity distributions in a cohesionless material discharging from a conical hopper. *Chemical Engineering Science*, 51, 3931-3942.
- MORENO-ATANASIO, R., ANTONY, J. & GHADIRI, M. 2004. Analysis of the effect of cohesion and gravity on the bulk behaviour of powders using Distinct Element Method. PARTECH 2004, International Congress for Particle Technology, 16 - 18 March, 2004 2004 Nuremberg, Germany. White Rose Consortium ePrints Repository.
- MUETH, D. M. 2003. Measurements of particle dynamics in slow, dense granular Couette flow. *Physical Review E*, 67, 011304.
- MUETH, D. M., DEBREGES, G. F., KARZMAR, G. S., ENG, P. J., NAGEL, S. R. & JAEGER, H. M. 2000. Signatures of granular microstructure in dense shear flows. *Nature*, 406, 385-389.

- MUETH, D. M., JAEGER, H. M. & NAGEL, S. R. 1998. Force distribution in a granular medium. *Physical Review E*, 57, 3164-3169.
- MULLARNEY, M. P. & LEYVA, N. 2009. Modeling pharmaceutical powder-flow performance using particle-size distribution data. *Pharmaceutical Technology*, 33, 126-134.
- MUNJIZA, A. 2004. *The combined finite-discrete element methods*, Chichester, Wiley Online Library.
- MURTHY, T. G., GNANAMANICKAM, E. & CHANDRASEKAR, S. 2012. Deformation field in indentation of a granular ensemble. *Physical Review E*, 85, 061306.
- MWAIKAMBO, L. & ANSELL, M. 2001. The determination of porosity and cellulose content of plant fibers by density methods. *Journal of materials science letters*, 20, 2095-2096.
- NAKASHIMA, H., SHIOJI, Y., KOBAYASHI, T., AOKI, S., SHIMIZU, H., MIYASAKA, J. & OHDOI, K. 2011. Determining the angle of repose of sand under low-gravity conditions using discrete element method. *Journal of Terramechanics* [Online], 48. Available: www.elsevier.com/locate/jterra.
- NASATO, D. S., GONIVA, C., PIRKER, S. & KLOSS, C. 2015. Coarse Graining for Large-scale DEM Simulations of Particle Flow – An Investigation on Contact and Cohesion Models. *Procedia Engineering*, 102, 1484-1490.
- NASUNO, S., KUDROLLI, A. & GOLLUB, J. P. 1997. Friction in Granular Layers: Hysteresis and Precursors. *Physical Review Letters*, 79, 949-952.
- NEDDERMAN, R. M. 1992. *Statics and Kinematics of Granular materials*, Oxford, UK, Cambridge Univ Press.
- NEDDERMAN, R. M. & TÜZÜN, U. 1979. A kinematic model for the flow of granular materials. *Powder Technology*, 22, 243-253.
- NEDDERMAN, R. M., TÜZÜN, U., SAVAGE, S. B. & HOULSBY, G. T. 1982. The flow of granular materials—I: Discharge rates from hoppers. *Chemical Engineering Science*, 37, 1597-1609.

- NGUYEN, T. K., COMBE, G., CAILLERIE, D. & DESRUES, J. 2014. FEM \times DEM modelling of cohesive granular materials: Numerical homogenisation and multi-scale simulations. *Acta Geophysica*, 62, 1109-1126.
- NGUYEN, T. V., BRENNEN, C. E. & SABERSKY, R. H. 1980. Funnel flow in hoppers. *Journal of Applied Mechanics, American society of mechanical engineers*, 47, 729-735.
- NOLLET, L. M. L. 2004. *Handbook of Food Analysis: Methods and instruments in applied food analysis*, CRC PRESS.
- NOSEWICZ, S., ROJEK, J., PIETRZAK, K. & CHMIELEWSKI, M. 2013. Viscoelastic discrete element model of powder sintering. *Powder Technology*, 246, 157-168.
- ODA, M. & IWASHITA, K. 1999. *An introduction to Mechanics of granular materials*, Rotterdam, A. A. Balkema.
- OKA, H., TAMURA, T., MIURA, Y. & TEKI, Y. 1999. Synthesis and Characterization of Poly(1,3-phenylene)-Based Polyradical Carrying Cyclic Nitroxides. Observation of Ferromagnetic Interaction. *Polym J*, 31, 979-982.
- ONWULATA, C. 2005. *Encapsulated and Powdered Foods*, CRC Press.
- OOI, J. Y., CHEN, J.-F., LOHNES, R. A. & ROTTER, M. J. 1996. Prediction of Static Wall Pressures in Coal Silos. *Construction and Building Materials*, 10, 109-116.
- PARKER, E. G. & O'BRIEN, J. F. Real-time deformation and fracture in a game environment. Proceedings of the 2009 ACM SIGGRAPH/Eurographics Symposium on Computer Animation, 2009. ACM, 165-175.
- PATTERSON, E. A. 1988. Automated photoelastic analysis. *Strain*, 24, 15-20.
- PENG, H.-H., LIN, C.-K. & CHUNG, Y.-C. 2014. Effects of Particle Stiffness on Mechanical Response of Granular Solid Under Confined Compression. *Procedia Engineering*, 79, 143-152.
- PITCHER, C., KÖMLE, N., LEIBNIZ, O., MORALES-CALDERON, O., GAO, Y. & RICHTER, L. 2015. Investigation of the properties of icy lunar polar regolith simulants. *Advances in Space Research*.

- PITMAN, E. B. 1986. Stress and velocity fields in two- and three-dimensional hoppers. *Powder Technology*, 47, 219-231.
- PLIMPTON, S. 1995. Fast Parallel Algorithms for Short-Range Molecular Dynamics. *Journal of Computational Physics*, 117, 1-19.
- PLUMPTON, A. J. 2013. *Production and Processing of Fine Particles: Proceedings of the International Symposium on the Production and Processing of Fine Particles, Montreal, August 28-31, 1988*, Elsevier Science.
- POTYONDY, D. O. & CUNDALL, P. A. 2004. Abonded-particle model for rock. *Int. J. Rock Mech. & Min. Sci.*, 41, 1329 - 1364.
- POULIQUEN, O. 1999. Scaling laws in granular flows down rough inclined planes. *Physics of Fluids (1994-present)*, 11, 542-548.
- QIU, J.-Y., ZHANG, J.-L., SUN, H., YAN, B.-J., LI, F.-G. & GUO, H.-W. 2014. DEM simulation and Experimental Investigation of Burden Distribution in the Parallel-Hopper Bell-I-Less Top Blast Furnace. *Applied Mathematics & Mechanics*, 35, 598.
- QUENOT, G. M., PAKLEZA, J. & KOWALEWSKI, T. A. 1998. Particle image velocimetry with optical flow. *Experiments in Fluids*, 25.
- QUINTANILLA, M. A. S., CASTELLANOS, A. & VALVERDE, J. M. 2001. Correlation between bulk stresses and interparticle contact forces in fine powders. *Physical Review E*, 64, 031301.
- RABINOVICH, Y. I., ESAYANUR, M. S. & MOUDGIL, B. M. 2005. Capillary Forces between Two Spheres with a Fixed Volume Liquid Bridge: Theory and Experiment. *Langmuir*, 21, 10992-10997.
- RADJAI, F., WOLD, D. E., ROUX, S., JEAN, M. & MOREAU, J. J. Force networks in dense granular media. *In: BEHRINGER, R. P. & JENKINS, J. T., eds. Powders and Grains, 1997* Rotterdam, The Netherlands. A. A. Balkema, 211-214.
- RADJAI, F., WOLF, D. E., JEAN, M. & MOREAU, J.-J. 1998. Bimodal character of stress transmission in granular packings. *Physical Review Letters*, 80, 61.

- RAMESH, K. 2000. Digital photoelasticity. IOP Publishing.
- RAMESH, K., KASIMAYAN, T. & NEETHI SIMON, B. 2011. Digital photoelasticity – A comprehensive review. *The Journal of Strain Analysis for Engineering Design*, 46, 245-266.
- RATHBONE, D., MARIGO, M., DINI, D. & VAN WACHEM, B. 2015. An accurate force–displacement law for the modelling of elastic–plastic contacts in discrete element simulations. *Powder Technology*, 282, 2-9.
- RAYLEIGH, L. 1906. IX. On an instrument for compounding vibrations, with application to the drawing of curves such as might represent white light. *Philosophical Magazine Series 6*, 11, 127-130.
- REDFERN, M. S., MARCOTTE, A. & CHAFFIN, D. B. 1990. A dynamic coefficient of friction measurement device for shoe/floor interface testing. *Journal of Safety Research*, 21, 61-65.
- REYNOLDS, O. 1885. LVII. On the dilatancy of media composed of rigid particles in contact. With experimental illustrations. *Philosophical Magazine Series 5*, 20, 469-481.
- RHODES, M. 2008a. Storage and Flow of Powders – Hopper Design. *Introduction to Particle Technology*. John Wiley & Sons, Ltd.
- RHODES, M. J. 1998. *Introduction to particle technology*, New York, John Wiley.
- RHODES, M. J. 2008b. *Introduction to Particle Technology*, Wiley.
- RICHARD, P., NICODEMI, M., DELANNAY, R., RIBIERE, P. & BIDEAU, D. 2005. Slow relaxation and compaction of granular systems. *Nat Mater*, 4, 121-128.
- ROBERTS, A. W. 1992. Modern technological developments in the storage and handling of bulk solids. *Chute Design Conference*. Australia: Bionic Research Institute.
- ROBERTS, A. W. & SCOTT, O. J. 1978. An investigation into the effects of sinusoidal and random vibrations on the strength and flow properties of bulk solids. *Powder Technology*, 21, 45-53.

- ROSE, H. E. & TANAKA, T. 1959. Rate of discharge of granular materials from bins and hoppers. *The Engineer*, 208, 465-469.
- ROSENTRATER, K. A. 2006. Some physical properties of distillers dried grains with solubles (DDGS). *Applied Engineering in Agriculture*, 22, 589-595.
- RYCROFT, C. H., GREST, G. S., LANDRY, J. W. & BAZANT, M. Z. 2006. Analysis of granular flow in a pebble-bed nuclear reactor. *Physical Review E*, 74, 021306.
- RYCROFT, C. H., KAMRIN, K. & BAZANT, M. Z. 2009a. Assessing continuum postulates in simulations of granular flow. *Journal of the Mechanics and Physics of Solids* [Online], 57. Available: www.elsevier.com/locate/jmps [Accessed 12-01-2011].
- RYCROFT, C. H., KAMRIN, K. & BAZANT, M. Z. 2009b. Assessing continuum postulates in simulations of granular flow. *Journal of the Mechanics and Physics of Solids*, 57, 828-839.
- SADOWSKI, A. J. & ROTTER, J. M. 2011. Steel silos with different aspect ratios: I— Behaviour under concentric discharge. *Journal of Constructional Steel Research*, 67, 1537-1544.
- SALISBURY, J. W. & GLASER, P. E. 2013. *The Lunar Surface Layer: Materials and Characteristics*, Elsevier Science.
- SALOT, C., GOTTELAND, P. & VILLARD, P. 2009. Influence of relative density on granular materials behavior: DEM simulations of triaxial tests. *Granular matter*, 11, 221-236.
- SAMADANI, A., PRADHAN, A. & KUDROLLI, A. 1999. Size segregation of granular matter in silo discharges. *Physical Review E*, 60, 7203-7209.
- SAMOILOV, V. M., DREMOVA, E. I. & SAMOILOV, D. V. 1996. Calculating grain-size composition for a polydisperse powder filler providing maximum particle packing density. *Powder Metallurgy and Metal Ceramics*, 34, 134-137.
- SARRAGUÇA, M. C., CRUZ, A. V., SOARES, S. O., AMARAL, H. R., COSTA, P. C. & LOPES, J. A. 2010. Determination of flow properties of pharmaceutical powders by near infrared spectroscopy. *Journal of pharmaceutical and biomedical analysis*, 52, 484-492.

- SATAKE, M., CHANG, C. S. & TOBITA, Y. 1999. Fundamentals for Mechanics of Granular Materials. In: ODAI, M. & IWASHITA, K. (eds.) *Mechanics of Granular Materials*. Netherlands: A. A. Balkema.
- SAVAGE, S. B. 1998. Analyses of slow high concentration flow of granular materials. *Journal of Fluid Mechanics*, 177, 1-26.
- SAWYER, W. G. & TICHY, J. A. 2001. Lubrication with granular flow: Continuum theory, particle simulations, comparison with experiment. *Journal of Tribology*, 123, 777-784.
- SAZZAD, M. & ISLAM, M. 2008. Macro and micro mechanical responses of granular material under varying interparticle friction. *Jl. Civil Engineering*, 36(2), pp. 87-96.
- SHELLART, W. P. 2000. Shear test results for cohesion and friction coefficients for different granular materials: scaling implications for their usage in analogue modelling. *Tectonophysics*, 324, 1-16.
- SCHMIDT, L. C. & WU, Y. H. 1989. Prediction of dynamic wall pressures on silos. *Int. J. Bulk Solid Handling*, 9, 333-338.
- SCHUBERT, H. 1984. Capillary forces-modeling and application in particulate technology. *Powder Technology*, 37, 105-116.
- SCHULZE, D. A new ring shear tester for flowability and time consolidation measurements. 1st International Particle Technology Forum, 1994 Denver, Colorado, USA. 11-16.
- SCHULZE, D. 1996. Flowability and time consolidation measurements using a ring shear tester. *Powder handling and processing*, 8, 221-226.
- SCHULZE, D. 2006a. *Flow properties of powders and bulk solids* [Online]. Dietmar Schulze. Available: <http://www.dietmarschulze.de/grdle1.pdf>.
- SCHULZE, D. 2006b. *Stresses in silos* [Online]. Dietmar Schulze. Available: <http://www.dietmarschulze.com/spanne.html>.
- SCHULZE, D. 2007. *Powders and Bulk Solids: Behavior, Characterization, Storage and Flow*, Springer Berlin Heidelberg.

- SCHULZE, D. 2008. Discussion of testers and test procedures. *Powders and Bulk Solids*. Springer Berlin Heidelberg.
- SCHULZE, D. & SCHWEDES, J. 1990. Storage and flow of bulk solids in silos and information for planning new installations. *VGB-Kraftwerkstechnik (English version)*, 70, 665-669.
- SCHWEDES, J. 2003. Review on testers for measuring flow properties of bulk solids. *Granular matter*, 5, 1-43.
- SEVILLE, J. P. K., WILLETT, C. D. & KNIGHT, P. C. 2000. Interparticle forces in fluidisation: a review. *Powder Technology*, 113, 261-268.
- SHAH, R. B., TAWAKKUL, M. A. & KHAN, M. A. 2008. Comparative evaluation of flow for pharmaceutical powders and granules. *AAPS PharmSciTech*, 9.
- SHEN, H. H. & BABIC, M. 1999. Rapid flow of granular materials. In: IWASHITA, K. & ODA, M. (eds.) *Mechanics of Granular materials*. A. A. Balkema Publishers.
- SHORT, N. M. 2011. *The remote sensing tutorial - Planetary remote sensing* [Online]. NASA. Available: http://rst.gsfc.nasa.gov/Sect19/Sect19_13a.html [Accessed December 7 2011].
- SIBILLE, L., CARPENTER, P., SCHLAGHECK, R. & FRENCH, R. A. 2005. Lunar regolith simulant materials: recommendations for standardization, production, and usage. *National Aeronautics and Space Administration: Marshall Space Flight Center*.
- SILBERT, L. E., ERTAS, D., GREST, G. S., HASLEY, T. C., LEVINE, D. & PLIMPTON, S. J. 2001. Granular flow down an inclined plane: Bagnold scaling and rheology. *Physics Review E*, 64, 051302.
- SIVAMANI, R. K., GOODMAN, J., GITIS, N. V. & MAIBACH, H. I. 2003. Coefficient of friction: tribological studies in man—an overview. *Skin Research and Technology*, 9, 227-234.
- SOCHI, T. 2010. Non-Newtonian flow in porous media. *Polymer*, 51, 5007-5023.
- SOCOLAR, J. E. S. 2003. Discrete Models of Force Chain Networks. *Discrete and Continuous Dynamic Systems-Series B*, 3, 17.

- SOMMIER, N., PORION, P., EVESQUE, P., LECLERC, B., TCHORELOFF, P. & COUARRAZE, G. 2001. Magnetic resonance imaging investigation of the mixing-segregation process in a pharmaceutical blender. *International Journal of Pharmaceutics*, 222, 243-258.
- SONG, C. Y. 2004. Effects of Patch Loads on Structural Behaviour of Circular flat-bottomed Steel Silos. *Thin-Walled Structures*, 42, 1519-1542.
- SRINIVASAN, G., COLSON, A., DEVINAT, A., L, H. J. & NAIR, P. 2008. Granular materials for textile treatment. Google Patents.
- STANFORD, M. K., DELLACORTE, C. & EYLON, D. Particle size effects on flow properties of PS304 plasma spray feedstock powder blend. *Ceramic Engineering and Science Proceedings*, 2003. American Ceramic Society, 577-586.
- STEINGART, D. A. & EVANS, J. W. 2005. Measurements of granular flows in two-dimensional hoppers by particle image velocimetry. Part I: Experimental method and results. *Chemical Engineering Science*, 60, 1043-1051.
- STURE, S., COSTES, N. C., BATISTE, S. N., LANKKTON, M. R., ALSHIBI, K. A., JEREMIC, B., SWANSON, R. A. & FRANK, M. 1998. Mechanics of granular materials at low effective stresses. *Journal of Aerospace Engineering (ASCE)*, 11, 67-72.
- SUIKER, A. S. J. & FLECK, N. A. 2004. Frictional Collapse of Granular Assemblies. *Journal of Applied Mechanics*, 71, 350-358.
- SUN, J. & SANKARAN, S. 2012. Radial hopper flow prediction using a constitutive model with microstructure evolution. *Soft Condensed Matter*.
- SUN, J., WANG, F., SUI, Y., SHE, Z., ZHAI, W., WANG, C. & DENG, Y. 2012. Effect of particle size on solubility, dissolution rate, and oral bioavailability: evaluation using coenzyme Q(10) as naked nanocrystals. *International Journal of Nanomedicine*, 7, 5733-5744.
- SUZUKI, A., TAKAHASHI, H. & TANAKA, T. 1968. Behaviour of a particle bed in the field of vibration II. Flow of particles through slits in the bottom of a vibrating vessel. *Powder Technology*, 2, 72-77.

- SYVITSKI, J. P. M. 2007. *Principles, Methods and Application of Particle Size Analysis*, Cambridge University Press.
- TAKAHASHI, H., SUZUKI, A. & TANAKA, T. 1968. Behaviour of a particle bed in the field of vibration I. Analysis of particle motion in a vibrating vessel. *Powder Technology*, 2, 65-71.
- TEJCHMAN, J. 2008. Theoretical Model. *Shear Localization in Granular Bodies with Micro-Polar Hypoplasticity*. Springer Berlin Heidelberg.
- TEJCHMAN, J. 2013. *Confined Granular Flow in Silos: Experimental and Numerical Investigations*, Springer International Publishing.
- THAKUR, S., IMOLE, O., WOJTKOWSKI, M., MAGNANIMO, V., MONTES, E., RAMAIOLI, M., AHMADIAN, H. & OOI, J. 2013. Characterization of cohesive powders for bulk handling and DEM modelling.
- THOM, N. & BROWN, S. The effect of grading and density on the mechanical properties of a crushed dolomitic limestone. Australian Road Research Board (ARRB) Conference, 14th, 1988, Canberra, 1988.
- THORNTON, A., WEINHART, T., LUDING, S. & BOKHOVE, O. 2012. Frictional dependence of shallow-granular flows from discrete particle simulations. *The European Physical Journal E*, 35, 1-8.
- THORNTON, C. & ANTONY, S. J. 1998. Quasi-static deformation of particulate media. *Philosophical Transactions of the Royal Society of London A: Mathematical, Physical and Engineering Sciences*, 356, 2763-2782.
- TIMOSHENKO, S. P. & GOODIER, J. N. 1970. *Theory of Elasticity*, McGraw-Hill Book Company.
- TIMOUNAY, Y., LORENCEAU, E. & ROUYER, F. 2015. Opening and retraction of particulate soap films. *EPL (Europhysics Letters)*, 111, 26001.
- TO, K., LAI, P.-Y. & PAK, H. 2001. Jamming of granular flow in a two-dimensional hopper. *Physical Review Letters*, 86, 71.

- TREMBLAY, L. B. & HAKAKIAN, M. 2006. Estimating the Sea Ice Compressive Strength from Satellite-Derived Sea Ice Drift and NCEP Reanalysis Data*. *Journal of Physical Oceanography*, 36, 2165-2172.
- TUCKER, J. R., SHADLE, L. J., GUENTHER, C., BENYAHIA, S., MEI, J. S. & BANTA, L. 2012. Characterization of the physical properties for solid granular materials. National Energy Technology Laboratory-In-house Research; National Energy Technology Laboratory (NETL), Pittsburgh, PA, and Morgantown, WV (United States).
- TÜZÜN, U., HOULSBY, G. T., NEDDERMAN, R. M. & SAVAGE, S. B. 1982. The flow of granular materials—II Velocity distributions in slow flow. *Chemical Engineering Science*, 37, 1691-1709.
- TYKHONIUK, R., TOMAS, J., LUDING, S., KAPPL, M., HEIM, L. & BUTT, H.-J. 2007. Ultrafine cohesive powders: From interparticle contacts to continuum behaviour. *Chemical Engineering Science*, 62, 2843-2864.
- VANEL, L., CLAUDIN, P., BOUCHAUD, J. P., CATES, M. E., CLÉMENT, E. & WITTMER, J. P. 2000. Stresses in Silos: Comparison Between Theoretical Models and New Experiments. *Physical Review Letters*, 84, 1439-1442.
- VANIMAN, D., DIETRICH, J., TAYLOR, G. J. & HEIKEN, G. 1991. Exploration, samples, and recent concepts of the Moon. *Lunar Sourcebook*, 5, 26.
- VERMEER, P. A., EHLERS, W., HERMANN, H. J. & RAMM, E. 2007. *Modelling of Cohesive-Frictional Materials: Proceedings of Second International Symposium on Continuous and Discontinuous Modelling of Cohesive-Frictional Materials (CDM 2004), held in Stuttgart 27-28 Sept. 2004*, CRC Press.
- VONDRAK, R. R. & CRIDER, D. H. 2003. Ice at the Lunar Poles. *American Scientists*, 91, 322-329.
- WALKER, D. M. 1966. An approximate theory for pressures and arching in hoppers. *Chemical Engineering Science*, 21, 975-997.
- WALTERS, J. K. 1973a. A theoretical analysis of stresses in axially-symmetric hoppers and bunkers. *Chemical Engineering Science*, 28, 779-789.

- WALTERS, J. K. 1973b. A theoretical analysis of stresses in silos with vertical walls. *Chemical Engineering Science*, 28, 13-21.
- WALTON, K. 1987. The Effective Elastic Moduli of a Random Packing of Spheres. *Journal of Mechanics and Physics of Solids*, 35, 13 - 226.
- WALTON, O. R. 2004. Potential discrete element simulation applications ranging from airborne fines to pellet beds. SAE Technical Paper.
- WALTON, O. R., PAMELADEMOOR, C. & GILL, K. S. 2007. Effect of gravity on cohesive behaviour of fine powders: Implications for processing Lunar regolith. *Granular matter* [Online]. [Accessed 12-07-2011].
- WANG, J. & YAN, H. 2012. DEM analysis of energy dissipation in crushable soils. *Soils and Foundations*, 52, 644-657.
- WANG, L. P., CAREY, V. P., GRIEF, R. & ABDOLLAHIAN, D. 1990. Experimental Simulation and Analytical modelling of two-phase Flow under Zero-Gravity Conditions. *International Journal Multiphase Flow*, 16, 407-419.
- WANG, Y. & OOI, J. Y. 2015. A Study of Granular Flow in a Conical Hopper Discharge Using Discrete and Continuum Approach. *Procedia Engineering*, 102, 765-772.
- WASHBURN, E. W. & BUNTING, E. N. 1922. POROSITY: VI. DETERMINATION OF POROSITY BY THE METHOD OF GAS EXPANSION*. *Journal of the American Ceramic Society*, 5, 112-130.
- WILLIAMS, J. R., HOCKING, G. & MUSTOE, G. G. W. 1985. The theoretical basis of the discrete element method. *NUMETA '85, Numerical Methods in Engineering Theory and Application*. Swansea: Balkema Publishers, Rotterdam.
- WILLIAMS, J. R., PERKINS, E. & COOK, B. 2004. A contact algorithm for partitioning N arbitrary sized objects. *Engineering computations*, 21 (2-4), 235-248.
- WILSON, T. J., PFEIFER, C. R., MEYSINGIER, N. & DURIAN, D. J. 2014. Granular Discharge rate for submerged hoppers. *Papers in Physics*, 6.

- WÓJCIK, M. & TEJCHMAN, J. 2009. Modeling of shear localization during confined granular flow in silos within non-local hypoplasticity. *Powder Technology*, 192, 298-310.
- WOODCOCK, C. & MASON, J. 2013. *Bulk solids handling: an introduction to the practice and technology*, Springer Science & Business Media.
- WOODCOCK, C. R. & MASON, J. S. 1987. *Bulk Solids Handling: An Introduction to the practice and technology*, USA, Chapman and Hall, New York.
- WOUTERS, I. M. F. & GELDART, D. 1996. Characterising Semi-Cohesive Powders using angle of repose. *Particle & Particle Systems Characterization*, 13, 254-259.
- WU, A. & SUN, Y. 2008. *Granular Dynamic Theory and Its Applications*, Springer Berlin Heidelberg.
- WU, W., WANG, W.-Q., YANG, D.-Z. & QI, M. 2007. Stent expansion in curved vessel and their interactions: A finite element analysis. *Journal of Biomechanics*, 40, 2580-2585.
- WU, Y. H. & SCHMIDT, L. C. 1992. A boundary element method for prediction of silo pressure. *Int J Comput Struct*, 45, 5-23.
- XU, Y., KAFUI, K., THORNTON, C. & LIAN, G. 2002. Effects of material properties on granular flow in a silo using DEM simulation. *Particulate Science and Technology*, 20, 109-124.
- YANG, J., SLIVA, A., BANERJEE, A., DAVE, R. N. & PFEFFER, R. 2005. Dry particle coating for improving the flowability of cohesive powders. *Powder Technology*, 158, 21-33.
- YANG, R. Y., ZOU, R. P. & YU, A. B. 2003. Effect of material properties on the packing of fine particles. *Journal of Applied Physics*, 94, 3025-3034.
- YANG, Y. & MISRA, A. 2012. Micromechanics based second gradient continuum theory for shear band modeling in cohesive granular materials following damage elasticity. *International Journal of Solids and Structures*, 49, 2500-2514.
- YANG, Y., OOI, J., ROTTER, M. & WANG, Y. 2011. Numerical analysis of silo behavior using non-coaxial models. *Chemical Engineering Science*, 66, 1715-1727.
- YU, C. M., CRAIG, K. & TICHY, J. A. 1994. Granular collision Lubrication. *J. Rheol*, 38, 921 - 936.

- YU, H. S., TAN, S. M. & SCHNAID, F. 2007. A critical state framework for modelling bonded geomaterials. *Geomechanics and Geoengineering*, 2, 61-74.
- ZEUCH, D. H., GRAZIER, J., ARGÜELLO, J. & EWSUK, K. G. 2001. Mechanical properties and shear failure surfaces for two alumina powders in triaxial compression. *Journal of materials science*, 36, 2911-2924.
- ZHANG-JI, L. 1987. Micropolar continuum mechanics is more profound than classical continuum mechanics. *Applied Mathematics and Mechanics*, 8, 939-946.
- ZHAO, Y. & TENG, J. G. 2004. Buckling Experiments on Steel Silo Transition Junctions II: Finite Element Modelling. *Journal of Constructional Steel Research*, 60, 1803-1823.
- ZHENG, X. M. & HILL, J. M. 1998. Molecular dynamics simulation of granular flows: Slip along rough inclined planes. *Computational Mechanics* [Online], 22.
- ZHOU, B., HUANG, R., WANG, H. & WANG, J. 2013. DEM investigation of particle anti-rotation effects on the micromechanical response of granular materials. *Granular matter*, 15, 315-326.
- ZHOU, Y. C., XU, B. H., YU, A. B. & ZULLI, P. 2002. An experimental and numerical study of the angle of repose of coarse spheres. *Powder Technology*, 125, 45-54.
- ZHU, H. P., WU, Y. H. & YU, A. B. 2005. Discrete and continuum modelling of granular flow. *China Particuology*, 3, 354-363.
- ZHU, H. P. & YU, A. B. 2004. Steady-state granular flow in a 3D cylindrical hopper with flat bottom using DEM simulation: microscopic analysis. *J. Phys. D. Appl Phys*, 37, 497-508.
- ZHU, H. P., ZHOU, Z. Y., YANG, R. Y. & YU, A. B. 2008. Discrete particle simulation of particulate systems: A review of major applications and findings. *Chemical Engineering Science*, 63, 5728-5770.
- ZHU, R., LI, S. & YAO, Q. 2013a. Effects of cohesion on the flow patterns of granular materials in spouted beds. *Physical Review E*, 87, 022206.
- ZHU, R., SHUIQING, L. & YAO, Q. Effect of cohesion on granular-fluid flows in spouted beds: PIV measurement and DEM simulations. POWDERS AND GRAINS 2013: Proceedings

of the 7th International Conference on Micromechanics of Granular Media, 2013b. AIP Publishing, 979-982.

ZHU, T. 2010. Some useful numbers on the engineering properties of materials (Geologic and Otherwise). www.stanford.edu [Online]. Available: <http://www.stanford.edu/~tyzhu/Documents/Some%20Useful%20Numbers.pdf> [Accessed April 23 2011].

List of Publications

S.J. Antony, T. Barakat, R. Hammond, K. Sheeba, T. Amanbayev, G. Okeke, S. Albaraki, B. C. Arowosola and A. Olugbenga (2014) “Multi-scale particulate mechanics in multi-disciplinary engineering applications” published in the proceedings of UK-China International Particle Technology Forum IV, Shanghai, China (347)

S. J. Antony, T. Amanbayev, B. C. Arowosola, and L. Richter (2012), “Flow behaviour of granular materials through confined geometries in low gravity and space environment” published in the proceedings of European Space Agency’s International Conference on Dust and Grains in Low Gravity and Space Environment, ESA/ESTEC, The Netherlands. (In CD)

Saeed Albaraki, S. J. Antony, B. C. Arowosola (2013), “Visualising shear stress distribution inside flow geometries containing pharmaceutical powder excipients using photo stress analysis tomography and DEM simulations” published in the AIP conference proceedings, Powders and Grains, Sydney, Australia. <http://dx.doi.org/10.1063/1.4812029>

Saeed Albaraki, B.C. Arowosola, Z. Afzal, S. J. Antony (2013) “Effect of granular microscopic characteristics on macroscopic flow behaviour” The Academy of Pharmaceutical Sciences Materials Conference proceedings, Nottingham, UK. (In CD)

S.J. Antony, S. Albaraki, B. C. Arowosola, N. Agarwal (2012) “Novel visual probing of shear stress distribution inside pharmaceutical powder packing with constrained geometries using photo stress analysis tomography” APS PharmSci 2012 International conference (The Science of Medicines) proceedings, Nottingham, UK)

S. J. Antony, B. C. Arowosola, S. Albaraki, A. Mandare (2014) “Current developments on the flow behaviour of particulate materials using advanced simulations and tomography experiments” Particulate Systems Analysis, Manchester, UK (In CD)

B. C. Arowosola, S. J. Antony, L. Richter, T. Amanbayev (2014) “Simulations of particulate flow under low gravitational environments” presented at Particle Systems Analysis, Manchester, UK

B. C. Arowosola, S. J. Antony, L. Richter, T. Amanbayev (2015) “Simulations of particulate flow under low gravitational environments” presented at Powder Flow – Fundamentals to Applications , Leeds, UK

Appendix A

Theory and concept of DEM modelling

A.1 Theory and concept of DEM modelling

This section introduces the discrete element model (DEM) for modelling granular flow and designing flow chambers under different gravity levels using particle flow code (PFC^{3D}). PFC is a DEM software (Itasca consulting group) used in this thesis for simulations. A discussion of the methodology of DEM using PFC^{3D} including the calculation cycle, constitutive model, contact detection are presented here.

The DEM technique takes a set of discrete elements which are usually spherical particles, applies Newton's law of motion (equations A.1 and A.2) and a force displacement model under the assumption that the element velocity is unchanged for a given time interval (Cundall and Strack, 1979).

$$F_i = ma_i \quad (\text{A.1})$$

$$M_i = m\omega_i \quad (\text{A.2})$$

where F , a , M and ω are the force, acceleration, moment and angular rotation acting on a particle mass, m in direction i .

A.2 DEM Calculation Cycle

The calculations performed in DEM alternate between the application of Newton's second law to the particles and a force-displacement law at the contacts. While Newton's second law helps to determine the motion of each particle arising from the contact and body forces that acts on it, the force-displacement law updates the contact forces which arise from the relative motion at each contact. The calculation cycle (Fig. 2.17) which is used in PFC^{3D} is a repetitive time-stepping algorithm and during the course of simulation, contacts between two particles or between a particle and the system boundary can be formed and broken automatically.

The method is based on the assumption of choosing a time-step that is very small and the inter-particle interactions considered are based on either a linear spring-dashpot model (Cundall and Strack, 1979) or established theories of contact mechanics (Thornton and Antony, 1998). At the beginning of each time-step, a set of contacts is updated from the known particle and boundary positions. Based on the relative motion between the entities at the contact and contact constitutive

models, the force displacement law is applied to each contact (Sazzad and Islam, 2008). The law of motion is then applied to each particle to update its velocity and position based on the resultant force and moment arising from contact forces and body forces acting on the particle. For every contact determined, the acting force is calculated in both the normal and tangential direction. Once the forces are determined, the equations of motions are used to calculate the motion of the particle (Kruggel-Emden et al., 2008) based on the un-balanced forces from the previous cycle.

A.2.1 Force displacement relations

The force-displacement relations applied in the DEM cycle is the relationship between the relative displacement between two bodies at contact and the contact force acting on the bodies (Cundall and Strack, 1979). The force-displacement law is mostly active at a contact and can be described in terms of the contact point on a contact plane defined by a unit normal vector, n_i (Fig. A.1). The contact point is within the interpenetration volume of the two bodies. Two types of contact exist which are the particle-particle contact and the particle-wall contact in which the contact force arises from contact occurring at a point. For particle-particle contact, the normal vector is directed along the line between the centers of the particles while for the particle-wall contact, the normal vector is directed along the line which defines the shortest distance between the center of the particle and the wall (Fig. A.2). The contact force has two components; normal and shear components which are related to the corresponding component of the relative displacement through the normal and shear stiffness at the contact. The normal component acts in the direction of the normal vector while the shear component acts on the contact plane. Models are usually designed for different types of particles which provide force-displacement laws that account for both normal and tangential interactions. The force-displacement is described using relevant equations as presented for particle-particle contacts using two spherical particles (Fig. A.1) and for particle-wall contacts using a spherical particle and a wall (Fig. A.2).

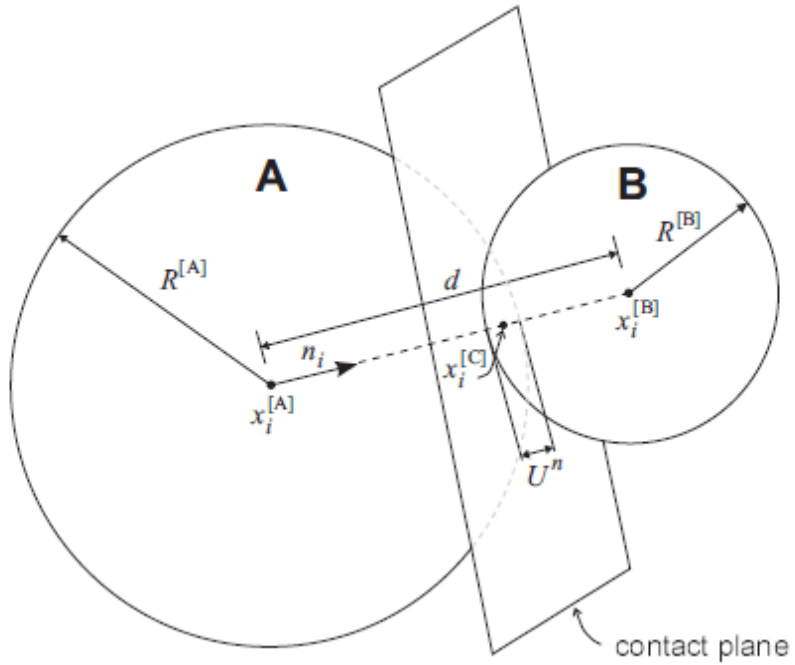


Fig. A. 1 Description of the particle-particle contact (ITASCA, 2004)

From Fig A.1, the contact plane is defined by the unit normal, n_i where;

$$n_i = \frac{x_i^{[B]} - x_i^{[A]}}{d} \quad (\text{A.3})$$

where $x_i^{[A]}$ and $x_i^{[B]}$ are the position vectors of the center of particles A and B and d is the distance between the particles.

The description of the particle-wall contact is given in Fig. A.2.

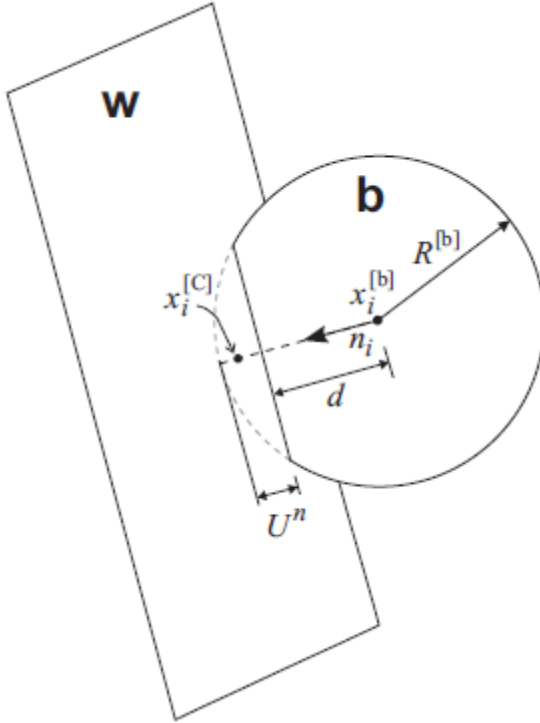


Fig. A. 2 Description of the particle-wall contact (ITASCA, 2004)

The normal direction for the particle-wall contact can be determined and the relative contact displacement in the normal direction is defined by the overlap, U_n given by

$$U_n = \begin{cases} R^{[A]} + R^{[B]} - d, & (\text{particle} - \text{particle}) \\ R^{[B]} - d, & (\text{particle} - \text{wall}) \end{cases} \quad (\text{A.4})$$

where $R^{[\varphi]}$ is the radius of the particle, φ .

The location at which the contact point exists is then given by

$$x_i^{[C]} = \begin{cases} x_i^{[A]} + \left(R^{[A]} - \frac{1}{2}U^n\right)n_i & (\text{particle} - \text{particle}) \\ x_i^{[B]} + \left(R^{[B]} - \frac{1}{2}U^n\right)n_i & (\text{Particle} - \text{wall}) \end{cases} \quad (\text{A.5})$$

The action of particle contact on both particle and wall can be resolved into normal and shear components for the contact force vector, F_i with respect to the plane as

$$F_i = F_i^n + F_i^s \quad (\text{A.6})$$

where F_i^n and F_i^s represents the normal and shear component vectors respectively.

The normal contact force vector is then calculated by

$$F_i^n = K^n U^n n_i \quad (\text{A.7})$$

where K^n is the normal stiffness (i.e. force/displacement) at the contact.

The shear component vector is also calculated in the form of an increment vector by

$$\Delta F_i^s = -K^s \Delta U_i^s \quad (\text{A.8})$$

Where ΔU_i^s is the shear component of the contact displacement-increment vector occurring over a timestep and K^s is the shear stiffness at the contact

The values of K^n and K^s depends on the type of contact model adopted in the DEM simulation.

A.2.2 Law of motion

The law of motion most applicable in DEM simulations is the Newton's second law of motion. This is the most powerful of Newton's three laws because it allows quantitative calculations of dynamics. The motion of a single rigid particle is said to be determined by the resultant force and moment vectors acting on it and is best described in terms of the translational motion of a point in the particle and the rotational motion of the particle. The total force, F_i , of the discrete elements with total momentum, M_i , acts on the center of the particle with the force originating from volume forces such as gravity forces or boundary forces (Kozicki and Donzé, 2008). The translational and rotational degrees of freedom are given by integrating Newton's equation of motion such that:

$$M_i x_i = F_i + m_i g \quad (\text{A.9})$$

where m_i is the mass of the discrete particle, x_i is the translational acceleration, F_i is the total force applied on the discrete particle as a result of the interactions and g is the acceleration due to gravity.

For a spherical particle of Radius R , having its mass uniformly distributed throughout its volume, the center of mass coincides with the sphere center and the rotational motion is given as:

$$M_i = I_i \omega_i = \left(\frac{2}{5} m R^2\right) \omega_i \quad (\text{A.10})$$

where I_i is the moment of inertia of the particle and ω_i is the angular velocity.

The equations of motion given in equations A.9 and A.10 are usually integrated using a centered finite-difference procedure involving a timestep.

A.2.3 Contact law

The equation of motion describes the global behaviour of impacting objects, while the contact force depends on the local contact law (Corwin et al., 2005). If particles are large enough, long range interactions such as van der Waals forces are negligible, in which case particles only interact at close range. Due to the forces exerted by the particles on each other, deformation tends to occur. However, in granular materials, particles have complicated shapes and their deformation as well as forces acting on them can be very complex. Thus, to reduce the computational cost in DEM, particles are usually modelled as spheres or disks and it is assumed that they are in contact when they overlap and the contact forces computed as a function of the overlap (Fig. A.3).

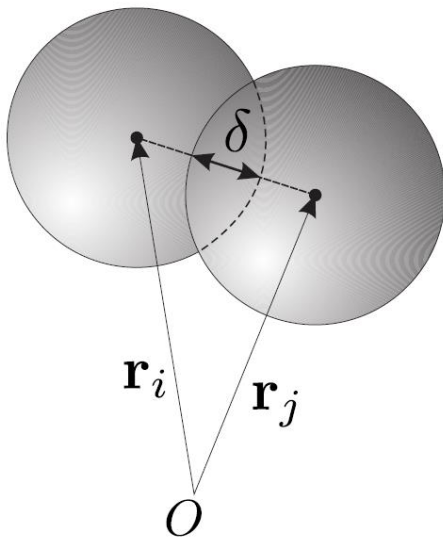


Fig. A. 3 Schematic description of the overlap, δ during collision

where r_i and r_j are the position vectors of the two particles overlapping each other

When particles collide, the shape changes and the distance between the two particles will be smaller than the sum of the diameters of the two particles. The way force contacts are computed depends on the different types of contact models used.

A.3 Contact Force Models

The force displacement model is an integral part of DEM simulations and used to define particle behaviour and geometry. The contact force is the result of elastic, viscous and frictional resistance between the moving particles which can be modelled using various force contact models. Most models assume that the normal contact force is independent of the tangential contact force, but the tangential contact force is dependent on the normal contact force. Tangential forces are attributed to surface friction between the particles and the friction is well modelled using Coulomb's law of friction. The overall constitutive behaviour of the particulate material is simulated by associating a simple constitutive model with each contact in PFC^{3D}. The constitutive model acting at a particular contact consists of three parts: the stiffness model, the slip model; and the bonding model.

A.3.1 Contact stiffness models

The contact stiffness model represents an elastic relationship between the contact force and the relative displacement in the normal and shear directions through equations A.7 and A.8. The normal stiffness is a secant stiffness as represented in equation A.7 because it relates the total normal force to the total normal displacement. The shear stiffness (equation A.8) is a tangent stiffness as it relates the increment of shear force to the increment of shear displacement. The contact stiffness model is generally of two types namely; linear model and a simplified Hertz-Mindlin model. The contact stiffness used in the simulation via equations A.7 and A.8 are assigned different values which depends on the type of contact stiffness model employed. In PFC^{3D}, contact between two particles operating under different contact stiffness models is not allowed due to its undefined behaviour.

A.3.1.1 Linear contact model

The linear contact model which is also known as the linear spring-dashpot model (Cundall and Strack, 1979) is one of the simplest force-displacement models used. This model is employed for the normal force which is combined with a slider for the tangential force (Corwin et al., 2005). A viscous damping constant, C_i ($i = n: normal, s: shear$) which is the dashpot is also included in the model (Fig. A.4).

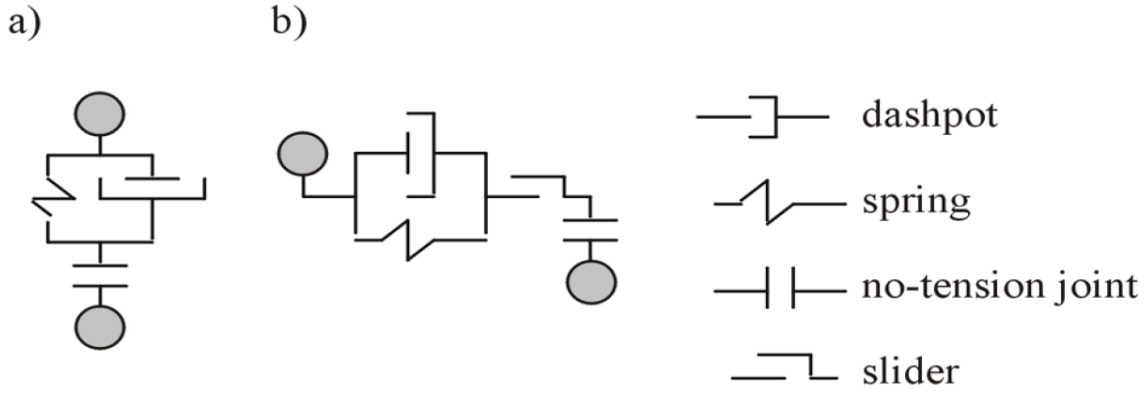


Fig. A. 4 Linear Spring-Dashpot Model for DEM simulations in (a) normal and (b) tangential directions

From Fig. A.4, the normal and shear stiffness K_n and K_s (spring) of the contacts occurring at both particle-particle and particle-wall defines the linear contact model. The contact stiffness for the linear contact model is computed based on assumptions that the stiffness at the two contacts acts in series. Thus, the contact normal secant stiffness is given by:

$$K^n = \frac{K_n^{[A]}K_n^{[B]}}{K_n^{[A]}+K_n^{[B]}} \quad (\text{A.11a})$$

and the contact shear tangent stiffness also given by:

$$K^s = \frac{K_s^{[A]}K_s^{[B]}}{K_s^{[A]}+K_s^{[B]}} \quad (\text{A.11b})$$

The subscripts $[A]$ and $[B]$ denote the two entities (particle-particle and particle-wall) in contact.

For the linear model, the normal secant stiffness is equal to the normal tangent stiffness, since

$$K^n = \frac{dF^n}{dU^n} = \frac{d(K^n U^n)}{dU^n} = K^n \quad (\text{A.12})$$

where K^n is as expressed in equation A.11a.

The linear model is well used and applied in DEM because they are less computationally expensive to calculate which in turn promotes its application in simulating larger systems (Rathbone et al., 2015).

A.3.1.2 Hertz-Mindlin contact model

The Hertz-Mindlin contact model is a non-linear contact elastic model based on an approximation of the theory of Deresiewicz and Mindlin (1952) and described in (Cundall, 1988). The model is strictly applicable only to spheres in contact and does not reproduce the continuous non-linearity in shear. It makes use of the initial shear modulus but however depends on the normal force. The model uses a spring-dashpot response to normal contact that exist between particles and/or geometry, a Coulomb friction coefficient μ for shear interactions and a second spring-dashpot response to tangential or rolling friction interaction (Fig. A.5). The two parameters used to define the model are the shear modulus G in terms of stress and Poisson's ratio ν which is dimensionless.

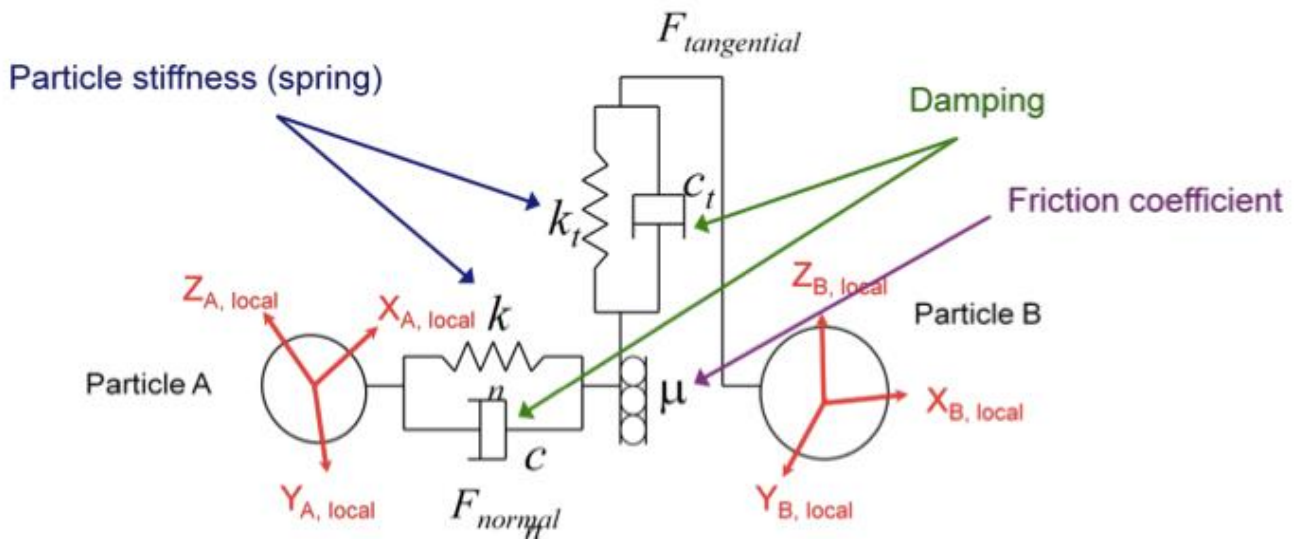


Fig. A. 5 An approximate of the Hertz-Mindlin Model (EDEM, 2012)

The Hertz-Mindlin model cannot be used in between particles that are joined by a contact model because the model does not support spheres that are in tension. The model however tends to produce the most accurate results (Jaeger, 2005) but can be computationally expensive to implement as smaller time-steps may be required as compared with the linear-spring dashpot model. In PFC^{3D}, when Hertz contact is active, the stiffness parameters k_n and k_s are ignored and the elastic properties G and ν are employed. The elastic properties are represented by mean values for particle to particle interactions, while for particle-wall interactions, the wall is assumed to be rigid and the elastic properties of the particles are used alone. The contact normal secant stiffness is given as:

$$K^n = \left(\frac{2\langle G \rangle \sqrt{2R}}{3(1-\nu)} \right) \sqrt{U^n} \quad (\text{A.13})$$

The contact shear tangent stiffness is also given as:

$$k^s = \left(\frac{2(\langle G \rangle^2 3(1-\nu)R)^{1/3}}{2-\nu} \right) |F_i^n|^{1/3} \quad (\text{A.14})$$

Where U^n is the sphere overlap $|F_i^n|$ is the magnitude of the normal contact force and R is the radius of the sphere. The multipliers to both equations A.13 and A.14 are a function of the two entities in contact. For the Hertz model, the normal-secant stiffness k^n is related to the normal-tangent stiffness by equation A.15.

$$k^n \equiv \frac{dF^n}{dU^n} = \frac{3}{2} K^n \quad (\text{A.15})$$

Where K^n is given by equation A.13.

A.3.2 Slip model

The slip model is an intrinsic property of the particle-particle or particle-wall contacts which does not provide normal strength in tension but allows slip to occur by limiting the shear force. The slip model is always present between contacts between the entities except a contact bond exists. In cases where contact bonds exist, the contact bonds supersede the slip model behaviour. The slip model and the contact bond model both describe the constitutive behaviour for particle contact which occurs at a point. The slip model is defined by the friction coefficient at the contact μ , where μ is assumed to be the minimum friction coefficient of the two bodies in contact. The contact between the particle-particle as well as the particle-wall is checked for slip conditions by calculating the maximum allowable shear contact force as given in equation A.16.

$$F_{max}^s = \mu |F_i^n| \quad (\text{A.16})$$

Thus, if $|F_i^s| > F_{max}^s$, then slip will occur during the next calculation cycle by setting the magnitude of F_i^s to be equal to F_{max}^s using equation A.17

$$F_i^s \leftarrow F_i^s (F_{max}^s / |F_i^s|) \quad (\text{A.17})$$

A.3.3 Bonding model

In DEM simulations using PFC^{3D}, particles are allowed to bond together and the two bonding models supported are the contact bond model and the parallel bond model. These bonds can be said to be a kind of glue joining two particles together in their individual distinct ways. The contact bond model joins two particles over a small area at the contact point while the parallel bond model can be termed as platen shaped contact of a finite size that acts over a circular cross-section lying on the contact plane between the particles. The contact bond model only supports the transmission of force while the parallel bond model supports the transmission of both force and moment. During simulation, both types of bonding model can be present and active at the same time but the presence of a contact bond will disable the default slip model. Also, once the particles are bonded, the contact continues to exist until the bond is broken and the bonds between the particles cannot be restored once broken. It is however important to note that bonds can only occur between the particle-particle contact and particles may not be bonded to a wall.

A.3.3.1 Contact-bond model

A contact bond can be represented by a pair of elastic springs with constant normal and shear stiffness acting on a contact point. The two springs have specified shear and tensile normal strengths and the slip is precluded due to the existence of contact bonds. Additionally, the contact bonds also give room for tensile forces to develop at the contact. The magnitude of the shear contact force is limited by the shear contact bond strength and the magnitude of the tensile normal contact force also limited by the normal contact strength.

A contact bond is characterized by the normal contact bond strength F_c^n and shear contact bond strength F_c^s with both measured in force units. The constitutive behaviour relating the normal and shear components of the contact force and relative displacement for particle contact that occurs at a point is presented in Fig. A.6.

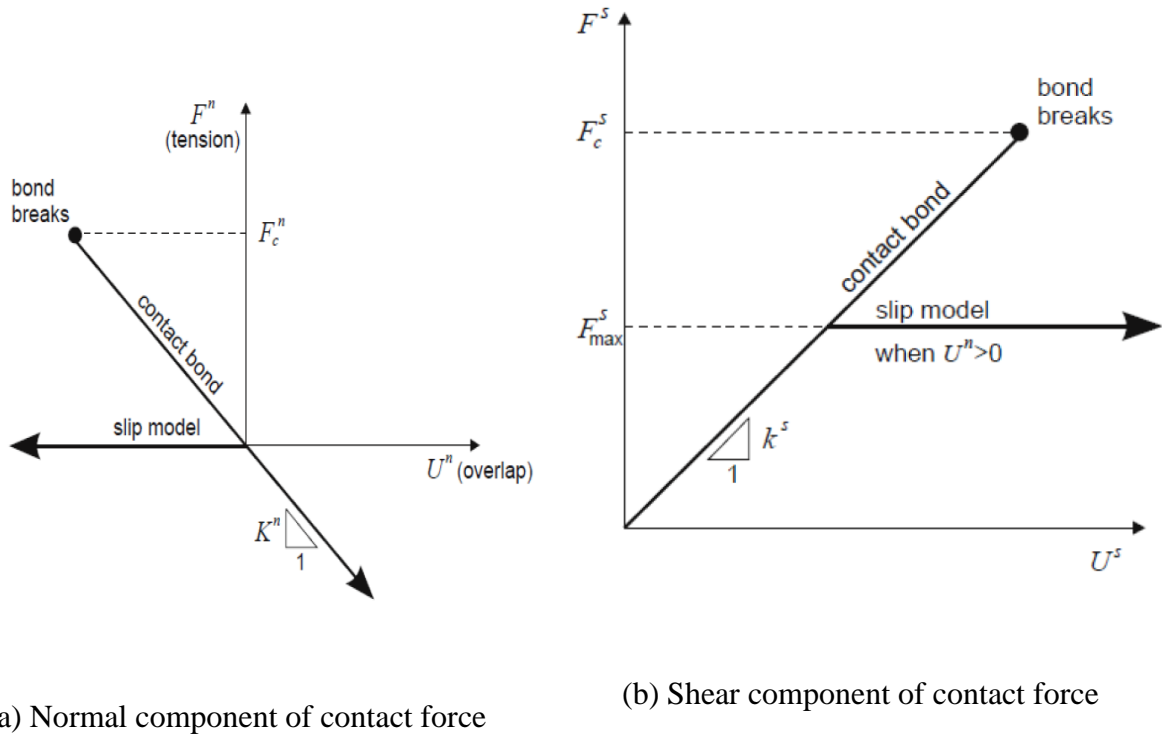


Fig. A. 6 Constitutive behaviours for point contact (ITASCA, 2004)

In Fig. 3.7, F^n is the normal contact force, U^n is the relative normal displacement, F^s is the magnitude of the total shear contact force and U^s is the magnitude of the total shear displacement measured relative to the location of the contact point at which the bond was formed. Conditions exist such that when $F^n > 0$, it indicates tension and when $U^n > 0$, it indicates an overlap. When the magnitude of the tensile normal contact force equals or exceed the normal contact bond strength, the bonds will break. After the breakage of the bonds, both the normal and shear contact forces reverts to zero.

A.3.3.2 Parallel-bond model

The parallel-bond model describes the behaviour of a finite-sized piece of cementitious material which is deposited between two particles. An elastic interaction is established by the bonds between the particles acting in parallel with the contact bond or slip models earlier discussed. Unlike in the application of contact bonds, the existence of parallel bonds does not preclude the possibility of slip. During simulation, parallel bonds may contribute to the resultant force and moment acting on the bonded particles because it is able to transmit both force and moments between particles. In the application of parallel-bond model in PFC^{3D}, the beam theory is applied

to calculate the stress within the parallel bond (Fig. A.7). The parallel bond is termed to be a set of elastic springs with constant normal and shear stiffness which is uniformly distributed over a circular area lying on the contact plane and centred at the contact point. After the parallel bond has been created, the relative motions at the contact causes the axial and shear forces (T and V , respectively) along with bending moment (M) and twisting moment (M_t) to develop within the bond material as a result of the parallel-bond stiffness. The forces and moments act on the bonded particles and can be related to maximum normal and shear stresses ($\bar{\sigma}$ and $\bar{\tau}$, respectively) acting within the bond material at the bond periphery as given in equation A.18.

$$\sigma_c = \frac{T}{A} + \frac{|M|\bar{R}}{I} \quad (\text{A.18a})$$

$$\tau_c = \frac{|V|}{A} + \frac{|M_t|\bar{R}}{J} \quad (\text{A.18b})$$

Where A and I are the area and moment of inertia of the parallel bond cross section, J is the polar moment of inertia of the parallel bond cross section and a positive T value indicates tension.

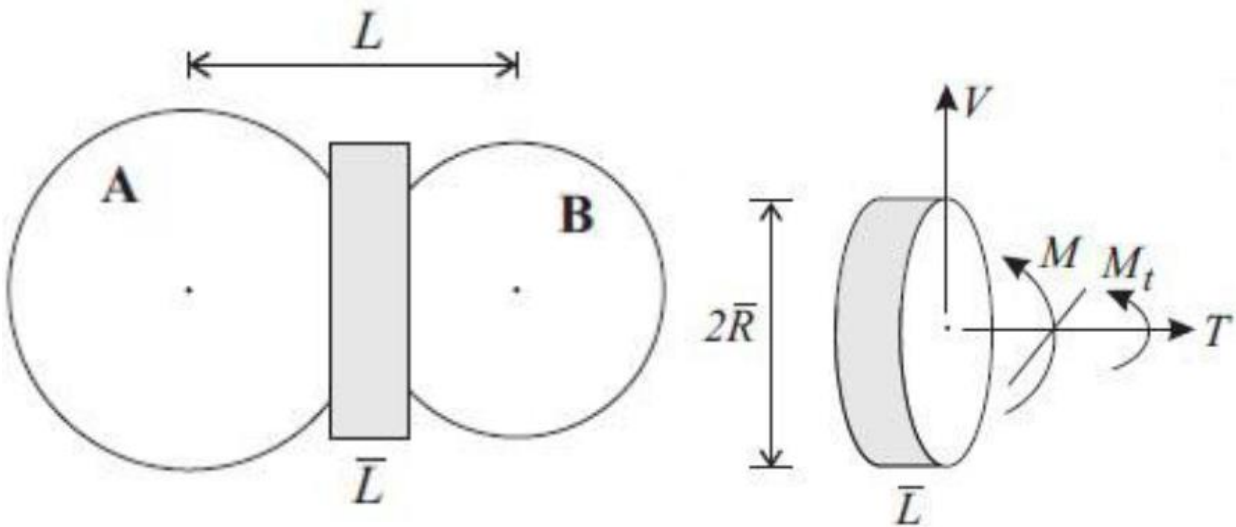


Fig. A. 7 Parallel bond idealization depicted as a cylinder of cementitious material

A parallel bond is defined by five parameters namely: normal and shear stiffness, \bar{k}^n and \bar{k}^s (stress/displacement); normal and shear strength, $\bar{\sigma}_c$ and $\bar{\tau}_c$ (stress); and bond radius \bar{R} . The bond radius is set by specifying $\bar{\lambda}$ as given in equation A.19:

$$\bar{R} = \bar{\lambda} \min(R^{[A]}, R^{[B]}) \quad (\text{A.19})$$

If either of the maximum stresses $\bar{\sigma}$ and $\bar{\tau}$ exceeds its corresponding bond strength, the parallel bond breaks. The beam cross-sectional area, moment of inertial and polar moment of inertia can be expressed as equations A.20, A.21 and A.22 respectively.

$$A = \pi \bar{R}^2 \quad (\text{A.20})$$

$$I = \frac{1}{4} \pi \bar{R}^4 \quad (\text{A.21})$$

$$J = \frac{1}{2} \pi \bar{R}^4 \quad (\text{A.22})$$

A.3.4 Alternative contact models

Other alternative methods exist in addition to the standard linear and Hertz models for the simulation of more complex contact behaviour (ITASCA, 2004). These models will only be mentioned here briefly and not elaborated in detail. The alternative contact models include: simple viscoelastic model (Nosewicz et al., 2013), simple ductile model (Peng et al., 2014), displacement-softening model (Peng et al., 2014), smooth-joint model (Lambert and Coll, 2014), Hysteretic damping model (Maia, 2009), Burger's model (Cai et al., 2013) and viscous damping model (Wang and Yan, 2012).

A.4 Critical Time-Step Determination

DEM belongs to a centred finite different scheme and in PFC^{3D}, the equations of motion are integrated using the scheme. The stability of the computed solutions produced by the equations depends on the time-step i.e. if the critical time-step related to the minimum Eigen period of the total system is not exceeded. Because of the large and constant changing system in DEM, it is impractical to calculate the global eigenvalue of the system. Thus, in PFC^{3D}, a simplified procedure is implemented to estimate the critical time-step of each calculation cycle and the actual time-step used in the cycle is a fraction of the estimated critical value.

The critical time-step for the solution stability is estimated by first considering a one-dimensional mass-spring system described by a point mass, m and spring stiffness, k as shown in Fig. A.8. The motion of the point mass is determined by the differential equation in equation A.23.

$$-kx = m\ddot{x} \tag{A.23}$$

The critical time-step for the system which corresponds to a second order finite difference scheme given by Bathe and Wilson (1976) is given in equation A.24.

$$t_{crit} = \frac{T}{\pi}; \quad T = 2\pi\sqrt{m/k} \tag{A.24}$$

where T is the period of the system.

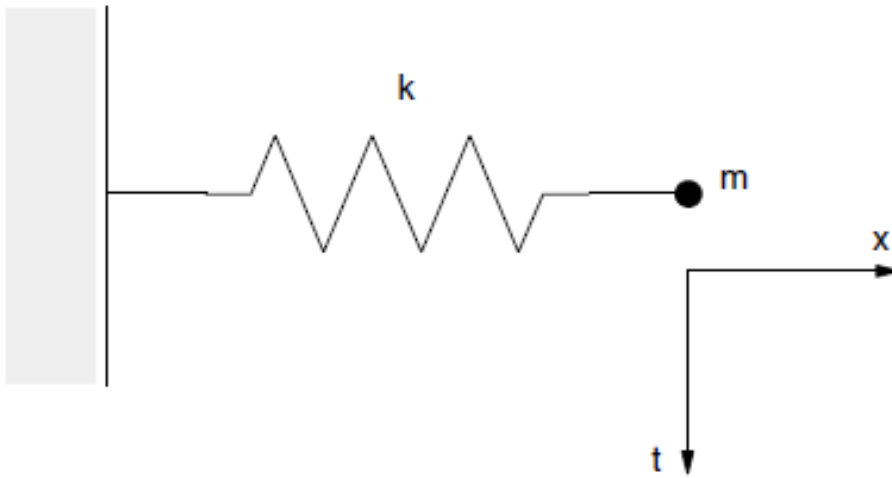


Fig. A. 8 Single mass-spring system

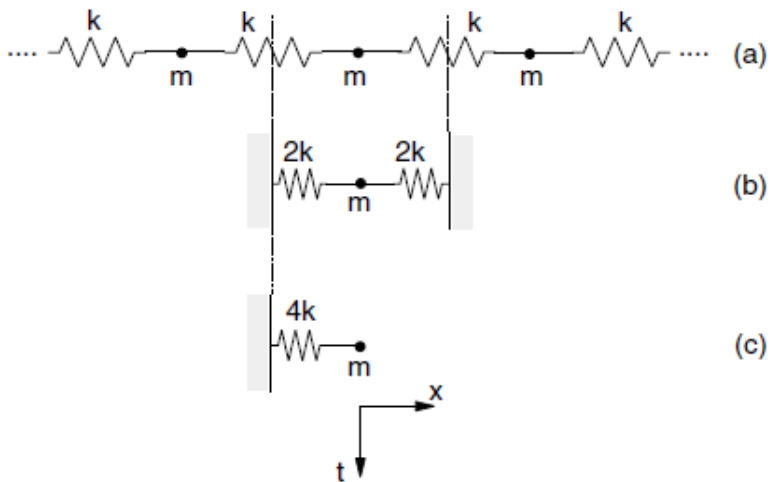


Fig. A. 1 Multiple mass-spring system

Further, for a system composed of infinite series of point masses and springs (Fig. A.9), the smallest period of the system is expected when the masses move in synchronized opposing motion in which there is no motion at the centre of each spring. Figs. A.9(b) and A.9(c) are two equivalent systems that describe the motion of a single point mass. Thus, from equation A.24, the critical time-step for this system can be expressed as:

$$t_{crit} = 2\sqrt{m/4k} = \sqrt{m/k} \quad (\text{A.25})$$

where k is the stiffness of each of the springs in Fig. A.9.

The translational motion can then be said to be characterized by the two systems in Figs. A.8 and A.9. Similarly, the rotational motion can be characterized by the same two systems but by replacing mass with the moment of inertia, I , of a finite sized particle as well as replacing the stiffness with rotational stiffness. The critical time-step for the generalized multiple mass-spring system can then be expressed as:

$$t_{crit} = \begin{cases} \sqrt{m/k^{tran}}, & (\text{translational motion}) \\ \sqrt{I/k^{rot}}, & (\text{rotational motion}) \end{cases} \quad (\text{A.26})$$

where k^{tran} and k^{rot} are the translational and rotational stiffness and I is the moment of inertia of the particle.

For a three-dimensional collection of particles and springs system using PFC^{3D} in which each may have a different mass and stiffness, equation A.26 is applied to estimate the critical time-step for each particle separately at each degree of freedom and assuming the degrees of freedom are uncoupled. The final critical time-step is then estimated to be the minimum of all the critical time-steps computed for all degrees of freedom of all particles.

A.5 Contact Detection Algorithm

It is very important to identify and determine whether particles are in contact with each other as this is a key step in DEM calculations as expressed in the DEM calculation cycle. A key point of analysis is to be able to define a way to efficiently determine the contacts and how many particles are in contact for each time-step in a given system. An efficient and robust contact detection algorithm is required because contact detection is a time consuming process and can take a considerable portion of the total computer processor time required to analyse the whole particulate system.

In PFC^{3D}, the scheme used to detect particle contacts is simple and requires less search time. The procedure is such that for particle A centred at (x_1, y_1) and particle B centered at (x_2, y_2) in a Cartesian coordinate system, a contact will exist if the distance d between their centers satisfies equation A.27.

$$d \leq \sqrt{(x_1 - x_2)^2 + (y_1 - y_2)^2} \quad (\text{A.27})$$

Thus, the scheme is such that particles are considered to be in contact only if the distance between the centres is less than the sum of their radii. Cundall (1988) presented a detailed description of the particle contact detection technique and its implementation in DEM.

Also, it is important to understand the contact detection and how the force-displacement law is applied at contacts between particles and the walls as expressed in Fig. A.10. In the force-displacement law, every particle parameter is transformed into the local coordinate system associated with the wall. In PFC^{3D}, Particles are also referred to as balls.

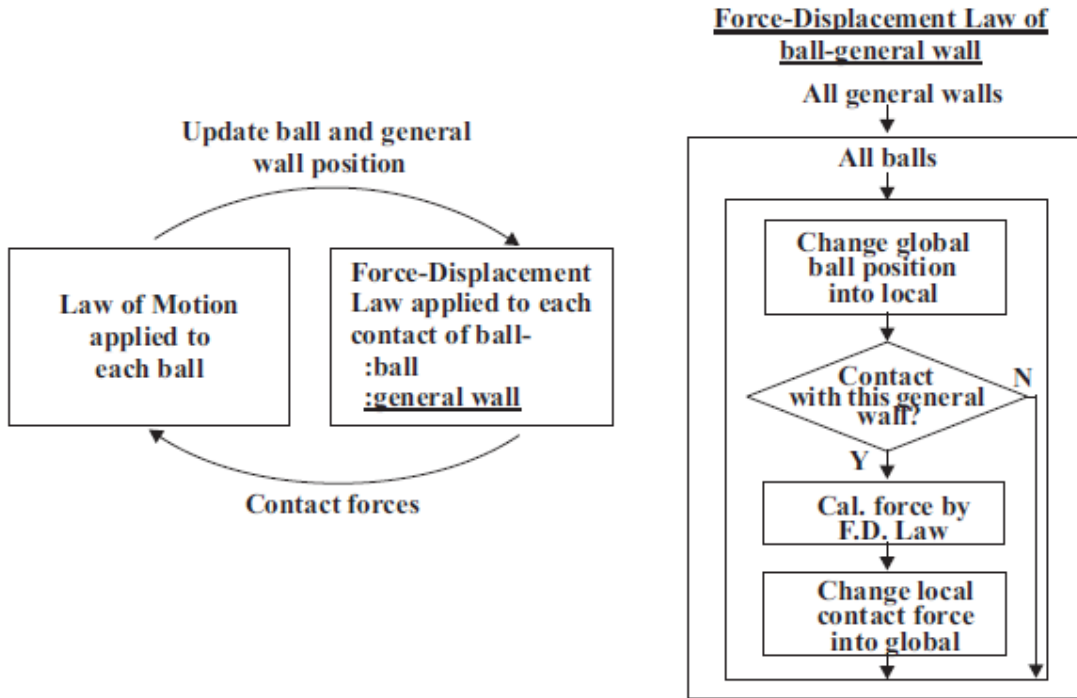


Fig. A. 2 Calculation cycle in PFC3D for the force-displacement law at particle-wall contacts

As the particle contacts the wall, the contact force is then updated by applying the force-displacement law of the contact and the process repeated for all the particles. The wall is driven with prescribed translational and rotational velocities and each particle obeys the Newton’s second law of motion.

A.6 Energy Tracing in DEM Simulations

The energy in the entire particle assembly can be tracked and the calculation of energy and work terms may be staggered by up to one whole time-step. The energy terms tracked in the DEM simulation using PFC^{3D} are body work, bond energy, boundary work, frictional work, kinetic energy, and strain energy.

A.6.1 Body work

The body work is the total accumulated work E_b , which is done by all the body forces on the assembly as given in equation A.28. Body forces are defined to be the gravity loading and applied forces and moments.

$$E_b \leftarrow E_b + \sum_{N_p} \left((mg_i + F_i)\Delta U_i + M_i\Delta\theta_i \right) \quad (\text{A.28})$$

where N_p , m , g_i , F_i , M_i , ΔU_i and $\Delta\theta_i$ are the number of particles, mass, gravitational acceleration vector, externally applied force, externally applied moment, computed displacement increment, and computed rotational increment, respectively, for a particle during current time-step.

The computation assumes that g_i , F_i and M_i are constant throughout the time-step and E_b may be either positive or negative, with the convention that work done by the body forces on the particles is positive.

A.6.2 Bond energy

This is the total strain energy, E_{pb} , of the assembly stored in parallel bonds such as given in equation A.29.

$$E_{pb} = \frac{1}{2} \sum_{N_{pb}} \left(\frac{|F_i^n|^2}{(Ak^n)} + \frac{|F_i^s|^2}{(Ak^s)} + \frac{|M_i^n|^2}{(Jk^s)} + \frac{|M_i^s|^2}{(Ik^n)} \right) \quad (\text{A.29})$$

Where N_{pb} is the number of parallel bonds and the equation contains notation for the forces, moments and stiffness associated with each parallel bond.

A.6.3 Boundary work

This is the total accumulated work, E_w that is done by all the walls on the assembly and given in equation A.30.

$$E_w \leftarrow E_w - \sum_{N_w} (F_i\Delta U_i + M_i\Delta\theta_i) \quad (\text{A.30})$$

where N_w is the number of walls; F_i and M_i are the resultant force and moment acting on the wall at the beginning of the current time-step; and ΔU_i and $\Delta\theta_i$ are the applied displacement and rotation occurring during the current time-step. In application, this is an approximation and it is assumed that F_i and M_i remain constant throughout the time-step. As with the body work case, E_w may be positive or negative, with the convention that work done by the walls on the particles is positive.

A.6.4 Frictional work

Frictional work is the total energy, E_f , that is dissipated by frictional sliding at all contacts and given as:

$$E_f \leftarrow E_f - \sum_{N_c} (\langle F_i^s \rangle (\Delta U_i^s)^{slip}) \quad (\text{A.31})$$

where N_c is the number of contacts; F_i^s and $(\Delta U_i^s)^{slip}$ are the average shear force and the increment of slip displacement, respectively, at the contact for the current time-step.

A.6.5 Kinetic energy

The kinetic energy is the total kinetic energy, E_k , of all bodies including spheres accounting for both translational and rotational motion. E_k is then expressed in equation A.32.

$$E_k = \frac{1}{2} \sum_{N_b} (m_i^i V_i^2 + I_i \omega_i \cdot \omega_i) \quad (\text{A.32})$$

where N_b , m_i , I_i , V_i and ω_i are respectively, the number of bodies, inertial mass, inertia tensor, and translational and rotational velocities of body i .

A.6.6 Strain energy

This is the total strain energy, E_c , of the whole assembly stored at all contacts assuming a linear contact-stiffness model which is given as:

$$E_c = \frac{1}{2} \sum_{N_c} (|F_i^n|^2 / k^n + |F_i^s|^2 / k^s) \quad (\text{A.33})$$

where N_c is the number of contacts; $|F_i^n|$ and $|F_i^s|$ are the magnitudes of the normal and shear components of the contact force; k^n and k^s are the normal and shear-contact stiffness. The strain energy value is not computed for nonlinear Hertz contact stiffness model.

A.7 Measurement Logic

During DEM simulation, a number of quantities in a PFC^{3D} model can be measured. The quantities are defined with respect to a specified measurement volume which is represented by a sphere termed as measurement sphere or circle. The quantities include coordination number, porosity, sliding fraction, stress and strain rate. Each of the measurement quantities is defined and the assumptions and approximations employed in their computations will further be described.

A.7.1 Coordination number

The coordination number C_n can be defined as the average number of active contacts that occur within the particle assembly per particle. An active contact is defined as that which either carries a non-zero normal force or has a parallel bond. Depending on the shape of the particles and bonding, the particle assembly can contain single particles and/or clump of particles. During the computation, only particles that their centroids within the measurement sphere are considered and this can be expressed as:

$$C_n = \frac{\sum_{N_p} n_c^{(p)} + \sum_{N_l} n_c^{(l)}}{N_p + N_l} \quad (\text{A.34})$$

where the summations are for both N_p particles and N_l clumps that have their centroids within the measurement sphere, and $n_c^{(p)}$ and $n_c^{(l)}$ are the number of active contacts of the particles and clumps respectively.

A.7.2 Porosity

The porosity, n , as defined earlier in chapter two is the ratio of the total void volume, V^{void} , within the measurement sphere to the measurement sphere volume, V^{sph} and given as:

$$n = \frac{V^{void}}{V^{sph}} = \frac{V^{sph} - V^{mat}}{V^{sph}} = 1 - \frac{V^{mat}}{V^{sph}} \quad (\text{A.35})$$

Where V^{mat} is the volume of the material in the measurement sphere and can be approximated as given in equation A.36:

$$V^{mat} = \begin{cases} \sum_{N_{p'}} V^{(p')} + \sum_{N_l} V^{(l)} - \sum_{N_c} V^{(c)} & B_v \neq 0 \\ \sum_{N_{p'}} V^{(p')} + \sum_{N_{l'}} V^{(l')} - \sum_{N_c} V^{(c)} - \sum_{N_r} V^{(r)} & B_v = 0 \end{cases} \quad (\text{A.36})$$

where, $N_{p'}$ is the number of particles that is unused by the clumps which lie fully within or intersect the measurement sphere, and $V^{(p')}$ is the volume of particle p' (equation A.37); N_l is the number of clumps with centroids that lie in the measurement sphere and $V^{(l)}$ is the clump volume (equation A.38); N_c is the number of active contacts that is not internal to a clump lying in the measurement sphere, and $V^{(c)}$ is the overlap volume of both particles in contact (c); $N_{l'}$ is the number of particles used by the clumps that are fully within or intersect the measurement sphere, and $V^{(l')}$ is the volume of particle (l') in the measurement sphere; and N_r is the number of clump-overlap regions with centroid in the measurement sphere, and $V^{(r)}$ is the volume of the clump-overlap region (r) which is the overlap volume of the two spheres defining the region.

A typical representation for a system containing both clump and particles is given in Fig. A.11.

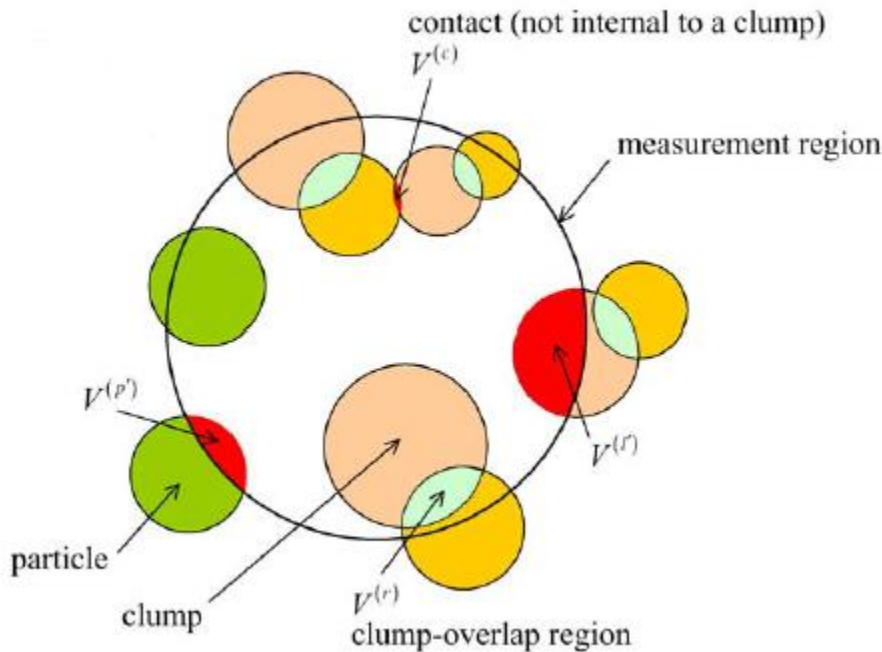


Fig. A. 3 Relevant quantities for porosity computation in a system with 4 clumps and 2 particles (ITASCA, 2004)

The particle volume can then be given as

$$V^{(p)} = \begin{cases} \pi R^2 t, & 2D (t = 1) \\ \frac{4}{3} \pi R^3, & 3D \end{cases} \quad (\text{A.37})$$

where R is the particle radius and the clump volume is represented in equation 3.38.

$$V^{(l)} = \begin{cases} \sum_{N_p} V^{(p)} - \sum_{N_r} V^{(r)}, & B_v = 0 \\ V_l, & B_v \neq 0 \end{cases} \quad (\text{A.38})$$

where N_p is the number of particles in the clump, and $V^{(p)}$ is the particle volume which is expressed in equation A.37; B_v is the volume-compute flag that is associated with each clump.

A.7.3 Sliding fraction

The sliding fraction is defined as the fraction of contacts that is slipping within the measurement sphere. As discussed earlier, the assumption is that slip will only occur at a contact in the absence of a contact bond and the magnitude of the shear component of the contact force is within one-tenth of a percent of the maximum allowable shear force. However, contacts with contact bonds that are intact are regarded as non-sliding regardless of the magnitude of the shear-force.

A.7.4 Stress measurements

Stress is a continuum quantity and in its application in DEM, it cannot exist at each point in a particle assembly due to the discrete characteristics of the medium. In the PFC^{3D} model, the contact forces and particle displacements are computed which provides useful information when studying the material behaviour on a microscale and not transferred directly to a continuum model. This introduces the averaging procedures which are necessary to make the step from microscale to a continuum. The average stress $\bar{\sigma}_{ij}$, in a volume V of a material is defined by

$$\bar{\sigma}_{ij} = \frac{1}{V} \int_V \bar{\sigma}_{ij} dV \quad (\text{A.39})$$

where $\bar{\sigma}_{ij}$ is the stress that acts throughout the volume.

However, for particulate materials that consist of spherical particles and clumps, stresses exists only in the particles/clumps and the integral can be expressed as a sum over the N_p particles and N_l clumps contained within V as:

$$\bar{\sigma}_{ij} = \frac{1}{V} \left(\sum_{N_p} \bar{\sigma}_{ij}^{(p)} V^{(p)} + \sum_{N_l} \bar{\sigma}_{ij}^{(l)} V^{(l)} \right) \quad (\text{A.40})$$

where $\bar{\sigma}_{ij}^{(p)}$ and $\bar{\sigma}_{ij}^{(l)}$ are the average stresses in particle (p) and clump (l) respectively.

Thus, in the same way, the average stresses in each entity (ϕ) where $\phi = \{p, l\}$ is given in equation A.41.

$$\bar{\sigma}_{ij}^{(\phi)} = \frac{1}{V^{(\phi)}} \int_{V^{(\phi)}} \bar{\sigma}_{ij}^{(\phi)} dV^{(\phi)} \quad (\text{A.41})$$

An expression for the average stress in a volume V , can be defined but could be problematic due to the particles/clumps that intersect the measurement sphere. This problem can be taken care of by noting that, in a statistically uniform assembly, there is a volume associated with each particle/clump such that:

$$V = \frac{\sum_{N_p} V^{(p)} + \sum_{N_l} V^{(l)}}{1-n} \quad (\text{A.42})$$

where n is the porosity of the measurement sphere. The average stress in the measurement sphere can then be expressed as given in equation A.43

$$\bar{\sigma}_{ij} = \left(\frac{1-n}{\sum_{N_p} V^{(p)} + \sum_{N_l} V^{(l)}} \right) \left(\sum_{N_p} \bar{\sigma}_{ij}^{(p)} V^{(p)} + \sum_{N_l} \bar{\sigma}_{ij}^{(l)} V^{(l)} \right) = \left(\frac{1-n}{\sum_{N_p} V^{(p)} \sum_{N_c^{(p)}} N_c^{(p)} + \sum_{N_l} V^{(l)} \sum_{N_c^{(l)}} N_c^{(l)}} \right) \left(\sum_{N_p} \sum_{N_c^{(p)}} \left(x_i^{(c)} - x_i^{(p)} \right) F_j^{(c,p)} + \sum_{N_l} \sum_{N_c^{(l)}} \left(x_i^{(c)} - x_i^{(l)} \right) F_j^{(c,l)} \right) \quad (\text{A.43})$$

where the summations are taken over the N_p particles and N_l clumps with centroid in the measurement sphere and the terms used are defined as:

$V^{(\phi)}$ is the volume of the body (ϕ), where ϕ is either the particle, p and clump l .

n is the porosity of the measurement sphere

$N_c^{(\phi)}$ is the number of contacts along the body surface (particle or clump)

$x_i^{(\phi)}$ and $x_i^{(c)}$ are the locations of the body centroid and its contact respectively.

$F_j^{(c,\phi)}$ is the force acting on a body (ϕ) at contact (c), which includes both contact and parallel bond forces but without the parallel-bond moment.

The above descriptions help to understand the methodology of DEM as well as describe different particle-scale parameters used as input to the DEM simulations.